

Heat and mass transfer during cooling and storage of agricultural products as influenced by natural convection

NN08201.805

K.J. Beukema

**Heat and mass transfer during cooling and storage of
agricultural products as influenced by natural convection**

Promotor: dr. ir. S. Bruin, hoogleraar in de proceskunde
Co-promotor: dr. ir. J. Schenk, hoogleraar in de technische natuurkunde

K.J. Beukema

Heat and mass transfer during cooling and storage of agricultural products as influenced by natural convection

Proefschrift
ter verkrijging van de graad van
doctor in de landbouwwetenschappen,
op gezag van de rector magnificus,
dr. H.C. van der Plas
hoogleraar in de organische scheikunde
in het openbaar te verdedigen
op vrijdag 16 mei 1980 des namiddags te vier uur
in de aula van de Landbouwhogeschool te Wageningen



Centrum voor landbouwpublicaties en landbouwdocumentatie

Wageningen – 1980

Abstract

Beukema, K.J. (1980) Heat and mass transfer during cooling and storage of agricultural products as influenced by natural convection. Agric. Res. Rep. (Versl. landbouwk. Onderz.) 897, ISBN 90 220 0728 6, (xii + 159 p., 101 figs, 24 tables, 155 refs, 2 app., Eng. and Dutch summaries.

Also: Doctoral thesis, Wageningen.

Three different models of bulk-stored agricultural products with air flow through the bulk, predicting the temperature profiles or the velocity of natural convection, are developed. The temperature distribution in a cylindrical container with insulated walls and open top and bottom, filled with heat-generating model material is studied experimentally, used to calculate the velocity of natural convection and compared with model predictions. A two-dimensional two-phase model of temperature and moisture distribution during cooling and storage of agricultural products in a cylindrical container is developed. The influence of convective transport (natural and forced convection), heat generation, heat conduction, evaporation, condensation and moisture diffusion is incorporated in the model equations. A sensitivity analyses with this model is presented. The model calculations are compared with the measured temperature course during self-heating of potatoes or model material. Three-dimensional natural convection in a closed container filled with heat-generating products is modelled with a three-dimensional one-phase model. Temperature measurements in a rectangular container filled with model material, potatoes or Brussels sprouts are discussed and compared with the model calculations. Literature on natural convection in porous media with or without heat generation and on models of bulk-stored agricultural products is reviewed.

Free descriptors: mathematical modeling, potatoe storage, porous medium, heat generation, three-dimensional air flow.

This thesis will be published as Agricultural Research Reports 897

© Centre for Agricultural Publishing and Documentation, Wageningen, 1980.

No part of this book may be reproduced and/or published in any form, by print, photoprint, microfilm or any other means without written permission from the publishers.

Stellingen

1. De aannname van Villa dat tijdens zijn experimenten de wateractiviteit aan het oppervlak van een geschildde aardappel niet verandert, is niet realistisch.

Villa, L.G., 1973, Ph.D. Thesis, Michigan State University.

2. Het gebruik van zowel de Darcy-term als de viskeuze wrijvingsterm in de bewegingsvergelijking voor een poreus medium is niet juist.

Hfdst. 2, dit proefschrift.

3. De conclusie van Hylmö dat de relatieve vochtigheid in een stapel aardappels overal 100% bedraagt, wordt door zijn metingen niet bevestigd.

Hylmö, B.T., T. Persson, C. Wikberg & W.C. Sparks, 1975, Acta Agr. Scand. 25: 81-87.

4. Het omdopen van de algemeen bekende Thiele-modulus tot Jüttner-modulus verdient geen navolging.

Wakao, N. & T. Funazkri, 1978, Chem. Engng Sci. 33: 1375-1384.

5. De conclusie van Ahuja, dat de warmteoverdrachtscoëfficiënt aan de buitenkant van een pijp een functie is van het vloeistofdebiet in de pijp, is het gevolg van een onjuiste toepassing van de Graetz-oplossing.

Ahuja, A.S., 1975, J. Appl. Phys. 46: 3408-3416.

6. Bij een aardappeltemperatuur beneden 4 °C levert het onderwatergewicht een te hoge waarde van het zetmeelgehalte.

7. Bij longemphyseem treedt in eerste instantie irreversibel elasticiteitsverlies van longweefsel op. In tegenstelling tot wat vermeld wordt in de literatuur bestaat er tevens een reversibele component van de bronchusobstructie die van belang is voor de prognose.

Postma, D.S., H.J. Sluiter, et al., 1979, Am. Rev. Resp. Dis. 119: 357-367.

8. Indien bij een verdubbeling van de rekensnelheid van een computer tevens de bedrijfszekerheid ervan verdubbelt, zijn computerberekeningen beter te plannen dan onder de huidige omstandigheden het geval is.

9. Het consequent uitdrukken van de snelheid van een auto in m/s maakt het een automobilist(e) eenvoudiger zich te realiseren dat hij/zij afstand moet houden.
10. Aangezien een verstandige jachtbeoefening bijdraagt tot het in stand houden van een gevarieerde fauna, moet beperking van de jacht worden tegengegaan.

Proefschrift van K.J. Beukema

Heat and mass transfer during cooling and storage of agricultural products as influenced by natural convection

Wageningen, 16 mei 1980.

Dankbetuiging

Door de hulp en stimulans van velen heb ik dit proefschrift kunnen voorbereiden en schrijven. Een aantal van hen wil ik met name bedanken:

- Mijn promotor prof. dr. ir. S. Bruin die door zijn belangstelling en adviezen steeds een stimulerende invloed had op mijn onderzoek.
- Mijn co-promotor prof. dr. ir. J. Schenk wiens belangstelling en kritische opmerking zeer nuttig waren.
- Mijn derde begeleider dipl. ing. H.F.Th. Meffert (Sprenger Instituut) die er voor zorgde dat de band met de praktijk niet verloren raakte.
- Mijn ex-collega's dr. ir. J.A.M. Spaninks en ir. K.Ch.A.M. Luyben voor hun stimulerende kritiek op mijn onderzoek.
- Ir. G. van Beek (Sprenger Instituut) met wie ik menige discussie over de praktische en theoretische aspecten van dit werk heb gevoerd.
- Dhr. J. G. de Swart (ITAL) voor zijn hulp bij het automatiseren van de temperatuurmetingen.
- De heren E. Janssen en W.J. Ackerman, alsmede de andere leden van de Centrale Dienst Biotechnion, voor het op kundige wijze maken van mijn experimentele opstellingen.
- Mevr. I. Teunis voor het snel en vakkundig uittypen van dit proefschrift.
- De heren C. Rijpma en M. Schimmel van de Centrale Dienst Biotechnion voor het vakkundig maken van het grote aantal figuren.
- De medewerkers van het Pudoc voor de uiteindelijke vormgeving van dit proefschrift.

Door hun aller belangstelling en medewerking is het mogelijk geweest mijn onderzoek aan de Landbouwhogeschool met dit proefschrift af te ronden.

Curriculum vitae

De auteur, geboren op 2 april 1951 te Hornhuizen (Gr.), bezocht van 1963-1968 de RHBS te Warffum. Na het behalen van het diploma HBS-B in 1968 begon hij in hetzelfde jaar met zijn studie scheikunde aan de Rijks Universiteit te Groningen. Na het kandidaats-examen in 1972 werd de studie voortgezet bij de vakgroep technische scheikunde met specialisatie fysische technologie. Het ingenieursdiploma werd behaald in maart 1975. Na het vervullen van de militaire dienstplicht trad hij in september 1976 als promotie-assistent in dienst bij de sectie proceskunde van de Landbouwhogeschool te Wageningen. In de periode 1976-1979 is het promotie onderzoek daar verricht. Sinds oktober 1979 is hij als researchmedewerker werkzaam bij de AVEBE te Veendam, waar hij betrokken is bij de winning van aardappelzetmeel en nevenprodukten.

Contents

List of symbols

1	Introduction	1
1.1	Storage and cooling of living products	1
1.2	Organization of this study.	6
2	Theory of natural convection	7
2.1	The governing equations	8
2.2	Natural convection in porous media without internal heat generation	10
2.3	Natural convection caused by heat generation	12
2.3.1	Heat-generating fluid	12
2.3.2	Heat-generating porous medium	12
2.4	Models of a heat-generating porous medium with pervious top and bottom	15
2.4.1	Heat transport by natural convection only	15
2.4.2	One-dimensional one-phase model with heat transport by convection and conduction	18
2.4.3	One-dimensional two-phase model with heat transport by convection and conduction	21
2.5	Pressure drop for flow through porous media	24
3	Physical modelling of bulk-stored agricultural and horticultural products	27
3.1	Review of literature	27
3.1.1	Comparison of various models in general	27
3.1.2	Models of bulk stored agricultural products	31
3.2	Physical properties used in the model equations	33
3.3	Derivation of the model equations for the SNC-model	40
3.4	Sensitivity analysis with the SNC-model	46
3.4.1	The base-case	46
3.4.2	Influence of different parameters	51
3.4.3	Conclusions	63
4	Experiments on one-dimensional natural convection in a container with insulated side walls	64
4.1	Materials and methods	64

4.1.1 Heat-generating model material	64
4.1.2 Temperature measurements	65
4.2 Experimental set-up	67
4.3 Results with model material for pervious bottom and pervious top	69
4.4 Results with model material for closed bottom and pervious top	85
4.5 Results with model material for closed bottom and closed top	88
4.6 Results with potatoes for pervious bottom and pervious top.	92
5 Application to cooling in closed containers	99
5.1 Conductive cooling models	99
5.2 Conductive cooling of a parallelepiped with a constant rate of heat generation	101
5.3 Model of three-dimensional natural convection in a porous medium with heat generation	106
5.3.1 Derivation of the model equations	106
5.3.2 The numerical solution	110
5.3.3 Results of the calculations	112
5.4 Experiments with model material	119
5.4.1 Experimental set-up	119
5.4.2 Experimental results	119
5.4.3 Comparison of measured and calculated temperatures	132
5.5 Experiments with real products	137
5.5.1 Potatoes	137
5.5.2 Brussels sprouts	141
6 Final remarks	145
6.1 Practical implications	145
6.2 Suggestions for futur research	145
Summary	147
Samenvatting	149
Appendices	151
Appendix A. Solution of the equations of the SNC-model	151
Appendix B. Physical data of the potatoes used in the experiments	152
References	154

List of symbols

a	thermal diffusivity	(m ² /s)
a_m	thermal diffusivity in the Raleigh number = $\lambda_0/(\rho c_p)_f$	(m ² /s)
A	specific surface	(m ² /m ³ product)
Bi	Biot number = $\alpha L/\lambda_0$	(1)
Bi'_L	Biot number at the top = $\alpha_L d_p/\lambda_0$	(1)
c	concentration	(kg/m ³)
c_p	heat capacity at constant pressure	(J/kgK)
C	dimensionless concentration	(1)
d	thickness	(m)
d_p	particle diameter	(m)
D	cylinder diameter	(m)
DD	diffusion coefficient	(m ² /s)
DD_e	axial dispersion coefficient	(m ² /s)
DD_r	radial dispersion coefficient	(m ² /s)
ϵ	radiative emissivity	(1)
F	heat capacity ratio = $(\rho c_p)_m/(\rho c_p)_a$	(1)
g	acceleration of the gravity	(m/s ²)
G	dimensionless heat of vaporization = $\Delta H_v L^2 kA(1-\epsilon)c_{sat,0}/\Delta T \lambda_{ax}$	(1)
k	mass transfer coefficient	(m/s)
K	correction factor in the Ergun equation	(1)
K_r	constant in calculating radial thermal conductivity	(1)
L	height	(m)
L_z	container height	(m)
Le	Lewis number = a/DD	(1)
\dot{m}	rate of total moisture loss	(kg/kg prod. h)
M	molecular weight	(kg/kmol)
n	molar concentration	(kmol/m ³)
Nu	Nusselt number = $\alpha L/\lambda_0$	(1)
\vec{O}	vorticity vector	(1/s)
P	pressure	(Pa)
Pe	Péclet number = vL/a	(1)
Po	Pomerantsev number = $QL^2/\lambda\Delta T$	(1)
Pr	Prandtl number = ν/a	(1)
Q	heat generation	(W/m ³)
Q_0	constant in temperature-dependent heat generation	(W/m ³)
Q_1	constant in temperature-dependent heat generation	(K)
r	radial coordinate	(m)

$r\delta$	variable in model of moisture loss	(m)
R	dimensionless radial coordinate = r/L	(1)
R	gas constant	(J/kmolK)
Ra_{cr}	critical Rayleigh number	(1)
Ra_E	external Rayleigh number = $\rho g \beta \kappa L \Delta T / \mu_f a_m$	(1)
Ra_I	internal Rayleigh number = $\rho g \beta \kappa L^3 Q / \mu_f a_m \lambda_0$	(1)
Re	Reynolds number = $\rho v d_p / \mu$	(1)
RH	relative humidity	(%)
R_0	radius	(m)
S	radiation number = $\epsilon \sigma L / \lambda_0 \Delta T$	(1/K ⁴)
S_c	dimensionless radiation number = $4 \epsilon \sigma L T_c^3 / \lambda_0$	(1)
Sh	Sherwood number = $k L / ID$	(1)
t	time	(s)
T	temperature	(K)
T_c	temperature at radiation loss	(K)
v	velocity	(m/s)
v_D	dimensionless velocity = $v L_z / a_m$	(1)
v_{FC}	velocity of forced convection	(m/s)
v_{NC}	velocity of natural convection	(m/s)
V	velocity potential	(m ³ /s)
V_D	dimensionless velocity potential = $V / a_m L_z$	(1)
x	distance coordinate	(m)
X	dimensionless distance coordinate = x / L_z	(1)
X_i	volume fraction component i	(1)
y	distance coordinate	(m)
Y	dimensionless distance coordinate = y / L_z	(1)
z	distance coordinate	(m)
Z	dimensionless distance coordinate = z / L_z	(1)
α	heat transfer coefficient	(W/m ² K)
α_L	effective heat transfer coefficient at top	(W/m ² K)
α_w	heat transfer coefficient at the wall	(W/m ² K)
β	thermal expansion coefficient	(1/K)
β_c	concentration expansion coefficient	(m ³ /kg)
β_p	pressure expansion coefficient	(1/Pa)
γ	fraction permeable to water vapour	(1)
ΔH_v	heat of vaporization	(J/kg)
Δm	integrated total moisture loss	(kg/kg product)
ΔP	pressure difference	(Pa)
ΔT	temperature difference	(K)
ϵ	porosity	(1)
η	thermal conductivity ratio = $\lambda_{rad} / \lambda_{ax}$	(1)
θ	dimensionless temperature = $(T - T_1) / (T_0 - T_1)$	(1)
θ_Q	dimensionless temperature = $(T - T_0) \lambda_0 / Q L^2$	(1)
κ	permeability	(m ²)
λ	thermal conductivity	(W/mK)

λ_c	thermal conductivity of continuous phase	(W/mK)
λ_d	thermal conductivity of dispersed phase	(W/mK)
λ_0	thermal conductivity of stagnant bed	(W/mK)
ρ	density	(kg/m ³)
ν	kinematic viscosity	(m ² /s)
μ	dynamic viscosity	(kg/ms)
σ	Stefan-Boltzmann constant	(kg/s ³ K ⁴)
σ_x	standard deviation	(1)
τ	dimensionless time = at/L^2	(1)
ϕ_m	mass flow	(kg/s)
ϕ_g''	heat flux	(W/m ²)
ψ	vector potential	(m ² /s)

Subscript

a	air
ax	axial
b	bulk
ext	external
f	fluid
int	internal
L	at height L
m	medium
ov	overall value
p	product
r	reference value
rad	radial
s	initial value
sat	saturated
sw	side wall
w	water
0	outside

Superscript

$\bar{}$	average value
\rightarrow	vector

1 Introduction

1.1 Storage and cooling of respiring products

Careful storage of agricultural and horticultural products is an important aspect of product quality control. Improper storage conditions may cause severe loss in quality. Storage conditions are not only important when products are kept in cold store, but also during transport. For instance flowers and vegetables need to be stored during transport by rail or by road from farm to auction and later to retailers. Sea transport of bananas, citrus fruit and apples is another example of this kind of storage. Storage is, of course, a prerequisite for consumption of a product all year round, since most of the products in question are harvested during a specific season. Potatoes, for instance, are harvested in the Netherlands from June to September, but they are available until June of the next year. Cereals can even be stored for some years and may be kept for when harvests are poor. Other products which are stored for long periods are cabbage, carrots, onions and fruit, like apples and pears.

Storage reduces the seasonal character of the food industry. Extension of the processing season, resulting in a prolonged on stream time of a plant or even in a year-round operation, has significant economic and social advantages, for example in potato processing and in milling industry. Another factor is that minimization of purchase costs of raw materials, i.e. buying at favourable market prices, requires storage facilities. Finally storage is necessary in order to damp out fast fluctuations in the delivery of raw materials. This last factor is important for example in canning and in the sugar industry.

The importance of careful storage is illustrated by some data on post-harvest food losses. The FAO (Willet, 1976) gave figures of estimated overall losses in the post-harvest period of 30 to 40% for perishable fruits and vegetables and 5 to 10% for cereals. In exceptional circumstances losses on cereals may increase to 20-40%. Willet did not indicate which part of the losses is caused by insects and rodents. However, when losses by insects and rodents are reduced or even prevented by fumigation and by a good construction of the storage room, there are still losses caused by other factors. Improved storage methods should reduce these losses.

Product quality may be lost by various kinds of deterioration. In order to select proper storage conditions, it is necessary to know these different kinds and to know which one dominates and therefore has to be prevented at first. Burton (1977) defined three different categories of deterioration: (1) microbial attack, (2) biochemical change and (3) evaporative losses. He stated that frequently one form terminates the useful storage period before either of the others becomes serious. Which form it is, depends upon the product.

Microbial attack causes rotting of the product. It is reduced by a low temperature or a low relative humidity of the air. A low temperature retards the growth rate of the micro-organism while bacteria and molds hardly grow below a relative humidity of 90 and 65%, respectively (Labuza, 1970). However a low relative humidity causes larger evaporative losses and only when these losses are unimportant, for instance with onions, may a low relative humidity be used. Another way to reduce microbial attack is a fungicide treatment of the produce, before it goes into store.

Biochemical change does not stop during storage of respiring products. It may change the taste (e.g. by breakdown of aroma components or by development of sugars) or the colour of the produce. Respiration, and its corresponding metabolism, is another form of biochemical change and this reaction is responsible for most of the heat generated by the products. The biochemical reactions are mostly retarded at lower temperatures. Some products, however, show undesirable reactions at low temperature; bananas should be stored above 12 °C, otherwise the skins turn brown.

Biochemical change is also influenced by the oxygen concentration of the environment. Lowering the partial pressure of oxygen retards the biochemical change. This is the so-called Controlled Atmosphere (CA) storage. The oxygen concentration may also be reduced by lowering the pressure of the air around the products: hypobaric storage.

Evaporative losses cause wilting and shrivelling of the product and also reduce the weight of saleable produce. They are important for products with a large specific surface area or a surface with a large permeability to water vapour, e.g. leafy vegetables like lettuce or endive. When storage for long periods is required, a small but continuous rate of evaporative loss is disastrous. This may occur in products such as potatoes and apples which are often stored for extended periods of time. Moisture is lost when the water vapour concentration of the air around the product is lower than the equilibrium water vapour concentration in the product. The smaller this difference in concentration, the lower the losses. Therefore a high relative humidity of the air around the product decreases evaporative losses. Sometimes the product is coated with wax, which reduces the permeability of the surface and therefore evaporative loss. The equilibrium water vapour concentration in the product decreases at decreasing temperatures. Therefore at the same relative humidity of the air, the water vapour pressure difference between product and air is smaller at a lower temperature. Thus a low temperature reduces evaporative losses.

Another factor influencing the final quality of the stored product is the condition of the product at the moment it goes into store. Unless a ripening period after harvest is necessary, storage can at most maintain quality, but never improves the product.

From the preceding survey it is obvious that product quality is influenced by the history of temperature, pressure and composition of the gas phase (especially water, oxygen and carbon dioxide content) during transport and storage (see Fig. 1). These environmental histories are governed by the imposed conditions of the gas phase (temperature, pressure, composition), the transient behaviour of the stored product when these conditions are imposed and the uniformity of the steady state. Table 1 summarizes the optimum storage temperature and the maximum storage time of some fruits and vegetables in air at atmospheric pressure, as recommended by different authors. A general

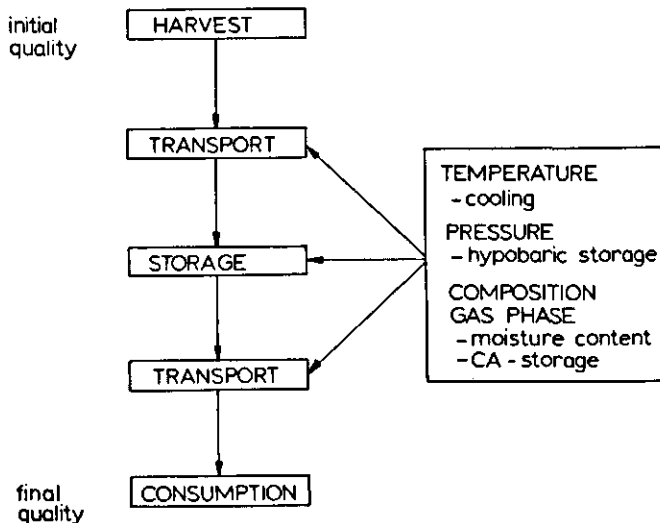


Fig. 1. Influences on quality of final product.

conclusion is that a low temperature and a high relative humidity are favourable. The minimum storage temperature is mostly determined by the freezing point of the product, since a lower temperature causes freezing injury which is unfavourable. There is a large variation in maximum storage time because different varieties of a product show different storage behaviour. For instance the apple variety Benoni cannot be stored for more than two weeks, whereas the variety Golden Delicious may be stored for five months.

Local differences in temperature and humidity in a storage room will cause different rates of deterioration in different places. When this happens, it is possible that storage has to be ended prematurely, because of unacceptable deterioration of the produce in some places. It is therefore important to create uniform storage conditions in a storage room.

Another factor affecting product quality is that the time required to bring the product from ambient conditions to the desired storage conditions should be optimized. The faster the optimum climate is attained the lower the moisture loss and deterioration of the produce will be. When harvested products go into store it is usually necessary to cool them. To attain rapid cooling, heat must be quickly transferred from the products to the air and the cooling capacity of the cold store must be large. This large cooling capacity is only used to attain the optimum storage temperature. A much smaller cooling capacity is required to maintain the low temperature of the product. It is therefore rather expensive to use a large cooling capacity in the cold store. This economic problem may be tackled by precooling the produce and placing it thereafter in a cold store with a small cooling capacity. At precooling, the products are cooled fast to the desired temperature in a special precooling unit. This system requires of course a larger investment in buildings and machinery and more handling of the produce. In the Netherlands most products are still cooled in a storage room with a small cooling capacity.

Two modes of cooling can be distinguished:

- Convective cooling. The cooling air is blown through a container with products or bulk-stored products. The heat is transferred directly from the product to the air.

Table 1. Optimum storage-conditions of some fruits and vegetables.

	O'Loughlin (1976)	Cheftel & Cheftel (1976)	Sprenger Institute (1972-1977)	Käppel & Weichmann (1977)	v.d. Berg & Lentz (1973)
<i>Apples</i>					
Temperature (°C)	0-2	-1-4	3-5		
Relative humidity (%)	88-90		90-95		
Storage time (month)	2-6	1-8	2-6		
<i>Pears</i>					
Temperature (°C)	-1	-2-1	-0.5-0		
Relative humidity (%)	88-90		92-95		
Storage time (month)	2	1-7	0.5-7		
<i>Oranges</i>					
Temperature (°C)	6	4-6			
Relative humidity (%)					
Storage time (month)	1.5-3	till 6			
<i>Peaches</i>					
Temperature (°C)	0	-1-1			
Relative humidity (%)	85-90				
Storage time (month)	0.5-1	0.25-1			
<i>Carrots</i>					
Temperature (°C)	0	-1-1	0-1	0	0
Relative humidity (%)	90-95		90-98	> 98	> 98
Storage time (month)	4-5	4-6	8		
<i>Beans</i>					
Temperature (°C)	0-7	0	5-6	8	
Relative humidity (%)	90-95		90-95	> 95	
Storage time (month)		0.25-0.75	0.25-0.5		
<i>Onions</i>					
Temperature (°C)	0	-3-0	-2-1	0	
Relative humidity (%)	75		80	70	
Storage time (month)	6	1.5	9		
<i>Cabbage</i>					
Temperature (°C)	0	0	0-1	0-1	
Relative humidity (%)	90		90-95	> 98	
Storage time (month)	3-4	2-4	6	7	
<i>Potatoes (table)</i>					
Temperature (°C)	7-10	5-10		4-8	
Relative humidity (%)	90-95			> 98	
Storage time (month)		4-8		9	
<i>Brussels sprouts</i>					
Temperature (°C)		-1-0	-1		
Relative humidity (%)			90-95		
Storage time (month)	0.75-1.5		1		

— Conductive cooling. The cooling air is blown around a container with the product. As the container is impervious to air flow, the heat is transported by conduction in the container to the wall and by convective heat transfer from the wall to the air.

Under conductive cooling conditions the product is cooled much more slowly than under convective cooling conditions, because conduction of heat through the container limits heat transfer. A combination of convective and conductive cooling is, of course, also possible.

During both convective and conductive cooling natural convection can occur. Natural or free convection is the movement of a fluid caused by buoyancy forces. The buoyancy force in a fluid is generated by density differences which may be caused by either temperature or concentration differences or both. It is obvious that temperature differences in the gas phase will occur during cooling of agricultural or horticultural products. For instance during conductive cooling of closed containers there exists a temperature difference between the centre and the walls of the container. This causes an air flow in the container which is directed downwards at the walls and upwards in the central part of the container. This natural convection accelerates the cooling. Natural convection also occurs during the storage of cereals in silos, when the side wall is heated during warm weather or cooled during cold weather. Then moisture accumulates on the top or the bottom of the stored grain (Carter & Farrar, 1943; Muir, 1973).

It is obvious that during cooling of both products that generate heat and those that do not natural convection will occur. When the steady state has been attained, natural convection ends for products that do not generate heat, whereas natural convection still occurs for heat-generating products. In the latter case heat generation causes temperature differences in the system and therefore natural convection does not end.

When products are stored in bulk and the average bulk temperature is higher than the temperature of the surroundings, natural convection can be used to lower the bulk temperature. If the cold air at the bottom of the bulk enters the bulk unrestrictedly, this air is sucked through the bulk and a natural cooling system is developed. The same principle is used in air cooling towers and in trickling filters for waste-water treatment.

Until now hardly any attention has been paid to the heat and mass transfer phenomena as influenced by natural convection during cooling and storage of agricultural and horticultural products. Burton et al. (1955) gave a simple model of natural convection in non-ventilated bulk stored potatoes. Mellor et al. (1962) described the faster cooling of fruit in containers with vents in the bottom and with open top, compared with conductive cooling. They indicated that about 10% open space in the bottom of the container gives this effect. Gafney (1977) stated that natural convection may influence the cooling of unvented containers, but he gave no real data. Lerew (1978) indicated the need for the description and simulation of natural convection in modelling potato storage.

The present work aims at studying natural convection and its influence on cooling and storage of agricultural and horticultural products. Most attention is paid to two extremes: (1) a system with air flow through a pervious bottom and a pervious top and (2) a completely closed container with only internal natural convection.

1.2 Organization of this study

After this introduction Chapter 2 starts with a review of literature on natural convection in systems, especially porous media, heated from below or with internal heat generation. In this chapter, I also give the mathematical analysis of natural convection and temperature distribution in heat-generating porous media with pervious top and bottom. Because pressure drop turns out to be important in modelling the air flow, the last section of this chapter is devoted to literature of pressure drop for flow through porous media or bulk-stored produce.

In Chapter 3 the modelling of bulk-stored agricultural and horticultural products is discussed. After a review of literature on this subject, including similar modelling in chemical reaction engineering, and a discussion of some of the physical constants used, a mathematical model, incorporating the influence of natural convection is derived. The use of this model is illustrated by a sensitivity analysis of the storage of apples.

Chapter 4 describes experimental work on natural convection and temperature distribution in a cylindrical set-up with model material or potatoes. Most experiments are performed in a cylindrical container with pervious bottom and pervious top. However experiments with closed bottom and pervious top or closed bottom and closed top are performed too.

Chapter 5 concerns natural convection during cooling and storage of agricultural or horticultural produce in closed containers. After a review of conductive cooling literature, a mathematical model of natural convection in a heat-generating container is derived. Hereafter my experiments on cooling or heating of a container with isothermal walls, filled with model material, potatoes or Brussels sprouts are discussed.

Chapter 6 summarizes the results of this thesis and contains recommendations for future research.

2 Theory of natural convection

In order to describe the velocity of natural convection in bulk-stored produce I have used the theories on natural convection in porous media. Although porous media mostly consist of particles with a much smaller diameter than agricultural or horticultural products, the results in the following chapters show that the application of these theories on stored produce gives good results.

Literature on natural convection in porous media is devoted to the following phenomena:

- When does natural convection start?
- How large is the increase in heat transfer rate compared with heat transfer by conduction only?
- Which kind of fluid flow (stable two-dimensional rolls, oscillatory three-dimensional flow) occurs?

The first question may be answered by calculating the critical Rayleigh number, which is the Rayleigh number above which natural convection starts. For a porous medium that is heated from below the Rayleigh number (Ra) is usually defined as follows:

$$Ra_E = \frac{\rho g \beta \Delta T L}{\mu_f a_m} \quad (2.1)$$

In a porous medium with volumetric heat sources Ra is given by

$$Ra_I = \frac{\rho g \beta \kappa L^3 Q}{\mu_f a_m \lambda_0} \quad (2.2)$$

Gasser & Kazimi (1976) defined these Rayleigh numbers as the external Rayleigh number (Ra_E) and the internal Rayleigh number (Ra_I), respectively.

The increase in heat transfer rate is commonly expressed as the heat loss under natural convection conditions, divided by the heat loss under conduction only. In literature on natural convection in porous media this ratio is often referred to as the Nusselt number (Nu). However, Nu is usually defined as the ratio between the resistance to heat transfer by conduction and the actual resistance to heat transfer at a surface. I therefore prefer to express the above-mentioned increase in heat transfer rate by a quotient:

$$\frac{Nu}{Nu_0} = \frac{\text{Resistance to heat transfer under conduction only conditions}}{\text{Resistance to heat transfer under natural convection conditions}} \quad (2.3)$$

2.1 The governing equations

In order to derive the critical Rayleigh number (Ra_{cr}), the Nu/Nu_0 values and the kind of fluid flow for different Rayleigh numbers theoretically, it is necessary to solve the governing equations for continuity, momentum and energy. These equations are given in many text-books, e.g. Bird et al. (1960):

Continuity:

$$\frac{\partial \rho}{\partial t} + \nabla \cdot (\rho \vec{v}) = 0 \quad (2.4)$$

Motion:

$$\frac{\partial}{\partial t} (\rho \vec{v}) + \vec{v} \cdot \nabla (\rho \vec{v}) = \rho \vec{g} - \nabla P - \mu \nabla^2 \vec{v} \quad (2.5)$$

inertia	buoyant	viscous
term	force	term

Energy:

$$\frac{\partial}{\partial t} ((\rho c_p)_m T) + \vec{v} \cdot \nabla ((\rho c_p)_f T) = \nabla \cdot (\lambda_0 \nabla T) + Q \quad (2.6)$$

In a rectangular coordinate system with, as usual, the z direction upwards the gravitational vector \vec{g} is given by $g(0,0, -g)$. The term Q in the energy equation incorporates all heat sources in the system. These sources may be viscous energy dissipation by fluid flow or internal heat generation by some other mechanism (e.g. chemical reaction).

Commonly the governing equations are simplified by neglecting inertia terms in the momentum equation, viscous heating by fluid flow and application of the Boussinesq approximation. The Boussinesq approximation implies constant fluid properties except the density in the term where it causes buoyant forces. This reduces the governing equations to:

Continuity:

$$\nabla \cdot \vec{v} = 0 \quad (2.7)$$

Momentum:

$$\rho \frac{\partial \vec{v}}{\partial t} = \rho \vec{g} - \nabla P + \mu \nabla^2 \vec{v} \quad (2.8)$$

Energy:

$$(\rho c_p)_m \frac{\partial T}{\partial t} + (\rho c_p)_f \vec{v} \cdot \nabla T = \lambda_0 \nabla^2 T + Q \quad (2.9)$$

In (2.9) the energy equation of a system consisting of one phase is given. As will be discussed in Chapter 3 it is sometimes necessary to distinguish in a porous medium between the solid and the fluid phase, both being assumed to be quasi-continuous. Heat transfer between the two phases is described by a velocity-dependent heat transfer coefficient. The solid phase is assumed to be stagnant. Thus the two-phase energy equations are

solid:

$$(1-\epsilon)(\rho c_p)_p \frac{\partial T_p}{\partial t} = (1-\epsilon)\lambda_p \nabla^2 T_p + Q_p + \alpha A (1-\epsilon)(T_f - T_p) \quad (2.10)$$

fluid:

$$\epsilon(\rho c_p)_f \frac{\partial T_f}{\partial t} + (\rho c_p)_f \vec{v} \cdot \nabla T_f = \epsilon \lambda_f \nabla^2 T_f + Q_f + \alpha A (1-\epsilon)(T_p - T_f) \quad (2.11)$$

From the integral form of the equation of motion Whitaker (1966) showed that in an incompressible, isotropic porous medium the viscous term may be given by

$$\mu \nabla^2 \vec{v} \equiv - \frac{\mu}{\kappa} \vec{v} \quad (2.12)$$

The term on the right side of this equation is the Darcy term, derived from Darcy's Law, giving the pressure drop for flow through porous media:

$$\frac{\Delta P}{L} = - \frac{\mu}{\kappa} v \quad (2.13)$$

Whitaker (1969) further showed that even when the inertial terms cannot be neglected, the linear dependence of the viscous term on the fluid velocity still may be used.

Brinkman (1947) introduced a momentum balance which incorporates both the viscous term and the Darcy term:

$$\frac{\partial}{\partial t} (\rho \vec{v}) + \vec{v} \cdot \nabla (\rho \vec{v}) = \rho \vec{g} - \nabla P - \frac{\mu}{\kappa} \vec{v} + \mu \nabla^2 \vec{v} \quad (2.14)$$

He used this equation to calculate the viscous force exerted by a flowing fluid on a dense swarm of particles. Other authors (e.g. Rudraiah & Prabhamani, 1974; Gasser & Kazimi, 1976; Walker & Homsy, 1977) used this form of the equation of motion to describe natural convection in porous media. Brinkman regarded the use of both viscous force and Darcy term in the equation of motion as an arbitrary interpolation in the region where the viscous force and the Darcy term are of the same magnitude. However as shown by Whitaker (1966, 1969), the Darcy term replaces the viscous force and therefore it is incorrect to use both terms in the same equation.

The choice of Darcy term or viscous force depends upon the dimensions of the reference volume (l) used to set up the equation of motion and the particle diameter (d_p).

When l is much larger than d_p , the porous medium may be considered as a continuum and the Darcy term may be used. However when l and d_p are of the same magnitude or when d_p is larger than l , the assumptions of Whitaker are not satisfied and the equation of motion should be solved with the viscous force instead of the Darcy term. Thus knowledge of local velocity profiles and distribution of pore diameter is required to solve the equation of motion.

2.2 Natural convection in porous media without internal heat generation

Literature of natural convection in porous media is mostly concerned with porous media heated from below. Lapwood (1948) was the first to calculate the critical Rayleigh number (Ra_{cr}) of an infinite horizontal layer with impervious isothermal top and bottom heated from below: $Ra_{cr} = 4\pi^2$. He also calculated the value of Ra_{cr} when the upper boundary has a constant pressure, as for instance in a porous medium with fluid above it: $Ra_{cr} = 27.1$. He further showed that a porous medium partly filled with fluid (free upper boundary) gives in a first order approximation the same critical Rayleigh number as a porous medium with an impervious upper boundary namely: $Ra_{cr} = 4\pi^2$. The three situations are summarized in Fig. 2.

Katto & Masuoka (1967) showed both experimentally and theoretically that the thermal diffusivity, to be used in the Rayleigh number, should be defined as:

$$a_m = \frac{\lambda_0}{(\rho c_p)_f} \quad (2.15)$$

Thus the thermal diffusivity is a combination of the bulk thermal conductivity and the fluid heat capacity. This combination is obtained when the energy equation is made dimensionless because convective transport only occurs in the fluid phase, whereas conductive transport occurs in solid and fluid phases.

Ribando & Torrance (1976) calculated Ra_{cr} in a porous medium with constant uniform heat flux at the bottom and a constant temperature at the top. They obtained $Ra_{cr} = 27.1$ and 17.1 with an impermeable and a constant pressure top, respectively.

Kassoy & Zebib (1975) and Epherre et al. (1976) reported a decrease of Ra_{cr} (based upon fluid properties at the top temperature) when a temperature-dependent viscosity was introduced in the governing equations. A decrease of Ra_{cr} was also measured (Lawson et al. 1976) for a fluid phase which was a mixture of two gases (N_2 and He).

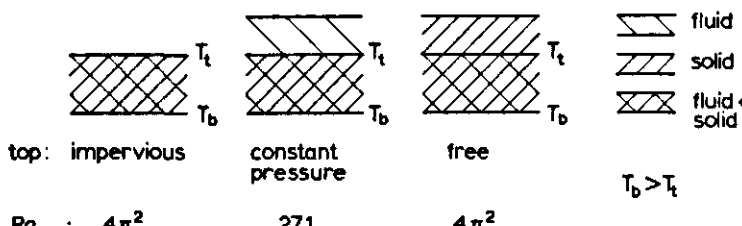


Fig. 2. Critical Rayleigh number for three different boundary conditions at the top and with heating from below.

Experimental work on the derivation of the relation between Nu/Nu_0 and Ra_E was reported by Elder (1967) and by Buretta & Berman (1976). Elder gave:

$$\frac{Nu}{Nu_0} = 0.025 Ra_E \quad (Ra_E < 1000) \quad (2.16)$$

This relation is only valid when Ra_E is not too large ($Ra_E < 1000$). Above some Ra_E value (depending upon the particle diameter) Nu/Nu_0 increases less because fluid velocities are higher at high Rayleigh numbers. Darcy's Law with a constant permeability is no longer valid. Buretta & Berman gave two relations:

$$\frac{Nu}{Nu_0} = 0.015 Ra_E^{1.15} \quad (40 < Ra_E < 100) \quad (2.17)$$

$$\frac{Nu}{Nu_0} = 0.061 Ra_E^{0.835} \quad (100 < Ra_E < 1000) \quad (2.18)$$

They also reported a deviation from this relation at higher Rayleigh numbers.

Theoretical calculations of Nu/Nu_0 as a function of Ra and a discussion of different kinds of fluid flow were given by Elder (1967), Palm et al. (1972) and Strauss (1974). Strauss calculated that at Rayleigh numbers between 40 and 380 two dimensional convective rolls will be stable.

Holst & Aziz (1972a) and Horne & O'Sullivan (1978) calculated the temperature and flow patterns when the fluid and porous medium properties are considered to be temperature dependent. The temperature dependence causes destabilization of the flow and higher values of Nu/Nu_0 .

The natural convection in inclined porous media heated from below has also been discussed by different authors (Holst & Aziz, 1972a; Bories & Combarous, 1973; Kaneko et al., 1974; Jaffrenou et al., 1974; Weber, 1975a). At small temperature differences between the upper and the lower boundary, there is an unicellular fluid movement parallel to the warmer bottom and colder top as given in Fig. 3. This unicellular flow is disturbed as the value of $Ra \cos \varphi$ becomes larger than $4\pi^2$, as has been shown by Bories & Combarous (1973), where φ is the angle between the bottom and the horizontal axis. The special case of $\varphi = 90^\circ$ gives rise to natural convection flow occurring in e.g. porous

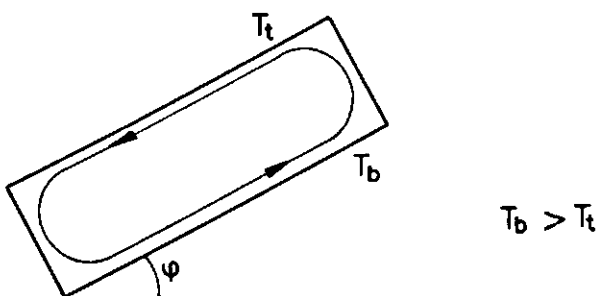


Fig. 3. Unicellular flow in an inclined porous medium.

insulation at the side walls of cold stores. This was theoretically discussed by Weber (1975b), whereas Seki et al. (1978) gave experimental results incorporating the influence of different height to width ratios in a rectangular cavity.

Because the assumption of horizontally infinite porous media is not always justified in practice, natural convection in closed rectangular containers was studied. These containers are heated from below, have impervious top and bottom and completely insulated impervious side walls. Holst & Aziz (1972b) solved the governing equations numerically to describe temperature and fluid velocity distribution inside the container. Beck (1972) calculated Ra_{cr} for different container geometries. He also calculated that the value of Ra_{cr} is influenced by the container geometry, but that the following relation always holds: $Ra_{cr} \geq 4\pi^2$. He also indicated the preferred cellular mode. By introducing a temperature-dependent viscosity, which is reported for the infinite extended porous medium, the value of Ra_{cr} in a container is lowered as shown by Zebib & Kassoy (1977). The dependence of Nu/Nu_0 on Ra and the stability of different fluid flows was discussed by Zebib & Kassoy (1977) and Strauss & Schubert (1978).

2.3 Natural convection caused by heat generation

2.3.1 Heat-generating fluid

Most literature on natural convection with internal heat generation deals with heat-generating fluids without a solid phase. This problem is important for safety analysis of nuclear reactors (melt down), geophysics and astrophysics. Most work is performed on systems which may be considered infinite in the horizontal direction, bounded on top and bottom by impervious isothermal layers of equal temperature (Kulacki & Goldstein, 1972; Kulacki & Goldstein, 1974; Catton & Suo-Antilla, 1974; Jahn & Reineke, 1974; Tveitereid, 1978) or with a higher temperature at the bottom (Cheung, 1978; Boon-Long et al., 1979). Kulacki & Emare (1977) and Cheung (1977) discussed systems with impervious isothermal top and impervious adiabatic bottom. Also natural convection in other geometries: a horizontal cylinder with isothermal walls (Jones, 1974), a sphere and a vertical cylinder (Kee et al., 1976) has been reported. The papers emphasized three subjects: (1) the distribution of heat losses between bottom and top for different rates of heat generation, (2) temperature and fluid velocity distribution inside the system and (3) stability of different fluid flow modes (laminar \rightarrow turbulent).

2.3.2 Heat-generating porous medium

Natural convection in porous media with internal heat generation has the same field of interest as the natural convection in fluids, described in Section 2.3.1. All literature deals with horizontally infinite porous layers. Most papers give the calculation of the critical Rayleigh number in different situations.

Hwang (1971) calculated Ra_{cr} in a heat-generating porous medium with impervious isothermal top and bottom. The bottom has a higher temperature than the top and the onset of natural convection is influenced by the rate of heat generation and by the temperature difference between bottom and top. Therefore Gasser & Kazimi (1976) gave values of the combination of the internal and external critical Raleigh numbers (defined

in Eqns 2.1 and 2.2). They used a free fluid surface on the top, occurring in a porous medium only partly filled with liquid. They studied both destabilizing ($T_b > T_t$) and stabilizing ($T_b < T_t$) temperature differences between bottom and top. There was a good agreement between their results and the data of Hwang on destabilizing temperature differences in spite of the different structure of the top layer: impervious for Hwang's calculations versus a free surface in the work of Gasser & Kazimi. As already described in Section 2.2 this agreement was also given by Lapwood (1948) in a system heated from below.

Kulacki & Ramchandani (1975) calculated Ra_{cr} in many different situations of fluid flow and temperature at top and bottom. The fluid flow was described for an impervious top and bottom and for a constant pressure top and bottom. The temperature followed from isothermal, adiabatic or imperfectly conducting top and bottom. The heat flux through an imperfectly conducting wall was represented by the value of the heat transfer coefficient at the wall (α). The limits of $\alpha \rightarrow 0$ or $\alpha \rightarrow \infty$ represent the adiabatic and the isothermal wall, respectively. The authors showed in various tables and graphs that Ra_{cr} is lower for a constant pressure top than for an impervious top, which causes more resistance to fluid flow. They also showed that a lower value of α at the bottom (and therefore a higher temperature) lowers Ra_{cr} too. Table 2 gives the data for adiabatic and isothermal, impervious or constant pressure top and bottom. It should be noticed that the combination of an adiabatic, impervious top and bottom describes heat generation without heat loss. This can only end in catastrophe.

Table 2 also gives Ra_{cr} of a system with impervious isothermal top and impervious adiabatic bottom calculated by Buretta (1972) and Tveitereid (1977). Buretta used an approximate solution to calculate Ra_{cr} and this may explain the difference between his

Table 2. Critical Rayleigh number in different situations of a porous medium with internal heat generation.

		TOP			
		Impervious		Constant pressure	
		adiabatic	isothermal	adiabatic	isothermal
BOTTOM	Impervious	adiabatic	238.2 ²	65.52 ¹ 61.86 ⁴	24.0 ²
		isothermal		471.4 ² 469.4 ³	235.2 ²
Constant pressure	adiabatic	245.0 ²			
	isothermal		472.4 ²		

1. Buretta (1972)

2. Kulacki & Ramchandani (1975)

3. Gasser & Kazimi (1976)

4. Tveitereid (1977)

$$Ra_I = \frac{\rho g \beta x L^3 Q}{\mu \sigma_m \lambda_0}$$

and Tveitereids data. The limiting value of Ra_1 when $Ra_E \rightarrow 0$ from the data of Gasser & Kazimi (1976) is also given in Table 2. The situation of a constant pressure top and a constant pressure bottom is discussed in Section 2.4.1.

Experiments giving the dependence of Nu/Nu_0 on Ra were performed by Buretta (1972), Buretta & Berman (1976) and Sun (1973). They used a porous medium with adiabatic impervious bottom and isothermal impervious top. Heat was generated by using 0.01 M copper sulphate solution to saturate the porous medium and by applying alternating current. In a porous medium without natural convection and an adiabatic bottom it can be derived from the energy equation (2.9) that the steady state temperature difference between top and bottom is given by

$$\Delta T = \frac{QL^2}{2\lambda_0} \quad (2.19)$$

In the work of Buretta (1972) and Sun (1973) Nu/Nu_0 was defined as:

$$\frac{Nu}{Nu_0} = \frac{QL^2}{2\lambda_0 \Delta T} \quad (2.20)$$

where ΔT represents the actual temperature difference between bottom and top. Therefore the value of Nu/Nu_0 is a comparison of the temperature difference between bottom and top for conduction only and the actual temperature difference. It may be more interesting to give the reduction of the maximum temperature for conduction only, compared with the maximum temperature with natural convection. The maximum temperature in a system determines the occurrence of other phenomena in that system e.g. boiling of a liquid phase, melting of the solid phase, deterioration of agricultural produce. The use of the maximum temperature implies, however, measurement of the internal temperature distribution.

Hardee & Nilsson (1977) performed experiments in a liquid saturated porous medium with adiabatic impervious bottom and an isothermal constant pressure top. They measured the temperature at different places in the bed, also with a high heat generation, which caused boiling of the liquid phase. They expected the onset of natural convection at $Ra_{cr} = 66$, as derived by Buretta (1972). However that value of Ra_{cr} is not to be expected with a boundary condition at the top of constant pressure, which occurs in the work of Hardee & Nilsson. From the work of Kulacki & Ramchandani (1975) it would be expected that Ra_{cr} is lower with a boundary condition at the top of constant pressure. In fact the plot of Nu/Nu_0 versus Ra_1 given by Hardee & Nilsson (1977) also indicates the onset of convection at a lower Ra_1 value: $Ra_1 = 24$.

Tveitereid (1977) analysed theoretically the stability of different kinds of flow patterns in a porous medium with impervious adiabatic bottom and impervious isothermal top. He concluded that there are no stable flows above $Ra > 8 Ra_{cr}$. At higher Rayleigh values the flow will show oscillatory instabilities.

The survey just presented shows that there are not many data available in the field of porous media with internal heat generation. Especially the data on the dependence of Nu/Nu_0 on Ra are rather scarce and the correspondence between theoretical and experimental work is not always sufficient. I have found no data at all on systems which cannot

be simplified to horizontally infinite parallel plates. These systems are of special interest for the storage of horticultural products in boxes and containers. Therefore I analysed the natural convection flow in rectangular containers, starting from the work of Holst & Aziz (1972b) and Tveitereid (1977). This analysis will be discussed in Chapter 5.

2.4 Models of a heat-generating porous medium with pervious top and bottom

2.4.1 Heat transport by natural convection only

The description of natural convection in porous media with pervious top and bottom should be used for bulk-stored produce that lies on a grate and is not covered. Heat generated by the produce in the bulk raises the temperature of the bulk and results in a temperature difference with the surroundings. In this system (see Fig. 4), with a constant pressure boundary on the top and on the bottom, the critical Rayleigh number will be zero. Therefore even when the rate of heat generation is very small, natural convection will occur.

The dependence of the steady-state velocity of natural convection (v_{NC}) on heat generation (Q) may be calculated from the governing equations. With the assumption of a horizontally infinite layer, the equation of energy (2.9) and momentum (2.8) with the Darcy term become in the steady state:

$$(\rho c_p)_a v_{NC} \frac{dT}{dz} = \lambda_0 \frac{d^2 T}{dz^2} + Q \quad (2.21)$$

$$0 = \frac{dP}{dz} + \rho g + \frac{\mu}{\kappa} v_{NC} \quad (2.22)$$

When v_{NC} is constant the integration of Eqn 2.22 over the height of the bulk ($0 \leq z \leq L$) yields with $P = P_0$ at $z = 0$ and $P = P_L$ at $z = L$

$$\frac{P_L - P_0}{L} + \bar{\rho} g + \frac{\mu}{\kappa} v_{NC} = 0 \quad (2.23)$$

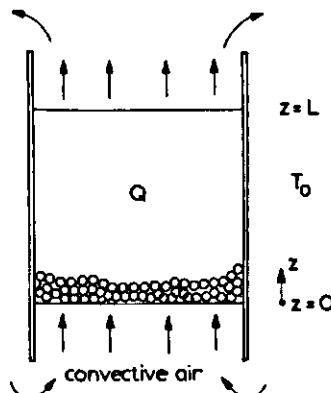


Fig. 4. The porous medium with internal heat generation.

where

$$\bar{\rho} = \frac{1}{L} \int_0^L \rho dz \quad (2.24)$$

The density differences between the outside air and the air in the product bulk may be caused by differences in temperature or water vapour concentration. Difference in water vapour concentration is caused by moisture loss of the produce. The change of density with temperature and water vapour concentration may be calculated from the air density:

$$\rho = n_w M_w + n_a M_a \quad (2.25)$$

where n_a and n_w denote the number of kmoles of air and water per m^3 gas and M_a and M_w the molecular weight of air and water. When it is assumed that water vapour and air behave as ideal gases, n_a and n_w as a function of pressure and temperature are given by

$$n_w = \frac{P_w}{RT} \quad (2.26)$$

$$n_a = \frac{P_a}{RT} = \frac{P - P_w}{RT} \quad (2.27)$$

where P_w and P_a are the partial pressure of water and air. P is the total pressure in the system, which is constant. Therefore

$$\rho = \frac{P_w M_w}{RT} + \frac{(P - P_w) M_a}{RT} \quad (2.28)$$

Substituting the ratio of the molecular weights of water and air:

$$\frac{M_w}{M_a} = \frac{18}{28.8} = 0.625 \quad (2.29)$$

gives

$$\rho = \frac{P - 0.375 P_w}{RT} M_a \quad (2.30)$$

The dependence of the density on water vapour pressure and temperature can be approximated by

$$\rho_{T,P} = \rho_r + \left(\frac{\partial \rho}{\partial T} \right)_{P_w} (T - T_r) + \left(\frac{\partial \rho}{\partial P_w} \right)_T (P_w - P_{w,r}) = \rho_r [1 - \beta(T - T_r) - \beta_P (P_w - P_{w,r})] \quad (2.31)$$

with

$$\beta = - \frac{1}{\rho_r} \left(\frac{\partial \rho}{\partial T} \right)_{P_w} = \frac{1}{T_r} \quad (2.32)$$

$$\beta_P = - \frac{1}{\rho_r} \left(\frac{\partial \rho}{\partial P_w} \right)_T = \frac{0.375}{P_t - 0.375 P_{w,r}} \quad (2.33)$$

The reference density (ρ_r) is the air density at temperature T_r and pressure P_r . Sometimes it is easier to use the water vapour concentration (c) instead of the pressure:

$$c = \frac{P_w M_w}{R T} \quad (2.34)$$

This gives

$$\rho = \rho_r [1 - \beta(T - T_r) - \beta_c(c - c_r)] \quad (2.35)$$

with

$$\beta_c = - \frac{1}{\rho_r} \left(\frac{\partial \rho}{\partial c} \right)_T = \frac{0.375}{\frac{P M_w}{R T_r} - 0.375 c_r} \quad (2.36)$$

In this section the models of natural convection for different rates of heat generation are restricted to systems without moisture loss and therefore the third term in Eqns 2.31 and 2.35 vanishes. When the reference value of the density is taken at the temperature of the outside air Eqn 2.35 becomes

$$\rho = \rho_0 [1 - \beta(T - T_0)] \quad (2.37)$$

With the assumption that the pressure drop over the bulk is due solely to the weight of the outside air, the combination of Eqns 2.37 and 2.23 yields:

$$\frac{\mu}{\kappa} v_{NC} = \rho_0 g \beta (\bar{T} - T_0) \quad (2.38)$$

In order to calculate the average temperature difference of the bulk with the outside air, the energy balance (2.21) is further simplified by neglecting heat conduction in the z direction relative to the heat convection in that direction. The solution of Eqn 2.21 with the boundary condition:

$$z = 0: \quad T = T_0 \quad (2.39)$$

is now given by

$$T = \frac{Q}{\bar{\rho} c_p v_{NC}} z + T_0 \quad (2.40)$$

Therefore the average bulk temperature is

$$\bar{T} = T_0 + \frac{QL}{2\bar{\rho}c_p v_{NC}} \quad (2.41)$$

Combination of Eqns 2.38 and 2.41 gives

$$v_{NC} = \sqrt{\frac{\kappa \rho_0 g \beta L Q}{2 \bar{\rho} c_p \mu}} \quad (2.42)$$

To make Eqn 2.42 dimensionless both sides are multiplied by $L/a_m = L(\rho c_p)_a / \lambda_0$. This yields

$$\frac{L v_{NC}}{a_m} = \sqrt{\frac{\rho_0 \bar{\rho} c_p g \beta \kappa L^3 Q}{2 \lambda_0^2 \mu}} \quad (2.43)$$

or

$$Pe = \sqrt{\frac{Ra_1}{2}} \quad (2.44)$$

This analysis shows a proportionality of the velocity of natural convection with the square root of the rate of heat generation and the height. The proportionality of v_{NC} with \sqrt{L} can also be derived from the data of Burton (1963) who gave the interchange of air at bulk storage of potatoes with an approximate rate of:

$$\phi = \frac{15}{\sqrt{L}} \text{ m}^3 \text{ air/ton potatoes h} \quad (2.45)$$

which, with a potato bulk density of 700 kg m^{-3} , can be rewritten as

$$v_{NC} = 2.9 \times 10^{-3} \sqrt{L} \text{ m/s} \quad (2.46)$$

It should be noticed that at higher air velocities ($Re > 10$) the permeability (κ) becomes a function of the air velocity as shown in Section 2.5. Eqn 2.42 was checked experimentally as is shown in Chapter 4.

2.4.2 One-dimensional one-phase model with heat transport by convection and conduction

To describe the distribution of steady-state axial temperature in a porous medium with a constant rate of heat generation and heat transfer by convection and conduction in the vertical direction only, the energy balance of the one-phase model, Eqn 2.9, can be simplified to:

$$(\rho c_p)_a v \frac{dT}{dz} = \lambda_0 \frac{d^2 T}{dz^2} + Q \quad (2.47)$$

The boundary condition at the bottom is derived from the assumption that heat transported by conduction through the porous medium to the bottom, is only used to heat the air before it enters the porous medium. Because at the bottom the temperature difference with the surroundings will be small, heat loss by radiation is neglected at the bottom. At the top of the porous medium heat loss by radiation to the colder surroundings and heat loss due to air flow at the top, which is described by an effective heat transfer coefficient (α_L), are assumed. The effective heat transfer coefficient is extensively discussed in Section 4.3.3. Thus the boundary conditions are

$$z = 0: \quad \lambda_0 \frac{dT}{dz} = (\rho c_p)_a v (T_b - T_0) \quad (2.48)$$

$$z = L: \quad -\lambda_0 \frac{dT}{dz} = e \sigma (T_L^4 - T_c^4) + \alpha_L (T_L - T_0) \approx 4e \sigma T_c^3 (T_L - T_c) + \alpha_L (T_L - T_0) \quad (2.49)$$

The different temperatures are defined in Fig. 5. The linearization of the boundary condition at $z = L$ is allowed when the temperature difference $T_L - T_c$ is not too large. A temperature difference of 10 K at room temperature gives an error of 5%. Substitution of the dimensionless parameters: $\theta = (T - T_0)/\Delta T$, where ΔT is an arbitrary temperature difference, and $Z = z/L$ leads to the dimensionless ordinary differential equation:

$$Pe \frac{d\theta}{dZ} = \frac{d^2\theta}{dZ^2} + Po \quad (2.50)$$

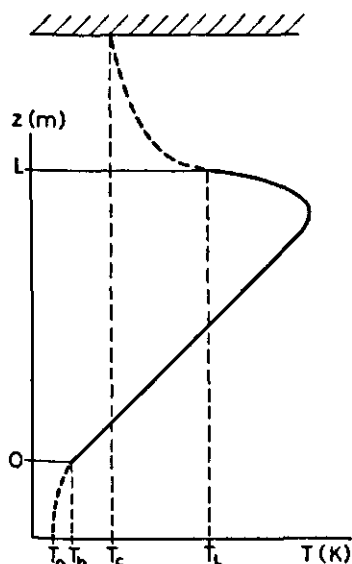


Fig. 5. Definition of the different temperatures used in the one-dimensional one-phase model.

with boundary conditions:

$$Z = 0: \quad \frac{d\theta}{dZ} = Pe \theta_0 \quad (2.51)$$

$$Z = 1: \quad \frac{d\theta}{dZ} = S_c (\theta_c - \theta_L) - Bi_L \theta_L \quad (2.52)$$

The solution of Eqn 2.50 with boundary conditions (2.51) and (2.52) is given by

$$\theta = C_1 e^{Pe(Z-1)} + C_2 (Pe Z + 1) \quad (2.53)$$

$$C_1 = \frac{\theta_c Pe^2 S_c - Po (Pe + (Pe + 1) (S_c + Bi_L))}{Pe^2 (Pe + S_c + Bi_L)} \quad (2.54)$$

$$C_2 = \frac{Po}{Pe^2} \quad (2.55)$$

The average temperature of the porous medium ($\bar{\theta}$) is given by the equation:

$$\bar{\theta} = \frac{C_1}{Pe} (1 - e^{-Pe}) + C_2 \left(1 + \frac{Pe}{2} \right) \quad (2.56)$$

When the temperature is made dimensionless with

$$\theta_Q = \frac{\theta}{Po} = \frac{(T - T_0) \lambda_0}{QL^2} \quad (2.57)$$

Equation 2.53 shows that the temperature profile of θ_Q is identical for different rates of heat generation, when Pe , S_c , Bi_L and θ_c are kept constant.

When typical numerical values, describing the experiments of Chapter 4, are introduced in Eqn 2.53, it turns out that because of the large values of Pe (Pe ranges from 10 to 50), the first term of Eqn 2.53 may be neglected for Z values below 0.8. Therefore the temperature gradient up to $Z = 0.8$ is given by

$$\frac{d\theta}{dZ} = \frac{Po}{Pe} \quad (2.58)$$

or in dimensional form

$$\frac{dT}{dz} = \frac{Q}{(\rho c_p)_a v} \quad (2.59)$$

2.4.3 One-dimensional two-phase model with heat transport by convection and conduction

To describe the distribution of steady-state axial temperature in a packed bed with a constant rate of heat generation and heat transfer by convection and conduction in the vertical direction only, the energy balance equations of the two-phase model (2.10) and (2.11) may be simplified to:

product:

$$0 = \lambda_0 \frac{d^2 T_p}{dz^2} + Q - \alpha(1-\epsilon)A(T_p - T_a) \quad (2.60)$$

air:

$$(\rho c_p)_a v \frac{dT_a}{dz} = \alpha(1-\epsilon)A(T_p - T_a) \quad (2.61)$$

In these equations T_p and T_a are the product and the air temperature, respectively. To describe the boundary conditions at the bottom of the bed, I used the model of Vortmeyer & Schaeffer (1974). They assumed that the heating of the gas from T_0 to $T_{a,b}$ is caused by heat transfer from the bottom, with a relative surface of $1-\epsilon$, to the gas under the packed bed. The heat transfer coefficient at the bottom is the same as that in the packed bed. The heat is transported to the bottom by conduction through the solid phase. On the top the boundary condition of the one-phase model, Eqn 2.49, is applied to the product phase. Therefore the boundary conditions are given by

$$z = 0: (\rho c_p)_a v (T_{a,b} - T_0) = \alpha(1-\epsilon) (T_{p,b} - T_{a,b}) \quad (2.62)$$

$$\lambda_0 \frac{dT_p}{dz} = \alpha(1-\epsilon) (T_{p,b} - T_{a,b}) \quad (2.63)$$

$$z = L: -\lambda_0 \frac{dT_p}{dz} = 4\epsilon\sigma T_c^3 (T_{p,L} - T_c) + \alpha_L (T_{p,L} - T_0) \quad (2.64)$$

The different temperatures used in these equations are defined in Fig. 6. Substitution of the dimensionless parameters: $\theta_p = (T_p - T_0)/\Delta T$, $\theta_a = (T_a - T_0)/\Delta T$ and $Z = z/L$ yields product:

$$0 = \frac{d^2 \theta_p}{dZ^2} + Pe - Bi(\theta_p - \theta_a) \quad (2.65)$$

air:

$$Pe \frac{d\theta_a}{dZ} = Bi(\theta_p - \theta_a) \quad (2.66)$$

with boundary conditions:

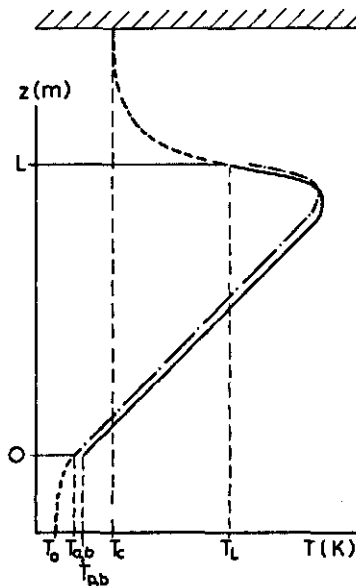


Fig. 6. Definition of the different temperatures used in the one-dimensional two-phase model.

$$Z = 0: \quad Pe \theta_{a,b} = Bi' (\theta_{p,b} - \theta_{a,b}) \quad (2.67)$$

$$\frac{d\theta_p}{dZ} = Bi' (\theta_{p,b} - \theta_{a,b}) \quad (2.68)$$

$$Z = 1: \quad \frac{d\theta_p}{dZ} = S_c (\theta_c - \theta_{p,L}) - Bi_L \theta_{p,L} \quad (2.69)$$

where $Pe = vL/a$, $Bi = \alpha A(1-\epsilon)L^2/\lambda_0$, $Po = QL^2/\lambda_0 \Delta T$, $Bi' = \alpha L(1-\epsilon)/\lambda_0$, $S_c = 4\epsilon\sigma LT_c^3/\lambda_0$ and $Bi_L = \alpha_L L/\lambda_0$.

To reduce the set of ordinary differential equations (2.65) and (2.66) to one ordinary differential equation in θ_p , Eqn 2.65 is differentiated with respect to Z . This yields

$$\frac{d^3\theta_p}{dZ^3} - Bi \left(\frac{d\theta_p}{dZ} - \frac{d\theta_a}{dZ} \right) = 0 \quad (2.70)$$

Substitution of Eqn 2.66 in Eqn 2.70 gives

$$\frac{d^3\theta_p}{dZ^3} - Bi \frac{d\theta_p}{dZ} + \frac{Bi^2}{Pe} (\theta_p - \theta_a) = 0 \quad (2.71)$$

This equation is reduced to an ordinary differential equation in θ_p by combination with Eqn 2.65. This yields finally:

$$\frac{d^3\theta_p}{dZ^3} + \frac{Bi}{Pe} \frac{d^2\theta_p}{dZ^2} - Bi \frac{d\theta_p}{dZ} + \frac{PoBi}{Pe} = 0 \quad (2.72)$$

This equation is solved with boundary conditions (2.67)-(2.69). Hereafter θ_a is calculated with Eqn 2.66. The solution is

$$\theta_p = C_1 e^{\lambda_1 Z} + C_2 e^{\lambda_2 Z} + C_3 + C_4 Z \quad (2.73)$$

$$\theta_a = \theta_p - \frac{C_1 \lambda_1^2 e^{\lambda_1 Z} + C_2 \lambda_2^2 e^{\lambda_2 Z} + Po}{Bi} \quad (2.74)$$

where $\lambda_1, \lambda_2, C_1, C_2, C_3$ and C_4 are defined by

$$\lambda_1 = \frac{-Bi + \sqrt{Bi^2 + 4BiPe}}{2Pe} \quad (2.75)$$

$$\lambda_2 = \frac{-Bi - \sqrt{Bi^2 + 4BiPe}}{2Pe} \quad (2.76)$$

$$C_1 = \frac{(A_1 - \lambda_2^2)(S_c \theta_c - C_3(S_c + Bi_L) - C_4(1 + S_c + Bi_L)) + (\lambda_2 + S_c + Bi_L)(A_1 C_3 - Po)e^{\lambda_2}}{(\lambda_1 + S_c + Bi_L)(A_1 - \lambda_2^2)e^{\lambda_1} + (\lambda_2 + S_c + Bi_L)(\lambda_1^2 - A_1)e^{\lambda_2}} \quad (2.77)$$

$$C_2 = \frac{(\lambda_1^2 - A_1)(S_c \theta_c - C_3(S_c + Bi_L) - C_4(1 + S_c + Bi_L)) - (\lambda_1 + S_c + Bi_L)(A_1 C_3 - Po)e^{\lambda_1}}{(\lambda_1 + S_c + Bi_L)(A_1 - \lambda_2^2)e^{\lambda_1} + (\lambda_2 + S_c + Bi_L)(\lambda_1^2 - A_1)e^{\lambda_2}} \quad (2.78)$$

$$C_3 = \frac{C_4(\lambda_1^2 - A_1) + (A_2 - \lambda_1)Po}{\lambda_1(\lambda_1 A_2 - A_1)} \quad (2.79)$$

$$C_4 = \frac{Po}{Pe} \quad (2.80)$$

$$A_1 = \frac{PeBi}{Pe + Bi'} \quad (2.81)$$

$$A_2 = \frac{PeBi'}{Pe + Bi'} \quad (2.82)$$

The average temperatures of the product and the air phase are given by

$$\bar{\theta}_p = \frac{C_1}{\lambda_1} (e^{\lambda_1} - 1) + \frac{C_2}{\lambda_2} (e^{\lambda_2} - 1) + C_3 + \frac{C_4}{2} \quad (2.83)$$

$$\bar{\theta}_a = \bar{\theta}_p - \frac{C_1 \lambda_1 (e^{\lambda_1} - 1) + C_2 \lambda_2 (e^{\lambda_2} - 1) + Po}{Bi} \quad (2.84)$$

Just as in the one-phase model, it turns out that only the last two terms in this equation are important, when typical numerical values, describing the experiments of Chapter 4, are introduced in Eqn 2.73. Therefore the temperature gradient in most of the system is given by Eqn 2.58 or 2.59.

2.5 Pressure drop for flow through porous media

The pressure drop necessary to obtain a specific superficial velocity in a porous medium may be calculated from Darcy's Law:

$$\frac{\Delta P}{L} = \frac{\mu}{\kappa} v \quad (2.85)$$

where v is the superficial velocity of the fluid. Commonly this equation is used at relatively low fluid velocities ($Re < 10$), because the permeability (κ) is constant in that flow regime. However when a velocity-dependent permeability is introduced, Eqn 2.85 can also be used at higher fluid velocities. The dependence of the permeability on the fluid velocity may be derived from a correlation between the pressure drop and the fluid velocity for flow through porous media.

Dullien (1975) gave a review of different models predicting the pressure drop for flow through porous media. He divided the models in three different groups:

- phenomenological models;
- models based on conduit flow;
- models based on flow around submerged objects.

He discussed each group thoroughly. From a general model (Whitaker, 1969), which averages the complete Navier-Stokes equations over certain representative volumes of the porous medium, Dullien derived that the flow resistance is the sum of a viscous resistance ($\propto v$) and an inertial resistance ($\propto v^2$):

$$\frac{\Delta P}{L} = C_1 v + C_2 v^2 \quad (2.86)$$

The constants C_1 and C_2 are still a function of the bed parameters (e.g. porosity, equivalent particle diameter, surface roughness). The viscous resistance is important at low rates of flow and the inertial resistance at high rates of flow. Both resistances are important at moderate rates of flow.

A well known equation which fulfils Eqn 2.86 is the Ergun equation (Ergun, 1952) which gives the pressure drop in packed beds of spherical particles:

$$\frac{\Delta P}{L} = \frac{1-\epsilon}{d_p \epsilon^3} \left(\frac{150(1-\epsilon)}{Re} + 1.75 \right) \rho v^2 \quad (2.87)$$

where Re is defined as:

$$Re = \frac{\rho v d_p}{\mu} \quad (2.88)$$

Bakker Arkema et al. (1969) and Patterson et al. (1971) showed that the Ergun equation may be modified to calculate the pressure drop in packed beds of granular material, such as cherry pits and grain. They multiplied the right side of the Ergun equation by a correction factor (K), because the particles were nonspherical. K values of 1.22 for cherry pits, 2.0 for navy beans (18% moisture) and 6.5 for corn (19% moisture) were reported.

Matthies (1956) proposed a similar equation to calculate the pressure drop of different agricultural products:

$$\frac{\Delta P}{L} = \frac{K_m \xi_{ks}}{2d_p \epsilon^4} \rho v^2 \quad (2.89)$$

where K_m is a product-dependent correction factor and ξ_{ks} is the air resistance of a packed bed with spheres. Matthies & Petersen (1974) used for ξ_{ks} the relation:

$$\xi_{ks} = \frac{47.92}{Re} + \frac{1.18}{Re^{0.1}} \quad (2.90)$$

This relation is derived from Fischer (1967) who gave the pressure drop in a packed bed of spheres. The equation of Fischer contains the porosity as a variable; for $\epsilon = 0.389$ Eqn 2.90 is obtained. Matthies & Petersen (1974) reported K_m values of many different agricultural products ranging from 1.1 for peas to 7.9 for seed of English rye-grass.

Recently Macdonald et al. (1979) analysed pressure drop data of many different authors. They advised the use of the Ergun equation with somewhat modified constants in engineering practice, to calculate the pressure drop in unconsolidated porous media. They gave

$$\frac{\Delta P}{L} = \frac{1 - \epsilon}{d_p \epsilon^3} \left(\frac{180(1 - \epsilon)}{Re} + C_1 \right) \rho v^2 \quad (2.91)$$

where C_1 is a function of particle surface roughness. The value of C_1 ranged from 1.8 (smooth particles) to 4.0. They stated that experimental values will lie within 50% of the predicted values. The values will be better when different constants are used for different kinds of porous media.

Neale & Messer (1976) measured the pressure drop of air, flowing through beds of potatoes, red beets, onions and carrots. They concluded that the pressure drop may be calculated from

$$\frac{\Delta P}{L} = K_N v^{1.8} \quad (2.92)$$

The constant K_N depends upon the product and is further influenced by the amount of adhering soil, sprouting, loose skins and tops of the different products. The air velocity in their experiments ranged from 0.04 to 0.3 ms^{-1} . It would be interesting to fit their data to the Ergun equation with correction factor. However it is impossible to do this with the data reported in the paper because they did not give an average diameter for the products. An estimated particle diameter of 0.05 m gives values of the Re number in their experi-

ments of 120-1000, which implies influence of both terms in the Ergun equation.

There are many other models of pressure drop in porous media or packed beds (see e.g. Rumpf & Gupte, 1971 and Molerus, 1977). However I have chosen to use the Ergun equation with the correction factor as proposed by Bakker Arkema et al. (1969).

The reasons for this choice are:

1. the good results of this model in the work of Bakker Arkema et al. (1969) and Patterson et al. (1971),
2. the physical base of the dependence of ΔP on v and v^2 as shown by Dullien (1975).

Therefore in my calculations the permeability will be calculated with

$$\kappa = \frac{\epsilon^3 d_p^2}{K(1-\epsilon)(150(1-\epsilon) + 1.75 Re)} \quad (2.93)$$

The correction factor K is not determined from pressure drop experiments but derived from measured temperature profiles, as shown in Section 4.3.5.

3 Modelling of bulk-stored agricultural and horticultural products

Models are made to describe the behaviour of a physical system. Mathematical modelling is merely the formulation of balances for conservation of mass, momentum and energy. This formulation usually leads to rather extensive equations. Therefore these equations are simplified by neglecting those factors that are unimportant in the described physical or chemical processes. Models are used in the following ways.

- To predict the influence of different parameters and the critical conditions of the process (sensitivity analysis).
- To predict the performance of designed facilities (planning).
- To search for optimal process conditions (optimization).

The use of a mathematical model does not imply the end of experimental work. Experiments are always necessary to obtain the different input data of the model calculations and to test the physical or chemical reality of the model by comparing calculated results with experimental data.

The aspects which should be considered for modelling bulk storage and cooling of respiring produce are: convective heat and mass transport (air flow), rate of heat generation (respiration), evaporative cooling, heat conduction and moisture diffusion. These influences will be described by heat and mass balances. Related kinds of balance occur in chemical engineering for the description of the performance of fixed bed catalytic reactors (Ray, 1972; Froment, 1974; Gilles, 1976) and gas adsorption in packed columns (Meijer & Weber, 1967; Ferrel et al., 1976; Brunovska et al. 1978) in food engineering in solid liquid extraction (Spaninks, 1979) and in agricultural engineering for convective grain drying (Bakker Arkema et al., 1977). Lerew (1978) gave an extensive review of different models of bulk-stored agricultural products.

In the next section of this chapter I describe different models which include convective transport, reported in a chemical engineering and agricultural engineering literature. Conductive cooling models will be discussed in Chapter 5.

3.1 Review of literature

3.1.1 Comparison of various models in general

In mathematical models of systems with convective transport, assumptions have to be made on the macro-scale (scale of the total system) and on the micro-scale (scale of the particles in the system). A subdivision is further possible:

- Macro-scale: one-dimensional and two-dimensional models
- Micro-scale: one-phase, two-phase and two-phase with internal gradient models.

One-dimensional models assume temperature and concentration gradients in the direction of the fluid flow only, whereas two-dimensional models assume temperature and

concentration gradients in two directions. The subdivision on micro-scale depends upon assumptions about temperature and concentration differences between gas and solid phase. In a one-phase model these differences are neglected and in a two-phase model not. In the two-phase model with internal gradients, temperature or concentration gradients in the, mostly spherical, solid phase are modelled too.

Two-dimensional models are frequently used to describe the radial temperature profile in cylindrical fixed bed reactors with cooling at the cylinder wall. The use of a two-dimensional model becomes more necessary when the heat transfer to the wall increases. Froment (1974) and Serpemen & Deckwer (1977) showed the difference between a one-dimensional and a two-dimensional model in o-xylol oxidation and ignition in a fixed bed catalytic reactor, respectively.

When the radial temperature profile can be approximated by a parabola a pseudo one-dimensional model can be used (Hlavacek, 1970). In this approach the axial temperature is calculated from the one-dimensional energy balance with radial heat losses described by an overall heat transfer coefficient at the wall. Hofmann (1974) gave criteria for choosing the right model representation.

All models of bulk-stored agricultural produce (Lentz et al., 1971; Rice, 1974; Hunter, 1976; Misener & Shove, 1976a; Baird & Gaffney, 1976; Lerew, 1978) are one-dimensional. Because of the relatively small heat generation and the large dimensions of a storage room, this simplification seems quite reasonable. Problems may arise when heat is lost at a wall which is completely impervious to water vapour. Condensation on a colder wall may occur and this cannot be modelled with a one-dimensional or pseudo one-dimensional model.

The general form of the energy and mass balance is, of course, too complicated to be practicable. Simplifying assumptions must be made to obtain balances which can be solved without insurmountable mathematical problems, but still give a good description of reality. General assumptions in a two-dimensional model are:

- the physical properties are constant;
- the axial velocity is uniform;
- heat is transported by convection and conduction;
- mass is transported by convection and diffusion;
- the radial gas velocity may be neglected.

In a two-dimensional two-phase model with a moving gas phase and a stagnant solid phase (see Fig. 7), these assumptions result in the following energy balance equations:

gas phase:

$$\epsilon(\rho c_p)_a \frac{\partial T_a}{\partial t} + (\rho c_p)_a v \frac{\partial T_a}{\partial z} = \epsilon \lambda_{ax,a} \frac{\partial^2 T_a}{\partial z^2} + \frac{\epsilon \lambda_{rad,a}}{r} \frac{\partial}{\partial r} \left(r \frac{\partial T_a}{\partial r} \right) + \alpha A (1-\epsilon) (T_p - T_a) \quad (3.1)$$

product phase:

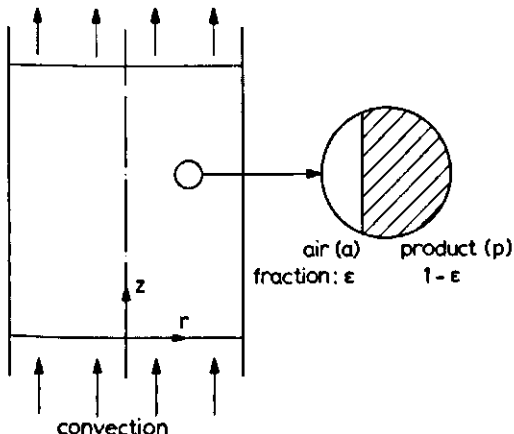


Fig. 7. The system in a two-dimensional two-phase model.

$$(1-\epsilon)(\rho c_p)_p \frac{\partial T_p}{\partial t} = (1-\epsilon)\lambda_{ax,p} \frac{\partial^2 T_p}{\partial z^2} + \frac{(1-\epsilon)\lambda_{rad,p}}{r} \frac{\partial}{\partial r} \left(r \frac{\partial T_p}{\partial r} \right) + Q + \alpha A (1-\epsilon) (T_p - T_a) \quad (3.2)$$

The velocity (v) in Eqn 3.1 is the superficial velocity. The mass balances can be given in a similar way. In fixed bed reactor and adsorption column models the energy and mass balance equations are coupled via Q , which represents the heat of reaction or the heat of sorption. In models of bulk-stored produce the important mass transfer is moisture loss from the products. This causes a negative source term in the energy balance equation because of the resulting heat of vaporization. The respiration of the products is a positive source term.

When a chemical reaction is highly exothermic or the temperature differences between the gas and the solid phase become large, the two-phase model has to be extended to describe internal temperature and concentration gradients in the different particles in the solid phase. When heat transfer from particle to particle is neglected, the energy balance of the product phase changes for spherical particles to:

product phase:

$$(\rho c_p)_p \frac{\partial T_p}{\partial t} = \frac{\lambda_p}{r^2} \frac{\partial}{\partial r} \left(r^2 \frac{\partial T_p}{\partial r} \right) + Q \quad (3.3)$$

with boundary conditions:

$$t = 0, \quad 0 \leq r \leq \frac{d_p}{2} \quad : \quad T_p = T_0 \quad (3.4)$$

$$t > 0, \quad r = 0 \quad : \quad \frac{\partial T_p}{\partial r} = 0 \quad (3.5)$$

$$r = \frac{d_p}{2} \quad : \quad \lambda_p \frac{\partial T_p}{\partial r} = -\alpha(T_{p,R} - T_a) \quad (3.6)$$

$T_{p,R}$ denotes the temperature of the product surface. The boundary condition at $t = 0$ is of course rather arbitrary and difficult to realize for storage of respiring produce. In practice some temperature differences will always occur. The energy balance of the gas phase, Eqn 3.1, also changes because T_p in the last term is replaced by $T_{p,R}$.

Lerew (1978) showed that the use of this two-phase model with internal temperature gradients gives about the same result as the two-phase model in describing the cooling of bulk-stored produce. Baird & Gaffney (1976) showed that the internal temperature gradients can be neglected at an air velocity of 0.13 ms^{-1} for the cooling of oranges ($d_p = 0.07 \text{ m}$) and that the two-phase model with internal temperature gradients should be used at an air velocity of 2.0 ms^{-1} .

The use of internal concentration gradients is not necessary in a model of bulk-stored agricultural produce because of the high moisture content (about 80%) and the rather low moisture loss from these products. Therefore a two-phase model with internal temperature gradients should be used in modelling precooling, but is not necessary to model normal bulk storage.

The two-phase model may be simplified when the temperature and concentration differences between gas and solid phase are rather small. Then the calculations are performed with the same temperature and concentration in the gas and the solid phase: the one-phase model. By adding Eqns 3.1 and 3.2 the resulting one-phase model equation is

$$(\rho c_p)_{\text{eff}} \frac{\partial T}{\partial t} + (\rho c_p)_a v \frac{\partial T}{\partial z} = \lambda_{ax} \frac{\partial^2 T}{\partial z^2} + \frac{\lambda_{rad}}{r} \frac{\partial}{\partial r} \left(r \frac{\partial T}{\partial r} \right) + Q \quad (3.7)$$

Lerew (1978) showed that the use of the one-phase model leads to substantial errors in the transient cooling of bulk-stored agricultural products. Nevertheless the one-phase and two-phase model predict the same steady state. Vortmeyer et al. (1974) and Simon & Vortmeyer (1978) incorporated the influence of the heat transfer coefficient of the two-phase model in the thermal conductivity of the one-phase model with

$$\lambda_{ax} = \lambda_0 + \frac{((\rho c_p)_a v)^2}{\alpha A (1-\epsilon)} \quad (3.8)$$

They reported nearly the same results with the one-phase model as with the two-phase model, when the thermal conductivity defined in Eqn 3.8 is used. The use of this thermal conductivity in the one-phase model will be further discussed in Section 4.3.

A further simplification of the models, mostly applied in one-dimensional models, is neglecting heat transport by conduction and mass transport by diffusion or by dispersion. When heat sources are also neglected, this leads in the two-phase model to the energy balances:

gas phase:

$$(\rho c_p)_a \frac{\partial T_a}{\partial t} + (\rho c_p)_a v \frac{\partial T_p}{\partial z} = \alpha A (1-\epsilon) (T_p - T_a) \quad (3.9)$$

solid phase:

$$(1-\epsilon) (\rho c_p)_p \frac{\partial T_p}{\partial t} = \alpha A (1-\epsilon) (T_a - T_p) \quad (3.10)$$

With the boundary conditions:

$$t = 0, \quad z \geq 0: \quad T_p = T_a = T_s \quad (3.11)$$

$$t > 0, \quad z = 0: \quad T_a = T_0 \quad (3.12)$$

$$z = \infty: \quad T_p = T_s \quad (3.13)$$

These equations were analytically solved by Anzelius (1926) and Schumann (1929). Furnas (1930) tabulated these solutions for a wide range of z and t values.

3.1.2 Models of bulk-stored agricultural produce

Businger (1955) neglected in Eqn 3.9 the accumulation in the gas phase and solved the resulting equations. He used this solution to predict the lower limit of the cooling time of bulk-stored produce. In this model, however, heat generation and moisture loss of the produce are neglected.

The use of the coupled energy and mass balances to describe temperature and moisture distribution in bulk-stored produce was proposed by van Arsdel (1955). He used a one-dimensional two-phase model to describe heat and mass transfer in batch grain drying. The heat and mass balance were coupled by the heat of vaporization. In this model heat generation of the produce was neglected because of the very low rate of heat generation of grain.

In the last decade different models of cooling bulk-stored agricultural produce have been proposed. Most of them have been solved numerically with the aid of a digital computer. Lentz et al. (1971) proposed a model which still is an analytical solution of the differential equations. They described the steady state of a one-dimensional one-phase model. Linear temperature-dependence of the heat generation and evaporative heat losses were incorporated in the model. Heat transport by conduction was neglected. Moisture loss was described by a constant mass transfer coefficient. Lentz et al. showed the influence of different parameters on temperature and moisture loss under conditions for storage of commodities such as carrots, parsnips and celery.

Rice (1974) described the heat and mass transfer with a one-dimensional two-phase model with heat generation and heat losses by evaporation. He did not describe the assumptions made in deriving the model equations. From the model equations it can be

seen that heat transfer by conduction is neglected. To determine moisture losses without employing the mass balance equations he further assumed that, because of moisture loss of the product, the gas phase is everywhere saturated. In spite of the overestimation of moisture losses by this last assumption he said that his calculations agreed reasonably well with physical experiments on potatoes.

The assumption of saturated air was also made by Hylmö et al. (1975a, 1975b). They developed a one-dimensional one-phase model of the cooling of bulk-stored potatoes. The rate of generation was assumed to be independent of temperature. Evaporative heat losses were incorporated. This model predicts a horizontal cooling front, because axial conduction is neglected.

Hunter (1976) described a steady-state one-dimensional two-phase model of bulk-stored potatoes without heat transport by conduction. Moisture losses were modelled with a two-film model, which assumes resistance to moisture loss in the solid and in the gas phase. Measured data were used for the rate of heat generation. Because he considered steady state solutions with continuous air flow only, he made the conclusion that cooling at a low air velocity reduces weight loss. This is not confirmed by other results. (Misener & Macdonald, 1975; Lerew, 1978).

Misener & Shove (1976a) and Misener & Macdonald (1975) presented a one-dimensional two-phase model of cooling bulk-stored potatoes, based upon models of shelled corn drying from Thompson et al. (1968) and Bloome & Shove (1971). They used a rate of heat generation with a linear temperature-dependence. They included the possibility of condensation of water vapour in a film on the product surface. The moisture loss in the beginning of the storage period was calculated from an experimental relation, given by Misener & Shove (1976b):

$$\dot{m} = \frac{C_1 \Delta P^{0.6}}{t^{0.35}} \quad (3.14)$$

The time dependence of the moisture loss is caused by change of the permeability of the skin of the potatoes in the beginning of a storage period. Therefore their results can only be applied to the start of a storage period.

Baird & Gaffney (1976) proposed a one-dimensional two-phase model with internal temperature gradients in the product phase to describe the precooling of bulk-stored produce. The model did not account for moisture loss, heat conduction from particle to particle and heat generation. These influences are modelled by the use of a heat transfer coefficient describing heat transfer product-air, which gives the best fit between experimental and measured cooling curves.

Lerew (1978) presented the most extensive model representation. He compared for a one-dimensional system the one-phase model, the two-phase model, and the two-phase model with internal temperature gradients. A heat generation with linear temperature-dependence and evaporative heat losses were included. The moisture losses were described with a two-film model, which assumes resistance to moisture loss in the product and in the air phase. Condensation on the product was possible. He concluded that the two-phase model was sufficient to describe the bulk storage of agricultural produce and that heat transport by conduction may be neglected.

This review shows that all models of bulk-stored agricultural products are one-dimen-

sional. In every model heat transport by conduction is neglected with respect to heat transport by convection. Heat generation is neglected, assumed to be constant or given by a linear function of temperature. Moisture loss of the products is neglected or given as a function of vapour pressure difference between product and air, of air velocity and, as in the model of Misener & Shove (1976), even of time.

The different models do not incorporate air flow by natural convection, though, especially when forced convection is stopped after cooling the produce, natural convection will certainly influence the temperature and moisture distribution. Therefore I developed a mathematical model of bulk-stored agricultural and horticultural produce, which includes the influence of natural convection: the Storage with Natural Convection or SNC-model. The SNC-model is a two-dimensional model. Thus influence of radial heat and moisture losses can be easily described. It is obvious from the work of Baird & Gaffney (1976) and Lerew (1978) that it is not necessary to model internal temperature gradients in the products. Therefore the equations of a two-phase model will be derived. The model further includes heat transport by conduction, which is necessary to describe radiative losses at the top of the bulk-stored produce.

3.2 Physical properties used in the model equations

Thermal conductivity In using a value of the thermal conductivity, different thermal conductivities should be distinguished:

- λ_p = thermal conductivity of the product.
- λ_0 = thermal conductivity of a packed bed with products and stagnant fluid phase.
- λ_{ax} = thermal conductivity in axial direction of a packed bed with products and a moving fluid phase.
- λ_{rad} = thermal conductivity in radial direction of a packed bed with products and a moving fluid phase.

In calculating λ_0 it is necessary to know the value of λ_p . Different methods of measuring λ_p were summarized by Reidy & Rippen (1971) and Mellor (1979). Because food consists of different components with similar thermal conductivities, λ_p is sometimes calculated by taking the sum of the thermal conductivities of the different components, each multiplied by the relevant volume fraction:

$$\lambda_p = \sum_i \lambda_i X_i \quad (3.15)$$

The preference of volume fractions to mass fractions was proposed by van den Berg & Lentz (1975), because thermal conductivity is defined in terms of length and not in terms of mass.

To calculate the thermal conductivity of materials consisting of small spheres dispersed in another continuous phase, Eucken (1940) used the following equation (derived from Maxwell's theory of electrical conductivity):

$$\lambda_p = \lambda_c \frac{3\lambda_d + 2\epsilon(\lambda_c - \lambda_d)}{\lambda_c - \epsilon(\lambda_c - \lambda_d)} \quad (3.16)$$

ϵ represents the volume fraction of the continuous phase. Eucken stated that this equation may be used up to $\epsilon = 0.5$ without large errors in the value of λ_p . This is, however, questionable, especially when the thermal conductivities of the pure components are quite different.

In the model of bulk-stored produce the thermal conductivity of the air phase is neglected. Therefore the thermal conductivity of the product phase is equal to λ_{ax} . As already stated in Section 3.1:

$$\lambda_{ax} = \lambda_0 \quad (3.17)$$

for a two-phase model.

Different models of calculating λ_0 are reviewed by Zehner & Schlünder (1970) and Kostaropoulos et al. (1975). Bauer & Schlünder (1977) gave an extended model which incorporates the influence of radiation, pressure (Smoluchovski effect), oxidation of the particles, non-uniform particle distribution and particle-to-particle contact area. The Smoluchovski effect may be neglected at atmospheric pressure. With uniform particle diameter, no oxidation of the particle surface and at atmospheric pressure, their equations reduce to:

$$\frac{\lambda_0}{\lambda_a} = \left(1 - \sqrt{1 - \epsilon}\right) \left(1 + \epsilon \frac{\lambda_R}{\lambda_a}\right) + \sqrt{1 - \epsilon} \left(\varphi \frac{\lambda_p}{\lambda_a} + (1 - \varphi) \frac{\lambda_0^*}{\lambda_a}\right) \quad (3.18)$$

$$\frac{\lambda_R}{\lambda_a} = \frac{4\sigma}{\left(\frac{2}{\epsilon} - 1\right)} T^3 d_p \quad (3.19)$$

$$\frac{\lambda_0^*}{\lambda_a} = \frac{2}{N - M} \left(\frac{BN - M}{(N - M)^2} \ln \left(\frac{N}{M} \right) - \frac{B - 1}{N - M} - \frac{B + 1}{2M} (1 - N - M) \right) \quad (3.20)$$

$$N = 1 + \frac{\lambda_R}{\lambda_p} \quad (3.21)$$

$$M = B \frac{\lambda_a}{\lambda_p} \quad (3.22)$$

$$B = C_c \left(\frac{1 - \epsilon}{\epsilon} \right)^{\frac{10}{9}} \quad (3.23)$$

C_c depends on the form of the particles (Zehner & Schlünder, 1970)

spheres	$C_c = 1.25$
cylinders	$C_c = 2.5$
broken particles	$C_c = 1.4$

T is the absolute temperature, φ denotes the contact area between two particles. Wakao & Kato (1969) have shown that the influence of φ may be neglected for rigid spheres, when

$\lambda_p/\lambda_a < 50$. This condition will be met for agricultural products stored in air and therefore $\varphi = 0$ in calculating λ_0 .

Different authors (e.g. Yagi & Kunii, 1957; Zehner & Schlünder; 1973, Bauer & Schlünder, 1977) have shown that the value of λ_{rad} is a function of the velocity of the fluid phase. This is caused by an increase of turbulent mixing with increasing velocity of the fluid phase. The general form of the relation is

$$\lambda_{rad} = \lambda_0 + \frac{Pe}{K_r} \lambda_a \quad (3.24)$$

with $Pe = v d_p (\rho c_p)_a / \lambda_a$. Yagi & Kunii (1957) gave $K_r = 8$, whereas Schlünder (1966) incorporated the influence of a finite diameter of the column by

$$K_r = 8 \left[2 - \left(1 - \frac{d_p}{R_0} \right)^2 \right] \quad (3.25)$$

Bauer & Schlünder (1977) showed that experimental data from different authors fit better with

$$K_r = 7 \left[2 - \left(1 - \frac{d_p}{R_0} \right)^2 \right] \quad (3.26)$$

In the model I used Eqn 3.24 with K_r given by Eqn 3.26 to describe the velocity dependency of λ_{rad} . Data of λ_0 are taken from experimental values. When these are not available the model of Bauer & Schlünder (1977) may be used.

Heat transfer coefficient There are no special correlations to calculate the heat transfer coefficient (α) of bulk-stored produce. Lerew (1978) showed that a large deviation exists between three correlations of α with the air velocity (v) in bulk-stored potatoes. The value of α is sometimes used to incorporate the influence of conduction and moisture loss (Baird & Gaffney, 1976). Such values of α are, of course, limited to that special product and that particular experimental situation.

In chemical engineering literature many data exist on heat transfer in packed beds. Reviews were given by Barker (1965), Balakrishnan & Pei (1979) and Wakao et al. (1979). Generally α is presented in the form of the dimensionless Nu -number which is correlated to Re and Pr . Wakao et al. (1979) gave for spherical particles:

$$Nu = 2 + 1.1 Re^{0.6} Pr^{0.33} \quad (15 < Re < 8500) \quad (3.27)$$

This correlation is obtained by correcting data of different authors for the influence of axial fluid thermal dispersion.

Because the bulk-stored products are assumed to be spherical particles, it is reasonable to use a correlation of packed beds with spherical particles to calculate α . The only difference between agricultural products and the materials used in literature of packed beds is the larger particle diameter of agricultural products. However this should not influence the kind of correlation. I have used the correlations of Bird et al. (1960):

$$Nu = 2.27 (1-\epsilon)^{0.51} Re^{0.49} Pr^{0.33} \quad (Re < 180) \quad (3.28)$$

$$Nu = 1.27 (1-\epsilon)^{0.41} Re^{0.59} Pr^{0.33} \quad (Re > 180) \quad (3.29)$$

Equation 3.28 was given for $Re > 13$ but I have extrapolated this relation to lower values. This relation predicts a 10% lower value of α than the correlation (3.27) of Wakao et al. (1979). However the values are still within the limits of the experimental data of different authors summarized by Wakao et al. (see Fig. 8).

Mass transfer coefficient The mass transfer from the product to the air is described with the two-film model (see Fig. 9), with resistance to mass transfer in both the product and the air phase. This results in an internal mass transfer coefficient (k_{int}) and an external mass transfer coefficient (k_{ext}). The overall mass transfer coefficient can be calculated with

$$\frac{1}{k} = \frac{1}{k_{int}} + \frac{1}{k_{ext}} \quad (3.30)$$

The value of k_{int} can be derived from data of moisture loss of a product.

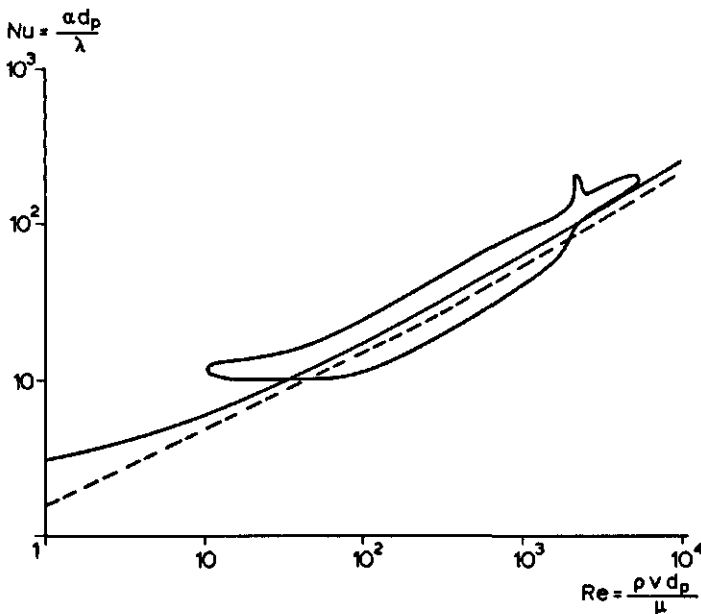


Fig. 8. Comparison of Eqn 3.27 and Eqn 3.28 and 3.29 with experimental data given by Wakao et al. (1979).

$\text{— } Nu = 2 + 1.1 Re^{0.6} Pr^{1/3}$
 $\text{--- } \{ \begin{array}{ll} Nu = 2.27 (1-\epsilon)^{0.51} Re^{0.49} Pr^{1/3} & (Re < 180) \\ Nu = 1.27 (1-\epsilon)^{0.41} Re^{0.59} Pr^{1/3} & (Re > 180) \end{array}$
 $\epsilon = 0.4$
 $Pr = 0.72$

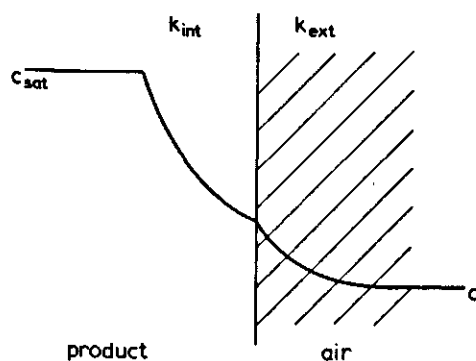


Fig. 9. Distribution of concentration in the two-film model.

Data on the moisture loss of many different products, showing a large scatter in the data were reported by Sastry et al. (1978) and van Beek & Ficek (1979). The data are presented by a transpiration coefficient. This is the quantity of mass or moisture transpired per unit mass of product per unit vapour pressure difference between product and surrounding air per unit time. The rate of moisture loss is the transpiration coefficient times the vapour pressure difference between product and air (ΔP). The transpiration coefficient is reported to be constant, or to increase with decreasing water vapour difference between product and air. The data of Misener & Shove (1976b) even showed a time dependence of the transpiration coefficient at the start of the storage period of potatoes. This is caused by the change in skin permeability of potatoes shortly after harvest.

Notwithstanding these data of moisture loss there exists in the current literature only one model of moisture loss from agricultural or horticultural produce (Fockens, 1967; Fockens & Meffert, 1972). This model was extended by Villa (1973) to describe moisture loss from potatoes, apples and sugar beets. Fockens divided the skin of the product into three parts: free water (fraction γ_1), permeable to water vapour (fraction γ) and impermeable to water vapour. The moisture transport is described with an internal and an external mass transfer coefficient (see Fig. 10). Moisture transport from the free water part is only restricted by the external mass transfer coefficient and is given by

$$\phi_{m,1} = k_{ext} \gamma_1 A (c_{sat} - c) \quad (3.31)$$

Moisture transport through the permeable part is determined by both the internal and the external mass transfer coefficient and is given by

$$\phi_{m,2} = \frac{\gamma A}{\frac{1}{k_{ext}} + \frac{1}{k_{int}}} (c_{sat} - c) \quad (3.32)$$

Total moisture loss follows from

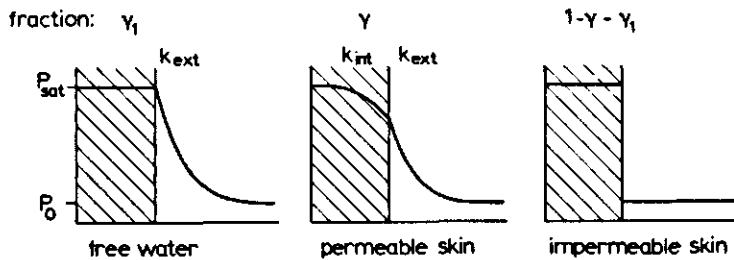


Fig. 10. Distribution of water vapour in the product and the air for three surface fractions of Fockens model.

$$\phi_m = \phi_{m,1} + \phi_{m,2} \quad (3.33)$$

Villa (1973) derived an experimental relation between the air velocity and k_{ext} from the measured weight loss of a peeled product during one hour. Because of the rather high air velocities during his experiments ($0.5\text{-}2 \text{ ms}^{-1}$) it is reasonable that internal moisture gradients in the product occur, which lowers the moisture loss. Thus it is possible that Villa underestimated the external mass transfer coefficient.

The experimental data of Fockens on apples and of Villa on apples and potatoes showed that the free water fraction of this products was negligible ($y_1 = 0$). They also found both that k_{int} is a function of the difference in water vapour pressure inside and outside the product. Villa described this concentration dependence with

$$k_{int} = \frac{ID}{a_1 + a_2(P_{sat} - P)} = \frac{ID}{r\delta} \quad (3.34)$$

Table 3 gives the value of γ , a_1 and a_2 from Villa and Fockens. The values given by Fockens are recalculated from his data. The value of γ deviates from the value he presented ($\gamma = 0.01$). The data in Table 3 show that k_{int} decreases with increasing water vapour difference. Respiring products have an internal protection against too large moisture losses.

Cannon et al. (1979) developed a rather similar model to describe the evaporation through the stomata of flat plant leaves. They incorporated the influence of evaporation of one stoma on the evaporation from other stomata, located downstream.

Table 3. Values of γ , a_1 and a_2 from Villa (1973) and Fockens (1976).

	$\gamma(-)$	$a_1(\text{m})$	$a_2(\text{m/Pa})$
<i>Villa</i>			
Manona potatoes	0.013	4.90×10^{-4}	3.31×10^{-6}
Jonathan apples	0.009	2.35×10^{-3}	4.07×10^{-6}
<i>Fockens</i>			
Laxton Superb apples	0.044	5.30×10^{-3}	1.6×10^{-5}

Because with the model of Fockens and Villa the influence of the vapour pressure difference between product and air can be included, I used their model representation to describe the moisture loss from the products.

There are no general correlations to derive the external mass transfer coefficient of bulk stored produce used in the model of moisture loss. Therefore I used a correlation derived for mass transfer in packed beds with spheres. Different correlations are proposed in literature as reviewed by e.g. Colquhoun-Lee & Stepanek (1974), Dwivedhy & Upadhyaya (1977) and Wakao & Funazkri (1978). I have used the relation of Bird et al. (1960), which, because of the well-known analogy between heat and mass transfer, has the same form as the relation of the heat transfer coefficient:

$$Sh = 2.27 (1-\epsilon)^{0.51} Re^{0.49} Pr^{0.33} \quad (Re < 180) \quad (3.35)$$

$$Sh = 1.27 (1-\epsilon)^{0.41} Re^{0.59} Pr^{0.33} \quad (Re > 180) \quad (3.36)$$

Heat transfer coefficient at the wall The radial temperature profile in a cylindrical packed bed may be presented as given in Fig. 11. The temperature in the cylinder decreases gradually towards the wall. The decrease becomes steeper near the wall. Fig. 11 shows further the temperature in the wall and in the ambient air. This part of the profile is influenced by the thermal conductivity and thickness of the wall and by the heat transfer coefficient on the outside of the cylinder (α_{ext}).

It is well known that temperature profiles in packed beds show a 'hump' near the wall (e.g. Lerou & Fromant, 1977; Dixon et al., 1978). This 'hump' may be caused by a higher air velocity near the wall, a lower thermal conductivity of the packed bed at the wall, or both. This steeper temperature decrease is normally modelled with a wall heat transfer coefficient (α_w). The dependence of α_w on the Re number is presented in different ways. Yagi & Kunii (1960) gave:

$$\frac{\alpha_w d_p}{\lambda_0} = \frac{\alpha_{w,0} d_p}{\lambda_0} + 0.054 Re Pr \quad (Re < 2000) \quad (3.37)$$

where $\alpha_{w,0}$ depends on the packing. Larger particle diameters gave a larger value of $\alpha_{w,0}$.

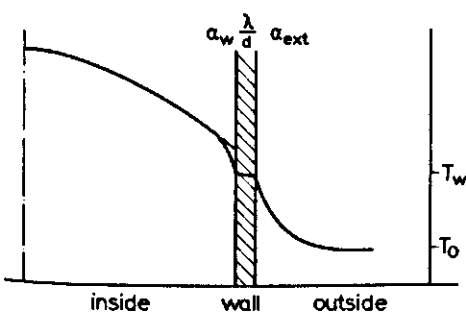


Fig. 11. Radial profile of temperature.

From those data that showed no effect of the length of the packed bed, Li & Finlayson (1977) derived the correlation:

$$\frac{\alpha_w d_p}{\lambda_0} = 0.17 Re^{0.79} \quad (20 < Re < 7000) \quad (3.38)$$

It may be expected that this relation cannot be extended to lower Re -values, because also in a packed bed with a stagnant fluid phase, resistance to heat transfer will be higher at the wall. This leads to a value of α_w greater than zero at $Re = 0$.

In fixed bed catalytic reactors, thin cylinder walls and high values of α_{ext} are usual. Therefore the heat flow through the wall, at a given value of T_0 , is determined by α_w . In modelling bulk-stored produce α_{ext} will mostly be rather low. Also the resistance to heat transfer in the wall can in general not be neglected. In order to simplify the model representation, I incorporated the influence of heat conduction through the wall, internal and external heat transfer coefficient in an overall heat transfer coefficient (α_{ov}) at the inner wall of the cylinder.

The mass transfer through the walls is modelled in the same way by an overall mass transfer coefficient (k_{ov}). However a value of $k_{ov} = 0$ will be rather common, because most walls are impermeable to water vapour.

3.3 Derivation of the model equations for the SNC-model

As already stated in the preceding section realistic simplifying assumptions are necessary to model complex physical reality: a system with internal heat generation, evaporation, condensation, convective transport, heat conduction, moisture diffusion and radiation. The following assumptions are made.

1. The system consists of two quasi-continuous phases: product and air.
2. The product and the air-phase are uniformly distributed in the system.
3. The system shows radial symmetry.
4. Thermal conductivity, heat capacity, diffusion coefficient and density are not dependent on temperature or moisture, except the density of the air when it causes buoyant forces.
5. The radial air velocity may be neglected.
6. The air flows in the axial direction in plug flow.
7. The air velocity is the sum of the natural and the forced convection velocity.
8. Heat generation is located in the product phase.
9. Heat generation and heat of vaporization have an exponential and a linear temperature-dependence, respectively.
10. The product phase conducts heat in both axial and radial direction.
11. Axial and radial heat conduction through the air-phase can be neglected.
12. Heat transfer from product to air may be described with a velocity-dependent heat transfer coefficient.
13. Accumulation of energy in the air-phase may be neglected towards the convective heat transport in that phase.
14. The only weight loss of the products results from water vapour transfer to the air.
15. The water vapour pressure in the product is the saturation pressure.

16. The moisture loss is restricted by an internal and an external resistance to moisture transfer (two-film theory).
17. The external resistance to moisture transfer can be described by a velocity-dependent mass transfer coefficient.
18. The radial dispersion coefficient depends on the air velocity.
19. Condensation on the product occurs when the calculated water vapour concentration in the air is higher than the saturated water vapour concentration in the product phase.
20. Condensation occurs in a thin water film on the product surface.
21. The product absorbs no water from the water film.
22. When the moisture content of the air reduces, the water film on the surface evaporates first, before further moisture loss from the product phase.
23. The initial local air and product temperatures are equal.
24. The initial water vapour concentration of the air is the saturated water vapour concentration at the initial temperature.
25. On the top of the bulk heat is lost or gained by radiation to or from the surroundings.
26. The heat and mass transfer from the radial boundaries to the surroundings can be described by an overall heat and mass transfer coefficient.
27. The heat transfer coefficient at the bottom of the bulk is equal to the heat transfer coefficient inside the bulk.
28. The water vapour concentration at the bottom is equal to the water vapour concentration of the outside air.

Some of these assumptions will now be explained further:

Assumption 7: The natural convection velocity (v_{NC}) is calculated with the relation derived in Chapter 2:

$$v_{NC} = \frac{\kappa}{\mu} \rho_1 g [\beta(\bar{T} - T_0) + \beta_c(\bar{c} - c_0)] \quad (3.39)$$

As given in Section 2.5 the permeability (κ) is calculated with the corrected Ergun-equation for particles of non-uniform shape:

$$\kappa = \frac{\epsilon^3 d_p^2}{K(1-\epsilon)} \frac{1}{[150(1-\epsilon) + 1.75 Re]} \quad (3.40)$$

Because the Re number is a function of the air velocity ($Re = \bar{\rho} v d_p / \mu$), combination of Eqn 3.39 and Eqn 3.40 gives:

$$C_1 v_{NC}^2 + C_2 v_{NC} + C_3 = 0 \quad (3.41)$$

where:

$$C_1 = \frac{1.75 K(1-\epsilon) d_p \bar{\rho}}{\mu} \quad (3.42)$$

$$C_2 = 150 K (1-\epsilon)^2 + \frac{1.75 K (1-\epsilon) \bar{\rho} d_p v_{FC}}{\mu} \quad (3.43)$$

$$C_3 = -\epsilon^3 d_p^2 \rho_1 g [\beta(\bar{T} - T_0) + \beta_c(\bar{c} - c_0)] \quad (3.44)$$

The average temperature and concentration in Eqn 3.44 are calculated from the temperature and concentration distribution in the system at the same moment. This calculated velocity of natural convection is used in the next time step to calculate the new temperature and concentration distribution.

Assumption 9: The temperature dependency of the rate of heat generation can be given in different forms. In most of the calculations I have used an Arrhenius-type equation, well known from the temperature dependence of a chemical reaction:

$$Q = Q_0 e^{-\frac{Q_1}{T}} \quad (3.45)$$

where T is the absolute temperature. Variables Q_0 and Q_1 are product dependent. Q_1 may be considered as the quotient of the activation energy of the heat generation reaction and the gas constant. Other types of temperature dependence or a constant rate of heat generation ($Q_1 = 0$) can be incorporated very easily in the model equations.

The heat of vaporization is calculated with

$$\Delta H_v = 3.154 \times 10^6 - 2.386 \times 10^3 T \quad (273 < T < 323) \quad (3.46)$$

where T is the absolute temperature. This relation yields ΔH_v in J/kg. The relation is used by Brooker (1967) in his mathematical model of the psychrometric chart.

Assumption 14: This assumption implies that mass losses by respiration, due to conversion of carbohydrates to carbon dioxide and water, are neglected. Carbon dioxide is lost by the product.

Assumption 15: The saturated water vapour concentration is calculated with the equation used by Brooker (1967):

$$c_{sat} = \frac{2.1669}{T} \exp \left(-\frac{6834.3}{T} + 53.525 - 5.1692 \ln T \right) \quad (3.47)$$

where T is the absolute temperature. c_{sat} is calculated in kg/m³. This equation is obtained by integrating the Clausius-Clapeyron equation, giving the temperature dependence of c_{sat} .

Assumption 18: The velocity dependence of the radial dispersion coefficient was given by de Ligny (1970):

$$ID_r = 0.67 ID + \frac{0.12 (v d_p)^2}{\epsilon v d_p + 78 \epsilon ID} \quad (3.48)$$

where ID represents the molar diffusion coefficient of water in air.

Assumption 27: Wicke (1975) discussed the boundary conditions of packed bed reactors. He concluded that the temperature at $z = 0$ will be above the temperature of the ambient air, whereas the concentration at $z = 0$ will be equal to the concentration in the ambient air, even when axial dispersion in the reactor is important. In order to derive a boundary condition at the bottom of the bulk, I assumed that at the bottom heat is transferred from the product to the air via the area $(1-\epsilon)\pi R_0^2$ (Vortmeyer & Schaeffer, 1974). This assumption results at $z = 0$ in an air temperature above the temperature of the ambient air. Because heat conduction in the air phase is neglected, this causes a discontinuity in the air temperature profile.

Because the air is heated before it enters the bed the unrealistic situation that heat is transported to the bottom (because the temperature gradient in the product phase is positive) whereas the air temperature does not rise, is avoided. Another way of solving this problem is to assume that there is no temperature gradient in the product phase at $z = 0$.

The use of the above-mentioned assumptions yields the following equations and boundary conditions:

Mass balance:

* air:

$$\epsilon \frac{\partial c}{\partial t} + v \frac{\partial c}{\partial z} = \epsilon ID_r \left[\frac{1}{r} \frac{\partial}{\partial r} \left(r \frac{\partial c}{\partial r} \right) \right] + kA(1-\epsilon)(c_{sat} - c) \quad (3.49)$$

Energy balances:

* product:

$$(1-\epsilon)(\rho c_p)_p \frac{\partial T_p}{\partial t} = \lambda_{ax} \frac{\partial^2 T_p}{\partial z^2} + \lambda_{rad} \left[\frac{1}{r} \frac{\partial}{\partial r} \left(r \frac{\partial T_p}{\partial r} \right) \right] - \alpha A(1-\epsilon)(T_p - T_a) - \Delta H_v k(1-\epsilon)(c_{sat} - c) + Q \quad (3.50)$$

* air:

$$(\rho c_p)_a v \frac{\partial T_a}{\partial z} = \alpha A(1-\epsilon)(T_p - T_a) \quad (3.51)$$

Boundary conditions:

$$t = 0, \forall r, z \quad : \quad c = c_{sat} \quad (3.52)$$

$$T_a = T_p = T_s \quad (3.53)$$

$$t > 0, \forall r, z = 0 \quad : \quad c = c_0 \quad (3.54)$$

$$\lambda_{ax} \frac{\partial T_p}{\partial z} = \alpha(1-\epsilon)(T_p - T_a) \quad (3.55)$$

$$(\rho c_p)_a v (T_a - T_0) = \alpha (1 - \epsilon) (T_p - T_a) \quad (3.56)$$

$$\forall r, z = L : \lambda_{ax} \frac{\partial T_p}{\partial z} = -e \sigma (T_p^4 - T_c^4) \quad (3.57)$$

$$\forall z, r = 0 : \frac{\partial c}{\partial r} = 0 \quad (3.58)$$

$$\frac{\partial T_p}{\partial r} = 0 \quad (3.59)$$

$$\forall z, r = R_0 : ID_r \frac{\partial c}{\partial r} = -k_{ov} (c - c_0) \quad (3.60)$$

$$\lambda_{rad} \frac{\partial T_p}{\partial r} = -\alpha_{ov} (T_p - T_0) \quad (3.61)$$

The different temperatures are already defined in Fig. 6. These equations are made dimensionless with the aid of the following dimensionless variables:

$$\theta = (T - T_0) / \Delta T, C = c / c_{sat,0}, \tau = \lambda_{ax} t / (\rho c_p)_p L^2, Z = z / L, R = r / L$$

and the numbers:

$$Pe = (\rho c_p)_p v L / \lambda_{ax}, Le = \lambda_{ax} / (\rho c_p)_p ID_r, Sh = k L / ID_r, Bi = \alpha L / \lambda_{ax}, \eta = \lambda_{rad} / \lambda_{ax},$$

$$G = \Delta H_v L^2 A (1 - \epsilon) c_{sat,0} / \lambda_{ax} \Delta T, Po = Q L^2 / \lambda_{ax} \Delta T, S = e \sigma L / \lambda_{ax} \Delta T$$

$$\text{and } Bi_{ov} = \alpha_{ov} L / \lambda_{ax}.$$

This yields:

Mass balance:

* air:

$$\epsilon \frac{\partial C}{\partial \tau} + Pe \frac{\partial C}{\partial Z} = \frac{\epsilon}{Le} \left[\frac{1}{R} \frac{\partial}{\partial R} \left(R \frac{\partial C}{\partial R} \right) + \frac{Sh L A (1 - \epsilon)}{\epsilon} (c_{sat} - c) \right] \quad (3.62)$$

Energy balances:

* product:

$$(1 - \epsilon) \frac{\partial \theta_p}{\partial \tau} = \frac{\partial^2 \theta_p}{\partial Z^2} + \frac{\eta}{R} \frac{\partial}{\partial R} \left(R \frac{\partial \theta_p}{\partial R} \right) - Bi L A (1 - \epsilon) (\theta_p - \theta_a) - G (c_{sat} - c) + Po \quad (3.63)$$

* air:

$$Pe \frac{\partial \theta_a}{\partial Z} = \frac{(\rho c_p)_p}{(\rho c_p)_a} (\theta_p - \theta_a) \quad (3.64)$$

Boundary conditions:

$$\tau = 0, \forall R, Z \quad : \quad C = C_{\text{sat}} \quad (3.65)$$

$$\theta_a = \theta_p = \theta_s \quad (3.66)$$

$$\tau > 0, \forall R, Z = 0 \quad : \quad C = C_0 \quad (3.67)$$

$$\frac{\partial \theta_p}{\partial Z} = Bi(1-\epsilon)(\theta_p - \theta_a) \quad (3.68)$$

$$\theta_a = \frac{\theta_p}{1 + \frac{(\rho c_p)_a v}{\alpha(1-\epsilon)}} \quad (3.69)$$

$$\forall R, Z = 1 \quad : \quad \frac{\partial \theta_p}{\partial Z} = -S(T_p^4 - T_c^4) \quad (3.70)$$

$$\forall Z, R = 0 \quad : \quad \frac{\partial C}{\partial R} = 0 \quad (3.71)$$

$$\frac{\partial \theta_p}{\partial R} = 0 \quad (3.72)$$

$$\forall Z, R = \frac{R_0}{L} \quad : \quad \frac{\partial C}{\partial R} = -Sh_{ov}(C - C_0) \quad (3.73)$$

$$\frac{\partial \theta_p}{\partial R} = -Bi_{ov} \theta_p \quad (3.74)$$

To simulate the cooling or heating of bulk-stored products the coupled differential equations (3.62) to (3.64) are solved with finite difference techniques. Because of the rather steep temperature gradients at the top of the bulk, I used a non-equidistant grid-point distribution in the axial direction. There are more grid-points in the upper part of the system. In writing the difference equations the first derivative in the R direction is written as a central difference and the first derivative in the Z direction as a backward difference. In the centre of the cylinder the following limit holds:

$$\lim_{R \rightarrow 0} \frac{1}{R} \frac{\partial}{\partial R} = \frac{\partial^2}{\partial R^2} \quad (3.75)$$

The solution of the equations is further given in Appendix A.

It is difficult to prove stability and convergence to the unique solution of the solution of the coupled differential equations (3.62) to (3.64). Therefore stability is tested by using different values of the time step. As stated in Appendix A both the small and the

large time-step have a limiting value above which the system becomes unstable.

The convergence to the unique solution may be proven by comparing the numerical solution with the analytical solution of the problem. However I have not succeeded in finding the analytical solution of Eqns 3.62-3.64. By neglecting some terms in the model equations, a set of equations may be obtained which can be solved analytically. This solution may be compared with the numerical solution. The convergence is also proven by comparing measured and calculated data. Both ways are discussed in Chapter 4 and show convergence to the unique solution within the experimental error. These results show that it may be assumed that the numerical solution of Eqns 3.62-3.64 describes the temperature and moisture distribution at cooling or heating of bulk-stored agricultural or horticultural products.

3.4 Sensitivity analysis with the SNC-model

3.4.1 *The base-case*

The SNC-model is used to calculate the influence of different parameters on temperature, water vapour concentration, moisture loss and natural convection velocity. The values of the different model parameters are chosen to describe the behaviour of apples. I choose apples because apples are normally stored in containers. With a two-dimensional model temperature and concentration differences in horizontal direction can be described too. The physical properties of the product are the average values given by the Sprenger Institute (1972). The value of Q_0 and Q_1 is calculated from their data on heat generation at different temperatures. Table 4 summarizes the base-case values. The results of the calculations with these standard values are summarized in Figs 12 to 18.

Fig. 12 shows the cooling of the product at different distances along the central axis of the cylinder and the transient behaviour of the average temperature. This figure shows a fast temperature drop at the top ($z = 1$ m) at the beginning of cooling, because the temperature at the top is influenced by radiation losses. The radiation losses are large at the beginning of cooling because of the large temperature difference between the top and the surroundings. As cooling proceeds the temperature at the top decreases and radiation losses become smaller. Consequently also the cooling rate of the top decreases. Fig. 12 further shows that under base-case conditions it takes about 120 h before the steady state is attained for cooling by natural convection only.

Fig. 13 gives the course of the dimensionless concentration at different distances. The change in concentration from the initial (saturated) value to the lower pseudo steady-state value (see Appendix A) is completed in 0.01 h. This is about the same time as the residence time of the air in the cylinder at the start of the cooling. Therefore the saturated air is at the start of the cooling process transported out of the cylinder by the air flow. The air remains unsaturated because the moisture loss of the products is too small. The change in concentration from the initial (saturated) value to the pseudo steady-state value is not shown in Fig. 13 because of the time-scale of this figure.

Fig. 14 shows the course of the velocity of natural convection. The velocity of natural convection decreases with time because of the decreasing average temperature in the cylinder.

The rate of total moisture loss (\dot{m}) is shown in Fig. 15. In the beginning the water

Table 4. Base-case values for the model calculations.

Cylinder height (L)	1.00 m
Cylinder radius (R_0)	0.50 m
Velocity of forced convection (v_{FC})	0 m/s
Overall heat transfer coefficient at the wall (α_{ov})	3 W/m ² K
Overall mass transfer coefficient at the wall (k_{ov})	7.5 x 10 ⁻⁴ m/s
Temperature of the ceiling (T_c)	10 °C
Initial temperature (T_s)	20 °C
Temperature of cooling air (T_o)	10 °C
Relative humidity of cooling air (RH_o)	90%
Density of air (ρ_a)	1.25 kg/m ³
Specific heat of air ($c_{p,a}$)	1020 J/kgK
Viscosity of air (μ)	1.77 x 10 ⁻⁵ kg/ms
Diffusion coefficient of water in air (D)	2.51 x 10 ⁻⁵ m ² /s
Bulk density (ρ_b)	475 kg/m ³
Density of product (ρ_p)	800 kg/m ³
Specific heat of product ($c_{p,p}$)	3640 J/kgK
Bulk thermal conductivity (λ_o)	0.30 W/mK
Specific surface area (A)	85.7 m ² /m ³ product
Radiative emissivity of product surface (ϵ)	1
Apple diameter (d_p)	0.07 m
Bulk porosity (ϵ)	0.406
Constant in heat generation equation (Q_0)	1.46 x 10 ¹² W/m ³ product
Constant in heat generation equation (Q_1)	7070 K
Correction factor in Ergun equation (K)	1.5
Permeable fraction of the surface (γ)	0.01
a_1 in Eqn 3.78	0.00235 m
a_2 in Eqn 3.78	0 m/Pa

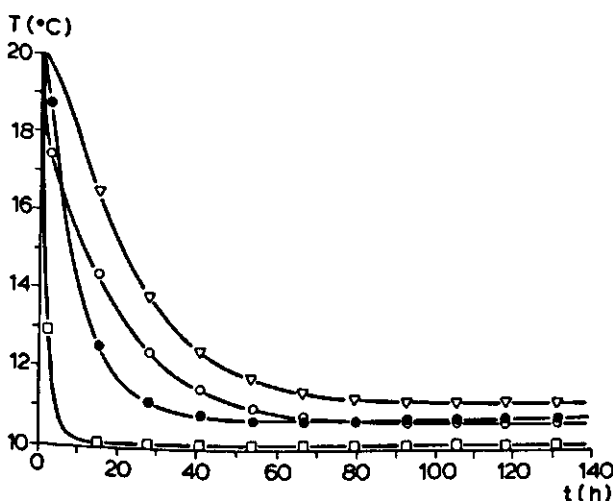


Fig. 12. Cooling by natural convection only. Changes in temperature with time at different distances along the central axis.

- $z = 0.00$ m
- $z = 0.40$ m
- ▽ $z = 0.88$ m
- $z = 1.00$ m

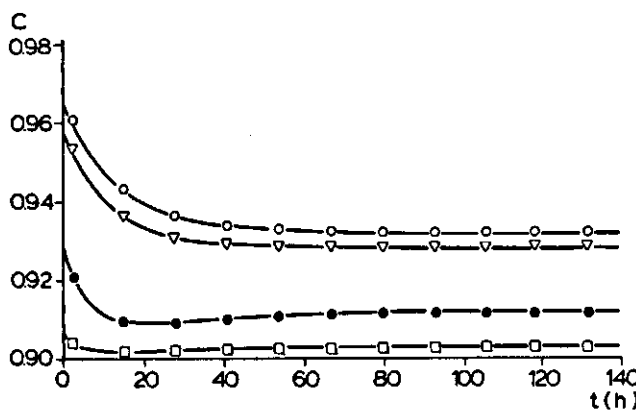


Fig. 13. Changes in dimensionless concentration with time at different distances along the central axis of the cylinder. Legend see Fig. 12.

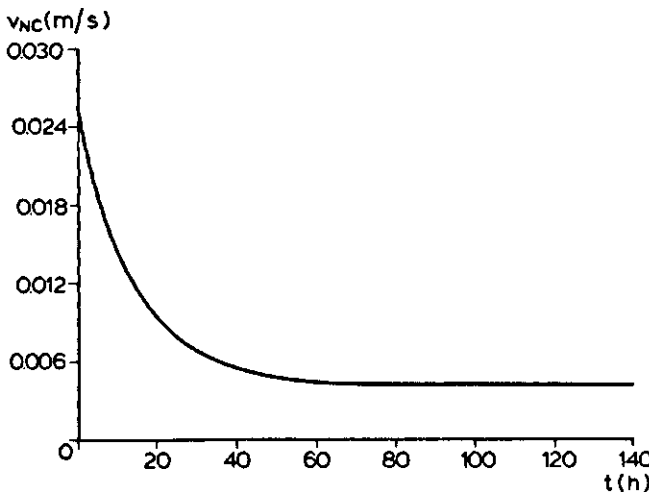


Fig. 14. Velocity of natural convection at different times.

vapour pressure difference between the product and the air is large so that moisture loss is high. During cooling the vapour pressure difference becomes less and the rate of moisture loss decreases too. A constant rate of total moisture loss is found in the steady state.

Fig. 16 shows the temperature profile along the central axis of the cylinder at different times. Obviously there is no sharp cooling front in the cylinder. This figure further shows that the lower part of the cylinder meets the steady state faster than the upper part.

Figs 17 and 18 give a survey of axial and radial temperature distribution for the steady state. The maximum temperature is located at $z = 0.82$ m and $r = 0.00$ m. Above this point radiation losses at the top cause cooling. As a result the radial temperature profile

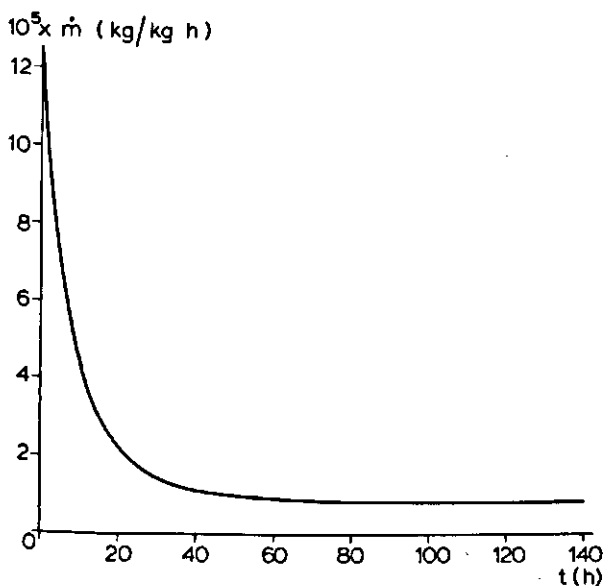


Fig. 15. Change in rate of total moisture loss with time.

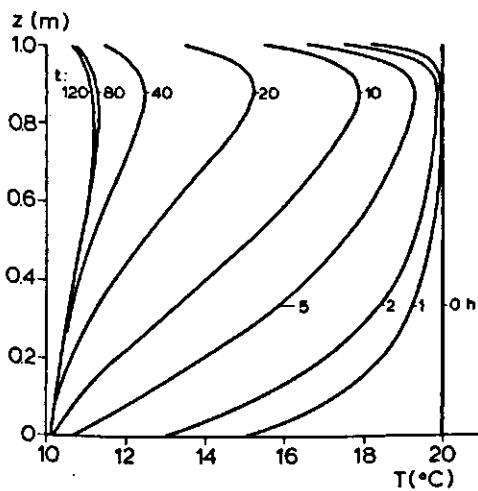


Fig. 16. Profile of temperature along the central axis of the cylinder at different times.

at $z = 1.00$ m is located between the profiles at $z = 0.20$ and 0.40 m. In a radial direction the temperature towards the wall decreases because of radial heat losses.

In the next part of this chapter I will discuss the influence on temperature, concentration, moisture loss and velocity of natural convection, of the model parameters:

- velocity of forced convection;
- mass transfer coefficient product to air;

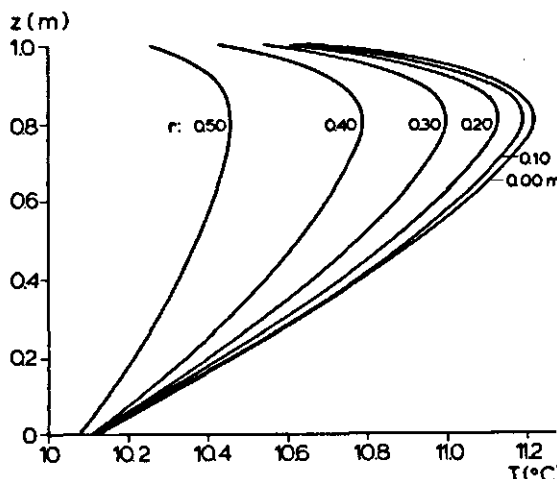


Fig. 17. Longitudinal steady-state profiles of temperature at different radii (r) from the axis.

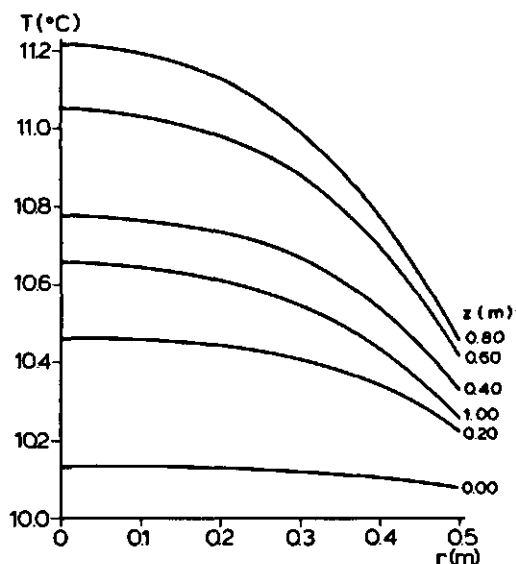


Fig. 18. Steady-state radial profile of temperature at different distances (z) along the cylinder.

- moisture content of the cooling air;
- porosity;
- heat and mass transfer at the wall;
- heat generation;
- bed height.

3.4.2 Influence of different parameters

Velocity of forced convection Fig. 19 gives the temperature course at $z = 0.88$ m and $r = 0.00$ m during pure natural convection and during cooling by both natural and forced convection with $v_{FC} = 0.01$ and 0.1 ms $^{-1}$. Evidently cooling by forced convection is much faster than cooling by natural convection only. This is also obvious from the 90% cooling time, defined as the time necessary to reduce the value of the average product temperature to 10% of its initial value, given in Table 5. This table further gives the steady-state values of maximum temperature, velocity of natural convection and moisture loss. A higher velocity of forced convection gives a lower maximum temperature. The average temperature in the cylinder will be lower too and as a result the velocity of natural convection is lower.

A higher velocity of forced convection gives more steady-state moisture loss, because the external mass transfer coefficient increases with increasing air velocity. This increase of the moisture loss will not continue at higher air velocities, for the moisture loss is limited by the internal mass transfer coefficient. Equation (3.30) shows that when k_{ext} becomes large the overall mass transfer coefficient (k) is determined by the value of k_{int} . When k_{int} is smaller than the value used in the actual calculations, this influence is more pronounced.

In spite of the higher rate of total moisture loss in the steady state with a higher velocity of forced convection, the integrated total moisture loss (Δm) at the moment the steady state is attained, is lower for a higher value of v_{FC} . This is shown in Fig. 20 which gives the integrated total moisture loss at different times during pure natural convection and during combined natural and forced convection ($v_{FC} = 0.1$ ms $^{-1}$). The steady state is attained after 120 and 15 h, respectively. Fig. 20 also shows that from 5 to 47 h the

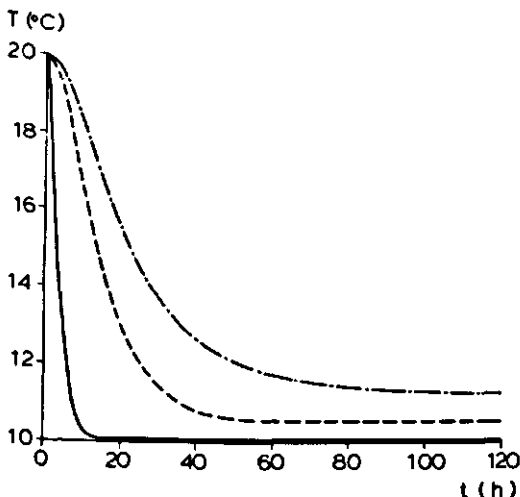


Fig. 19. Changes in temperature at a distance of 0.88 m on the central axis with natural convection only ($v_{FC} = 0$) (—) or with forced convection at 0.01 (---) and 0.10 m/s (—).

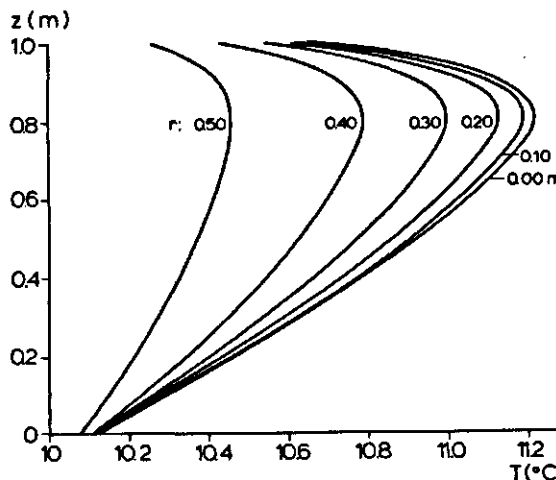


Fig. 17. Longitudinal steady-state profiles of temperature at different radii (r) from the axis.

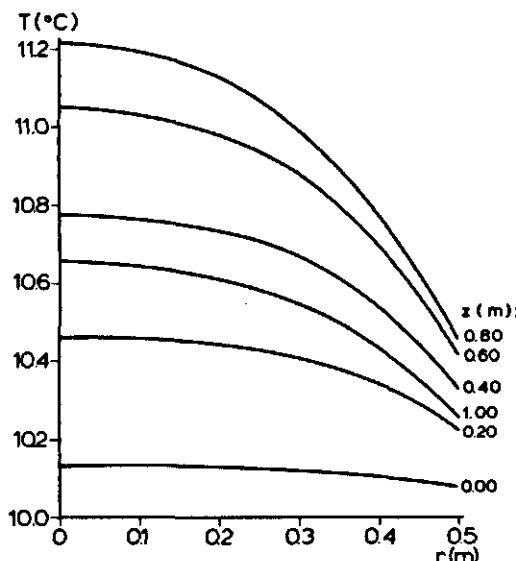


Fig. 18. Steady-state radial profile of temperature at different distances (z) along the cylinder.

- moisture content of the cooling air;
- porosity;
- heat and mass transfer at the wall;
- heat generation;
- bed height.

3.4.2 Influence of different parameters

Velocity of forced convection Fig. 19 gives the temperature course at $z = 0.88$ m and $r = 0.00$ m during pure natural convection and during cooling by both natural and forced convection with $v_{FC} = 0.01$ and 0.1 ms^{-1} . Evidently cooling by forced convection is much faster than cooling by natural convection only. This is also obvious from the 90% cooling time, defined as the time necessary to reduce the value of the average product temperature to 10% of its initial value, given in Table 5. This table further gives the steady-state values of maximum temperature, velocity of natural convection and moisture loss. A higher velocity of forced convection gives a lower maximum temperature. The average temperature in the cylinder will be lower too and as a result the velocity of natural convection is lower.

A higher velocity of forced convection gives more steady-state moisture loss, because the external mass transfer coefficient increases with increasing air velocity. This increase of the moisture loss will not continue at higher air velocities, for the moisture loss is limited by the internal mass transfer coefficient. Equation (3.30) shows that when k_{ext} becomes large the overall mass transfer coefficient (k) is determined by the value of k_{int} . When k_{int} is smaller than the value used in the actual calculations, this influence is more pronounced.

In spite of the higher rate of total moisture loss in the steady state with a higher velocity of forced convection, the integrated total moisture loss (Δn) at the moment the steady state is attained, is lower for a higher value of v_{FC} . This is shown in Fig. 20 which gives the integrated total moisture loss at different times during pure natural convection and during combined natural and forced convection ($v_{FC} = 0.1 \text{ ms}^{-1}$). The steady state is attained after 120 and 15 h, respectively. Fig. 20 also shows that from 5 to 47 h the

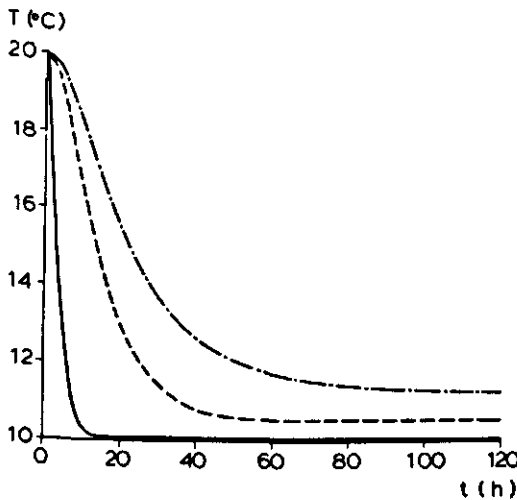


Fig. 19. Changes in temperature at a distance of 0.88 m on the central axis with natural convection only ($v_{FC} = 0$) (---) or with forced convection at 0.01 (---) and 0.10 m/s (—).

Table 5. Steady-state values for different velocities of forced convection.

v_{FC} (m/s)	90% cooling time (h)	T_{max} (°C)	$10^2 \times v_{NC}$ (m/s)	$10^5 \times \dot{m}$ (kg/kgh)
0	32.3	11.2	0.42	0.90
0.005	24.5	10.8	0.22	0.99
0.01	17.5	10.5	0.12	1.11
0.02	14.5	10.3	0.05	1.30
0.05	6.6	10.1	0.01	1.67
0.10	4.2	10.05	0.002	2.05

integrated total moisture loss is less when $v_{FC} = 0.1 \text{ ms}^{-1}$. During this period the average temperature of the cylinder is much lower when the value of v_{FC} is higher. This results in a much lower vapour pressure difference between the product and the air and therefore a lower driving force of moisture loss. On the other hand the overall mass transfer coefficient product to air will be higher for a higher value of v_{FC} . However as shown in Fig. 20 the influence of the smaller vapour pressure difference is more pronounced up to about 20 hours.

In practice cooling by forced convection should not proceed, of course, when the steady state has been attained. Therefore Fig. 20 also shows the integrated total moisture loss when forced convection cooling is stopped after 15 h. The temperature in the cylinder will then rise gradually till the steady-state situation of cooling with natural convection only is attained. Because the integrated total moisture loss in the situation with forced convection is less when convection is stopped, the integrated total moisture loss is always less than for cooling with natural convection only. Fig. 20 therefore shows the advantage of precooling produce with a high velocity of forced convection before the produce is stored for longer periods.

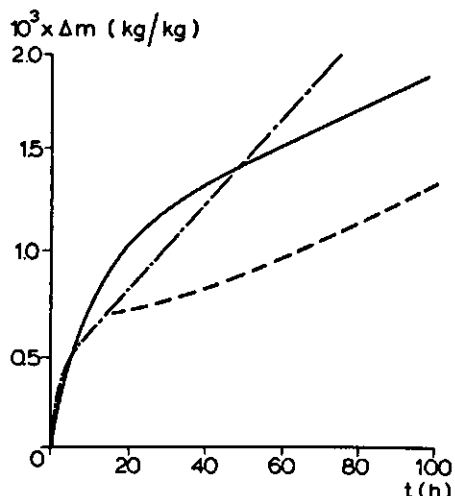


Fig. 20. Integrated total moisture loss with forced convection at 0.10 m/s (—) and without forced convection (—). --- integrated total moisture loss when forced convection is stopped after cooling for 15 hours.

Mass transfer coefficient product to air As shown in Section 3.2 the overall mass transfer coefficient product to air is given by

$$k = \frac{\gamma}{\frac{1}{k_{\text{ext}}} + \frac{1}{k_{\text{int}}}} = \frac{\gamma}{\frac{1}{k_{\text{ext}}} + \frac{r\delta}{ID}} \quad (3.76)$$

Fig. 21 shows the influence of the fraction of surface permeable to water vapour (γ) on the steady-state temperature distribution along the central axis of the cylinder. A higher value of γ gives a higher rate of total moisture loss and therefore lower temperatures. In the lower part of the cylinder the temperature becomes even lower than the temperature of the cooling air, because of the large evaporative cooling in this part of the cylinder. As shown in Table 6 the steady-state velocity of natural convection decreases and the steady-state moisture loss increases with an increasing value of γ .

In this calculations it is assumed that $r\delta$ does not depend upon the vapour pressure difference between product and air. Therefore it is possible to get the same steady-state temperature profile and therefore the same v_{NC} for different combinations of γ and $r\delta$. Equation 3.76 may be rewritten as

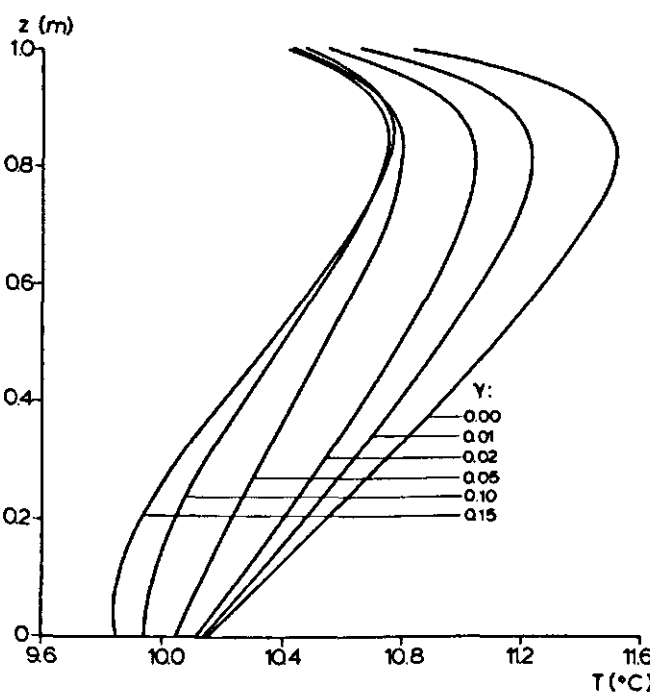


Fig. 21. Influence of the permeable fraction of the product skin (γ) on the axial steady-state profile of temperature along the central axis of the cylinder.

Table 6. Steady-state rate of total moisture loss and natural convection velocity for different values of the fraction of surface permeable to water vapour.

	$\gamma(-)$					
	0	0.01	0.02	0.05	0.10	0.15
$10^5 \times \dot{m}$ (kg/kg h)	0	0.90	1.42	2.23	2.71	2.84
$10^2 \times v_{NC}$ (m/s)	0.47	0.42	0.38	0.31	0.27	0.25

$$\gamma = \frac{k}{k_{ext}} + \frac{k}{ID} r\delta \quad (3.77)$$

With the calculated value of v_{NC} at specific values of γ and $r\delta$, k_{ext} and k may be calculated from Eqn 3.35 or 3.36 and Eqn 3.76. When these values are substituted in Eqn 3.77, the combination of γ and $r\delta$ values is obtained which gives the same steady-state temperature profile. It is therefore also possible to plot Fig. 21 with a constant value of γ and different values of $r\delta$. A larger value of $r\delta$ reduces the rate of total moisture loss. However in order to obtain a large rate of total moisture loss, it may be necessary to use negative values of $r\delta$. These negative values cannot be accepted in physical reality.

The dependence of $r\delta$ on ΔP was given by Villa (1973) as:

$$r\delta = a_1 + a_2 \Delta P \quad (3.78)$$

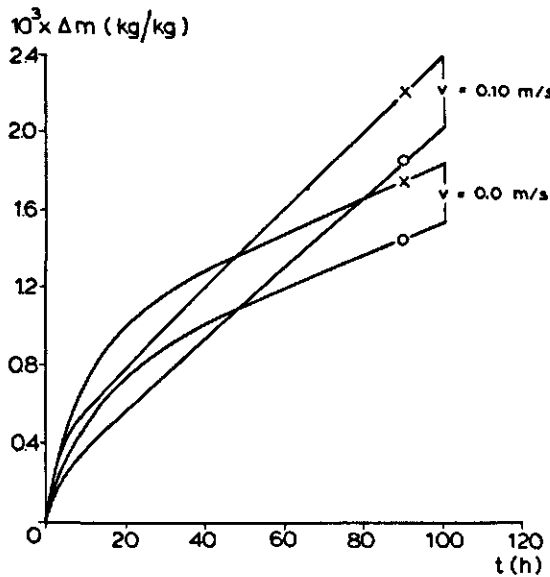


Fig. 22. Integrated total moisture loss with and without forced convection; influence of a_2 (Eqn 3.78).

— x — $a_2 = 0$
— o — $a_2 = 4.07 \times 10^{-6}$ m/Pa.

Table 7. Steady-state rate of total moisture loss (kg/kgh) for different values of forced convection velocity and a_2 (Eqn 3.78)

v_{FC} (m/s)	a_2 (m/Pa)	$10^5 \times \dot{m}$ (kg/kgh)
0	0	0.90
0	4.07×10^{-6}	0.87
0.10	0	2.16
0.10	4.07×10^{-6}	1.94

When Villa's data of a_1 and a_2 for apples (Table 2) are used, the calculated integrated total moisture loss is less than when there is no dependence of ΔP (Fig. 22). The value of a_2 has the largest influence on the integrated total moisture loss at the beginning of the cooling period. This is obvious because the vapour pressure difference between product and air is large at the beginning of the cooling period.

The steady-state rate of total moisture loss (Table 7) is less when the influence of ΔP is incorporated, because $r\delta$ in Eqn 3.76 becomes larger and therefore k is smaller. This influence is somewhat more pronounced at $v_{FC} = 0.1 \text{ ms}^{-1}$, because k_{ext} is larger at this higher velocity, and $r\delta$ has therefore more influence on k . The steady-state temperature profile is almost the same at the two values of a_2 . The temperature difference was $0.01 \text{ }^{\circ}\text{C}$. As a result the velocities of natural convection are equal too.

Moisture content ambient air A lower moisture content of the ambient cooling air (C_0) leads to a higher rate of total moisture loss and, because of the influence of evaporative cooling, to lower temperatures in the cylinder (see Fig. 23). Consequently the velocity of

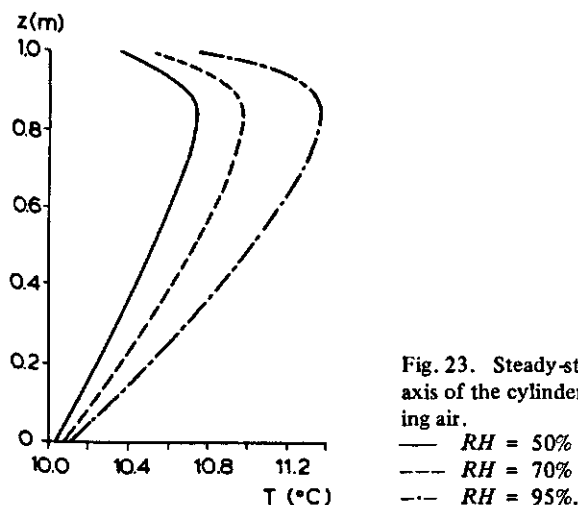


Fig. 23. Steady-state profile of temperature along the central axis of the cylinder at different relative humidities of the cooling air.

— $RH = 50\%$
 - - - $RH = 70\%$
 - · - $RH = 95\%$.

Table 8. Steady-state rate of total moisture loss and velocity of natural convection for different relative humidities of the ambient air (C_0).

C_0 (%)	50	60	70	80	90	95	100
$10^5 \times \dot{m}$ (kg/kgh)	2.64	2.32	1.92	1.45	0.90	0.62	0.30
$10^2 \times v_{NC}$ (m/s)	0.25	0.29	0.33	0.37	0.42	0.44	0.46

natural convection is lower. The steady state velocities of natural convection and rates of total moisture loss at different C_0 -values are summarized in Table 8. Moisture loss even occurs at $C_0 = 100\%$ because the temperature in the cylinder is above the temperature of the ambient air. The relative humidity of the air in the cylinder is therefore below 100% and moisture loss is possible.

For the base-case value of $\gamma = 0.01$ no condensation occurs in the cylinder when $C_0 = 100\%$. The relative humidity in the whole cylinder is below 100% (see Fig. 24). However, as also shown in Fig. 24, when $\gamma = 0.10$ condensation at the top of the cylinder occurs at cooling with $C_0 = 100\%$.

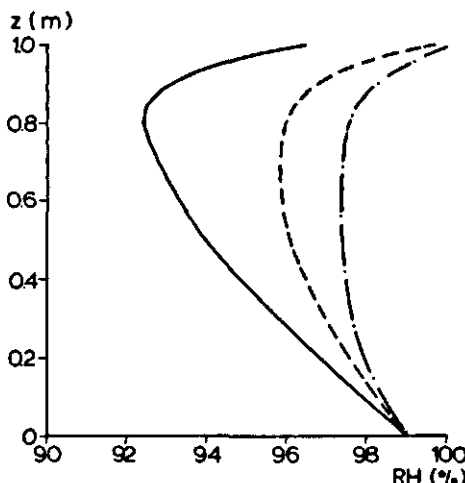


Fig. 24. Steady-state profile of temperature along the central axis of the cylinder at different values of the fraction of the surface permeable to water vapour and $C_0 = 100\%$.

- $\gamma = 0.01$
- - $\gamma = 0.05$
- · - $\gamma = 0.10$

Porosity The porosity (ϵ) influences rate of heat generation and the pressure drop of the air flowing through the cylinder. As porosity increases volumetric heat generation decreases, because there is less product per unit volume, and also pressure drop decreases. The temperature difference with the surroundings is assumed to be equal for the different values of the porosity. Therefore the pressure drop at the start of the cooling will be equal too. As a result the velocity of natural convection at the start of the cooling is high and cooling is faster at high values of porosity (see Figs 25 and 26). In the steady state the velocity of natural convection is higher for $\epsilon = 0.43$ than for $\epsilon = 0.38$, in spite of the lower average temperature in the cylinder (see Table 9). The pressure drop of the air flowing through the cylinder is so much reduced by the higher porosity that, in spite of the lower driving force of natural convection, a higher air velocity results. Table 9 further shows that, because of the higher velocity of natural convection, for $\epsilon = 0.43$ the rate of total moisture loss in the steady state is somewhat higher than at $\epsilon = 0.38$. Nevertheless, when it is possible to modify the porosity, it seems better to have a high porosity because of the lowered maximum temperature at about the same rate of total moisture loss. With a high porosity, of course, more storage volume is necessary used to store the same weight of produce.

These data show that a rather small change in porosity has a relatively large influence on temperature distribution and velocity of natural convection. It is therefore important to measure rather accurately the bulk porosity of stored produce (in spite of difficulties with measurement), when model calculations of the storage are to be performed. It is also obvious that the results of the SNC-model cannot be applied to bulk-stored produce with large varieties in porosity at different positions in the container (e.g. because of adhering soil), because the SNC-model assumes a uniform porosity distribution.

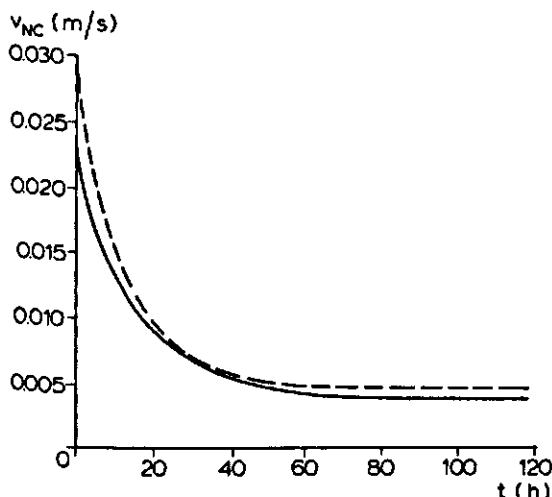


Fig. 25. Velocity of natural convection at different porosities.

— $\epsilon = 0.38$
- - - $\epsilon = 0.43$.

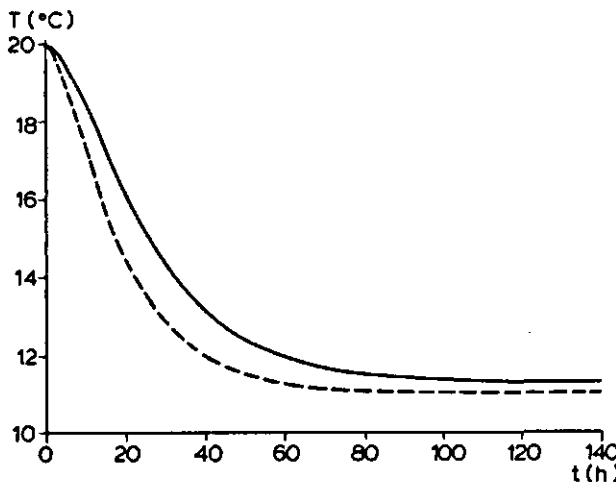


Fig. 26. Influence of porosity on changes in temperature with time at a distance of 0.88 m on the central axis for pure natural convection. Legend: see Fig. 25.

Table 9. Steady-state rate of total moisture loss and velocity of natural convection for different values of bulk porosity.

ϵ (-)	0.38	0.406	0.43
$10^4 \times \dot{m}$ (kg/kgh)	0.887	0.895	0.905
$10^3 \times v_{NC}$ (m/s)	0.37	0.42	0.46

Heat and mass transfer coefficient at the wall As stated in Section 3.2 heat and mass transfer at the wall is described by overall heat and mass transfer coefficients (α_{ov} and k_{ov}). The influence of α_{ov} on the steady-state rate of total moisture loss and velocity of natural convection is given in Table 10. A decreasing value of α_{ov} gives an increasing velocity of natural convection, because of the higher average temperature in the cylinder. Fig. 27 gives the radial temperature distribution at $z = 0.4$ m for different values of α_{ov} . The radial temperature distribution becomes more uniform with decreasing α_{ov} . The value of α_{ov} has only a small influence on the steady state profile of temperature along the central axis of the cylinder, as shown in Fig. 28. The increased heat loss with an increasing heat transfer coefficient at the wall is reduced by the decreased heat transport due to convection (v_{NC} becomes lower). Eventually there is a higher temperature along the central axis of the cylinder at higher values of α_{ov} . Only at the top is the temperature lower, because of the larger influence of radiation losses at the top when velocities of natural convection are low.

Table 10. Steady-state rate of total moisture loss and natural convection velocity for different values of the overall heat transfer coefficient at the wall.

α_{ov} (W/m ² K)	1000	15	6	3	1.5	0.6	0
$10^5 \times \dot{m}$ (kg/kg h)	0.76	0.80	0.85	0.90	0.96	1.02	1.08
$10^3 \times v_{NC}$ (m/s)	0.34	0.36	0.39	0.42	0.45	0.48	0.51

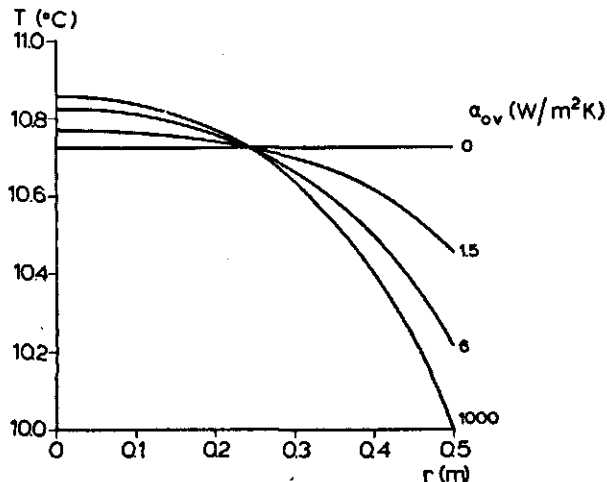


Fig. 27. Radial profile of temperature at $z = 0.4$ m, for different values of the overall heat transfer coefficient at the wall.

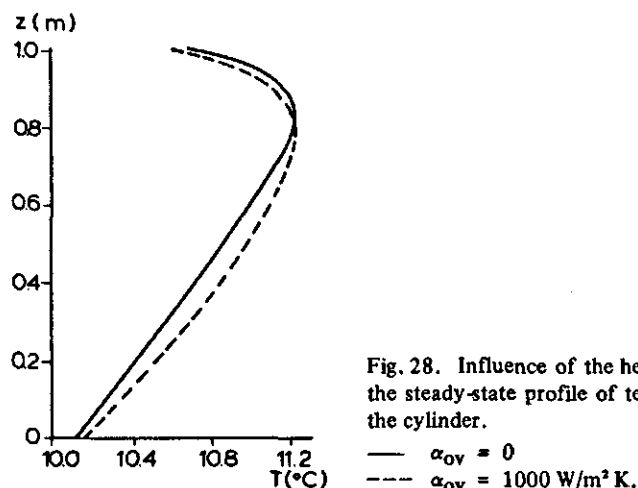


Fig. 28. Influence of the heat transfer coefficient at the wall on the steady-state profile of temperature along the central axis of the cylinder.

— $\alpha_{ov} = 0$
 - - - $\alpha_{ov} = 1000$ W/m²K.

The calculated data show that under conditions of cooling by natural convection the temperature on the central axis is not reduced by a large heat transfer coefficient at the wall. Therefore product deterioration by higher temperatures is not reduced by increased heat transfer at the wall. However, because of the lower average temperature in the cylinder, the rate of total moisture loss is less at a higher value of α_{ov} (Table 10).

A decrease of k_{ov} results in an increase of the relative humidity at the wall. This influence is more pronounced at higher values of α_{ov} because of the resulting lower wall temperatures. The calculations for $C_0 = 100\%$ showed that for $k_{ov} = 0$ condensation at the wall occurred when $\alpha_{ov} \geq 15 \text{ Wm}^{-2} \text{ K}^{-1}$. With $C_0 = 90\%$ and a very high value of α_{ov} ($1000 \text{ Wm}^{-2} \text{ K}^{-1}$) the maximum relative humidity at the wall was 92.5%. Therefore when $C_0 = 90\%$, condensation at the wall will never occur.

Heat generation Different kinds of products have widely different rates of heat generation and even for the same product large differences occur. The rate of heat generation used in the preceding calculations is the average rate of heat generation of apple varieties which can be stored for long periods. Apple varieties which can be stored for only rather short periods have a higher rate of heat generation, which is given by $Q_0 = 2.98 \times 10^{13} \text{ Wm}^{-3}$ and $Q_1 = 7796 \text{ K}$. The calculation of the cooling of these apples leads to a higher steady-state temperature and therefore a higher velocity of natural convection ($v_{NC} = 0.0055 \text{ ms}^{-1}$). The cooling of these two kinds of apple is compared in Fig. 29. At a height of 0.40 m the temperature difference becomes only clear after cooling for about 15 h.

Brussels sprouts have a much higher rate of heat generation than apples (150 Wm^{-3} vs. 20 Wm^{-3} at 10°C). Average physical properties of Brussels sprouts are given in Table 11. These data are summarized from data of the Sprenger Institute (1972). The values for γ and $r\delta$ are chosen in order to give a specific moisture loss of $2.4 \times 10^{-9} \text{ kg/kg Pa}$ when $v = 0.1 \text{ ms}^{-1}$, as given by van Beek & Ficek (1979). The other data used in the calculations are taken from Table 4.

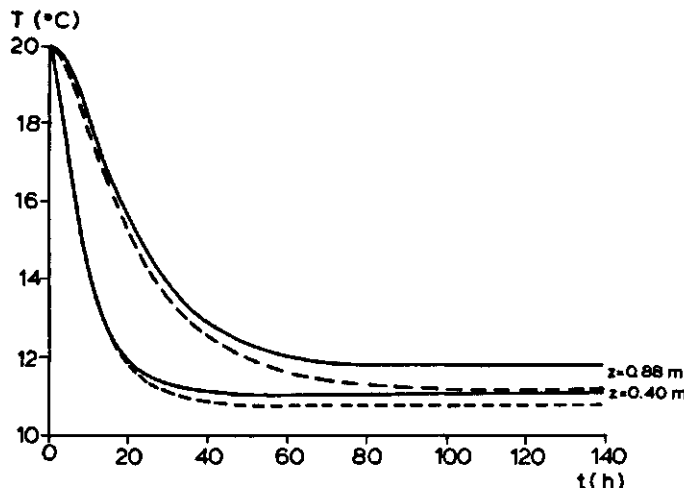


Fig. 29. Cooling by natural convection at a high (—) and a low (---) rate of heat generation.

Table 11. Physical properties of Brussels sprouts.

Bulk density (ρ_b)	516 kg/m ³
Density of product (ρ_p)	860 kg/m ³
Specific heat of product ($c_{p,p}$)	3910 J/kgK
Bulk thermal conductivity (λ_b)	0.30 W/mK
Specific surface area (A)	200 m ² /m ³ product
Particle diameter (d_p)	0.03 m
Bulk porosity (ϵ)	0.40
Constant in heat generation equation (Q_0)	2.06 x 10 ¹⁵ W/m ³ product
Constant in heat generation equation (Q_1)	8559 K
Correction factor in Ergun equation (K)	1.5
Permeable fraction of the surface (γ)	0.20
a_1 in Eqn 3.78	0.0021 m
a_2 in Eqn 3.78	0 m/Pa

Fig. 30 shows the cooling of Brussels sprouts with pure natural convection at different points along the central axis of the cylinder. At the top the product is at first somewhat cooled by radiation losses. Thereafter the temperature rises by the heating in the upper part of the cylinder as shown by the temperature at 0.88 m. In the steady state the temperature is lower than at the beginning of the cooling, but the temperature differences

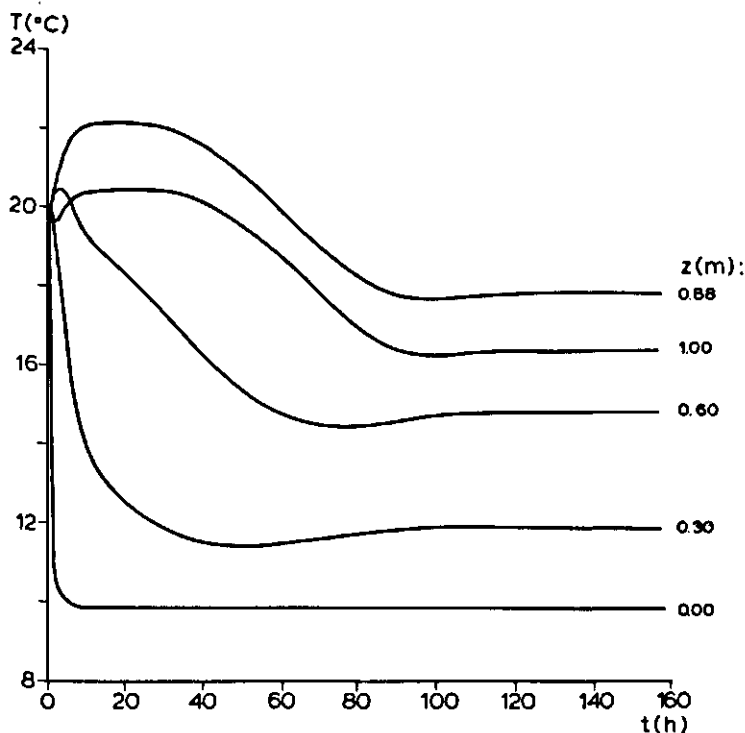


Fig. 30. Cooling of Brussels sprouts at different distances along the central axis of the cylinder.

within the cylinder are too large to make cooling by natural convection only, acceptable as the best way to store Brussels sprouts.

The steady-state velocity of natural convection is 0.0048 ms^{-1} . Notwithstanding the higher average temperature difference with the surroundings, this velocity is not much higher than for apples. This small difference is caused by the higher pressure drop necessary to maintain the air flow through the cylinder. The pressure drop is higher because the particle diameter of the Brussels sprouts is smaller than that of apples.

Bed height The influence of the height of the bed on the temperature profile along the central axis of the cylinder is shown in Fig. 31. The steady-state rate of total moisture loss and natural convection velocity are given in Table 12. At a larger height the average bulk temperature is higher so that the velocity of natural convection is higher. This higher air velocity gives rise to more moisture loss and a slower increase in temperature with the bed height (see Fig. 31). Fig. 31 also shows a non-linear temperature rise with height. This is caused by the larger influence of radial heat losses when the temperatures in the cylinder increase. Under base-case conditions the increased radial heat loss overwhelms the increased rate of heat generation at increased temperatures.

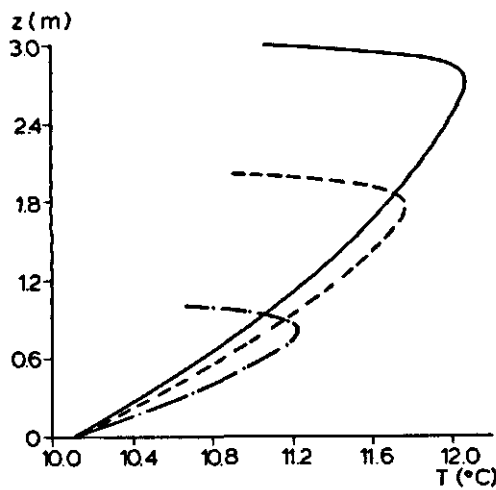


Fig. 31. Steady-state profile of temperature along the central axis of the cylinder at different heights of the bed.

— $L = 1 \text{ m}$
 - - - $L = 2 \text{ m}$
 — $L = 3 \text{ m}$.

Table 12. Steady-state rate of total moisture loss and velocity of natural convection at different bed heights.

	$L \text{ (m)}$		
	1	2	3
$10^5 \times \dot{m} \text{ (kg/kgh)}$	0.90	0.97	1.02
$10^2 \times v_{NC} \text{ (m/s)}$	0.42	0.53	0.61

3.4.3 Conclusions

In practical storage the aim is a low and uniformly distributed temperature and as little moisture loss as possible. The calculations with the SNC-model have shown that moisture loss and temperature distribution are influenced by different parameters. For the storage of one special product the product parameters discussed: fraction of surface permeable to water vapour, internal mass transfer coefficient, rate of heat generation and bulk porosity cannot be modified easily. Only a higher content of carbon dioxide of the cooling air (CA-storage) might influence rate of heat generation and waxing the product lowers the moisture loss. However, to obtain reliable predictions of the influence of the discussed external parameters (velocity of forced convection, moisture content cooling air, heat and mass transfer at the wall and bulk height), it is necessary to have rather accurate values of the product parameters. Especially the parameters describing the moisture loss from product to air have a strong influence on moisture loss and temperature. As already stated there are only few reliable data on this subject. Further research to derive values of the moisture loss parameters, and especially their dependence on difference in water vapour pressure between product and air, is necessary.

The calculations have shown the following influence of the external parameters for cooling by pure natural convection.

1. A high moisture content of the cooling air is the best way to reduce moisture loss.
2. Large heat losses by the side walls reduce moisture loss but do not influence the maximum bulk temperature.
3. A higher bed height gives a higher maximum temperature and more moisture loss.
When the influence of forced convection is incorporated it is also shown:
4. When the temperatures in the bulk become too high with cooling by natural convection only, moisture loss is more reduced by cooling for a short time with a high velocity of forced convection than by cooling longer with a lower velocity of forced convection.

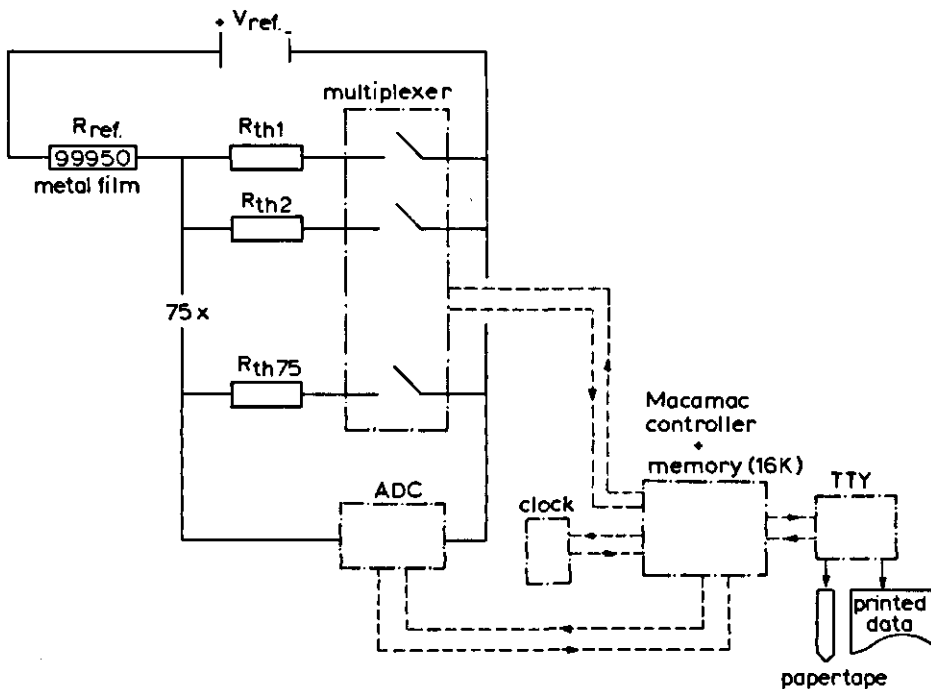


Fig. 33. The 75-point measuring system.

by a BASIC programmable microprocessor, as shown in Fig. 33. This figure also shows that measuring the thermistor resistance was based on a constant voltage over the thermistor and a reference resistance (99950Ω). It was possible to measure 75 different temperatures. I used Philips thermistors (resistance at 25°C : $10 \text{ k}\Omega \pm 20\%$) embedded in a glass envelope (length 5 mm, diameter 1.5 mm). Further details of the measuring system are given by Beukema & de Swart (1979).

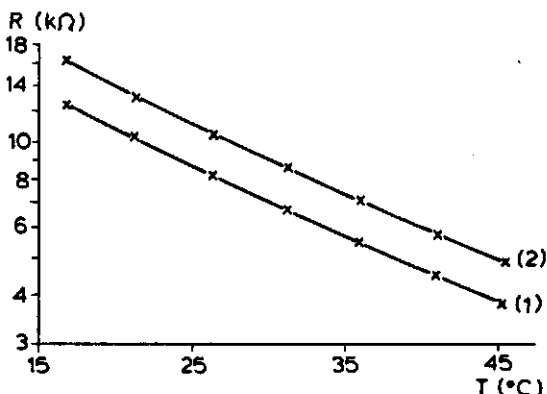


Fig. 34. Thermistor calibration curves, $\ln R = C_1 T^2 + C_2 T + C_3$.

$$(1) C_1 = 1.336 \times 10^{-4} \text{ } ^\circ\text{C}^{-2}, C_2 = -4.832 \times 10^{-2} \text{ } ^\circ\text{C}^{-1}, C_3 = 10.2049.$$

$$(2) C_1 = 1.354 \times 10^{-4} \text{ } ^\circ\text{C}^{-2}, C_2 = -4.919 \times 10^{-2} \text{ } ^\circ\text{C}^{-1}, C_3 = 10.4949.$$

The temperature dependence of the thermistor resistance is described by the empirical relation:

$$R = e^{C_1 T^2 + C_2 T + C_3} \quad (4.1)$$

where C_1 , C_2 and C_3 are the calibration constants. R is the thermistor resistance (Ω) and T the temperature ($^{\circ}\text{C}$). C_1 , C_2 and C_3 were determined for each sensor by a second order polynomial regression of $\ln R$ versus T . Fig. 34 shows two representative calibration curves. The deviation from the specific calibration curve of each of the 75 thermistors used in the experiments was $0.05\text{ }^{\circ}\text{C}$ or less. The calibration constants of the different thermistors were incorporated in the measuring program of the microprocessor controller.

4.2 Experimental set-up

To investigate the influence of natural convection on convective cooling of bulk-stored agricultural or horticultural products, I used a cylindrical container as shown in Fig. 35. The cylinder is made of epoxy glass fibre and built by piling up four sections, each with an inner diameter of 1.00 m and a height of 0.50 m. The upper and the lower section stabilize the air flow. The products rest on an iron grate. The pressure drop to the air flow caused by this grate is negligible compared with that of the packed bed of products. The air flow towards the grate is not hindered substantially by the set-up. The distance from the grate to the floor is 1.00 m.

The cylinder was insulated to reduce radial heat losses by a layer of insulating material (polyurethane foam) around the cylinder wall. The foam was covered by brass shielding. The temperature of the brass shielding was controlled by heating tape. Heat losses would have been too large if only insulating material had been used. The aim of the temperature control was to ensure that the outer wall at any height had the same temperature as the products in the cylinder at that height. The lower rim of the brass shielding was kept at room temperature by pumping water of room temperature around the cylinder at the height of the grate. At distances of 0.30, 0.55, 0.73 and 0.85 m upwards from the grate, heating tapes were fixed around the brass shielding. Each heating tape was controlled by a temperature controller. The input signal of the controller was the amplified voltage of 5 copper-constantan thermocouples in series (Fig. 36). These 5 thermocouples were spaced at equal distances around the cylinder circumference. The cold junctions were connected to the brass outer wall just above the heating tape and the warm junctions were placed on the inner wall. I used 5 thermocouples around the cylinder to determine the average temperature difference between the inner and the outer wall at one height. Another advantage of 5 thermocouples in series was the resulting higher input voltage of the amplifier. The temperature controller was regulated to restrict the temperature differences between inner and outer wall up to $0.1\text{ }^{\circ}\text{C}$. The total amount of heat lost through the wall was always less than 1% of the heat generated in the cylinder. The heat loss was not the same at every place on the cylinder wall, but the maximum amount of heat loss never exceeded 2% of the generated heat.

To measure the local temperatures the thermistors were placed in the air between the model material at different places in the cylinder as shown in Fig. 37. To measure whether the expected small differences between product and air temperature occur in

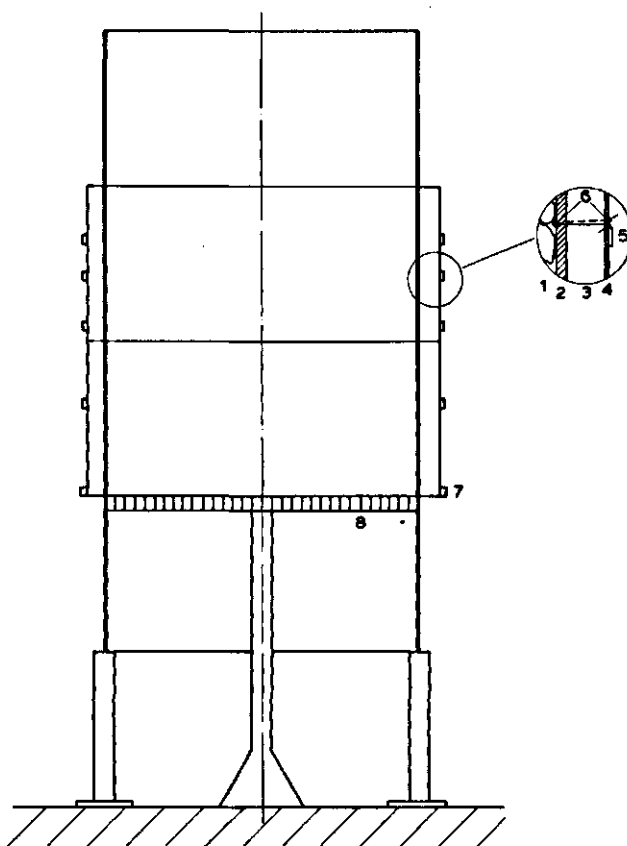
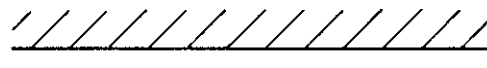


Fig. 35. The cylindrical set-up.

- 1 = model material
- 2 = cylinder wall (epoxy glass fibre)
- 3 = polyurethane foam insulation
- 4 = brass shielding
- 5 = heating tape
- 6 = thermocouple junctions
- 7 = cooling ring
- 8 = grate
- 9 = ceiling

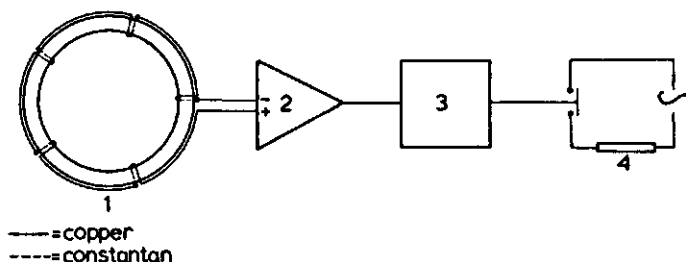


Fig. 36. The brass shielding temperature control system

- 1 = cylinder wall with thermocouples
- 2 = amplifier
- 3 = temperature controller
- 4 = heating tape

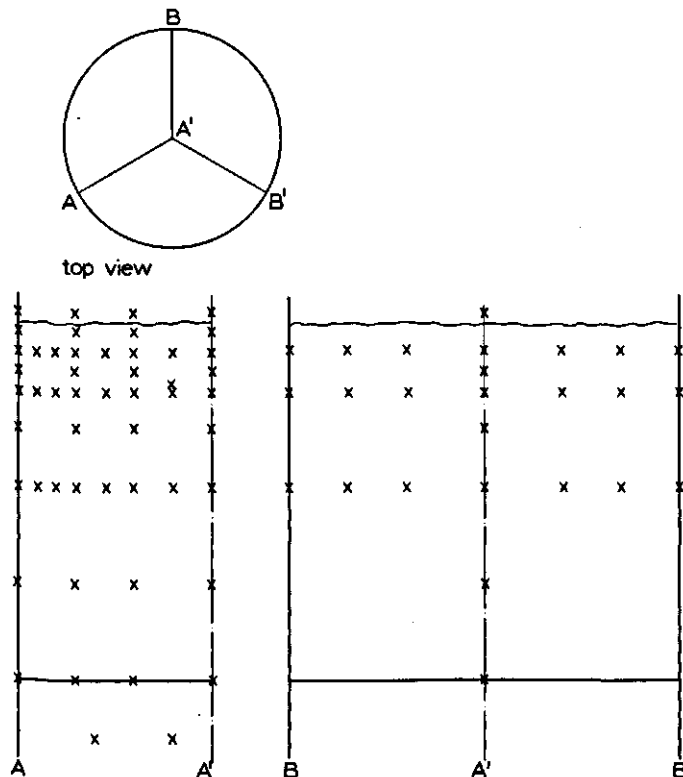


Fig. 37. Location of the thermistors inside the cylinder with model material.

practice, one thermistor was embedded in the wall of a model product. Four other thermistors were connected to the ceiling above the cylinder, to measure the ceiling temperature. These temperatures were used to calculate the heat lost by radiation from the top of the cylinder.

4.3 Results with model material for pervious bottom and pervious top

The experimental set-up was used to measure temperature for different rates of heat generation. Most experiments were performed with an open top and bottom. Some experiments were performed with an open top and closed bottom and a closed top and bottom. 'Open' means that air flow through the bottom or top is unrestricted, whereas 'closed' indicates that air flow is impossible.

I investigated the open bottom-open top and closed bottom-closed top situations, because they are the two extremes of practical storage. The open bottom-open top situation represents the bulk storage of produce in large storage rooms, cooled by convective cooling. The closed bottom-closed top situation represents storage in closed containers. This kind of storage is more extensively discussed in Chapter 5. The closed bottom-open top situation is an intermediate between the extremes.

Self-heating of the products When bottom and top are open, the heat generated is removed by natural convection as shown in Section 2.4. Fig. 38 and Fig. 39 show the measured temperature course for different distances along the central axis of the cylinder for a rate of heat generation of 51 and 274 W m^{-3} , respectively. It is remarkable that especially in the lower parts of the cylinder the temperature course shows a maximum. The reason for this maximum is that the temperatures in the upper part of the cylinder are still below the steady state temperature when, for example, the temperature at a height of 0.25 m is equal to the steady state temperature. This occurs at a rate of heat generation of 51 W m^{-3} after heating about 30 h (see Fig. 38). Then the average temperature in the cylinder is lower than in the steady state. The difference between the average temperature in the cylinder and the temperature of the outside air is the driving force of natural convection. Therefore the lower average temperature results in a velocity of natural convection lower than in the steady state. The lower velocity of natural convection causes less cooling and as a result the temperature at, for example, 0.25 m rises above its steady-state value. When the self-heating proceeds, the average temperature

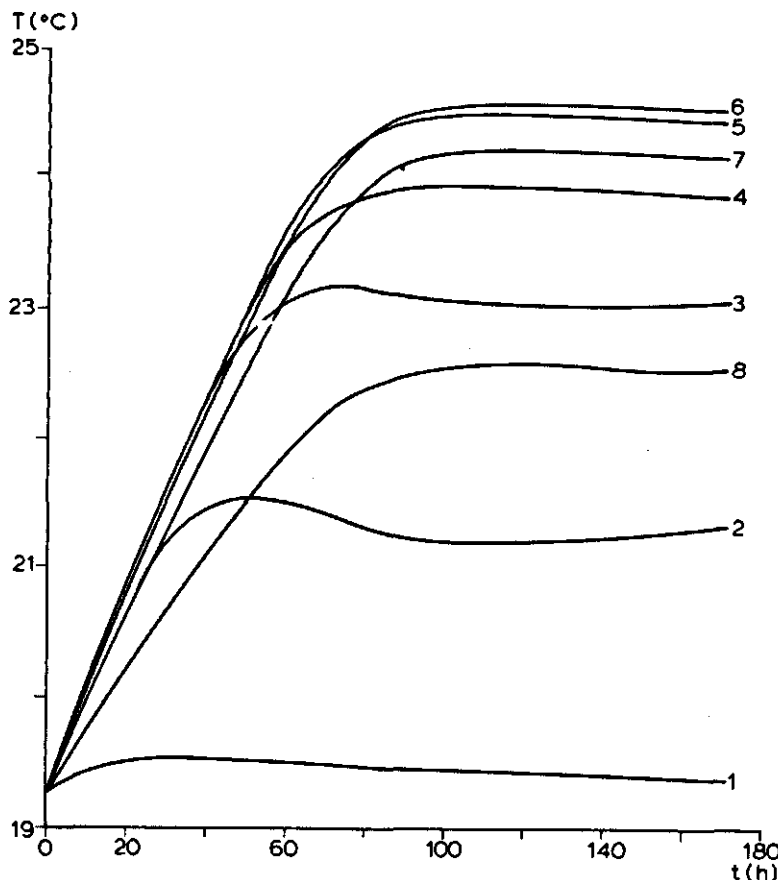


Fig. 38. Changes in temperature with time for a rate of heat generation of 51 W m^{-3} at different distances along the central axis of the cylinder.

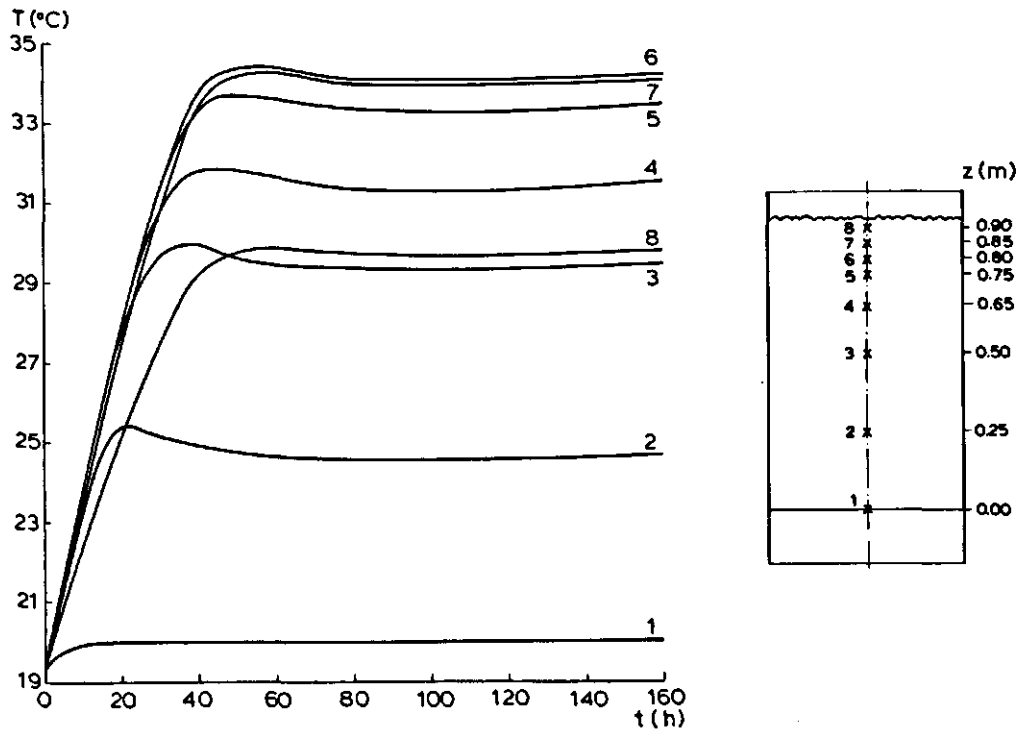


Fig. 39. Changes in temperature with time for a rate of heat generation of 274 W/m^3 at different distances along the central axis of the cylinder.

rises and the velocity of natural convection increases too. Because of the increasing velocity of natural convection the temperature at a height of 0.25 m decreases until the steady state is attained.

The steady-state profiles of temperature corresponding with Figs 38 and 39 are given in Fig. 40. The linear temperature rise in the lower part of the cylinder is clearly shown. Fig. 41 gives the steady-state profiles of the dimensionless temperature:

$$\theta_Q = \frac{(T - T_0) \lambda_0}{QL^2} \quad (4.2)$$

As shown in Section 2.4.2, for a constant air velocity and equal dimensionless heat losses, the temperature profile of θ_Q is equal for various rates of heat generation. In Fig. 41, however, the measured dimensionless temperature decreases with increasing rate of heat generation at any height. This decrease is caused by the higher velocity of natural convection at higher rates of heat generation because of the larger average temperature in the cylinder. The higher velocity of natural convection gives the smaller increase of θ_Q with the height for higher rates of heat generation.

The steady state is attained faster at a higher rate of generation, see Fig. 38 and Fig. 39. At a rate of heat generation of 274 Wm^{-3} the steady state is attained after about 50 h and at a rate of heat generation of 51 Wm^{-3} after about 90 h. The cylinder has to be

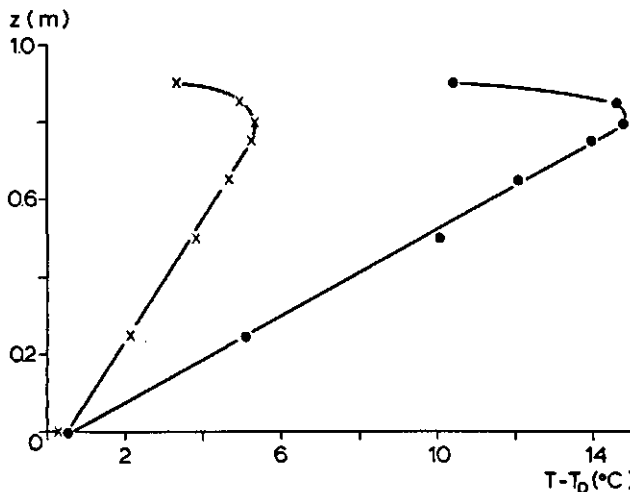


Fig. 40. Steady-state profile of temperature along the central axis of the cylinder with a rate of heat generation of 51 (x) and 274 (●) W/m^3 .

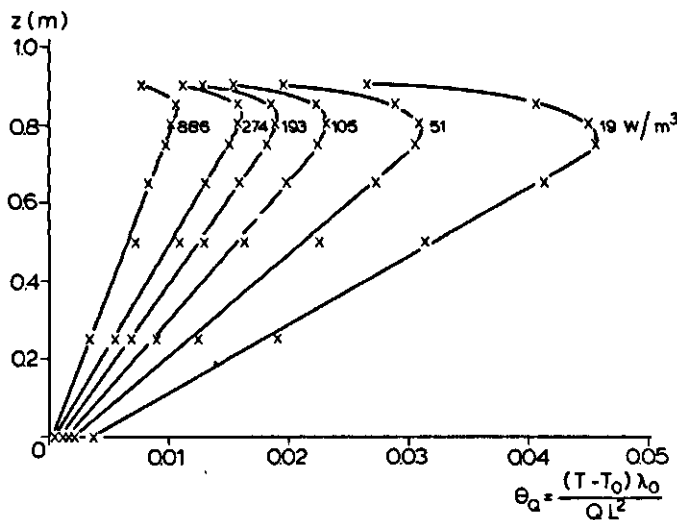


Fig. 41. Dimensionless steady-state profile of temperature along central axis of the cylinder with different rates of heat generation.

heated relatively less at a higher rate of heat generation, because more heat is removed by the higher velocity of natural convection.

Radial temperature distribution The radial profiles of temperature in the direction A-A' (see Fig. 37) at different heights in the cylinder at a rate of heat generation of 51 Wm^{-3} are given in Fig. 42. The measured temperatures in the directions A'-B and A'-B' at a

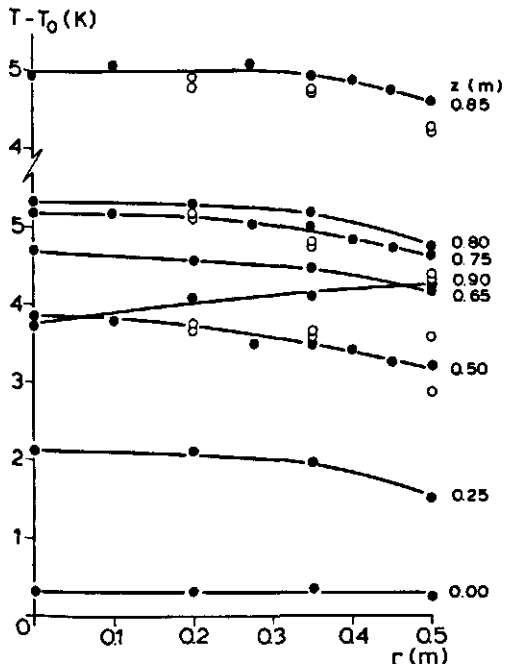


Fig. 42. Radial profiles of temperature at different distances for $Q = 51 \text{ W/m}^3$.

○ = same distance, but other radial directions.

height of 0.50, 0.75 and 0.85 m are also shown (x). The radial temperatures are presented in another way by the contoured print-plot of the temperature distribution in one radial direction. Fig. 43 and Fig. 44 show the contoured print-plots at $Q = 51$ and 274 Wm^{-3} , respectively. A contoured print-plot is made in the following way. Temperatures at other positions in the cylinder are calculated from the measured temperatures by linear interpolation. The value of the temperature of the surroundings (T_0) is subtracted from every temperature. The resulting temperatures are divided by the maximum value of $T - T_0$. Therefore normalized temperatures between 0 and 1 result. In the contoured print-plot a 0 is plotted when the normalized temperature is between 0.000 and 0.025, a 1 indicates a temperature between 0.075 and 0.125, etc., while temperatures between 0.975 and 1.000 are indicated by *. Other values of the temperature (e.g. between 0.025 and 0.075) are not indicated. Figs 43 and 44 show that the radial temperature gradients increase as the rate of heat generation increases.

The radial heat flux towards the wall of the cylinder, resulting from the radial temperature gradient is larger than the heat flux through the insulated wall. The heat losses at the inner wall of the cylinder consist of two parts: radial conduction through the wall and axial convection by natural convection. Near the wall the velocity of natural convection is higher than in the centre of a packed bed, because the porosity of a packed bed increases and therefore the resistance to air flow decreases near the wall. Consequently in convective heat transport, radial temperature gradients even occur in a packed bed with a perfectly insulated side wall. The lower temperatures at higher porosity are also shown by

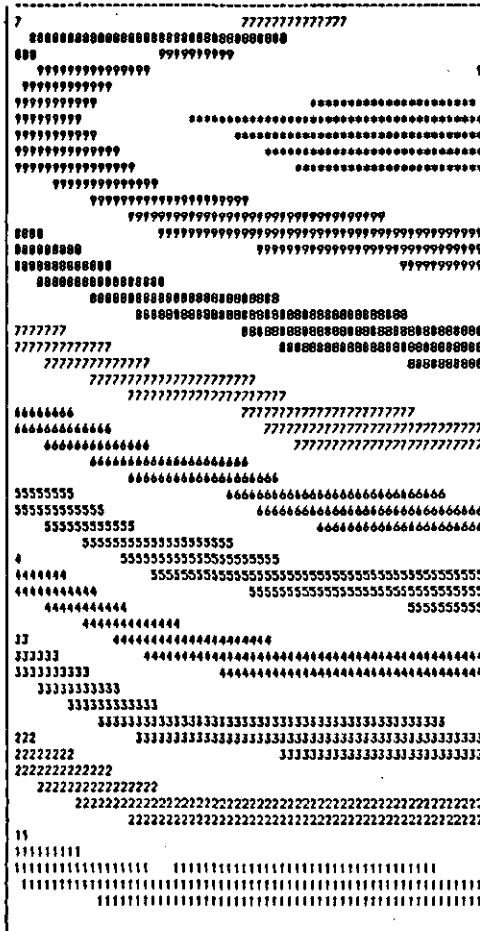


Fig. 43. Contoured print-plot of the experimental temperature distribution in the cylinder at $Q = 51 \text{ W/m}^3$. Maximum temperature difference with the surroundings: 5.3°C .

the calculations in Section 3.3.

I measured temperatures at three different heights (0.50, 0.75 and 0.85 m), in three radial directions, at three radial distances (0.20, 0.35 and 0.50 m, see Fig. 37) to check the radial symmetry in the cylinder. The mean ($\bar{T} - T_0$), the standard deviation (σ_x) and the relative standard deviation ($\sigma_x / (\bar{T} - T_0)$) of the steady-state temperatures with the same r and z coordinate were calculated. The mean of the relative standard deviation for different rates of heat generation is given in Table 13. This table shows that temperature differences at the same height and the same radial distance are rather small, especially at $r = 0.20$ and 0.35 m. The larger differences at $r = 0.50$ m may be caused by differences in the porosity at the wall and by somewhat different heat losses through the wall at different radial positions.

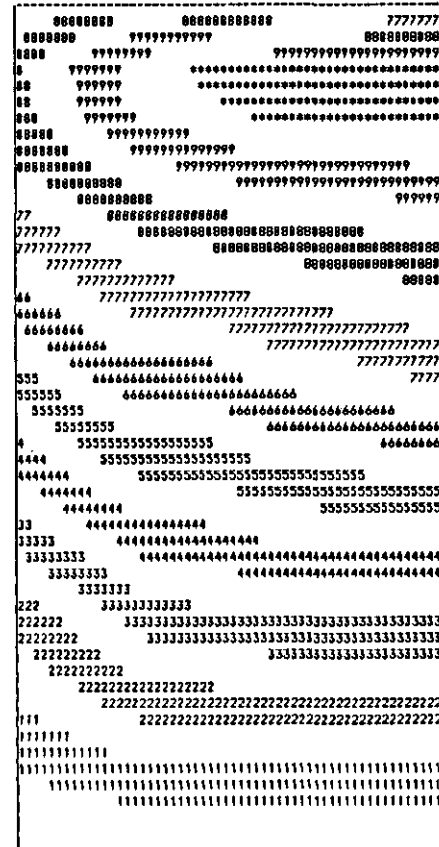


Fig. 44. Contoured print-plot of the experimental temperature distribution in the cylinder at $Q = 274 \text{ W/m}^3$. Maximum temperature difference with the surroundings: 14.7°C .

Table 13. Mean relative standard deviation at different heights and distances from the cylinder centre.

z (m)	r (m)		
	0.20	0.35	0.50
0.85	0.017	0.026	0.047
0.75	0.004	0.015	0.037
0.50	0.011	0.019	0.075

From these measurements it can be concluded that temperature measurements in one radial direction give a good description of the temperatures at other places in the cylinder. The cylindrical symmetry is good with this experimental set-up.

Axial temperature distribution As shown in Section 2.4 both the one-dimensional one-phase and two-phase model give, in the lower part of the cylinder, a linear temperature rise with height. The slope of the temperature profile is given by

$$\frac{dT}{dz} = \frac{Q}{(\rho c_p)_a v} \quad (4.3)$$

It is therefore possible to calculate the natural convection velocity from the slope (dT/dz) of the measured temperature profile:

$$v = \frac{Q}{(\rho c_p)_a \frac{dT}{dz}} \quad (4.4)$$

Table 14 summarizes the velocities of natural convection for different rates of heat generation, calculated in this way. The density of the air (ρ_a) is taken at the average temperature of the air in the cylinder and a pressure of 1 bar. The data for a rate of heat generation of 105 W m^{-3} are the result of two measurements.

It is possible to calculate the steady-state axial profiles of temperature, as predicted by

Table 14. Velocity of natural convection and heat transfer coefficient at the top for different rates of heat generation.

	Q (W/m ³)						
	18.9	50.8	105	105	193	274	886
v_{NC} (m/s)	0.0041	0.0063	0.0087	0.0085	0.0106	0.0128	0.0204
α_L (W/m ² K)	4.7	7.0	8.6	10.4	12.5	13.0	18.5

Table 15. Physical data of the model material.

Density (ρ_p)	1038 kg/m ³
Specific heat ($c_{p,p}$)	3560 J/kg K
Bulk thermal conductivity (λ_b)	0.25 W/mK
Porosity (ϵ)	0.364
Equivalent diameter (d_p)	0.0527 m

the one-dimensional one-phase or two-phase model with the air velocities of Table 14 and the physical data of the model material (given in Table 15) and air. The necessary equations are given in Sections 2.4.2 and 2.4.3. Fig. 45 shows these temperatures at $Q = 274 \text{ W m}^{-3}$, assuming heat losses at the top by radiation only. There is a good fit of the calculated temperatures from both the one-phase and two-phase model with the measured temperatures up to a height of 0.80 m. It is obvious that the heat lost at the top by radiation to the surroundings is not sufficient to explain the low temperatures measured in the upper part of the cylinder.

I studied the flow pattern of the air at the top of the cylinder qualitatively by observation of the smoke pattern, used to visualize the air flow. The air flowing through the cylinder mixed with the colder air of the surroundings and caused contact of the

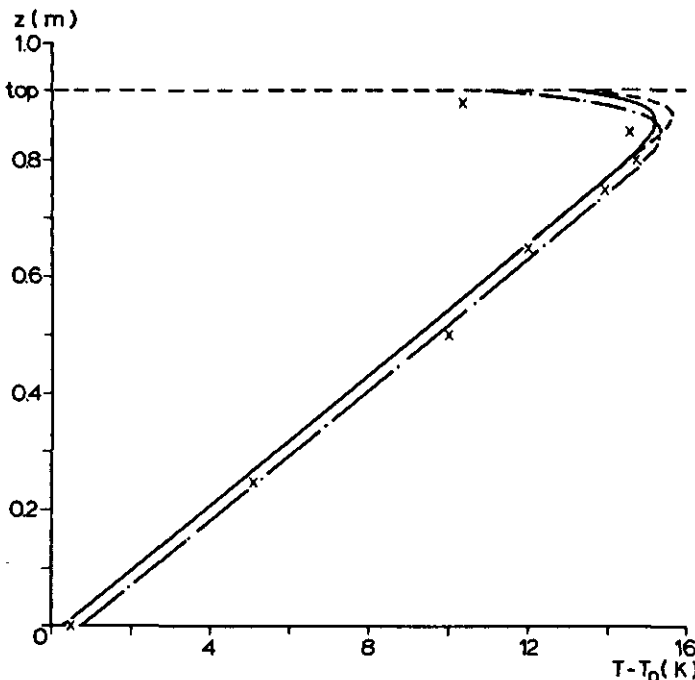


Fig. 45. The temperature calculated with the one-phase model (---) and two-phase model (T_p (---) and T_a (—)) at $Q = 274 \text{ W/m}^3$. (---) and T_a (---) at $Q = 274 \text{ W/m}^3$.

x = temperatures measured along the central axis at $Q = 274 \text{ W/m}^3$.

colder air with the top layer of the products in the cylinder. This contact gave extra cooling of the top. I described this cooling by introducing an effective heat transfer coefficient at the top (α_L). These heat losses at the top are introduced in the boundary condition at the top of the one-phase and two-phase model, as shown in Sections 2.4.2 and 2.4.3.

The value of α_L in the two-phase model is calculated by the Least Squares Method to minimize the difference between the measured and the calculated values of T_p . Table 14 summarizes the α_L values for different rates of heat generation calculated in this way. Fig. 46 gives the calculated product temperature at $\alpha_L = 0$ and $13.0 \text{ W m}^{-2} \text{ K}^{-1}$ together with the measured temperatures. It is obvious that the introduction of α_L in the model equations gives a better description of the measured temperatures.

As shown in Section 2.4.2 the Biot number:

$$Bi_L = \frac{\alpha_L L}{\lambda_0} \quad (4.5)$$

is obtained when Eqn 2.49 is made dimensionless. However because the occurrence of α_L is coupled to the air turbulences at the top of the cylinder, it is better to use the equivalent particle diameter (d_p) as the characteristic length in the Biot number. Thus:

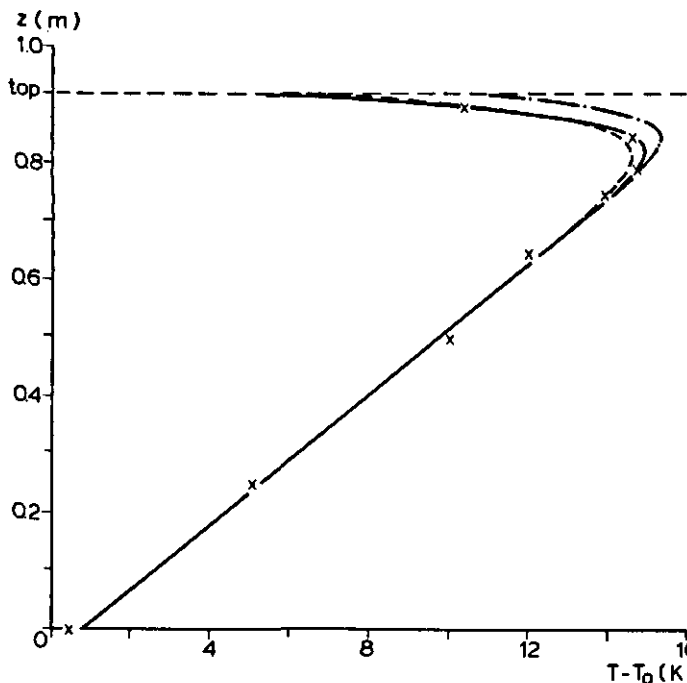


Fig. 46. Product temperature of the two-phase model at $\alpha_L = 0.0$ (---) and 13.0 (—) $\text{W/m}^2 \text{ K}$ and the temperature of the one-phase model (----) at $\alpha_L = 13.0 \text{ W/m}^2 \text{ K}$ and $\lambda_{ax} = 0.655 \text{ W/mK}$ with a rate of heat generation of 274 W/m^3 .

$$Bi'_L = \frac{d_p}{L} Bi_L = \frac{\alpha_L d_p}{\lambda_0} \quad (4.6)$$

The dependence of α_L on the velocity of natural convection is shown in Fig. 47, which shows a linear dependence of Bi'_L on Re . Re is calculated with the value of v_{NC} given in Table 14. The relation between Bi'_L and Re is given by

$$Bi'_L = 0.063 Re \quad (4.7)$$

This relation is used in the calculations with the SNC-model in Section 4.3.

An explanation of the linear dependence of α_L on the velocity of natural convection may be found in the theories of axial dispersion in packed beds. It is well known (e.g. Wicke, 1975) that the Pe number based on dispersion in packed beds is constant at Re numbers above 20:

$$Pe = \frac{v d_p}{ID_e} = 2 \quad (Re > 20) \quad (4.8)$$

At constant heat capacity of the air, the heat flux by dispersion is given by

$$\phi''_q = ID_e (\rho c_p)_a \frac{dT}{dz} \quad (4.9)$$

At the top the heat flux is modelled with

$$\phi''_q = \alpha_L (T_L - T_0) \quad (4.10)$$

Therefore the heat flux is proportional to two different groups:

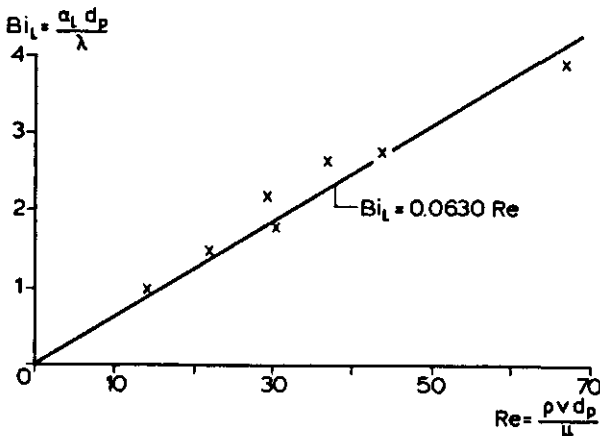


Fig. 47. Dependence of Bi'_L on Re .

$$\phi''_q \approx D_e (\rho c_p)_a \frac{\Delta T}{d_p} = \frac{v(\rho c_p)_a}{2} \Delta T \quad (4.11)$$

and

$$\phi''_q \approx \alpha_L \Delta T \quad (4.12)$$

Because the heat capacity of the air is assumed to be constant combination of Eqns 4.11 and 4.12 gives

$$\alpha_L \approx v \quad (4.13)$$

It should be noticed that the relation between Bi'_L and Re cannot be applied directly to other bulk storage problems. The larger heat transfer at the top is influenced by the experimental set-up. When, for example, the top section of the cylinder becomes shorter, the cold air from the surroundings will mix more easily with the air flowing through the cylinder and α_L should be higher.

Thermal conductivity in the one-phase model As shown in Section 2.4 the equations of the one-phase model are less complex than the equations of the two-phase model. It is therefore easier to calculate temperature profiles when the one-phase model gives a good description of the measured temperature profile. However, as shown in Fig. 45, the two-phase model gives, even at $\alpha_L = 0$, a better description of the measured temperatures, especially at the top. Also the introduction of other α_L values does not substantially improve the description with the one-phase model. A real improvement of the one-phase model is obtained by introducing a velocity-dependent thermal conductivity, as shown by Vortmeyer & Schaefer (1974).

From the two-phase model Vortmeyer & Schaefer (1974) theoretically derived a one-phase model that includes the influence of a higher heat transfer coefficient at higher air velocities. Because the air and product temperature profiles had a similar shape, they assumed that:

$$\frac{d^2 T_p}{dz^2} = \frac{d^2 T_a}{dz^2} \quad (4.14)$$

With this assumption they derived from the energy equations of the two-phase model an equation that is mathematically identical to the energy equation of the one-phase model. For spherical particles the equations are equal when the thermal conductivity of the one-phase model (λ_{ax}) is equal to:

$$\lambda_{ax} = \lambda_0 + \frac{Re^2 Pr^2}{6(1-\epsilon) Nu} \lambda_a \quad (4.15)$$

where λ_0 is the effective thermal conductivity of the stagnant bed. Introduction of the relation of Bird et al. (1960) to calculate Nu values:

$$Nu = 2.26(1-\epsilon)^{0.51} Re^{0.49} Pr^{0.33} \quad (13 < Re < 180) \quad (4.16)$$

in Eqn 4.15 yields:

$$\lambda_{ax} = \lambda_0 + 0.0734 \frac{Re^{1.51} Pr^{1.67}}{(1-\epsilon)^{1.51}} \lambda_a \quad (4.17)$$

From temperature measurements in packed beds of glass beads, metallic balls and broken pieces of limestone, Yagi et al. (1960) found the experimental relation:

$$\lambda_{ax} = \lambda_0 + \delta Re Pr \lambda_a \quad (4.18)$$

where:

$\delta = 0.7$ for lead and steel balls ($0 < Re < 40$).

$\delta = 0.8$ for glass beads and broken pieces of limestone ($0 < Re < 15$).

Vortruba et al. (1972) derived from experimental work in packed beds of sand, glass spheres and metallic spheres, with $2.5 \times 10^{-4} < d_p < 5 \times 10^{-3}$ m, the empirical relation:

$$\lambda_{ax} = \lambda_0 + \frac{0.0145 Re Pr}{d_p \left(1 + \frac{C_v}{Re Pr} \right)} \quad (0.1 < Re < 100) \quad (4.19)$$

C_v is an experimentally determined constant, which ranges between 0 and 5. At $C_v = 0$ this equation gives a linear dependence of λ_{ax} on Re just as Eqn 4.18.

The thermal conductivity of the one-phase model in the experiments was calculated by the Least Squares Method to minimize the difference between the measured steady-state temperatures in the centre of the cylinder, and the temperatures calculated from the one-phase model. The value of α_L for the different measurements is taken from Table 14. The calculated thermal conductivities for different rates of heat generation are given in Table 16. The dependence of λ_{ax} on Re is given in Fig. 48. Fig. 48 also shows that the λ_{ax} values of my experiments are lower than the values predicted by Vortmeyer & Schaefer (1974) and Yagi et al. (1960), but higher than the value predicted by Vortruba et al. (1972). The theoretical curves of λ_{ax} were calculated with $\lambda_0 = 0.224 \text{ W m}^{-1} \text{ K}^{-1}$.

Table 16. Thermal conductivity of the one-phase model and velocity of natural convection for different rates of heat generation.

$Q (\text{W/m}^3)$							
	18.9	50.8	105	105	193	274	886
$10^2 \times v_{NC} (\text{m/s})$	0.41	0.63	0.87	0.85	1.06	1.28	2.04
$\lambda_{ax} (\text{W/mK})$	0.353	0.443	0.535	0.518	0.586	0.655	0.885

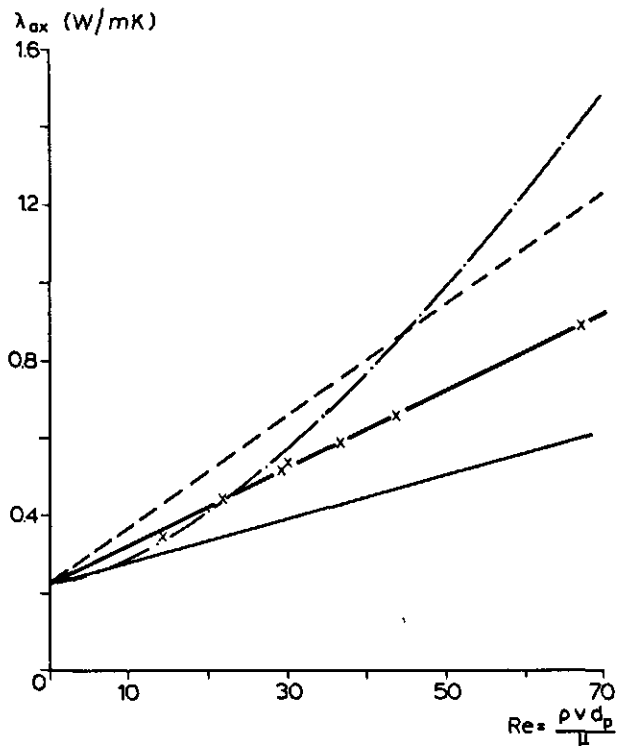


Fig. 48. Different correlation of the thermal conductivity in the one-phase model and the measured values (X).

$$\begin{aligned}
 \text{—} \quad \lambda_{ax} &= 0.224 + 0.56 Re Pr \lambda_a & & \\
 \text{—} \quad \lambda_{ax} &= 0.224 + 0.28 Re Pr \lambda_a & \text{(Vortruba et al., 1972)} & \\
 \text{---} \quad \lambda_{ax} &= 0.224 + 0.8 Re Pr \lambda_a & \text{(Yagi et al., 1960)} & \\
 \text{---} \quad \lambda_{ax} &= 0.224 + \frac{0.0734 Re^{1.51} Pr^{1.67}}{(1-\epsilon)^{1.51}} \lambda_a & \text{(Vortmeyer & Schaefer, 1974).} &
 \end{aligned}$$

The dependence of λ_{ax} on Re can be given with the relation:

$$\lambda_{ax} = 0.224 + 0.56 Re Pr \lambda_a \quad (4.20)$$

The value of λ_0 (0.224) agrees rather well with the experimental value of $\lambda_0 = 0.25 \text{ W m}^{-1} \text{ K}^{-1}$.

The dependence of λ_{ax} on $Re^{1.5}$, as predicted by Vortmeyer & Schaefer (1974) was not confirmed by these measurements. Their assumption of the identity of the second derivatives of T_p and T_a is not valid in the upper part of the cylinder (see Fig. 45). The value of λ_{ax} was determined mainly by the temperatures in the upper part of the cylinder. The temperature profile in the lower part of the cylinder was not determined by the value of λ_{ax} but by the value of the air velocity.

Correction factor in the Ergun equation It is possible to calculate the correction factor in the Ergun equation (K), as defined in Section 2.5, with the natural convection velocity of Table 14. When Eqn 2.38 is modified by introducing $\kappa = \kappa'/K$, where κ' represents the permeability of a packed bed of spheres with the particle diameter of the products and the same porosity as the packed bed with products, K can be calculated from

$$K = \frac{\rho_1 g \beta \kappa' (\bar{T} - T_{in})}{\mu v_{NC}} \quad (4.21)$$

The average temperature in Eqn 4.21 can be calculated in different ways:

- from the experimental values in the centre of the cylinder,
- with the one-phase model temperatures,
- with the product temperature of the two-phase model,
- with the air temperature of the two-phase model and
- from the assumption of a linear temperature rise.

The last method was already introduced in Section 2.4.1. where a relation between Pe and Ra was developed. This relation can be modified to:

$$K = \frac{Ra'_1}{2Pe^2} \quad (4.22)$$

where Ra' represents the Rayleigh number calculated with the permeability κ' .

Table 17 summarizes the values of K , calculated in the different ways: The average experimental temperature in the cylinder was calculated from the eight temperatures measured along the central axis of the cylinder by the trapezoidal rule. The model of linear temperature rise predicted a lower value of K than the other models, even though the temperature at the top was overestimated in this model. This difference was caused by the lower average temperature in the model of linear temperature rise, because this model did not predict a temperature jump at the entrance of the bed (see Fig. 49). It predicted, therefore, too low temperatures in most parts of the bed. This influence was partly compensated by the higher temperature at the top. However the area S_1 in Fig. 49, which represents the underestimation of the average temperature, was still larger than the

Table 17. Value of K for different rates of heat generation, calculated in different ways.

Q (W/m ³)	Experimental	One-phase	Two-phase product	Two-phase air	Linear temp. rise
18.9	1.74	1.72	1.72	1.69	1.65
50.8	1.80	1.76	1.77	1.71	1.68
105	1.80	1.74	1.76	1.69	1.67
105	1.88	1.85	1.88	1.81	1.79
193	1.98	1.98	2.01	1.93	1.91
274	1.81	1.82	1.86	1.77	1.75
886	1.95	1.94	2.01	1.88	1.87
$\bar{K} \pm \sigma_x$	1.85 ± 0.09	1.83 ± 0.09	1.86 ± 0.11	1.78 ± 0.09	1.76 ± 0.10

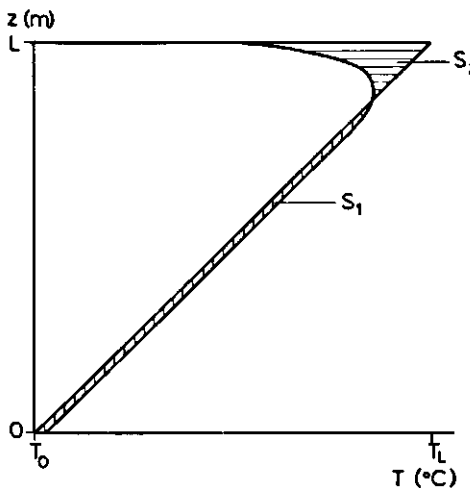


Fig. 49. Axial profile of temperature of the linear temperature rise model and the one-phase or two-phase model.

area S_2 , which represents the overestimation of the average temperature. Therefore the K value from the model of linear temperature rise was lower than the K value from the other models.

The K value from the air temperature of the two-phase model ($K = 1.78$) was used in further calculations. I used the average temperature calculated with a model instead of the measured temperatures, because the average temperature could be calculated more accurately from a formula than from the eight experimental temperatures. The two-phase model was preferred to the other models because it gave the best fit to the experimental temperatures. I used the air temperature instead of the product temperature, because air was the medium that was transported by natural convection.

The Pe-Ra relation To check whether Eqn 2.44, derived from the model of linear temperature rise is able to predict the velocity of natural convection, I calculated the Pe and Ra_1 values for the different measurements. The air density was taken at the average temperature on the central axis of the cylinder. The resulting data are given in Fig. 50 which also shows the curve calculated with Eqn 2.44. The simple relation between Pe and Ra_1 provided a satisfactory description of the velocity of natural convection for different rates of heat generation even though the temperature profile predicted by this model was not the real temperature profile to be expected in the bulk. It is therefore possible to predict the natural convection velocity in a packed bed with a constant rate of heat generation, open top and bottom and adiabatic walls with the relation:

$$Pe = \sqrt{\frac{Ra_1}{2}} = 0.7 \sqrt{Ra_1} \quad (4.23)$$

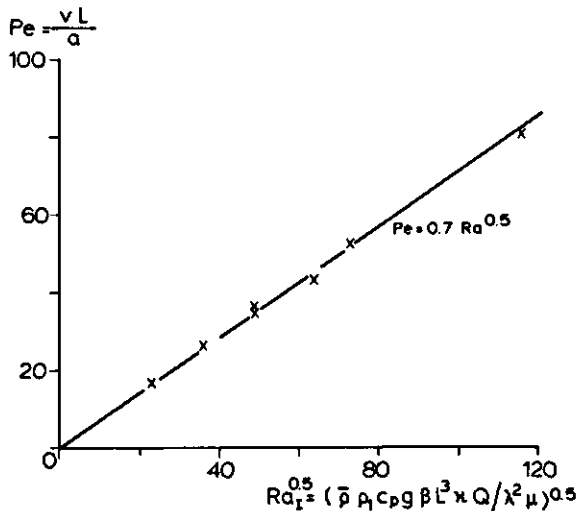


Fig. 50. Experimental Péclet numbers (x) and the theoretical relation between Pe and $Ra_I^{0.5}$.

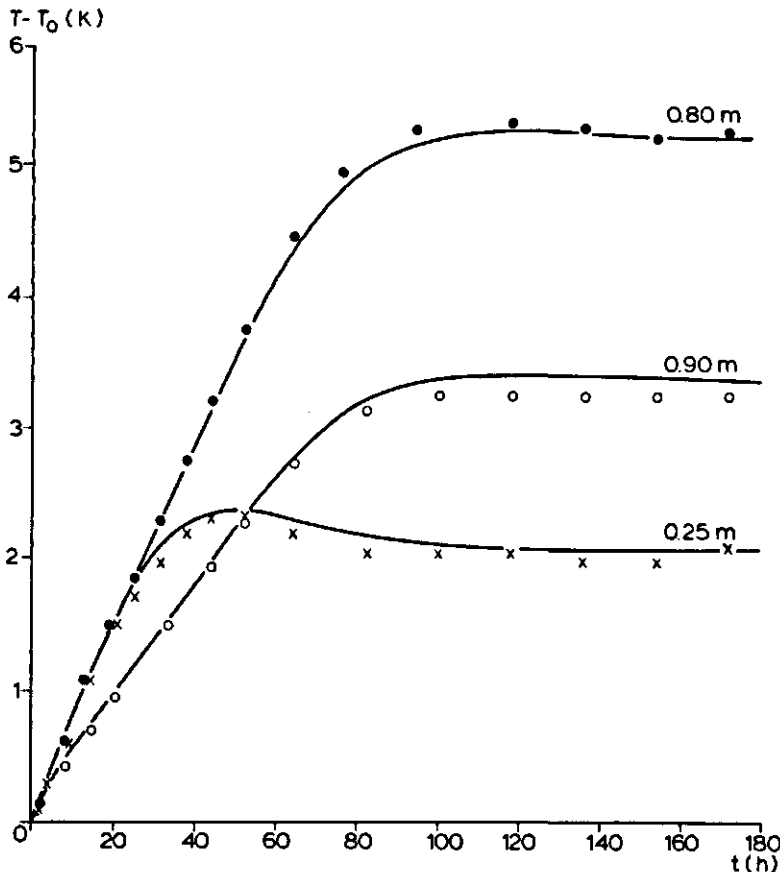


Fig. 51. Measured and calculated (—) temperature changes with time for a rate of heat generation of 51 W/m^3 .

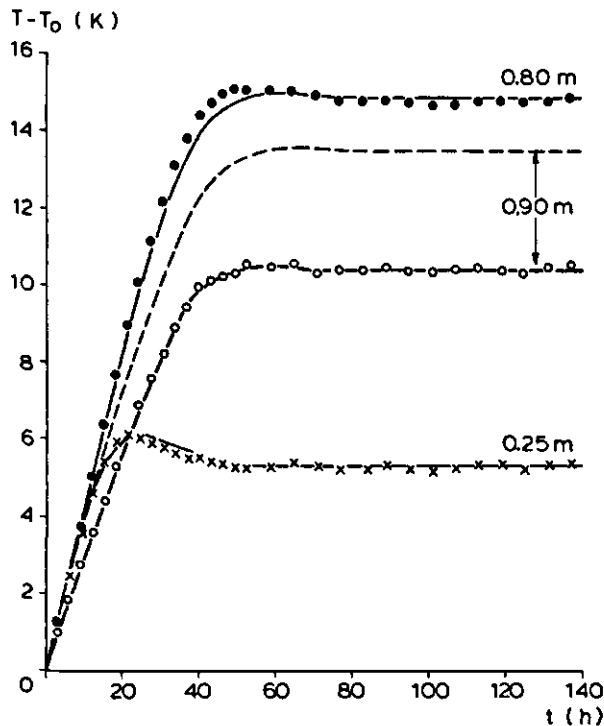


Fig. 52. Measured and calculated (—) temperature changes with time for a rate of heat generation of 274 W/m^3 .
 (---) = heating at $\alpha_L = 0$.

Comparison with the SNC-model The SNC-model, derived in Section 3.2 can also be used to simulate the heating of the cylindrical container with model material. This solution can be obtained without recourse to the mass balance, because of the absence of moisture loss. However it serves as a useful check of the solution to the energy balance in the model approximation. Figs 51 and 52 compare the measured and the calculated temperature rise at a rate of heat generation of 50.8 and 274 Wm^{-3} and heights of 0.25 , 0.80 and 0.90 m . Equation 4.7 is used in calculating α_L . Fig. 52 also shows the heating at 0.90 m with $\alpha_L = 0.0 \text{ Wm}^{-2}\text{K}^{-1}$. The influence of α_L is obvious. The temperatures at 0.25 m and 0.80 m are not influenced by this change in α_L .

These results show that the SNC-model gives a good prediction of the measured temperature course and the steady-state temperature distribution in a cylindrical container filled with model material which has a constant rate of heat generation and no moisture loss.

4.4 Results with model material for closed bottom and pervious top

To get an impression of natural convection in systems with no air flow through the bottom, I closed the bottom of the experimental set-up just under the iron grate with a

polyethylene sheet. The bottom was kept at room temperature by blowing air of room temperature on to the outside of the bottom. The temperature control of the brass shielding was not used during these experiments, because in this type of experiment temperature was not expected to increase linearly with height. The temperature control system would have had an unacceptable influence on the measured temperatures, if it had been applied.

The radial temperature distribution in the steady state at a rate of heat generation of 50.7 W m^{-3} (see Fig. 53) shows different temperatures in different radial directions. There is no radial symmetry in the cylinder. Visualization of the air flow by smoke showed that

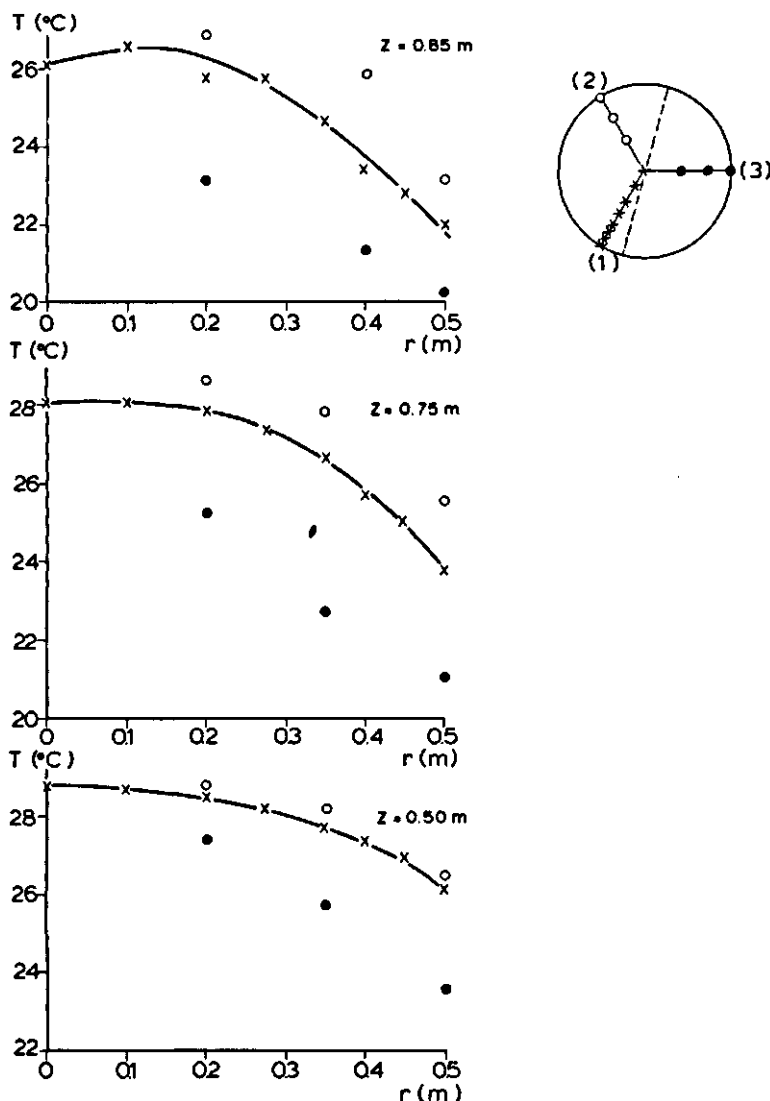


Fig. 53. Radial temperature distribution at $Q = 50.7 \text{ W/m}^3$; bottom closed.

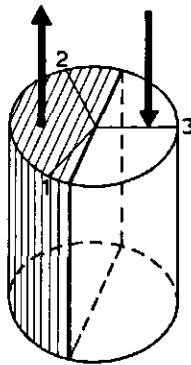


Fig. 54. The air-flow on the top of a cylinder with a closed bottom, 1, 2 and 3 are the three directions of temperature measurements (Fig. 53).

the air was sucked into the container by one half of the top surface and left the container by the other half (see Fig. 54). This kind of air flow pattern could be reproduced after cooling the container to room temperature and reheating. I expect that the existence of this special air distribution is coupled to the experimental set-up. This could have been confirmed by repacking the container or by turning the container. However because of



Fig. 55. Contoured print-plot in measuring direction (1) at $Q = 50.7 \text{ W/m}^3$. Maximum value: $T - T_0 = 9.3^\circ\text{C}$.

the large quantity of work in relation to the minor importance of these results, such experiments were not performed. For the same reason the experiments were not repeated in another temperature-controlled room to investigate the influence of the surroundings.

The pattern of air flow inside the cylinder cannot be derived from the temperature measurements. The gradually changing temperatures in the contoured print-plot at a rate of heat generation of 50.7 Wm^{-3} (Fig. 55) only indicate that there is not much mixing of the air inside the cylinder.

These experiments confirm the difficulties in predicting flows due to natural convection. They indicate only that significant natural convection currents occur in containers with a closed bottom.

4.5 Results with model material for closed bottom and closed top

The influence of natural convection in a completely closed container was investigated by closing the bottom (as described in Section 4.4) and the top of the experimental set-up with a polyethylene sheet. The polyethylene was in direct contact with the model material on the top of the cylinder to give good heat transfer from the top to the surroundings. There was no forced air flow on the outside of the top. Experiments were performed for three different rates of heat generation (9.3, 25.6 and 50.7 Wm^{-3}). Just as in the previous experiments, the temperature control of the wall was not used during these experiments because a linear temperature rise with the height was not expected.

Just as for the open cylinder, the radial symmetry was checked by calculating the relative standard deviation of the temperatures with equal r and z coordinates. The results are given in Table 18. The values of the relative standard deviation are somewhat larger than the values from the open cylinder in Table 13, but the measured temperatures in the main radial direction still give a good impression of the temperature distribution in the closed cylinder.

The dimensionless temperatures ($\theta_Q = (T - T_0) \lambda_0 / QL^2$) along the central axis of the cylinder with different rates of heat generation and a theoretical profile are given in Fig. 56. The theoretical profile is the temperature distribution along the central axis of a finite cylinder with a constant rate of heat generation and for heat transfer by conduction only; $\theta_Q = 0$ at the bottom and the top, and heat losses at the cylinder wall are described by an overall heat transfer coefficient (α_{ov}). The value of α_{ov} follows from the assumption that the resistance to heat loss is complete situated in the insulated cylinder wall. Therefore

Table 18. Relative standard deviation (in %) of temperature with equal r and z coordinates for different rates of heat generation, closed bottom and closed top.

$Q (\text{W/m}^2)$	$z = 0.50 \text{ m}$			$z = 0.75 \text{ m}$			$z = 0.85 \text{ m}$					
	$r (\text{m})$	0.20	0.35	0.50	$r (\text{m})$	0.20	0.35	0.50	$r (\text{m})$	0.20	0.35	0.50
9.3	1.9	6.6	3.3	1.6	4.3	6.6	2.9	6.7	17.7			
25.6	1.2	1.7	4.0	0.8	4.4	4.7	1.3	4.8	16.2			
50.7	1.0	2.7	2.1	2.8	9.1	17.0	2.6	8.8	18.8			

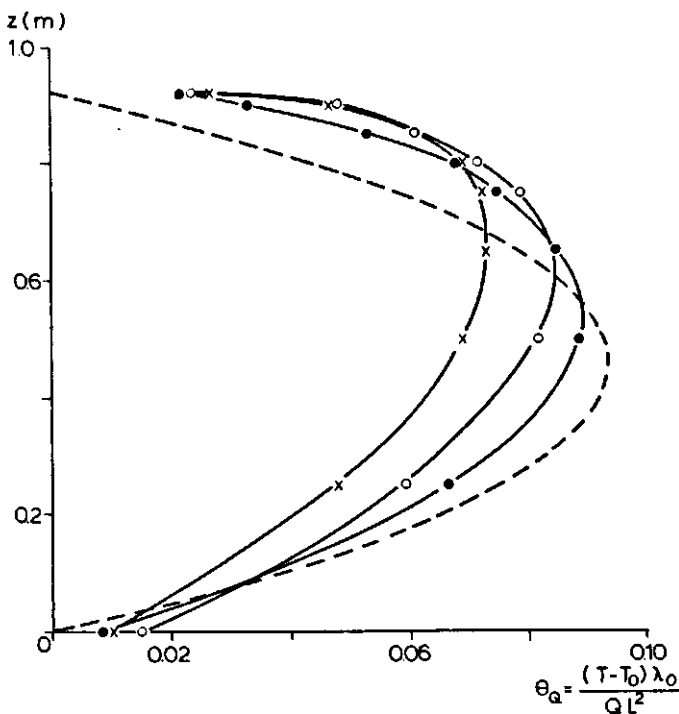


Fig. 56. Temperature profiles along the central axis of the cylinder with different rates of heat generation and the theoretical profile (---) for conduction only.

- $Q = 9.3 \text{ W/m}^3$
- $Q = 25.6 \text{ W/m}^3$
- $Q = 50.7 \text{ W/m}^3$

$\alpha_{ov} = \lambda_{iso}/d_{iso} = 0.5 \text{ W m}^{-2}\text{K}^{-1}$. The theoretical temperature profile was calculated with the SNC-model for the assumption of no moisture loss and no air flow.

The deviations of the measured profiles from the theoretical one were probably caused by natural convection. The temperatures in the steady state along the central axis and also the contoured print-plots of these experiments (Fig. 57) suggest an air movement in the cylinder as given in Fig. 58. The air flows downwards in the vicinity of the cold walls and upwards in the centre of the cylinder. The influence of natural convection increased with increasing rate of heat generation, as is shown by the position of the maximum temperature for different rates of heat generation. At higher rates of heat generation the maximum temperature was situated higher in the cylinder because the air rose faster in the central part of the cylinder.

The measured radial temperature distribution was not the same as the radial temperature distribution in a cylinder without natural convection. As shown in Fig. 57 a comparison of the contoured print-plot of the situation without natural convection with that of the measured temperatures shows differences in the radial temperature gradients. In the upper part of the cylinder warm air moves from the central axis to the wall so that the temperature near the central axis is higher and the radial temperature gradient is steeper than in the theoretical situation. In the lower part of the cylinder cold air moves from the



a



b

Fig. 57. Contoured print-plot in measuring direction (1) at:

- $Q = 9.3 \text{ W/m}^3$; $(T-T_0)_{\max} = 2.6^\circ\text{C}$.
- $Q = 25.6 \text{ W/m}^3$; $(T-T_0)_{\max} = 6.8^\circ\text{C}$.
- $Q = 50.7 \text{ W/m}^3$; $(T-T_0)_{\max} = 11.6^\circ\text{C}$.
- $Q = 50.7 \text{ W/m}^3$; $(T-T_0)_{\max} = 14.9^\circ\text{C}$ (calculated for conduction only and $\alpha_{\text{ov}} = 0.5 \text{ W/m}^2 \text{ K}$).

wall to the central axis. This causes cooling of the central part and a decrease of the radial temperature gradient. Both influences are shown in the contoured print-plots.

The influence of closing the bottom, or the top and the bottom of a container with heat-generating material is shown in Fig. 59. This figure shows the temperature profiles along the central axis of the cylinder in three different systems but at the same rate of heat generation: (1) open bottom and top, (2) closed bottom and open top and (3) closed bottom and top. It is obvious that the open system with least hindrance to natural convection, gives the lowest temperatures. The natural convection helps to keep the temperature low.

C

Fig. 57 (continued)

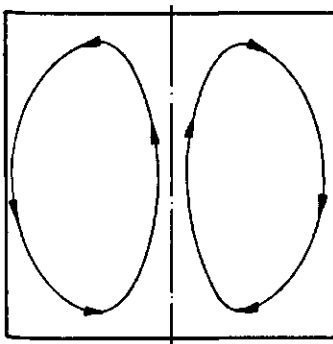


Fig. 58. Air movement in the closed cylinder.

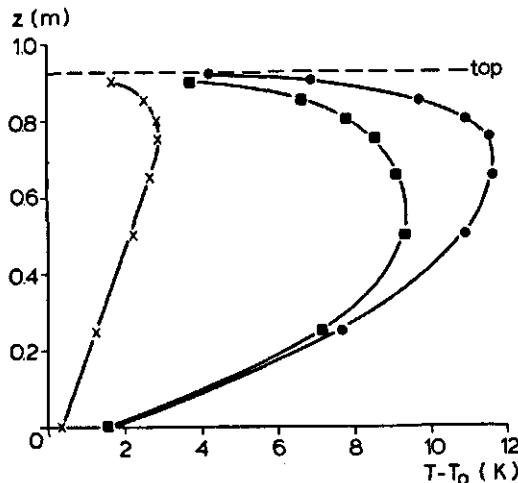


Fig. 59. Distribution of steady-state temperature along the central axis at $Q = 51 \text{ W/m}^3$ in three different systems.

- open bottom and open top;
- closed bottom and open top;
- closed bottom and closed top.

4.6 Results with potatoes for pervious bottom and pervious top

The experiments on the model material provided data on the behaviour of bulk-stored products with a constant rate of heat generation. To compare these experimental results with the behaviour of real products, I performed experiments with the cylindrical set-up, described in Section 4.1, filled with potatoes (variety: Bintje). The main differences between potatoes and model material are the moisture loss and the temperature-dependent rate of heat generation of the potatoes. The physical properties of the potatoes were measured or calculated as given in Appendix B.

The experiments were performed at two relative humidities (RH) of the cooling air: 78% and 96%. The temperature control system of the measuring room produced a gradual cyclic change of the RH between a maximum and a minimum value with a period of 20 minutes. The given RH value was the average of the measured RH . The RH was measured with a psychrometer. At 96% the RH ranged between 93 and 99% and at 78% between 76 and 80%.

The radial temperature distribution in the cylinder at $RH = 96\%$ was checked at $z = 0.36 \text{ m}$ and 0.80 m . There was a good radial symmetry at 0.36 m . The measured temperatures at the same r and z coordinate differed less than $0.1 \text{ }^\circ\text{C}$. The symmetry was less perfect at 0.80 m . At this height the maximum value of the temperature was not situated along the central axis, but in measuring direction (1), 0.05 m from the central axis. See Fig. 60. This disturbance may have been caused by a radial air flow in the upper part of the cylinder or by a disturbance of the temperature profile at the top due to the rising air mixing with the outside air. The disturbed temperature profile at the top, of course, influences the temperature distribution underneath.

Fig. 61 shows the measured steady-state temperature distribution along the central

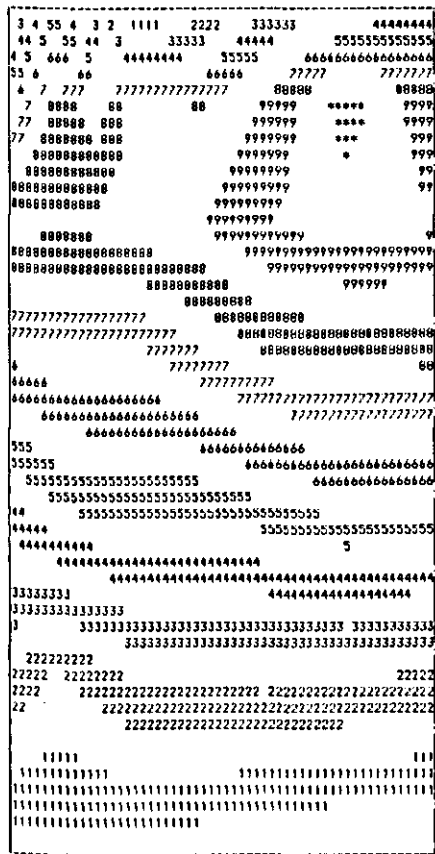


Fig. 60. Contoured print-plot of the distribution of steady-state temperature of potatoes at $RH = 90\%$. Maximum value $T - T_0 = 1.8^\circ\text{C}$.

axis for the two relative humidities. At a RH of 96% the shape of the temperature profile is similar to the measured profile for the model material (Fig. 40). At a lower RH the bulk cooling due to moisture loss from the products became much more important. In the lower part of the bulk the largest moisture loss occurred and therefore much heat was needed to evaporate the water. Because this amount of heat, required for evaporation, even exceeded the rate of heat generation, the product was cooled below the ambient temperature, resulting in a temperature decrease with height. Rising through the bulk the air became more and more saturated and as a result the moisture loss of the product was less at greater height and therefore less heat was required for evaporation. The relative influence of the heat generation thus became more important in the middle region; a temperature increase instead of a decrease with the height resulted. In the top region of the container heat losses due to radiation and air mixing became larger than the heat generated and the temperature again decreased with increasing height.

A lower RH of the ambient air gave a lower average temperature in the cylinder. Therefore the driving force of natural convection was smaller and the velocity of natural convection was smaller too. This is shown in Fig. 61 by the larger temperature gradient for a lower RH (2.6 and 3.1°C m^{-1} at $RH = 96$ and 78% , respectively).

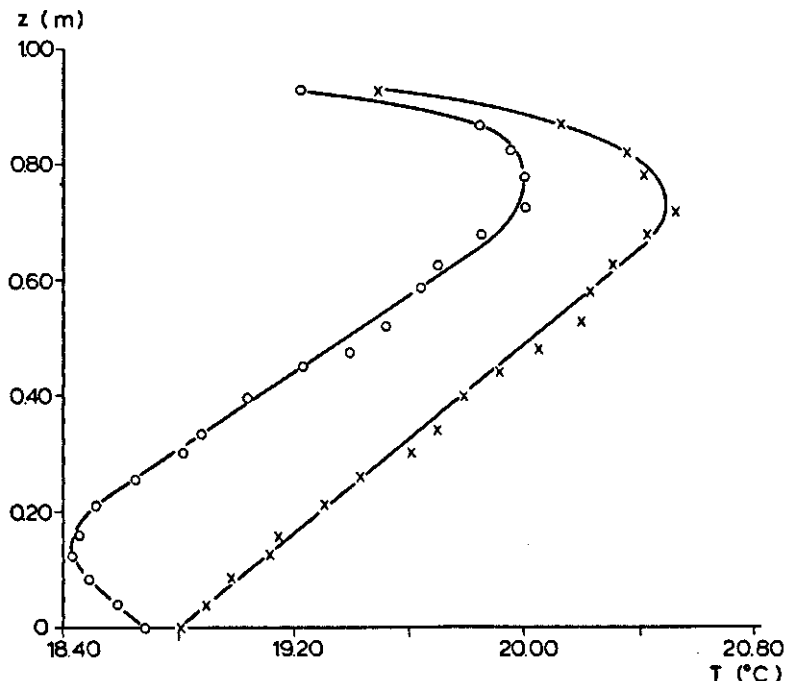


Fig. 61. Distribution of measured steady-state temperature along the central axis of the cylinder with potatoes at a RH of 78% (○) and 96% (x).

In Section 4.3, describing the results of the experiments with the model material, I calculated the natural convection velocity directly from the value of the slope of the measured linear temperature profile and the rate of heat generation. This procedure cannot be used to calculate the velocity of natural convection in these experiments. The potatoes lose moisture by vaporization of water. The required heat of vaporization is withdrawn from the potatoes. Therefore the steady-state sensible heat transferred from the potatoes to the air is lowered by vaporization. The rate of heat generation, which should be used in Eqn 4.4 to calculate v_{NC} , therefore is not the measured rate of heat generation of the potatoes, but the difference between the rate of heat generation and the heat lost by the evaporation of water. However the amount of water evaporating at the different heights cannot be derived from the measurements. This I used the SNC-model (given in Chapter 3) to calculate the velocity of natural convection.

The calculations were also performed to compare the measured temperature rise with the calculated values, starting from the measured initial temperature distribution. Table 19 summarizes the calculated velocity of natural convection and the value of $r\delta$ which at $\gamma = 0.10$ gives a good fit of the measured and the calculated steady-state profile of temperature. The increase of v_{NC} with increasing RH , as derived from Fig. 61, was confirmed by these calculations. The decrease of $r\delta$ with decreasing RH was also found by Fockens (1967) for apples and by Villa (1974) for apples and potatoes.

Fig. 62 gives the measured and the calculated temperature course at $RH = 96\%$ and heights of 0.16, 0.36, 0.55 and 0.85 m. The comparison of the measured and the calcu-

Table 19. Value of v_{NC} and $r\delta$ giving a good fit of the calculated temperatures to the measured temperatures at $\gamma = 0.10$ and for different RH .

RH (%)	v_{NC} (m/s)	$r\delta$ (m)
96	0.0029	0.005
78	0.0020	0.028

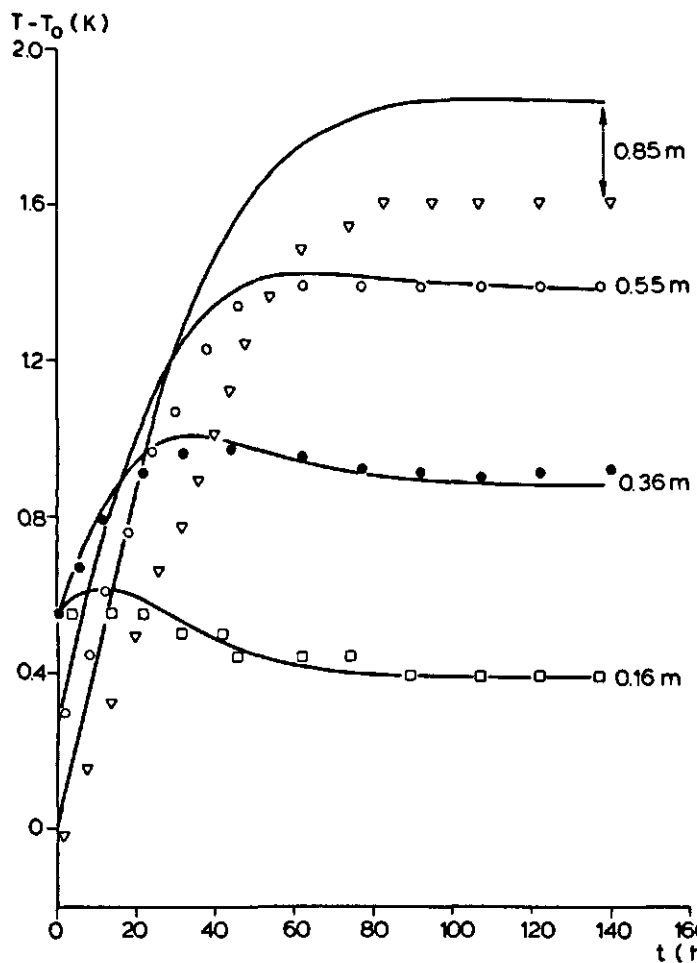


Fig. 62. Measured and calculated heating at different distances along the central axis of the cylinder with potatoes.

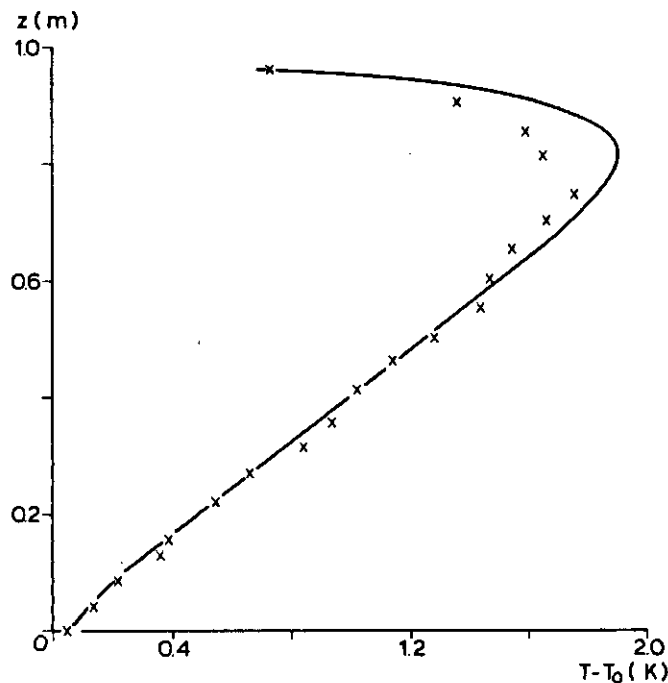


Fig. 63. Measured (x) and calculated (—) steady-state temperature distribution along the central axis of the cylinder with potatoes ($RH = 96\%$).

lated temperatures shows that the SNC-model is not able to predict the measured temperature course in the upper part of the cylinder correctly. See Fig. 63. The measured and the calculated temperature profiles are different above a height of about 0.75 m. This difference may be caused by the measured disturbance of the radial symmetry of the temperature in the upper part of the cylinder, as already discussed. Because the SNC-model assumes radial symmetry it is impossible to predict the measured temperatures exactly with the SNC-model, but a good impression of the temperature development is still obtained. ment is still obtained.

In fig. 62 the calculated temperature-time curve at a height of 0.85 m shows a sudden change in temperature rise after 32 h. This can be explained as follows. Because of the lower temperatures in the upper part of the cylinder at the start of the experiments, the calculation predicts condensation in this part. The condensation causes a faster temperature rise than in the lower part, because the heat of condensation also heats the potatoes. At a height of 0.85 m condensation stops after 32 h. Hereafter the condensed water film on the product surface evaporates. The evaporation from the free water film is much faster than the moisture loss from the inside of the potatoes. Therefore much heat produced by the respiration of the potatoes is used to evaporate the water. As a result less heat is available to heat the potatoes as can be seen from the rather slow temperature rise at a height of 0.85 m from 32 to 35 h. When the water film on the product surface is completely evaporated, moisture loss from the inside of the potatoes starts. This evapora-

tion is much more restricted and the resulting temperature rise of the potatoes is therefore faster again, but still less than during the condensation period.

In the steady state the calculations predict condensation at the top of the cylinder above a height of 0.95 m. Visual inspection during the experiment showed condensation above a height of 0.90 to 0.95 m. In the top layer the condensation was not visible on the upper side of the potatoes but only on the under side. Probably the mixing of the surrounding air and the air rising through the cylinder lowers the *RH* around the upper side of a potato and prevents condensation on the upper side.

An example of the influence of the internal mass transfer coefficient on the temperature profile at a *RH* of 78% is shown in Fig. 64. A lower value of $r\delta$ gives more evaporation and therefore lower temperatures. Fig. 64 also shows a good fit of the measured and the calculated temperatures at $r\delta = 0.028$ m and $\gamma = 0.10$, except at the top and the bottom of the cylinder. The deviation at the top has already been discussed. The deviation at the bottom may be caused by radiation from the warmer floor to the bottom of the cylinder. This influence is not incorporated in the boundary condition at the bottom.

Lowering the relative humidity of the air leads to a more intensive cooling in the lower part of the cylinder and a decrease in average temperature. When the average temperature becomes lower than the temperature of the surroundings, the air flow will invert and

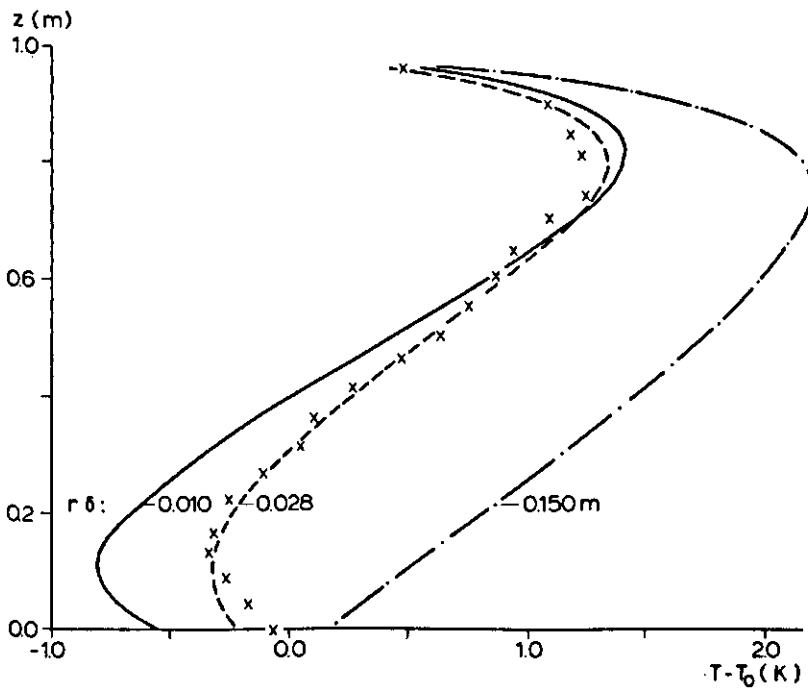


Fig. 64. Measured (x) and calculated temperature profile along the central axis of a cylinder filled with potatoes with a relative humidity of the ambient air of 78%.

- $r\delta = 0.010$ m
- - - $r\delta = 0.028$ m
- ... $r\delta = 0.150$ m.

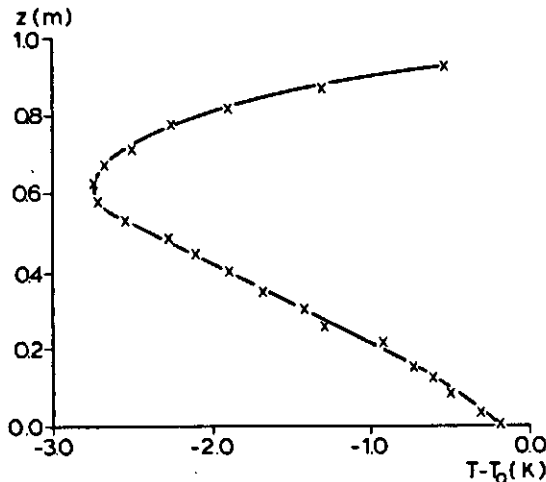


Fig. 65. Measured temperature distribution along the central axis of the cylinder with potatoes at $RH = 40\%$.

move downwards through the cylinder instead of upwards. Fig. 65 shows the measured steady-state temperature distribution along the central axis of the cylinder at a RH of 40%. It is obvious that the average temperature is below the temperature of the surroundings and consequently air flow should be downwards. The use of smoke to visualize the air flow confirmed the downward movement of the air.

5 Application to cooling in closed containers

In order to make a good design of a cold store for conductive cooling of produce, it is important to know the cooling rate of the produce. When a container is cooled fast, much heat is transferred from the container to the cold store. Therefore a large cooling capacity of the cold store is necessary to keep the temperature of the cold store constant. It is also important to know the maximum temperature of the produce in the container to predict the maximum storage period of the products. Different models have been developed to calculate cooling rate and temperature but none of these models includes the influence of natural convection, even though natural convection always occurs during conductive cooling of containers: relatively warm containers are placed in a cold store. As the container walls cool down, temperatures at the walls become lower than in the centre of the container. Because of this temperature difference the air will move downwards near the wall and upwards in the centre.

The influence of natural convection on cooling closed containers with heat-generating produce is discussed in this chapter. However first I will review various conductive cooling models.

5.1 Conductive cooling models

The development of temperature in solid material of simple geometry (infinite plate, infinite cylinder, sphere) with a constant rate of heat generation is given in different text-books (e.g. Carslaw & Jaeger, 1959; Luikov, 1968). The temperature at different times and positions is obtained by solving the energy equation:

$$\rho c_p \frac{dT}{dt} = \lambda \nabla^2 T + Q \quad (5.1)$$

with the appropriate boundary conditions. In the literature different kinds of boundary conditions at the wall are discussed: constant temperature (boundary condition of the first kind), given heat flux (boundary condition of the second kind) though not very important for the present problem, or heat losses to be described with a heat transfer coefficient (boundary condition of the third kind). Luikov discussed the analytical solutions for heat sources dependent on time and distance (exponential, power series).

The cooling of an infinite slab with a temperature-dependent rate of heat generation (exponential) was calculated numerically by Gögüs et al. (1972). The boundary condition at the wall is a boundary condition of the third kind. They introduced the rate of heat generation at different temperatures as:

$$Q = A e^{BT} \quad (5.2)$$

where A and B are product-dependent constants and T is the temperature in K. They determined A and B by fitting the rate of heat generation to different temperatures of various fruits and vegetables. However when their values of A and B are used, the calculated rate of heat generation is much too low. There must be some error in their calculation of A and B .

Gonlag (1975) calculated the cooling rate of heat-generating infinite cylinders numerically. He also used a boundary condition of the third kind at the wall. His equation to calculate the heat generation is the Arrhenius type equation:

$$Q = Q_0 e^{-\frac{Q_1}{T}} \quad (5.3)$$

This type of heat generation equation is also used by Eelkman Rooda & van Beckum (1978) who calculated the cooling of infinite slab, infinite cylinder and sphere with a boundary condition of the third kind at the wall. They also discussed the numerical stability of the implicit scheme used in their calculations. They concluded that the implicit scheme is stable when the rate of heat generation of the produce is not so large that it gives a continuous increase of the temperature within the container dimensions used.

When the constants A and B or Q_0 and Q_1 in Eqn 5.2 or 5.3 are calculated by fitting these equations to measured heat generation data at different temperatures, the rate of heat generation may be calculated with Eqn 5.2 or 5.3. As shown in Table 20, giving the measured and calculated rate of heat generation of tomatoes, the calculated rates of heat generation never differ more than 3% in the temperature range of 0-20 °C. Because of the much larger differences in the experimental data, both equations are suitable for calculating the rate of heat generation. However, because of the physical nature of the Arrhenius-type equation (5.3), this equation should be preferred for describing the temperature dependence of the rate of heat generation.

Yavuzkurt et al. (1976) repeated the calculation of the temperature distribution in an infinite slab with a temperature-dependent rate of heat generation (given by Eqn 5.2) but also incorporated the influence of evaporative cooling. They accounted for the cooling effect by evaporation with an additional negative term for rate of heat generation (the rate of moisture loss times the heat of vaporization) in the differential equation. The mass

Table 20. Measured (Sprenger Institute, 1972) and calculated (Eqns 5.2 and 5.3) heat generation of tomatoes.

Temperature (°C)	Measured data (W/kg)	Average (W/kg)	Q from (5.2) (W/kg)	Q from (5.3) (W/kg)
0	0.014-0.018	0.016	0.0145	0.0143
2	0.016-0.020	0.018	0.0176	0.0175
5	0.020-0.022	0.021	0.0234	0.0236
10	0.031-0.041	0.036	0.0376	0.0382
15	0.053-0.087	0.070	0.0604	0.0609
20	0.080-0.102	0.091	0.0972	0.0955

balance equation was solved taking into account the terms for moisture transport by diffusion, evaporation from the product surface and moisture accumulation. They presented only calculated data of the temperature and moisture distribution after cooling a short period (10 h). Then the steady state was not attained at all and therefore it is difficult to draw any conclusion from their data.

Besides numerical solutions of the energy and mass balance equations to describe the cooling of horticultural produce, analytical solutions are also proposed in the literature. Meffert & Potters (1970) used the analytical solution of the heating of a cube with a constant rate of heat generation (Carslaw & Jaeger, 1959) to reproduce the experimental heating of model material and horticultural products (apples and tomatoes). The comparison between calculated data and experiments indicated the need of incorporating the influence of evaporative heat losses in the energy equation.

Meffert & Rudolphy (1972) used the solutions of Luikov (1968) of the temperature distribution at a constant rate of heat generation to predict cooling or heating of different kinds of produce in containers with different geometries. The occurrence of either cooling or heating when a container is placed in a cold store, is determined by the temperature dependence of the rate of heat generation. Heat generation causes temperature rise. At the higher temperature the rate of heat generation is higher. As long as the amount of heat generated is higher than the heat lost to the surroundings a self-heating process results, accelerating temperature rise and decomposition of the produce.

The prediction of heating or cooling is further extended by using the safe radius concept. The safe radius was described by Van Geel (1966) to predict selfignition of hazardous material. The safe radius of a heat-generating material was defined as the distance from the centre to the wall which keeps the steady-state temperature within a given limit. Meffert & Van Beek (1976) applied this concept to predict the container dimensions with which there is no overheating of the product. For the calculation of the safe radius, the rate of heat generation at the maximum temperature is assumed at every position in the container. Correction for evaporative heat losses is given by subtracting the amount of heat lost by evaporation from the amount of heat generated.

5.2 Conductive cooling of a parallelepiped with a constant rate of heat generation

In a rectangular parallelepiped (drawn in Fig. 66) with a uniform and constant rate of internal heat generation and heat transport by conduction only, the energy equation can be written as:

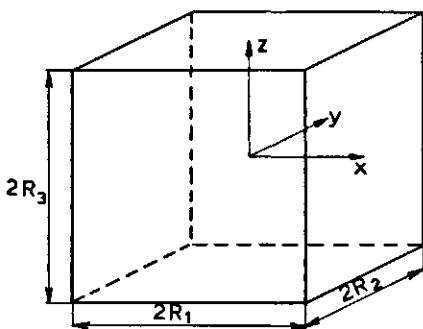


Fig. 66. The rectangular parallelepiped.

$$(\rho c_p)_m \frac{\partial T}{\partial t} = \lambda_0 \left(\frac{\partial^2 T}{\partial x^2} + \frac{\partial^2 T}{\partial y^2} + \frac{\partial^2 T}{\partial z^2} \right) + Q \quad (5.4)$$

The initial and boundary conditions, which describe a uniform initial temperature distribution, a constant temperature at the wall and symmetry around yz , xz and xy planes are:

$$t = 0, \forall (x, y, z): \quad T = T_s \quad (5.5)$$

$$t > 0, \forall (y, z), x = 0: \quad \frac{\partial T}{\partial x} = 0 \quad \text{and } x = R_1: \quad T = 0 \quad (5.6)$$

$$\forall (x, z), y = 0: \quad \frac{\partial T}{\partial y} = 0 \quad \text{and } y = R_2: \quad T = 0 \quad (5.7)$$

$$\forall (x, y), z = 0: \quad \frac{\partial T}{\partial z} = 0 \quad \text{and } z = R_3: \quad T = 0 \quad (5.8)$$

Equation (5.4) may be solved by separating T in two contributing functions $T_1 (x, y, z, t)$ and $T_2 (x, y, z, t)$:

$$T = T_1 + T_2 \quad (5.9)$$

Substitution of Eqn 5.9 in Eqn 5.4 gives:

$$\begin{aligned} a \left(\frac{\partial^2 T_1}{\partial x^2} + \frac{\partial^2 T_1}{\partial y^2} + \frac{\partial^2 T_1}{\partial z^2} \right) - \frac{\partial T_1}{\partial t} &= -a \left(\frac{\partial^2 T_2}{\partial x^2} + \frac{\partial^2 T_2}{\partial y^2} + \frac{\partial^2 T_2}{\partial z^2} \right) \\ &\quad - \frac{Q}{(\rho c_p)_m} + \frac{\partial T_2}{\partial t} \end{aligned} \quad (5.10)$$

The boundary conditions (5.5)-(5.8) are also separated in two parts. The boundary conditions of T_1 :

$$t = 0, \forall (x, y, z): \quad T_1 = T_s \quad (5.11)$$

$$t > 0, \forall (y, z), x = 0: \quad \frac{\partial T_1}{\partial x} = 0 \quad \text{and } x = R_1: \quad T_1 = 0 \quad (5.12)$$

$$\forall (x, z), y = 0: \quad \frac{\partial T_1}{\partial y} = 0 \quad \text{and } y = R_2: \quad T_1 = 0 \quad (5.13)$$

$$\forall (x, y), z = 0: \quad \frac{\partial T_1}{\partial z} = 0 \quad \text{and } z = R_3: \quad T_1 = 0 \quad (5.14)$$

The boundary conditions of T_2 :

$$t = 0, \forall (x, y, z): \quad T_2 = 0 \quad (5.15)$$

$$t > 0, \forall (y, z), x = 0: \quad \frac{\partial T_2}{\partial x} = 0 \quad \text{and } x = R_1: \quad T_2 = 0 \quad (5.16)$$

$$\forall (x, z), y = 0: \quad \frac{\partial T_2}{\partial y} = 0 \quad \text{and } y = R_2: \quad T_2 = 0 \quad (5.17)$$

$$\forall (x, y), z = 0: \quad \frac{\partial T_2}{\partial z} = 0 \quad \text{and } z = R_3: \quad T_2 = 0 \quad (5.18)$$

Because the left side and right side of Eqn 5.10 are arbitrary functions of the independent variables x, y, z and t , they can only be equal if they are constant, e.g. equal to C_1 . Therefore the solution of Eqn 5.10 should satisfy:

$$a \left(\frac{\partial^2 T_1}{\partial x^2} + \frac{\partial^2 T_1}{\partial y^2} + \frac{\partial^2 T_1}{\partial z^2} \right) - \frac{\partial T_1}{\partial t} = C_1 \quad (5.19)$$

$$a \left(\frac{\partial^2 T_2}{\partial x^2} + \frac{\partial^2 T_2}{\partial y^2} + \frac{\partial^2 T_2}{\partial z^2} \right) + \frac{Q}{(\rho c_p)_m} - \frac{\partial T_2}{\partial t} = C_1 \quad (5.20)$$

A particular solution of Eqn 5.19 is:

$$T_1 = -C_1 t \quad (5.21)$$

The reduced equation of Eqn 5.19 with initial and boundary conditions (5.11)-(5.14) describes the well-known cooling of a rectangular parallelepiped. The solution is given in many text-books on heat transfer (e.g. Carslaw & Jaeger, 1959; Luikov, 1968):

$$T_1(x, y, z, t) = \frac{64}{\pi^3} T_s \sum_{l=0}^{\infty} \sum_{m=0}^{\infty} \sum_{n=0}^{\infty} \left[\frac{(-1)^{l+m+n}}{(2l+1)(2m+1)(2n+1)} \cos\left(\frac{(2l+1)\pi x}{2R_1}\right) \right. \\ \left. x \cos\left(\frac{(2m+1)\pi y}{2R_2}\right) \cos\left(\frac{(2n+1)\pi z}{2R_3}\right) e^{-bt} \right] \quad (5.22)$$

where

$$b = \frac{\pi^2}{4} a \left(\frac{(2l+1)^2}{R_1^2} + \frac{(2m+1)^2}{R_2^2} + \frac{(2n+1)^2}{R_3^2} \right) \quad (5.23)$$

From the requirement that the temperature T_1 must be finite at large times, it may be concluded that $C_1 = 0$. Therefore the solution of the reduced equation is also the solution of Eqn 5.19.

The solution of Eqn 5.20 with boundary conditions (5.15)-(5.18) with $C_1 = 0$, is given by Carslaw & Jaeger (1959):

$$\begin{aligned}
T_2(x,y,z,t) = & \frac{256Q}{\pi^5 \lambda_0} \sum_{l=0}^{\infty} \sum_{m=0}^{\infty} \sum_{n=0}^{\infty} \left[\frac{(-1)^{l+m+n}}{(2l+1)(2m+1)(2n+1)} \cos\left(\frac{(2l+1)\pi x}{2R_1}\right) \right. \\
& \times \cos\left(\frac{(2m+1)\pi y}{2R_2}\right) \cos\left(\frac{(2n+1)\pi z}{2R_3}\right) \\
& \left. \frac{1-e^{-bt}}{\frac{(2l+1)^2}{R_1^2} + \frac{(2m+1)^2}{R_2^2} + \frac{(2n+1)^2}{R_3^2}} \right] \quad (5.24)
\end{aligned}$$

Therefore the solution of Eqn 5.4 is:

$$\begin{aligned}
T = T_1 + T_2 = & \frac{64}{\pi^3} \sum_{l=0}^{\infty} \sum_{m=0}^{\infty} \sum_{n=0}^{\infty} \left[\frac{(-1)^{l+m+n}}{(2l+1)(2m+1)(2n+1)} \cos\left(\frac{(2l+1)\pi x}{2R_1}\right) \right. \\
& \times \cos\left(\frac{(2m+1)\pi y}{2R_2}\right) \cos\left(\frac{(2n+1)\pi z}{2R_3}\right) \left(T_s e^{-bt} + \right. \\
& \left. \left. \frac{Q}{(\rho c_p)_m b} (1-e^{-bt}) \right) \right] \quad (5.25)
\end{aligned}$$

Fig. 67 presents T_1 , T_2 and T at $x = 0$, $y = 0$ and $z = 0$ calculated with a rate of heat generation of 235 Wm^{-3} and the data of Table 21.

It follows from Eqn 5.25 that the maximum temperature in the steady state is the centre temperature of the parallelepiped:

$$T_{\max} = \frac{256Q}{\pi^5 \lambda_0} \sum_{l=0}^{\infty} \sum_{m=0}^{\infty} \sum_{n=0}^{\infty} \left[\frac{(-1)^{l+m+n}}{(2l+1)(2m+1)(2n+1) \left[\frac{(2l+1)^2}{R_1^2} + \frac{(2m+1)^2}{R_2^2} + \frac{(2n+1)^2}{R_3^2} \right]} \right] \quad (5.26)$$

Tchumak et al. (1970) gave the maximum temperature in a rectangular parallelepiped with a constant rate of heat generation and dimensions $l_1 \times l_2 \times l_3$:

$$T_{\max} = \frac{Ql_3^2}{\lambda_0} C_1 \quad (5.27)$$

In this equation l_3 is the smallest side of the parallelepiped. They only gave a graph of C_1 as a function of l_3/l_1 and l_3/l_2 . However the data of this graph can be calculated with Eqn 5.26.

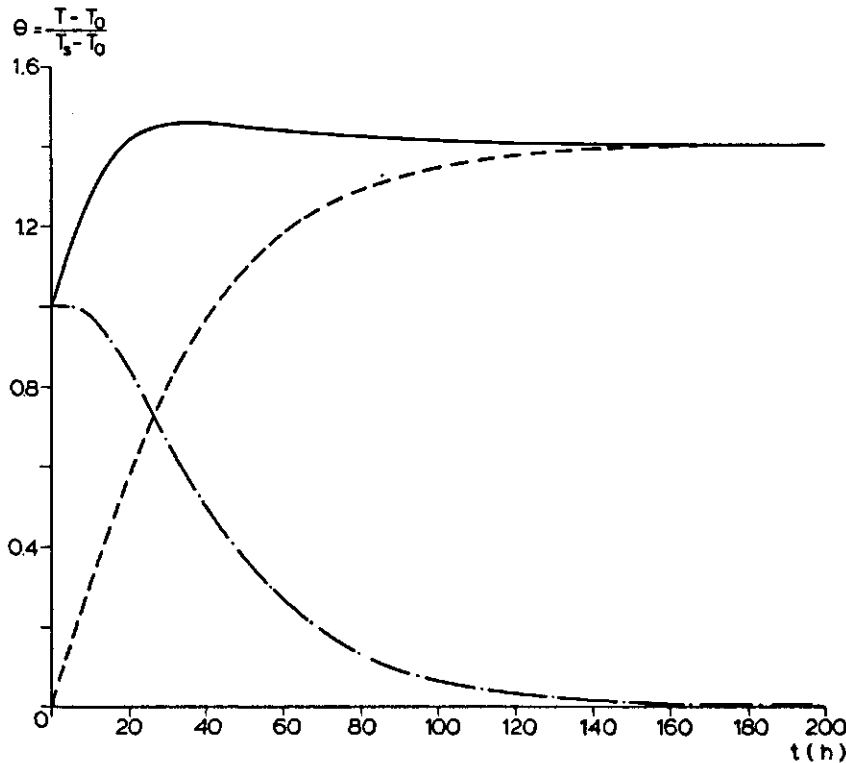


Fig. 67. Changes in temperature with time at $x = 0, y = 0$ and $z = 0$ of T_1 (---), T_2 (---) and T (—), $Q = 235 \text{ W/m}^3$.

Table 21. Data used in the calculations.

Bulk thermal conductivity (λ_b)	0.25 W/mK
Heat capacity air ($(\rho c_p)_a$)	1230 J/m ³ K
Heat capacity medium ($(\rho C_p)_m$)	$2.30 \times 10^6 \text{ J/m}^3\text{K}$
Porosity (ϵ)	0.378
Heat generation (Q)	60 W/m ³
Permeability (κ)	$1.45 \times 10^{-6} \text{ m}^2$
Heat transfer coefficient at bottom top and side walls ($\alpha_b, \alpha_t, \alpha_{sw}$)	1000 W/m ² K
Initial temperature (T_s)	28.75 °C
Wall temperature (T_0)	19.2 °C
Length (R_1)	0.38 m
Width (R_2)	0.38 m
Height (L_z)	0.50 m

5.3 Model of three-dimensional natural convection in a porous medium with heat generation

5.3.1 Derivation of the model equations

To describe the cooling or heating of containers with respiring produce mathematically, the bulk in the container is considered to be a porous medium. The temperature distribution can be described with a one-phase model. At the walls of the container the heat transfer to the surroundings is described with an overall heat transfer coefficient.

The mathematical formulation of natural convection in a porous medium with internal heat generation is given by the continuity equation, the equations of motion and the energy equation (see Section 2.1):

Continuity equation:

$$\nabla \cdot \vec{v} = 0 \quad (5.28)$$

Equation of motion:

$$\rho \frac{\partial \vec{v}}{\partial t} = -\nabla P + \rho_r [1 - \beta(T - T_r)] \vec{g} - \frac{\mu}{\kappa} \vec{v} \quad (5.29)$$

Energy equation:

$$(\rho c_p)_m \frac{\partial T}{\partial t} + (\rho c_p)_s \vec{v} \cdot \nabla T = \lambda_0 \nabla^2 T + Q \quad (5.30)$$

Aziz & Hellums (1967) showed that in a fluid-filled parallelepiped elimination of pressure in the equation of motion leads to a set of equations which are solved more easily than the original set of equations. Holst & Aziz (1972b) showed that this elimination may also be applied for a porous medium. Pressure is eliminated by the vector potential-vorticity method. Vector potential ($\vec{\psi}$) and vorticity (\vec{O}) are defined by

$$\vec{v} = \nabla \times \vec{\psi} \quad (5.31)$$

$$\vec{O} = \nabla \times \vec{v} \quad (5.32)$$

The vector potential may be looked upon as the three-dimensional extension of the two-dimensional stream function. Hirasaki & Hellums (1968) showed that, when \vec{v} is solenoidal ($\nabla \cdot \vec{v} = 0$), $\vec{\psi}$ exists and is solenoidal too. The equation of continuity (5.28) shows that \vec{v} is solenoidal and therefore also $\vec{\psi}$ is solenoidal. This property of the vector potential combined with the definition of the vorticity leads to:

$$\vec{O} = \nabla \times \vec{v} = \nabla \times (\nabla \times \vec{\psi}) = -\nabla^2 \vec{\psi} \quad (5.33)$$

Analysis of Eqns 5.29 and 5.30 showed that velocity attained the steady state much faster than temperature. Therefore, being interested in the temperature course, the time derivative of \vec{v} may be neglected in Eqn 5.29. This yields:

$$\vec{v} = -\frac{\kappa}{\mu} \left(\nabla P - \rho_r [1 - \beta(T - T_r)] \vec{g} \right) \quad (5.34)$$

Because $\nabla \times \nabla P = 0$ the vorticity is:

$$\vec{\Omega} = \frac{\kappa}{\mu} \nabla \times (\rho_r [1 - \beta(T - T_r)] \vec{g}) = -\frac{\kappa}{\mu} \nabla \times (\rho_r \beta T \vec{g}) \quad (5.35)$$

Combination of Eqns 5.33 and 5.35 with $\vec{g} = g(0, 0, -g)$ yields:

$$\nabla^2 \psi_x = -\frac{\kappa}{\mu} \frac{\partial}{\partial y} (\rho_r g \beta T) \quad (5.36)$$

$$\nabla^2 \psi_y = -\frac{\kappa}{\mu} \frac{\partial}{\partial x} (\rho_r g \beta T) \quad (5.37)$$

$$\nabla^2 \psi_z = 0 \quad (5.38)$$

The boundary conditions of this set of equations are given by the system: a rectangular parallelepiped with the walls which are impervious to fluid flow (see Fig. 68). Because of the symmetry in the parallelepiped the governing equations need only to be solved in a quarter of the parallelepiped. The quarter of interest is indicated in Fig. 68. The centre of the coordinate system is located in the centre of the parallelepiped. The bottom, right side, back and top are rigid and therefore the fluid velocity is zero at these walls. At the left side and front fluid flow is possible.

Hirasaki & Hellums (1968) derived the boundary conditions of the vector potential on the walls without fluid flow:

$$x = R_1 \quad : \quad \frac{\partial \psi_x}{\partial x} = \psi_y = \psi_z = 0 \quad (5.39)$$

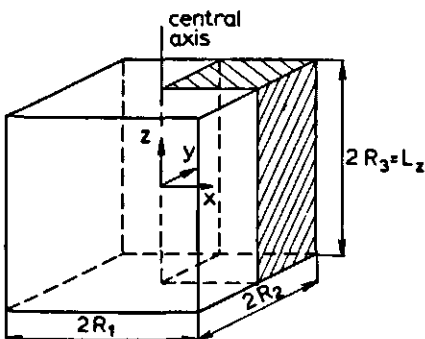


Fig. 68. The rectangular parallelepiped with the coordinate centre, the dimensions and the quarter of interest.

$$y = R_2 \quad : \quad \psi_x = \frac{\partial \psi_y}{\partial y} = \psi_z = 0 \quad (5.40)$$

$$z = -R_3, R_3 \quad : \quad \psi_x = \psi_y = \frac{\partial \psi_z}{\partial z} = 0 \quad (5.41)$$

Equation 5.38 with boundary condition (5.41) gives:

$$\psi_z = 0 \quad (5.42)$$

The boundary conditions of ψ_x and ψ_y are completed with the symmetry conditions:

$$x = 0 \quad : \quad \frac{\partial \psi_x}{\partial x} = 0, \quad \psi_y = 0 \quad (5.43)$$

$$y = 0 \quad : \quad \psi_x = 0, \quad \frac{\partial \psi_y}{\partial y} = 0 \quad (5.44)$$

By solving the coupled differential equations (5.30), (5.36) and (5.37) with appropriate boundary conditions, the temperature and velocity at different times and different locations in the container may be calculated. However this set of equations contains two elliptic differential equations of which the numerical solution is very computer-time consuming. Tveitereid (1977, 1978) introduced the velocity potential (V), which reduces the two elliptic differential equations to one. He defined the velocity potential only in terms of velocity:

$$v_x = \frac{\partial^2 V}{\partial x \partial z} \quad (5.45)$$

$$v_y = \frac{\partial^2 V}{\partial y \partial z} \quad (5.46)$$

$$v_z = - \left(\frac{\partial^2 V}{\partial x^2} + \frac{\partial^2 V}{\partial y^2} \right) \quad (5.47)$$

One of the above mentioned equations is not necessary for defining V , because, when two of these equations are given, the third relation can be derived from the continuity equation (5.28).

There exist, of course, relations between velocity potential and vector potential:

$$\psi_x = \frac{\partial V}{\partial y} \quad (5.48)$$

$$\psi_y = - \frac{\partial V}{\partial x} \quad (5.49)$$

With these relations Eqns 5.36 and 5.37 may be reduced to:

$$\nabla^2 V = -\frac{\rho_r g \beta \kappa}{\mu} (T - T_r) \quad (5.50)$$

The boundary conditions of V become:

$$x = 0, R_1: \quad \frac{\partial V}{\partial x} = 0 \quad (5.51)$$

$$y = 0, R_2: \quad \frac{\partial V}{\partial y} = 0 \quad (5.52)$$

$$z = 0, R_3: \quad \frac{\partial V}{\partial z} = 0 \quad (5.53)$$

Therefore, by solving the coupled differential equations (5.30) and (5.50) with boundary conditions (5.51)-(5.53) it is possible to calculate the temperature and velocity (with Eqns 5.45-5.47) distribution at different times. Of course boundary conditions for the temperature are required too. I described heat transfer with a constant heat transfer coefficient at the fixed walls and assumed symmetry around the xz plane and the yz plane. I used the set of equations with the velocity potential because this set of differential equations only requires the solution of one elliptic differential equation instead of two, using the equations with the vector potential, (5.36) and (5.37).

These equations are made dimensionless with:

$$\theta = (T - T_0)/\Delta T, \tau = a_m t / L_z^2, v_D = v L_z / a_m, \nabla_D = L_z \nabla, \nabla_D^2 = L_z^2 \nabla^2, V_D = V / a_m L_z, \\ X = x / L_z, Y = y / L_z, Z = z / L_z, F = (\rho c_p)_m / (\rho c_p)_a$$

and the dimensionless numbers:

$$Po = Q L_z^2 / \lambda_0 \Delta T, Ra_E = \rho_r g \beta \kappa L_z \Delta T / \mu a_m \text{ and } Bi = \alpha L_z / \lambda_0.$$

This yields the following set:

$$F \frac{\partial \theta}{\partial \tau} - \vec{v}_D \cdot \nabla_D \theta = \nabla_D^2 \theta + Po \quad (5.54)$$

$$\nabla_D^2 V = -Ra_E (\theta - \theta_r) \quad (5.55)$$

with the boundary conditions:

$$t = 0, \forall (X, Y, Z) \quad : \quad \theta = 1, \quad V_D = 0 \quad (5.56)$$

$$t > 0, \forall (Y, Z), X = 0 \quad : \quad \frac{\partial \theta}{\partial X} = 0, \quad \frac{\partial V_D}{\partial X} = 0 \quad (5.57)$$

$$\forall (Y, Z), X = \frac{R_1}{L_z} \quad : \quad \frac{\partial \theta}{\partial X} = -Bi_{sw} \theta, \quad \frac{\partial V_D}{\partial X} = 0 \quad (5.58)$$

$$\forall (X, Z), Y = 0 \quad : \quad \frac{\partial \theta}{\partial Y} = 0, \quad \frac{\partial V_D}{\partial Y} = 0 \quad (5.59)$$

$$\forall (X, Z), Y = \frac{R_2}{L_z} \quad : \quad \frac{\partial \theta}{\partial Y} = -Bi_{sw} \theta, \quad \frac{\partial V_D}{\partial Y} = 0 \quad (5.60)$$

$$\forall (X, Y), Z = -\frac{1}{2} \quad : \quad \frac{\partial \theta}{\partial Z} = -Bi_b \theta, \quad V_D = 0 \quad (5.61)$$

$$\forall (X, Y), Z = \frac{1}{2} \quad : \quad \frac{\partial \theta}{\partial Z} = -Bi_t \theta, \quad V_D = 0 \quad (5.62)$$

while \vec{v} is calculated with the aid of:

$$v_x = \frac{a_m}{L_z} \frac{\partial^2 V_D}{\partial X \partial Z} \quad (5.63)$$

$$v_y = \frac{a_m}{L_z} \frac{\partial^2 V_D}{\partial Y \partial Z} \quad (5.64)$$

$$v_z = -\frac{a_m}{L_z} \left(\frac{\partial^2 V_D}{\partial X^2} + \frac{\partial^2 V_D}{\partial Y^2} \right) \quad (5.65)$$

To calculate the driving force of natural convection in the parallelepiped the reference air density (ρ_r) should be calculated from the average temperature in the container (T_r). I used the equation giving the density of dry air at atmospheric pressure as a function of temperature (Handbook of Chemistry and Physics, 1976), assuming the Ideal Gas Law:

$$\rho_r = \frac{353.13}{T_r} \quad (5.66)$$

with T_r as absolute temperature.

5.3.2 The numerical solution

The parabolic differential equation (5.54) and the elliptic differential equation (5.55) are both solved with an Alternating Direction Implicit Procedure (ADIP) (Douglas & Rockford, 1956), as recommended by Marsall (1976). In writing the difference equations the first derivative in time is written as a forward difference and the first derivative in X , Y or Z direction as a central difference. The mixed derivatives in X and Z direction or Y

and Z direction in the calculation of the velocity are also written as central differences. Because the temperature gradients are steeper near the wall, I used a non-equidistant grid-point distribution in X , Y and Z direction. There are more grid-points near the wall than in the central part of the parallelepiped. The calculations were performed with 9 grid-points in the X and Y direction and 15 in the Z direction.

After giving the initial value to the parameters, the calculation of temperature and velocity proceeds in the following way:

- The dimensionless temperature in the grid-points after a time-step $\Delta\tau$ is calculated.
- The average temperature in the container is calculated with the trapezoidal rule. The reference density is calculated with Eqn 5.66.
- The value of V_D in the grid-points is calculated by iteration. The iteration is finished when the maximum relative error in Eqn 5.55 is less than 0.005:

$$\left| \frac{\nabla^2 V_D - Ra(\theta - \theta_r)}{Ra(\theta - \theta_r)} \right|_{\max, i, j, k} < 0.005 \quad (5.67)$$

The grid-points with a very small value of $Ra(\theta - \theta_r)$ (< 0.001) are excluded from the calculation of the maximum relative error. In these grid-points the absolute error in Eqn 5.55 should be less than 0.001:

$$|\nabla^2 V_D - Ra(\theta - \theta_r)|_{i, j, k} < 0.001 \quad (5.68)$$

- The value of the air velocity in the X , Y and Z direction in the grid-points is calculated.
- A new value of the time step ($\Delta\tau$) is calculated by introducing a value of $\Delta\tau$ which does not give rise to an estimated change of θ in any grid-point of more than 7% of the initial value of θ . The value of 7% is determined by comparing calculations with different maximum temperature changes. Higher values give rise to instabilities of the numerical scheme. The choice of the new time-step is restricted by the demand that the new time-step is never more than 1.5 times the old time-step and is not larger than 0.01.
- A check of the accuracy of the calculated temperatures is performed by calculating the heat loss in the last time-step in two ways: (1) from the heat capacity of the product and the decrease of the average temperature and (2) from the heat flux through the walls. When these two values differed more than 1% the new time-step is reduced 10 times to improve accuracy.
- The above mentioned procedure is repeated until the steady state is attained in the calculations. The calculation is finished then.

Just as with the SNC-model, it is difficult to prove stability and convergence to the unique solution of the coupled differential equations (5.54) and (5.55). The stability is tested by using different values of the maximum time-step. The calculation shows that the numerical scheme becomes unstable when the dimensionless time-step is larger than 0.01. The convergence to the unique solution is shown in the next chapter by comparing measured and calculated temperature profiles.

5.3.3 Results of the model calculations

The model developed in the preceding chapter is used to calculate the cooling rate of heat-generating model material in a container. I used the data of Table 21 in the calculations. The container dimensions are those of the container used in my experiments (Section 5.4). The permeability was calculated from Eqn 2.93 with $Re = 0$ and $K = 1.78$.

Fig. 69 shows the temperature course at different positions along the central axis of the container. Just after the start of cooling, temperature differences in the container are only small and therefore the velocity of natural convection is small too. The cooling rate of the product is then determined by heat conduction. Therefore fast cooling near the wall and heating in other parts of the container occurs. After cooling for about 10 h, the temperature differences in the container are larger. As a result the velocity of natural convection is larger too, as shown in Fig. 70. Therefore convective heat transport in the container becomes more important. The air flows downwards near the cold walls ($x = 0.37, y = 0.18, z = -0.20$ and $x = 0.32, y = 0, z = 0$) and upwards in the central part of the container ($x = 0, y = 0, z = 0$). The rising air in the container causes heat transport from the centre to the upper part of the container. The larger heat transport causes the lower temperature decrease at a height of 0.15 m and 0.20 m after about 10 h, see Fig. 69.

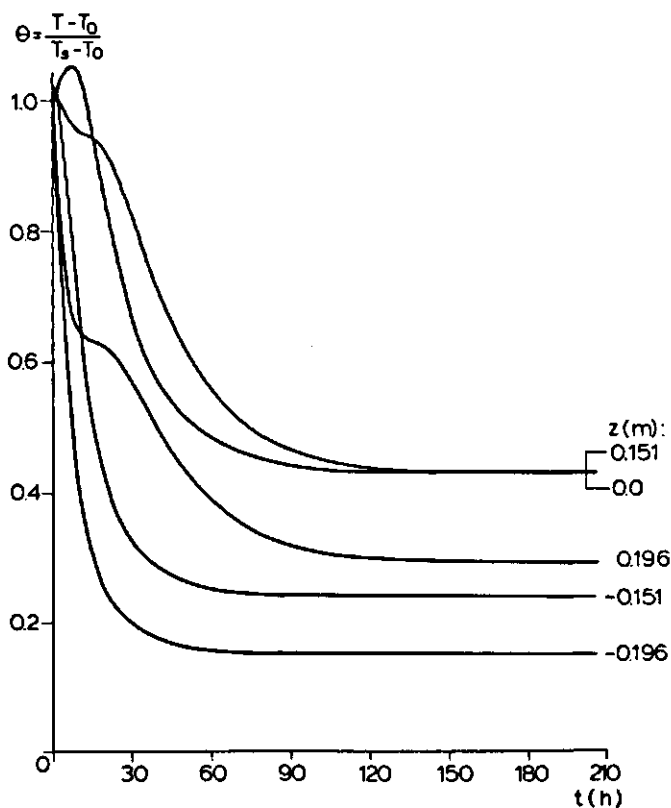


Fig. 69. Calculated changes in temperature with time at different locations along the central axis of the container.

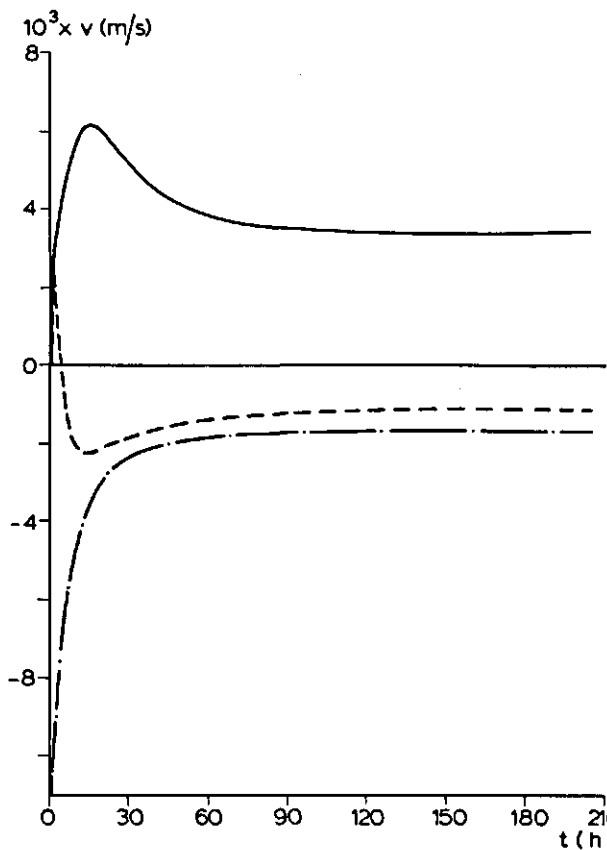


Fig. 70. Changes in velocity of natural convection in z direction with time at different locations in the container.

— $x = 0, y = 0, z = 0$; --- $x = 0.37, y = 0.18, z = -0.20$; -.- $x = 0.32, y = 0, z = 0$.

When cooling further proceeds the absolute value of the velocity of natural convection decreases again and therefore the influence of convective heat transport decreases. As a result the temperature decreases more rapidly again after about 20 h.

The rising air in the centre also causes an upwards displacement of the position of the maximum temperature of the product, compared with conductive cooling only. This is shown in Fig. 71 which gives the calculated steady-state profile of temperature along the z axis and the steady-state profile for conductive cooling only. Fig. 72 gives the temperature profile in the x direction at a height of 0.0 m at cooling with and without internal natural convection. The natural convection changes the shape of the temperature profile in the x direction. Because of the rising air, the parabolic temperature profile at conduction only is flattened towards the centre of the container when natural convection is not neglected.

The temperature distribution in the container in the xz plane at different y -values is given by the contoured print-plots in Fig. 73. This figure shows that the maximum temperature in every vertical section is situated above the middle ($z = 0.0$ m) of the section.

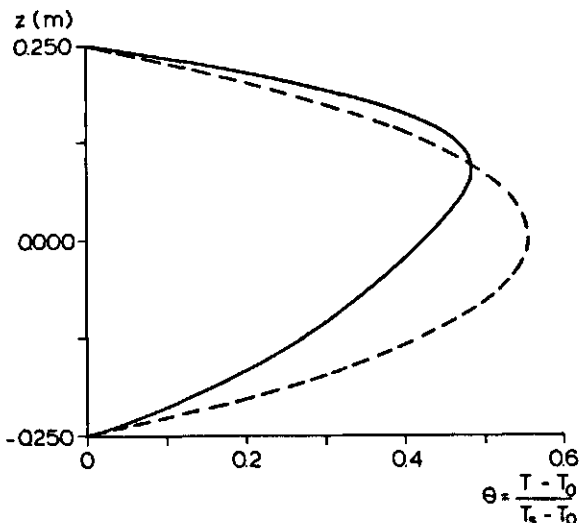


Fig. 71. Calculated steady-state temperature profile along the central axis with (—) and without (---) natural convection.

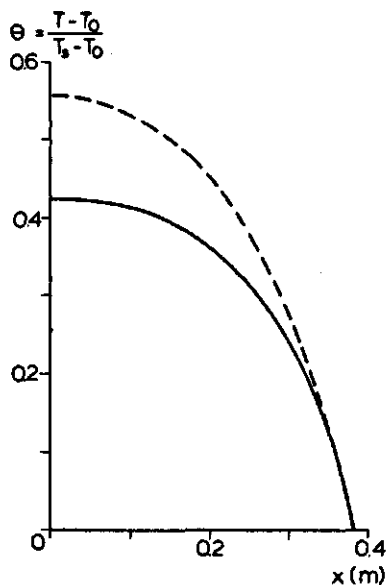
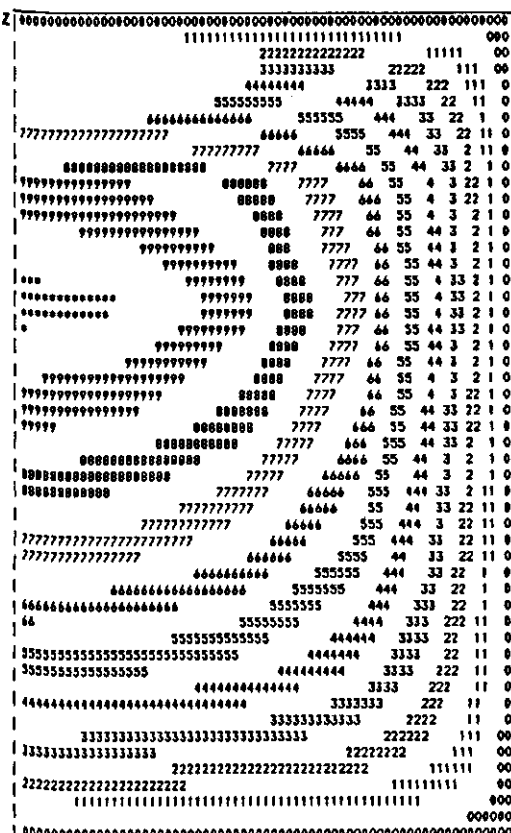
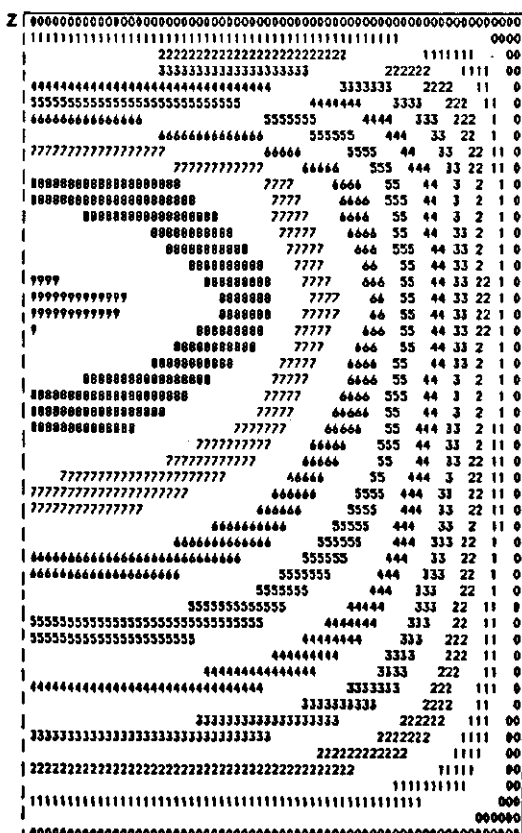


Fig. 72. Calculated steady-state temperature profile in the x direction ($y = 0, z = 0$) with (—) and without (---) natural convection.

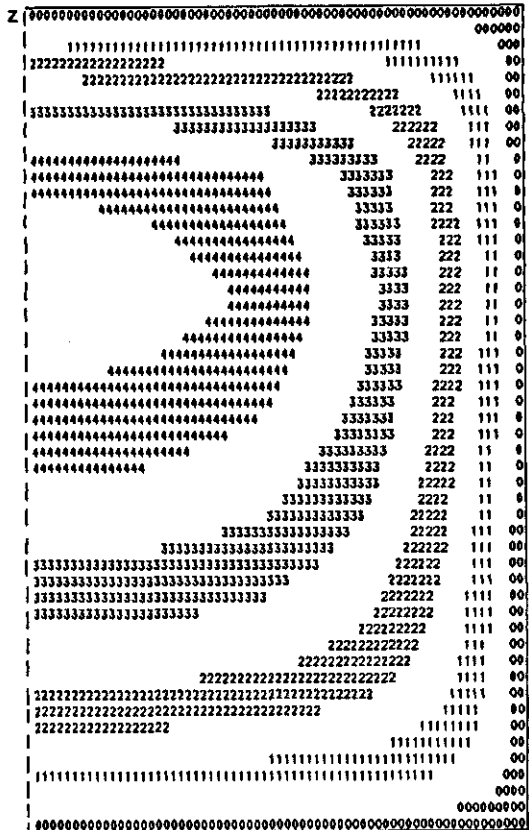


$y=0.0m$



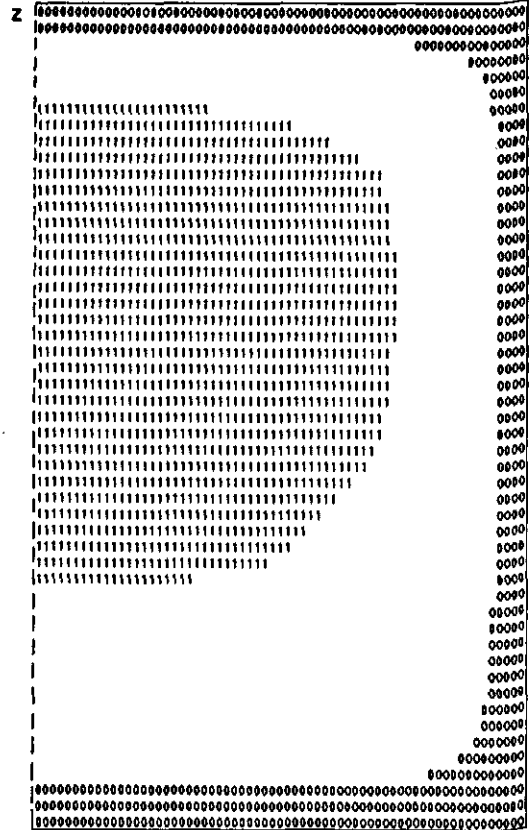
$y=0.176m$

Fig. 73. Contoured print-plots of the calculated temperatures in the xz plane and different y -values.



$y=0.317 \text{ m}$

x



$y=0.367 \text{ m}$

x

Fig. 73 (continued)

The velocity of natural convection passes a maximum or minimum value during cooling, as shown in Fig. 70. The velocity has a maximum or minimum value when temperature differences in the container are largest: then the driving force of natural convection has its largest value.

The steady-state velocity in the x and in the z direction at different positions in the xz plane is shown in the contoured print-plots, Figs 74 and 75. At $y = 0$ the velocity in the y direction is zero and therefore the air movement in the xz plane at $y = 0$ is shown in these two figures: upwards in the central part, to the side wall at the top, downwards near the side wall and to the central part at the bottom. The maximum value of v_z ($7.2 \times 10^{-3} \text{ ms}^{-1}$) is directed downwards and located near the side wall. The maximum value of v_x ($3.1 \times 10^{-3} \text{ ms}^{-1}$) is directed to the side wall near the top of the container. This implies a sharp velocity decrease quite near the wall because the velocity at the wall will be zero.

The velocity potential at different positions in the xz plane at $y = 0$ is shown in the contoured print-plot of the velocity potential in Fig. 76.

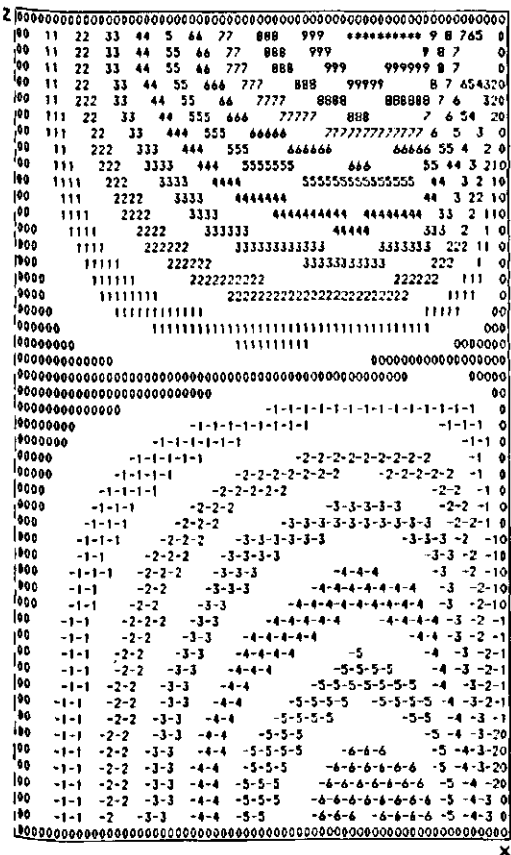


Fig. 74. Contoured print-plot of the steady-state velocity in the x direction in the xz plane at $y = 0$.

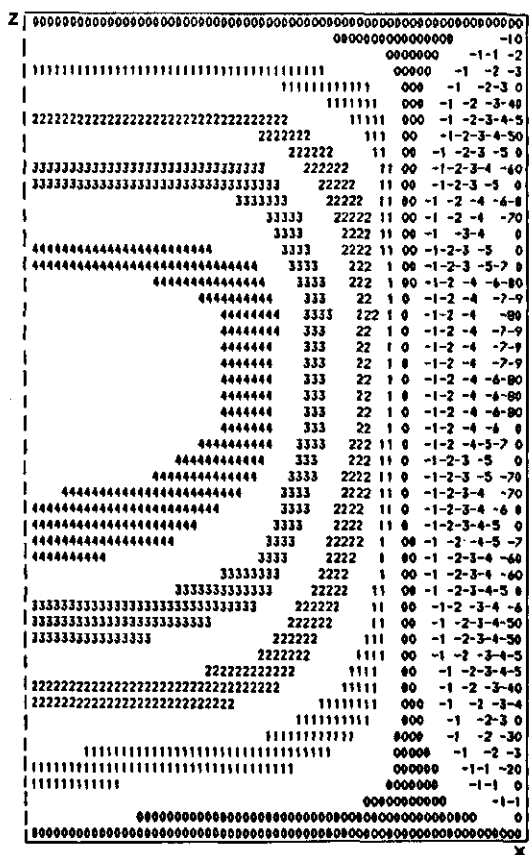


Fig. 75. Contoured print-plot of the steady-state velocity in the z direction in the xz plane at $y = 0$.

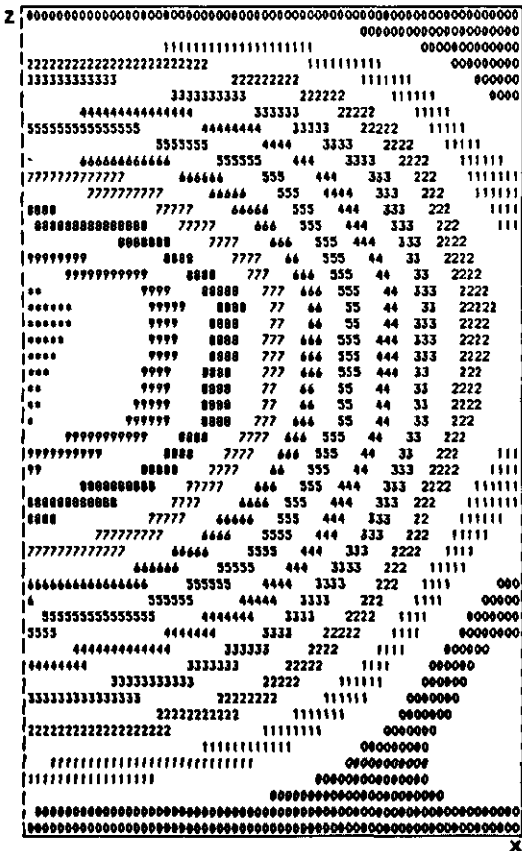


Fig. 76. Contoured print-plot of the steady-state velocity potential in the xz plane at $y = 0$.

5.4 Experiments with model material

5.4.1 Experimental set-up

The conductive cooling of agricultural and horticultural products in containers was studied experimentally in a brass container ($0.76 \text{ m} \times 0.76 \text{ m} \times 0.50 \text{ m}$) with isothermal walls, filled with model material (described in Section 4.1), potatoes or Brussels sprouts. The wall temperature was kept constant by pumping methanol from a thermostatic bath (accuracy: $\pm 0.01 \text{ }^{\circ}\text{C}$) through pipes which had good thermal contact with the six walls of the container (see Fig. 77). The top of the container could be removed to fill the container. To be able to blow air through the container for cooling or heating by forced convection, five holes ($0.035 \text{ m} \times 0.65 \text{ m}$) were made in the bottom. During the experiments the holes were closed with brass plates. The contact wires of the model material were passed through a hole in the container wall, 0.05 m from the top of one side wall. This hole was also closed during the measurements.

The temperature at different places in the container was measured with thermistors. Fig. 78 shows the positions of the thermistors in the container for the experiments with model material. The automatic system for measuring temperature, discussed in Section 4.1, was also used during these experiments.

5.4.2 Experimental results

An experiment was usually started by removing the top, opening the bottom holes and blowing air through the container to heat the products or model material up to about $30 \text{ }^{\circ}\text{C}$. When the content of the container had attained this temperature, bottom and top were closed. Then the wall cooling and heat generation of the model material were started. At the start of a cooling experiment the temperatures at different positions in the container did not differ by more than $1.0 \text{ }^{\circ}\text{C}$. The experiments were stopped when the steady state was attained.

Experimental verification showed that the temperature rise of the liquid cooling the walls, was less than $0.1 \text{ }^{\circ}\text{C}$ except in the first ten minutes of an experiment, when the temperature rise decreased exponentially from about $1.0 \text{ }^{\circ}\text{C}$ to $0.1 \text{ }^{\circ}\text{C}$. However because of the rather long duration of one experiment (about one week) and the large temperature differences at the start, the temperature of the cooling liquid was assumed to be constant during the experiment.

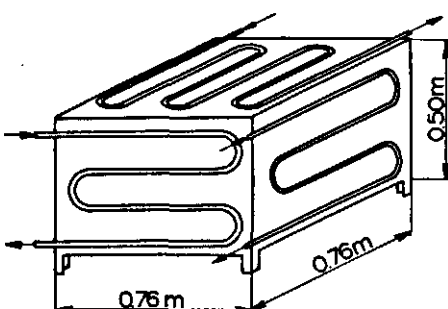


Fig. 77. Brass container with cooled walls.

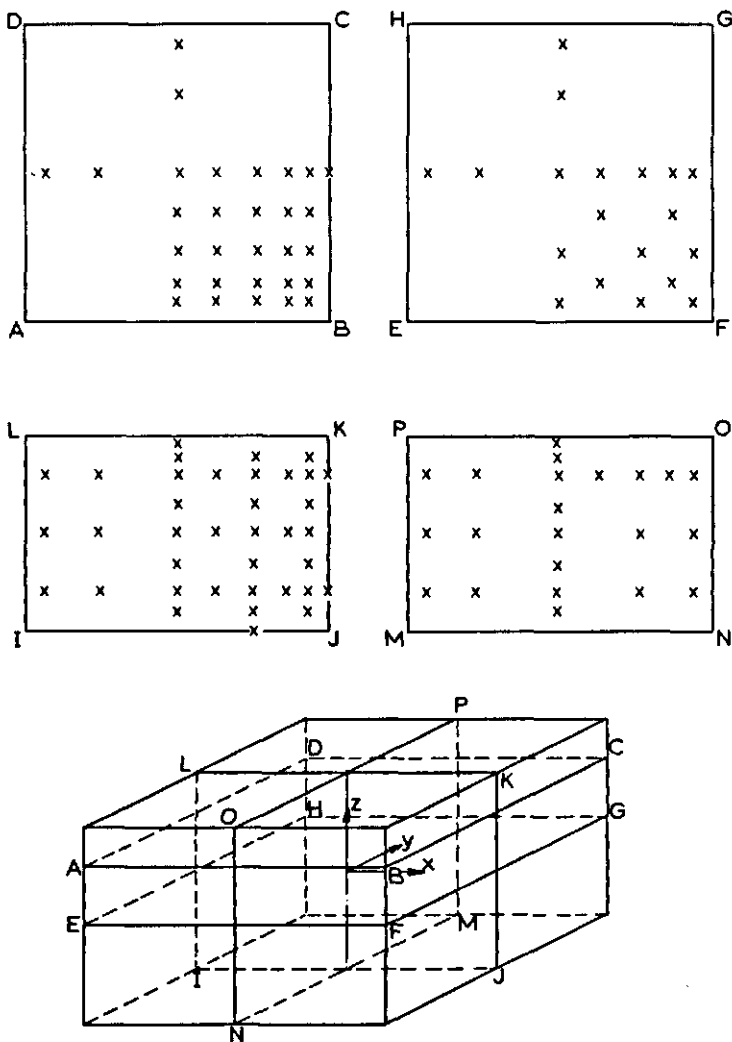


Fig. 78. Distribution of the thermistors in the container.

Figs 79 and 80 show the temperature course at different positions along the central axis at a rate of heat generation of 60 and 235 Wm^{-3} , respectively. The wall temperature in these experiments was 19.2 and 20.0°C , respectively. The temperature profiles at 0.150 and 0.195 m show after about 10 h a decreasing rate of cooling and afterwards transformation into heating. This result is caused by the increasing influence of heat transport by natural convection as already discussed in Section 5.3.3.

Figs 81-84 show the course of the dimensionless temperature (θ) on the z axis at a height of -0.005 , 0.065 , 0.150 and 0.195 m with different rates of heat generation. The temperatures are made dimensionless according to:

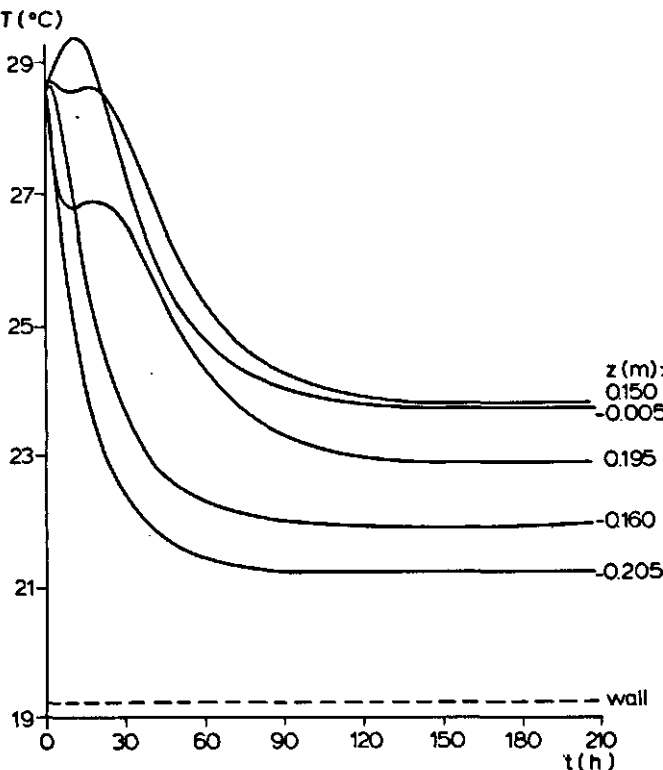


Fig. 79. Changes in temperature with time along the central axis with a rate of heat generation of 60 W/m^3 and a wall temperature of 19.2°C .

$$\theta = \frac{T - T_0}{T_s - T_0} \quad (5.69)$$

so that cooling experiments with different initial product and wall temperatures can be compared. As shown in Table 22 the value of $T_s - T_0$ differs somewhat between the different measurements.

Figs 81 and 82 show the faster heating during the initial stage of the experiment and the higher maximum temperature at higher rate of heat generation. For a rate of heat generation above 60 Wm^{-3} the maximum temperature is higher at 0.065 m than at -0.005 m . Figs 83 and 84 show both the slower decrease or faster increase of the temperature course after about 10 h (as already discussed in Section 5.3.3), even for cooling without heat generation. This effect was more pronounced at a higher rate of heat generation because the temperature differences and therefore also the velocities of natural convection were higher with higher rates of heat generation. At a height of 0.195 m the temperature always decreased in the beginning of the cooling, because this position was near the top of the container. At a height of 0.150 m it depended upon the rate of heat generation whether heating or cooling occurred in the beginning of the experiment.

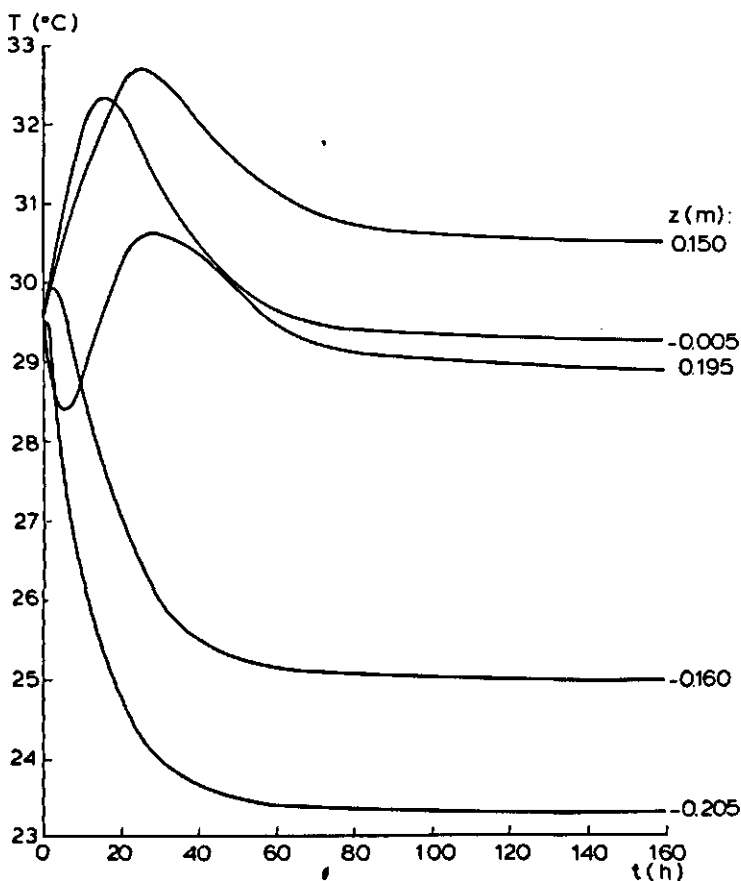


Fig. 80. Changes in temperature with time along the central axis with a rate of heat generation of 235 W/m^3 and a wall temperature of $20.0 \text{ }^\circ\text{C}$.

Table 22. Difference between initial and wall temperature and steady-state maximum and wall temperature for different rates of heat generation.

$Q \text{ (W/m}^3\text{)}$						
	15	28	60	115	171	235
$T_s - T_w \text{ (K)}$	9.1	10.7	9.55	10.35	11.10	12.30
$T_{\max} - T_w \text{ (K)}$	1.31	2.37	4.73	7.92	10.98	13.71

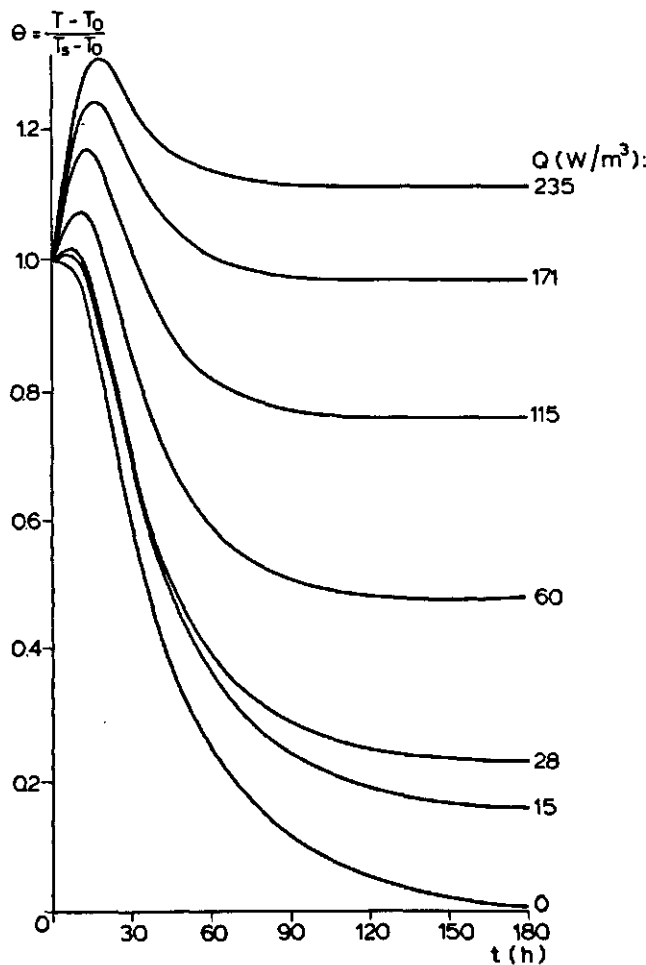


Fig. 81. Changes in temperature with time at $x = 0$, $y = 0$ and $z = -0.005$ m with different rates of heat generation.

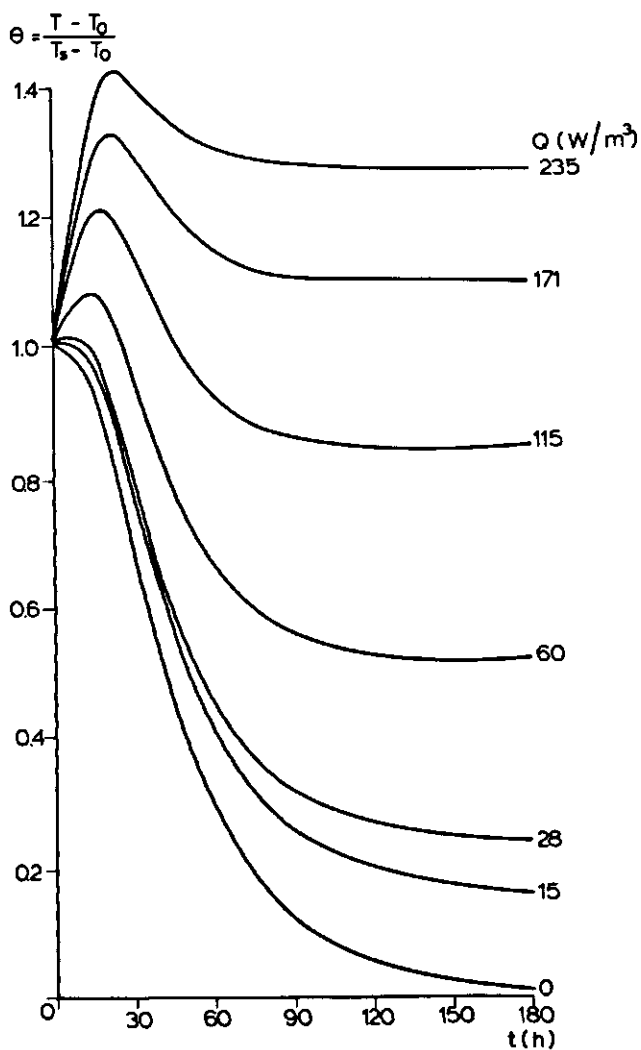


Fig. 82. Changes in temperature with time at $x = 0$, $y = 0$ and $z = 0.065$ m with different rates of heat generation.

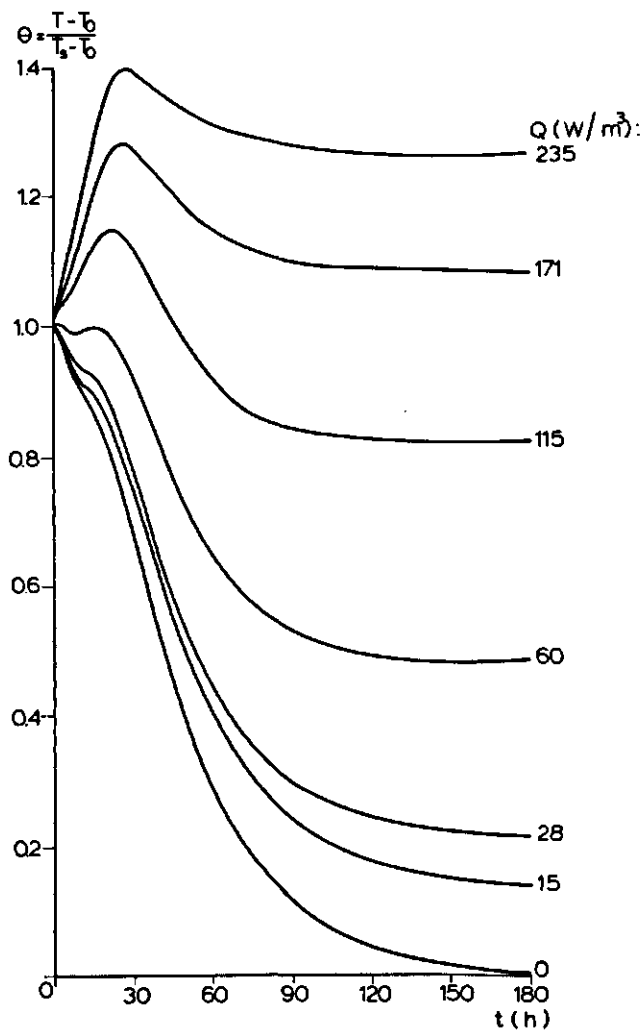


Fig. 83. Changes in temperature with time at $x = 0$, $y = 0$ and $z = 1.150$ m with different rates of heat generation.

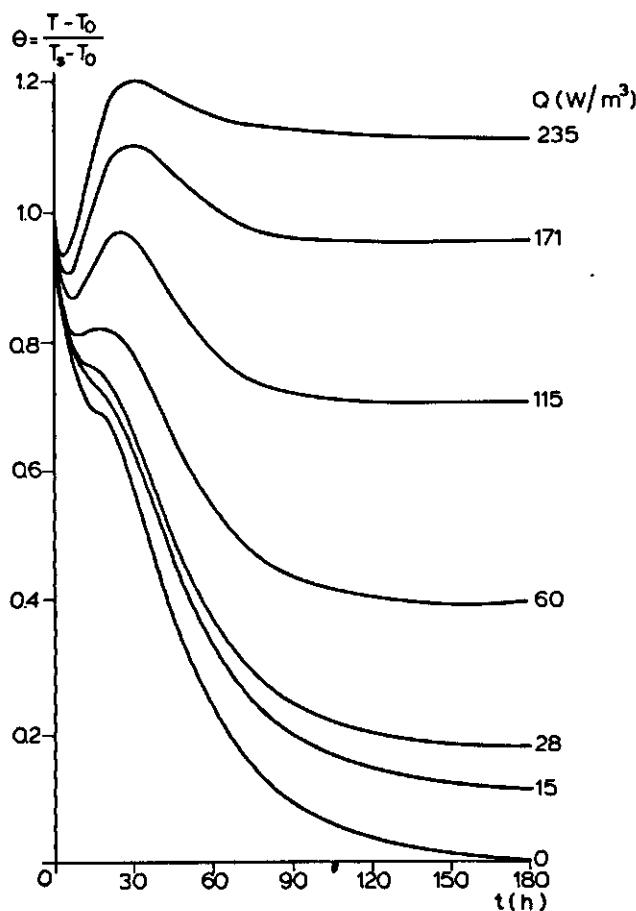


Fig. 84. Changes in temperature with time at $x = 0$, $y = 0$ and $z = 0.195$ m with different rates of heat generation.

Because heat losses by conduction and convection in the centre of the cylinder are very small during the first hours of an experiment, the heating rate in the centre is only determined by the rate of heat generation and the heat capacity of the heat-generating produce:

$$(\rho c_p)_m \frac{dT}{dt} = Q \quad (5.70)$$

It is therefore possible to calculate the heat capacity of the product from the initial heating rate in the centre of the container. In one experiment in which the initial temperature in the container was equal to the temperature of the cooling liquid, the linear temperature rise with time was maintained for 18 h (see Fig. 85). From this experiment the heat capacity of the model material, given in Table 20 was calculated. This value agrees well with the value calculated from the composition of the model material and the

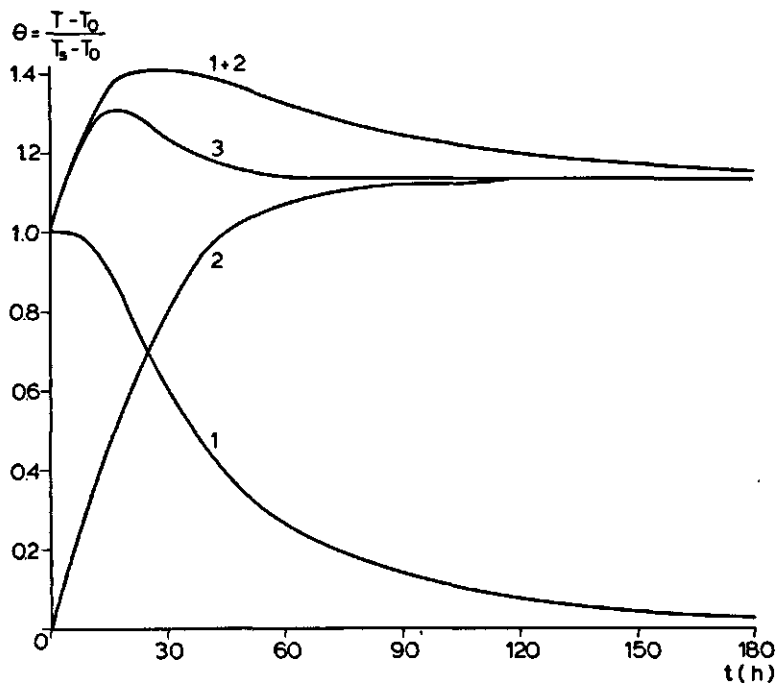


Fig. 85. Changes in temperature with time at $x = 0$, $y = 0$ and $z = 0$.

- (1) Cooling without heat generation.
- (2) Self heating; $Q = 235 \text{ W/m}^3$, $\theta_s = 0$.
- (3) Self heating; $Q = 235 \text{ W/m}^3$, $\theta_s = 1$.

The sum of (1) and (2) is also indicated.

porosity of the filled container.

Fig. 85 also shows that the sum of the temperature course in an experiment with $T_s \neq T_w$ and $Q = 0$ (1) and in an experiment with $T_s = T_w$ and $Q = 235 \text{ Wm}^{-3}$ (2) is not equal to the measured temperature profile at $T_s \neq T_w$ and $Q = 235 \text{ Wm}^{-3}$. As shown in Section 5.2 these two temperature histories should coincide exactly when heat transport is only by conduction. Here again the influence of natural convection is shown. The actual maximum temperature (Curve 3) is significantly lower than the value predicted by the pure conduction model, curve (1)+(2).

Cooling of the product at a rate of heat generation of 235 Wm^{-3} was accelerated more by natural convection than cooling without heat generation. The self-heating of the container with an initial temperature equal to the wall temperature at a rate of heat generation of 235 Wm^{-3} was also only slightly influenced by natural convection in the beginning of self-heating. Therefore the sum of the self-heating and cooling experiment predicts slower cooling and higher temperatures than the real situation. This result shows that cooling closed containers with respiring products cannot be analysed when conductive cooling only is assumed.

The temperature at a height of 0.15 m was measured at different positions as shown in Fig. 78. These temperature measurements served as a check of the symmetry with respect

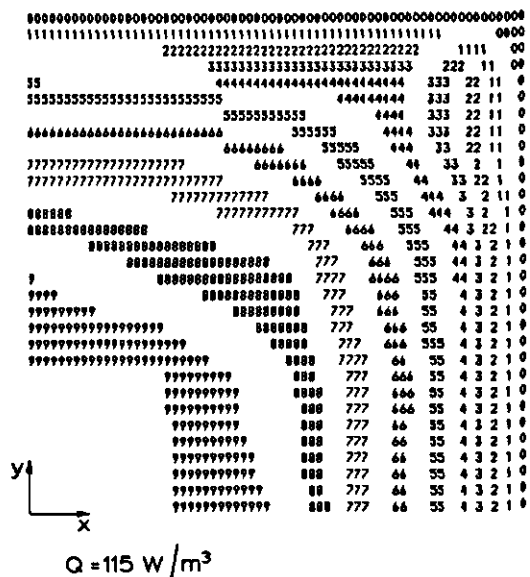
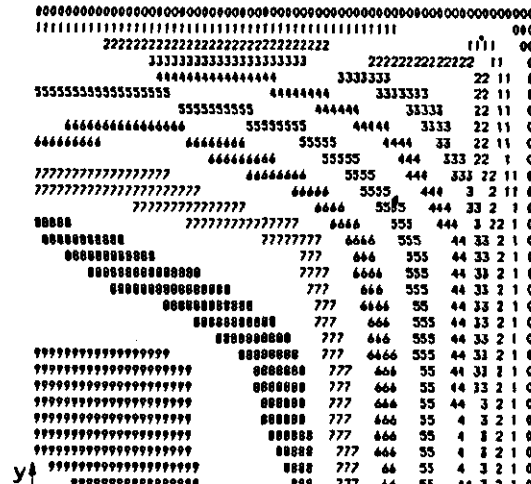
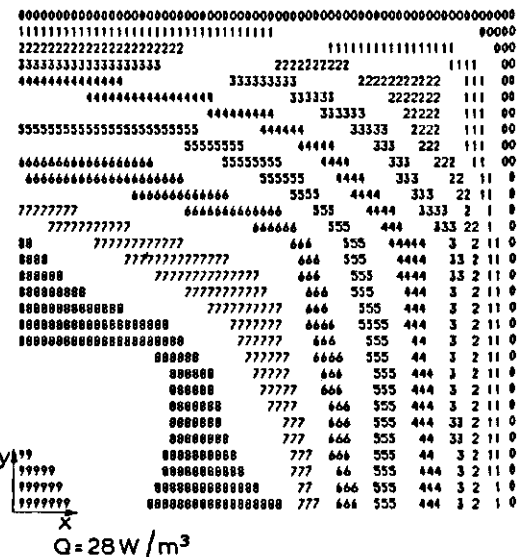


Fig. 86. Contoured print-plot of the temperature in the xy plane at $z = 0.15$ m with different rates of heat generation.

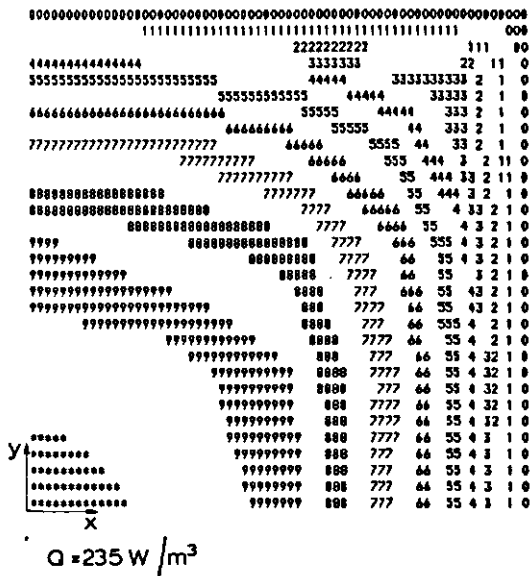
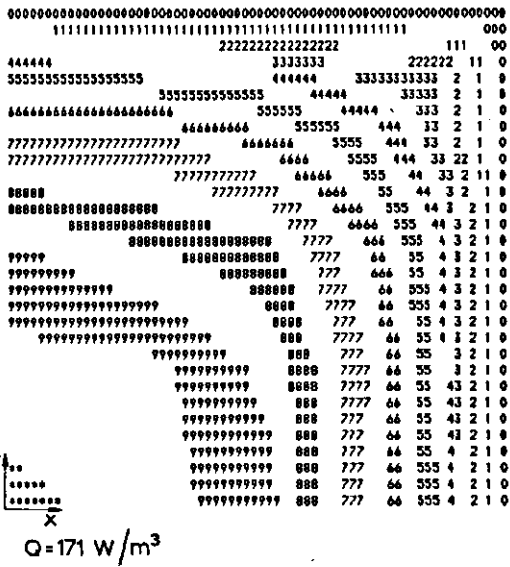


Fig. 86 (continued)

to the plane with equal x and y coordinates. The temperatures are shown in the contoured print-plots in Fig. 86. The temperatures were normalized by dividing $T - T_0$ by the difference between the maximum temperature in the container and T_0 (given in Table 22), instead of using the maximum temperature at the given height as in the other plots. The contoured print-plots show a good symmetry with respect to the line $y = x$. Therefore the heat losses by the walls $x = R_1$ and $y = R_2$ did not differ very much. The values of the temperature in the centre ($x = 0, y = 0, z = 0.15$) for the different rates of heat generation, confirm the higher position of the maximum temperature of the product with an increasing rate of heat generation.

Fig. 87 shows the steady-state temperature distribution along the z axis ($x = 0, y = 0$). In this figure the temperature is given as the dimensionless temperature θ_Q :

$$\theta_Q = \frac{(T - T_0) \lambda_0}{Q L_z^2} \quad (5.71)$$

It may be shown from Eqn 5.25 that by using θ_Q the temperature profiles for conductive cooling only, will be equal for different rates of heat generation. The pure conduction cooling profile, calculated with Eqn 5.25 is shown in Fig. 87. The figure shows that at one height the dimensionless steady-state temperature decreases with increasing rate of heat generation. At a higher rate of heat generation the actual maximum temperature difference between bulk and wall is higher of course. Therefore the driving force of natural convection is higher. The higher velocity of natural convection gives larger heat loss and thus the value of θ_Q will be lower when the rate of heat generation is on the increase.

The higher velocity of natural convection is also shown by the rise in position of the

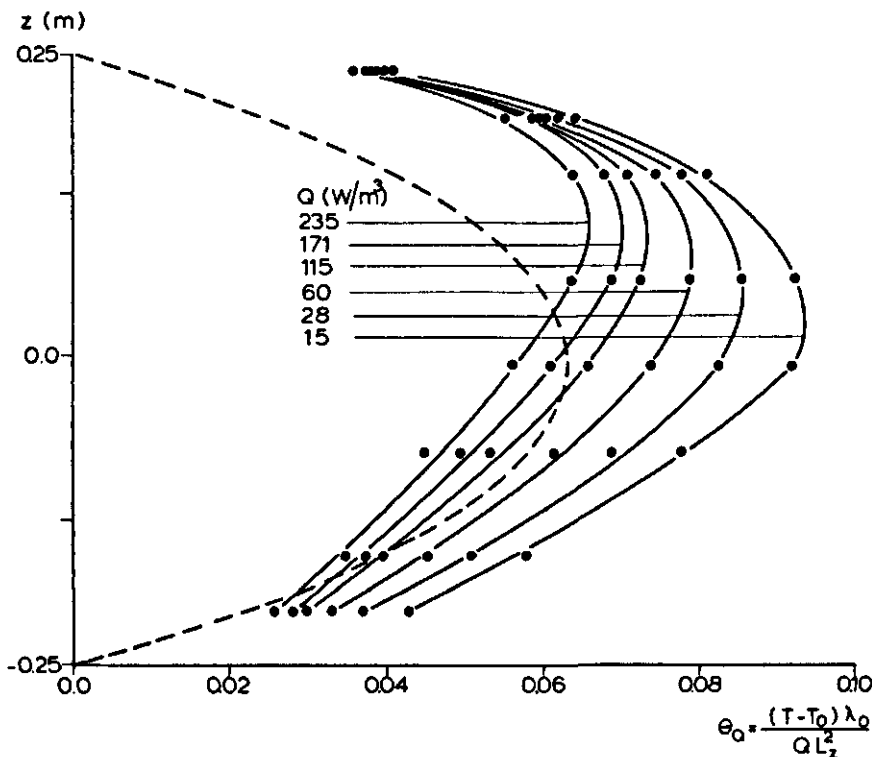


Fig. 87. Steady-state profile of dimensionless temperature along the central axis with different rates of heat generation.
 --- pure conduction, $\lambda_0 = 0.25 \text{ W/mK}$.

maximum temperature at increasing rate of heat generation. The air rises in the centre of the container. This causes the observed rise of the maximum temperature in the container from the centre where it is located for conduction only.

Fig. 87 also shows that the heat transfer at the top and the bottom of the container is not perfect. Extrapolation of θ_Q to the temperature at the wall does not give the value $\theta_Q = 0$. There is a resistance to heat transfer near the wall. This resistance may be modelled with a wall heat transfer coefficient, as discussed in Section 3.2. Fig. 88 gives the dimensionless temperature in the x direction at $y = 0.0$ and $z = 0.0 \text{ m}$. It shows that the heat transfer at the side walls is also restricted.

The heat flux through the wall may be calculated from thermal conductivity times temperature gradient at the wall or from heat transfer coefficient at the wall times the difference between the extrapolated wall temperature (T_e) and the real wall temperature (T_0), (see Fig. 89):

$$q = -\lambda_0 \frac{dT}{dx} = \alpha_{ov} (T_e - T_0) \quad (5.72)$$

It is therefore possible to estimate α_{ov} from an extrapolation of the measured tempera-

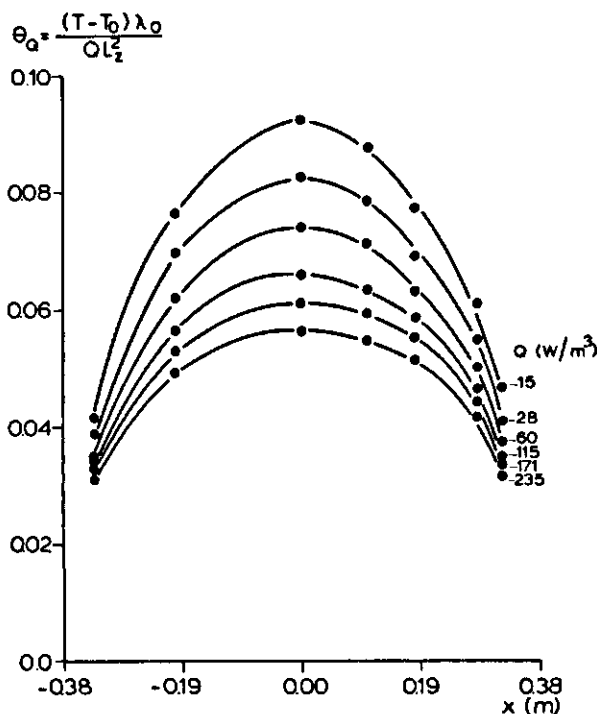


Fig. 88. Steady-state profile of dimensionless temperature in the x direction at $y = 0$ and $z = 0$ with different rates of heat generation.

ture profile to the wall. Table 23 summarizes the values of α_{ov} at the bottom and the side wall at different x and z values, calculated with Eqn 5.72 and for a linear extrapolation of the measured temperatures to obtain T_e . However, because the temperatures used in the extrapolation were measured at a distance of 0.05 and 0.10 m from the wall, the calculated wall heat transfer coefficients are not very accurate. The value of α_{ov} varied between $\pm 25\%$ at $Q = 235 \text{ W m}^{-3}$, $z = 0.25 \text{ m}$ and $\pm 265\%$ at $Q = 15 \text{ W m}^{-3}$, $x = 0.33 \text{ m}$.

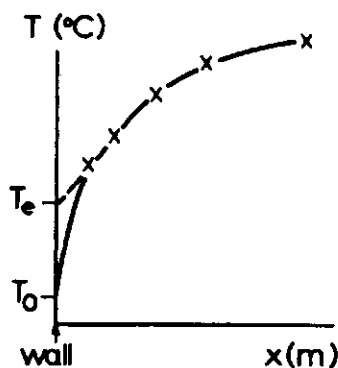


Fig. 89. Temperature profile with additional resistance at the wall.

Table 23. Heat transfer coefficient at the bottom and the side wall for different x and z values and different rates of heat generation.

Q (W/m ³)	Bottom x (m)			Side wall z (m)		
	0.00	0.20	0.33	0.10	0.25	0.40
15	3.6	5.6	1.7	5.9	4.2	3.5
28	4.0	4.8	3.5	5.8	5.3	3.1
60	3.8	4.6	3.4	5.9	5.3	3.8
115	3.2	3.7	4.8	3.8	5.0	3.0
171	3.2	2.9	3.5	3.6	4.9	2.8
235	3.5	2.9	4.1	3.6	4.6	2.5

Therefore the calculated values give only a rough estimation.

The value of α_{ov} may also be calculated by comparing measured and calculated temperature profiles as is discussed in the next section.

5.4.3 Comparison of measured and calculated temperatures

I used the mathematical model of the temperature distribution in a container with heat-generating produce and internal natural convection to predict the temperature course and the steady-state temperature distribution in the container with model material. The physical properties of the model material have already been given in Table 21. Figs 90 and 91 show the calculated steady-state temperature profiles at a rate of heat generation of 60 Wm⁻³ and different heat transfer coefficients at the wall. Figs 90 and 91 also give the measured steady-state temperature distribution. The figures show that temperature profiles with the right shape are obtained by using the following set of heat transfer coefficients at bottom (α_b), top (α_t) and side walls (α_{sw}) respectively: 7, 10 and 20 Wm⁻²K⁻¹.

The difference in the values of the heat transfer coefficient at top, bottom and side walls, for a good fit of the measured and calculated temperatures may be caused by the different air velocities near top, bottom and side walls. As shown in Section 3.2 the heat transfer coefficient at the wall is proportional to the air velocity. In Section 5.3.3 I have shown that the highest air velocity was located near the side walls and that the air velocity was higher at the top than at the bottom of the container. Therefore the highest heat transfer coefficient was expected at the side walls and the smallest heat transfer coefficient at the bottom. This expectation was confirmed by the 'best' values of α_b , α_t and α_{sw} .

The influence of natural convection on the steady-state temperature profile is also notable in Figs 90 and 91 from the calculated temperature profile for conductive cooling only. In this calculation the heat transfer coefficients at bottom, top and side walls are also 7, 10 and 20 Wm⁻²K⁻¹, respectively. The comparison of the temperature profile with and without natural convection obviously shows that the location of the maximum temperature above the centre of the container is not caused only by the higher heat

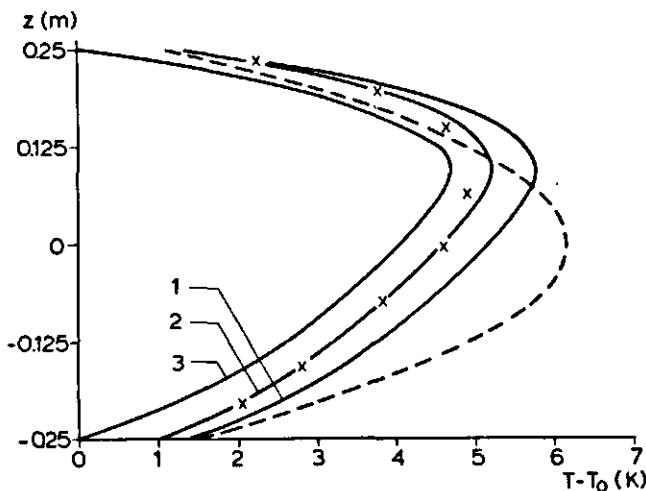


Fig. 90. Distribution of steady-state temperature along the central axis for different heat transfer coefficients at the walls.

(1) : $\alpha_b = 5 \text{ W/m}^2 \text{ K}$, $\alpha_t = 9 \text{ W/m}^2 \text{ K}$ and $\alpha_{sw} = 6.5 \text{ W/m}^2 \text{ K}$.
 (2) : $\alpha_b = 7 \text{ W/m}^2 \text{ K}$, $\alpha_t = 10 \text{ W/m}^2 \text{ K}$ and $\alpha_{sw} = 20 \text{ W/m}^2 \text{ K}$.
 (3) : $\alpha_b = 1000 \text{ W/m}^2 \text{ K}$, $\alpha_t = 1000 \text{ W/m}^2 \text{ K}$ and $\alpha_{sw} = 1000 \text{ W/m}^2 \text{ K}$.

— x Measured temperatures;
 - - - Profile for conduction only and α values of set (2).

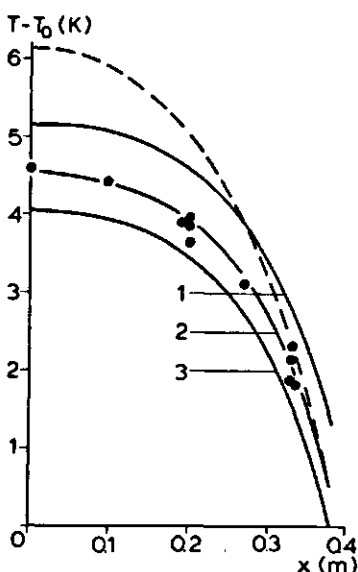


Fig. 91. Distribution of steady-state temperature in the x direction ($y = 0$ and $z = 0$) for different heat transfer coefficients at the wall. Legend: see Fig. 90.
 ● = Measured in positive and negative x and y direction.

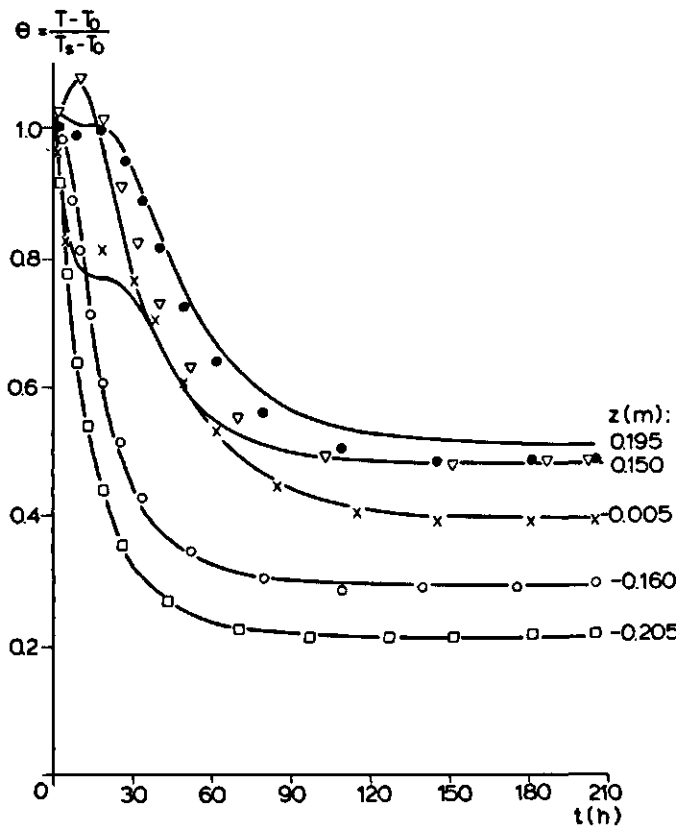


Fig. 92. Measured and calculated (—) temperature changes with time at different locations along the central axis. $Q = 60 \text{ W/m}^3$, $\alpha_b = 7 \text{ W/m}^2 \text{ K}$, $\alpha_t = 10 \text{ W/m}^2 \text{ K}$ and $\alpha_{sw} = 20 \text{ W/m}^2 \text{ K}$.

transfer coefficient at the top, but mainly by the influence of natural convection.

Fig. 92 shows that the course of the measured temperatures is also predicted well by the model calculations. Figs 93 and 94 show the measured and the calculated course of the temperature, with and without natural convection. The heat transfer coefficients at the walls are the same as used in Fig. 92. In the centre of the container the difference between cooling with and without natural convection is very large. At a height of 0.15 m the difference is less, but the rather constant temperature in the first 20 h of the cooling process is not predicted when natural convection is neglected. Fig. 93 also shows that the steady state is attained sooner at cooling with natural convection.

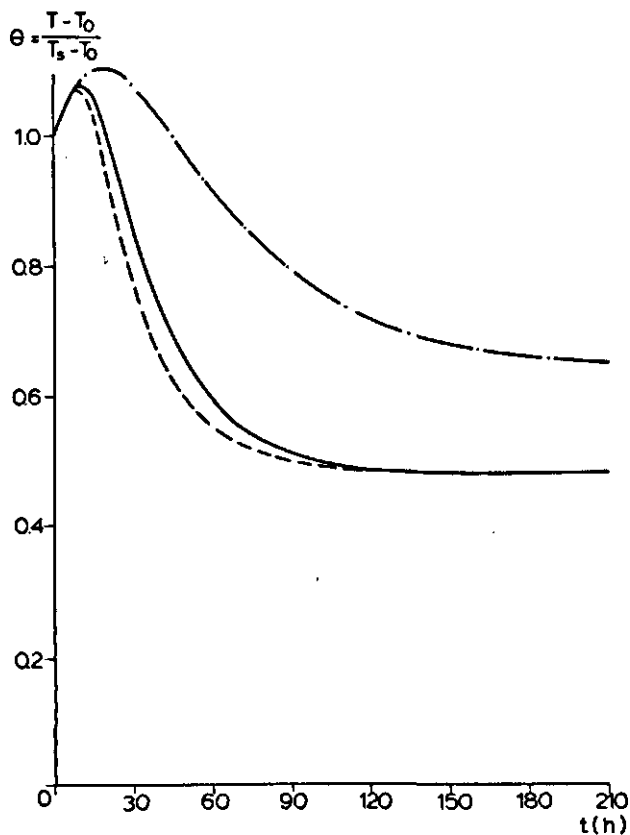


Fig. 93. Changes in temperature with time at $x = 0$, $y = 0$ and $z = -0.005$ m.

- measured temperatures
- calculated; with natural convection
- calculated; without natural convection

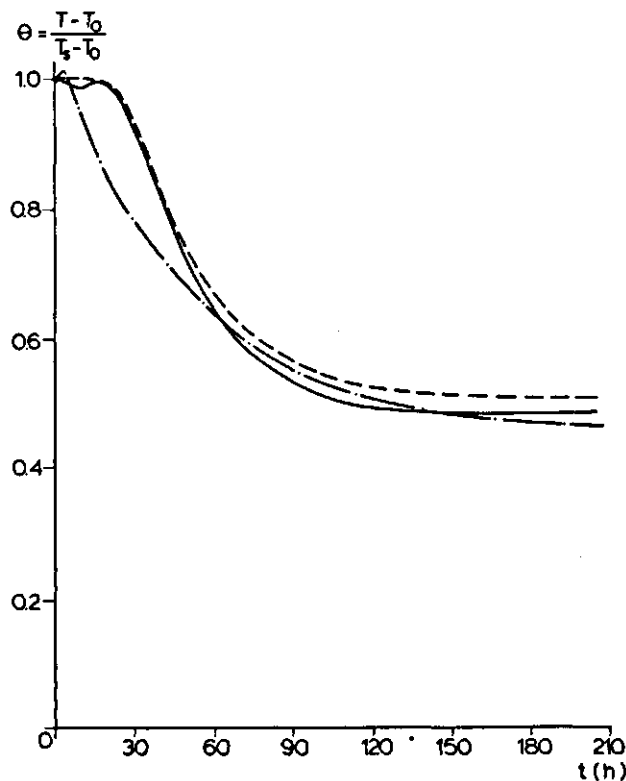


Fig. 94. Changes in temperature with time at $x = 0$, $y = 0$ and $z = 0.150$ m. Legends: see Fig. 93.

5.5 Experiments with real products

To compare the storage in containers of real products and model material, I performed experiments on the container filled with potatoes or Brussels sprouts. During cooling and storage of these real products a new variable was introduced, namely moisture loss of the products. This variable could not be studied in the experiments with model material. Moisture loss of the products causes a rise of the moisture content of the air in the container. Because of the temperature differences in the container the air may become saturated with water vapour in the colder parts of the container, resulting in condensation of water on the products and on the wall of the container.

5.5.1 Potatoes

The potatoes used in these experiments came from the same bulk as those used in the experiments with the open cylinder. After the curing period the potatoes were stored for one month at 5 °C. Two days before the start of the experiment the potatoes were acclimatized at 20 °C. The physical properties of the potatoes are given in Appendix B. The rate of heat generation is given by the experimental data of November in Table B1. This rate of heat generation was measured at the end of these experiments in the closed container.

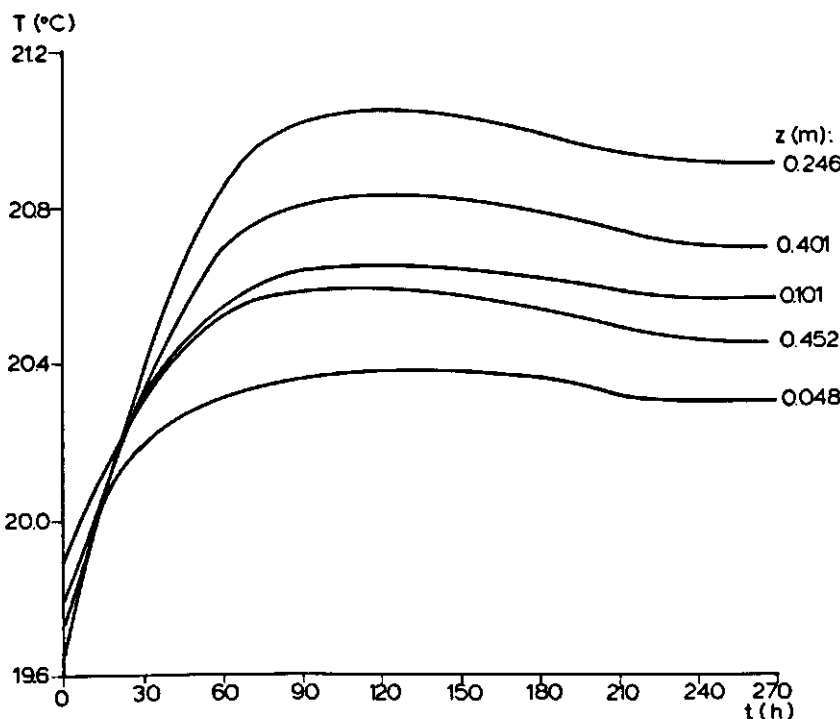


Fig. 95. Changes in temperature with time at different locations along the central axis with self-heating of the container with potatoes.

In the first experiment the container with potatoes was closed, the wall temperature was kept at 19.9 °C and the temperature course at different positions in the container was recorded. As shown in Fig. 95 the temperature in the container rises because the potatoes generate heat. From the initial temperature rise the rate of heat generation was calculated with Eqn 5.70. The calculated rate of heat generation was 13 Wm^{-3} . This value is 20% higher than the figure of 11 Wm^{-3} given in Appendix B, which was measured after the experiments. Perhaps the acclimatization of the potatoes for two days was too short, and the rate of heat generation decreased during the experiment. A decrease in rate of heat generation after some time would also explain the slowly decreasing temperatures after about 120 h.

The second experiment was the cooling of a heated container with potatoes. At the start of the cooling the temperature of the potatoes was about 29.5 °C. The wall temperature was kept at 19.9 °C. Fig. 96 shows the temperature course at different positions in

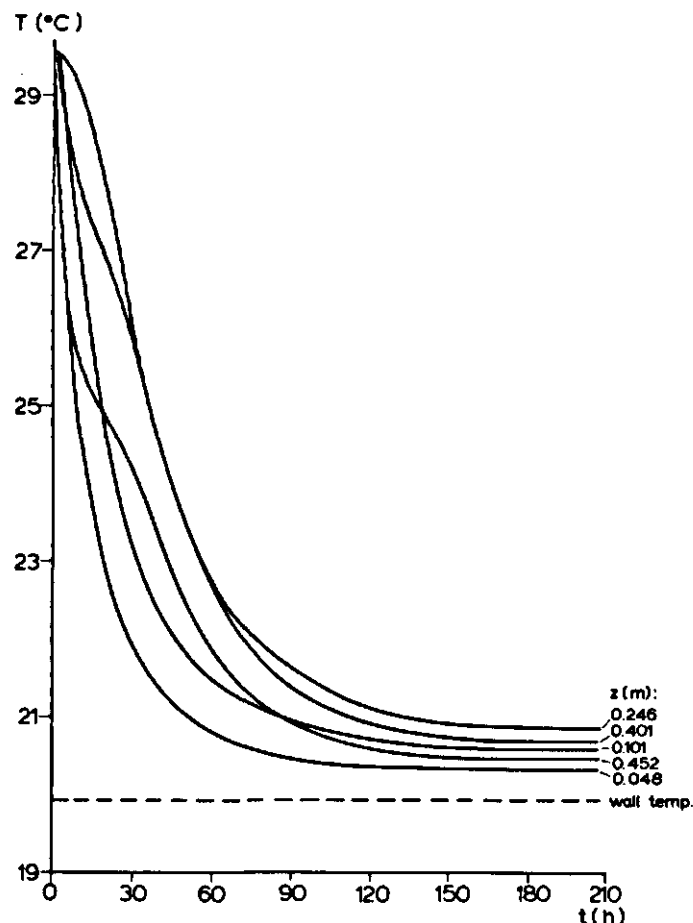


Fig. 96. Changes in temperature with time at different locations along the central axis for cooling potatoes.

the container. Just as in the experiments with model material, the temperature decrease at a height of 0.15 m and 0.20 m became less after cooling about 10 h and increased again thereafter. It is obvious that heat transport by natural convection also occurs during cooling of a container with potatoes.

Fig. 97 shows that the course of the dimensionless temperature in the beginning of the cooling was not the same as the temperature course during the cooling of the model material with a rate of heat generation of 15 W m^{-3} . During cooling of potatoes the temperature decreased right from the beginning of the experiment in every position in the container (see Fig. 96). During cooling of the model material, even in the experiments without heat generation such a fast temperature decrease could not be achieved (see Fig. 81). The rapid temperature decrease in the beginning of the cooling was caused by evaporative cooling of the potatoes. The air, used to heat the potatoes up to 29.5°C had a relative humidity of about 70%. Therefore at the start of the cooling the air in the container was not saturated. The amount of heat lost by evaporative cooling exceeded the amount of heat generated by the potatoes. Therefore the temperature decreased directly at the start of the cooling.

The steady-state temperature distribution for model material was also different from

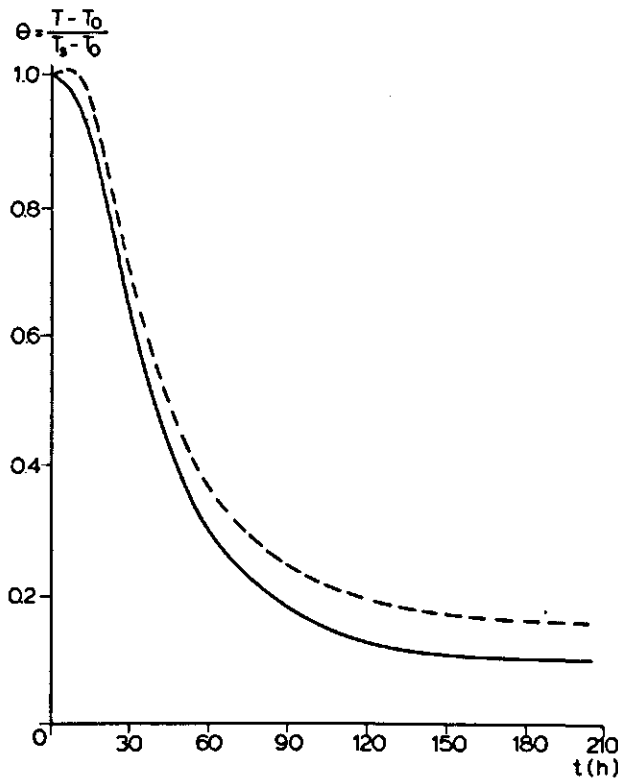


Fig. 97. Changes in temperature with time at $x = 0$, $y = 0$ and $z = -0.005 \text{ m}$.

— potatoes;
--- model material ($Q = 15 \text{ W/m}^3$).

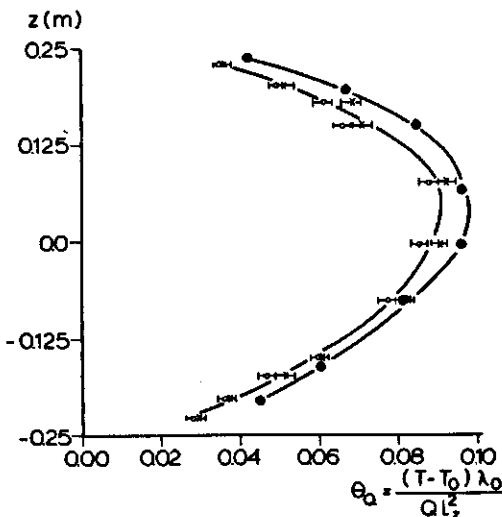


Fig. 98. Steady-state profile of temperature along the central axis of potatoes (○ and x) and model material (●). The accuracy of the temperature is indicated (—).

that of potatoes as shown in Fig. 97. However it should be noticed that the value of $T_s - T_0$ used for calculating θ was 9.7 K for potatoes and 9.1 K for model material. Fig. 98 gives the steady-state profiles of θ_Q along the central axis for the two experiments on potatoes ($Q = 11 \text{ W m}^{-3}$) and for the experiment with model material at a rate of heat generation of 15 W m^{-3} . It is shown in Fig. 87 that, for model material, θ_Q increases as the rate of heat generation decreases. The potatoes had a lower rate of heat generation than the model material, but θ_Q of the potatoes was lower too. This result may be caused by a higher value of the heat transfer coefficient at the wall, because the equivalent diameter of the potatoes was smaller than the equivalent diameter of the model material.

In these experiments the heat transfer coefficient at the wall was not calculated from the mathematical model of the container with internal natural convection, because moisture loss of the products, which occurs in these experiments, is not incorporated in the model equations.

Fig. 98 also shows that the two experiments with potatoes gave the same steady-state temperature profile, within the accuracy of the temperature measurements. Thus the steady-state rate of heat generation of the potatoes was about the same in both experiments.

After opening the container, I saw condensed water on the top and the side walls of the container. In the upper third part of the container condense had also formed on the potatoes. As shown in Fig. 98 the upper third part is that part of the container where the temperature decreases with increasing height. The air rising in the central part of the container will be almost saturated. Therefore, when the temperature of the air decreases, condensation occurs.

5.5.2 Brussels sprouts

The Brussels sprouts used in the experiments (variety: Dorema, size: 22-32 mm) were bought at the auction and acclimatized for one day at 16 °C. The rate of heat generation was measured at the Sprenger Institute with an adiabatic calorimeter (see Appendix B). The rate of heat generation at 15 °C and 20 °C is given in Table 24, together with some other physical properties. Thermal conductivity, product density and specific heat are literature values (Sprenger Institute, 1972).

In the first experiment with Brussels sprouts the container was filled, the wall temperature kept at 16.0 °C and the change in temperature with time was measured at different places in the container. Fig. 99 shows the temperature course on the z axis of the container. The temperature distribution at the start of the experiment was not uniform because the container could not be filled instantaneously. The temperature course shows a maximum after about 25 h. This may have been caused by the decreasing O₂ concentration and the increasing CO₂ concentration in the container as a result of the high respiration rate of the Brussels sprouts. The rate of respiration and the resulting heat generation are reduced at a higher CO₂-content and a lower O₂-content of the air. The CO₂ and O₂ concentrations in the container were not measured during the experiments. Therefore this assumption cannot be proven.

Fig. 99 also shows an increasing temperature after about 120 h, especially at the places with a higher temperature. This rise in temperature may be caused by an increasing heat generation due to deterioration of the Brussels sprouts. Deterioration will start sooner at higher temperatures. When the Brussels sprouts were removed from the container after the experiment, there was some rotting of the sprouts and the leaves were yellow where the temperature had been higher.

In the second experiment the change in temperature with time in the container filled up to a height of 0.45 m with Brussels sprouts was investigated. The Brussels sprouts of this experiment were stored for one week at 5 °C and acclimatized for one day at 16 °C before the container was filled. Fig. 100 shows the temperature course at different positions along the central axis. Comparison of Fig. 99 and Fig. 100 shows that the maximum in the temperature course is much higher in the first experiment. This may be caused by a higher rate of heat generation of the Brussels sprouts at the start of the first experiment. The rate of heat generation decreases after 25 h.

The second experiment also shows a temperature rise in the container after about 100 h. The temperature rises more than in the completely filled container. This result may be

Table 24. Physical data of Brussels sprouts used in the experiments.

Heat generation (Q) 15 °C:	0.55 W/kg
20 °C:	0.66 W/kg
Bulk density (ρ_b)	525 kg/m ³
Equivalent diameter (d_p)	0.029 m
Product density (ρ_p)	860 kg/m ³
Thermal conductivity (bulk) (λ_b)	0.30 W/mK
Specific heat ($c_{p,p}$)	3910 J/kg K

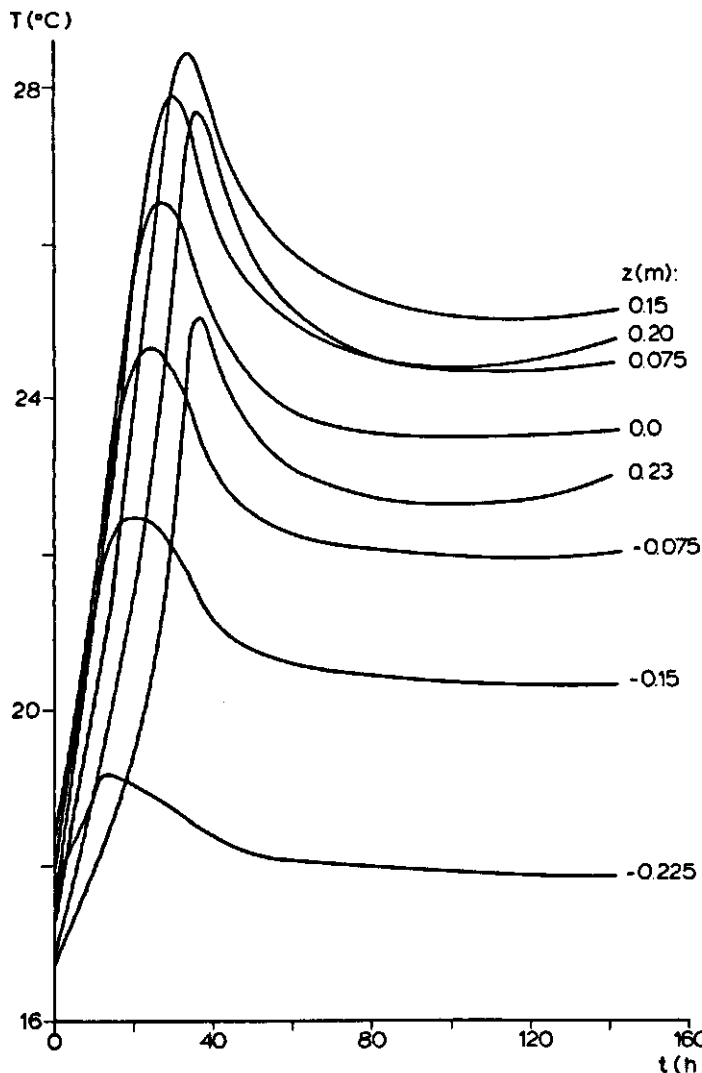


Fig. 99. Changes in temperature with time along the central axis of the container completely filled with Brussels sprouts. Wall temperature: 16.0 °C.

due to the faster deterioration of the Brussels sprouts in the second experiment, as the product had already been stored for one week at 5 °C. It is well known (Sprenger Institute, 1972) that storage of Brussels sprouts for one week at 5 °C reduces the storage period at 15 °C by about two days. Visual inspection after the experiment also showed more decay and discolouration than in the first experiment.

The pseudo steady-state profile of temperature on the z axis ($x = 0, y = 0$) in the two experiments (Fig. 101) shows that during the period of constant temperature the temperature was lower when the container was 90% filled. Better cooling due to better air circu-

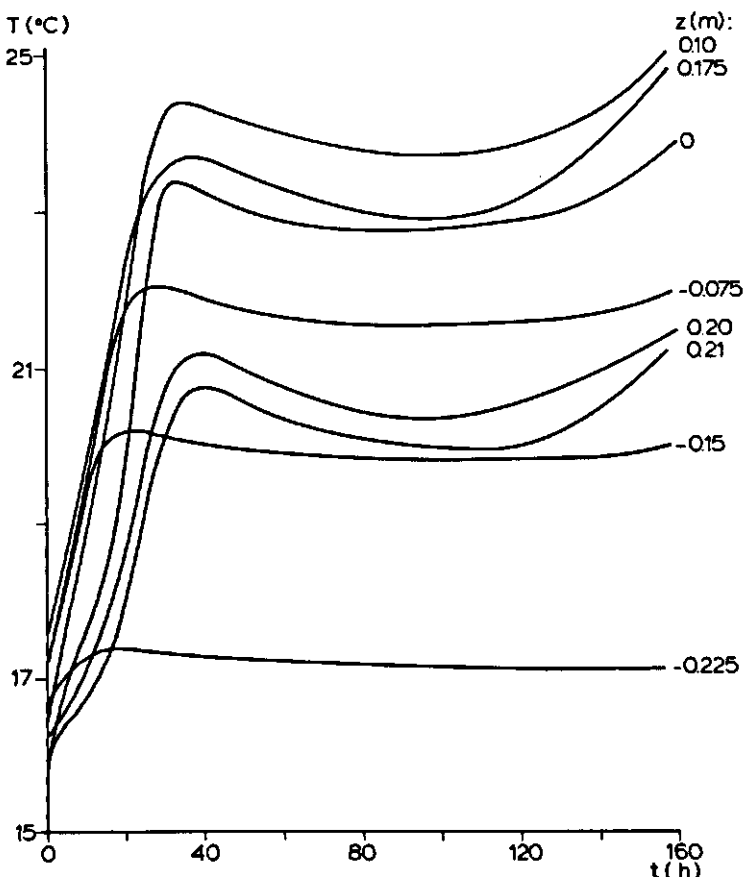


Fig. 100. Changes in temperature with time along the central axis of the container filled 90% with Brussels sprouts. Wall temperature: 16.0 °C.

lation may have produced this result, or even a lower rate of heat generation may account for it. As the rate of heat generation was only measured at the start of the first experiment, it is impossible to confirm this idea. Fig. 101 also shows that the temperature rise in the last period of the experiment is higher in the 90% filled container than in the completely filled container.

Condensation on the walls and on the Brussels sprouts also occurred in these experiments. More water vapour condensed than in the experiments with potatoes, because the moisture loss of Brussels sprouts was higher.

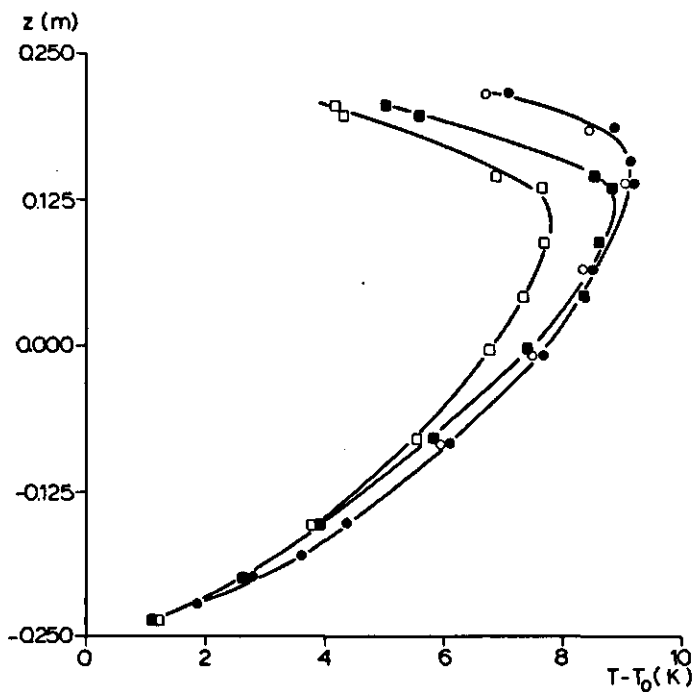


Fig. 101. Pseudo steady-state profile of temperature along the central axis:

- container 100% filled, after 100 h;
- container 100% filled, after 144 h;
- container 90% filled, after 98 h;
- container 90% filled, after 146 h.

6 Final remarks

This work has provided some insight in existing problems, but (as usual) it also has given rise to new questions and ideas, which are worth investigating further. At first the practical implications of this study are discussed and thereafter recommendations for future research are given.

6.1 Practical implications

The experimental results show that in a system with open top and open bottom the temperature rise of bulk-stored respiring produce is significantly reduced by natural convection, when the temperature of the ambient air is lower than the average temperature of the bulk. Acceptable low temperatures of bulk-stored produce can be attained without resorting to forced convection. However, when restriction of moisture loss is very important, temperature should be controlled by cooling with forced convection. The occurrence of natural convection, when forced convection is switched off, should then be hindered by closing all holes at bottom and side walls of the bulk.

As shown by the experimental results the value of the velocity of natural convection can be calculated from the assumption that the pressure drop caused by the flow through the bed is equal to the driving force of natural convection.

With the SNC-model, developed in this study, we can calculate the influence of different storage conditions on temperature, moisture distribution and moisture loss of stored produce. In the calculations of the present research heat was always generated by respiration. However this model can also be used to calculate the influence of other chemical reactions or microbial growth during storage of different materials, where heat is transported by natural or forced convection. The SNC-model may be of help in designing storage rooms, for example to calculate whether too high temperatures will develop in the system of interest or to calculate which cylinder diameter still gives acceptable temperatures of material stored in cylinders.

With the equations of the model of three-dimensional natural convection in a closed container it is possible to calculate the cooling rate of heat-generating products in closed containers with internal natural convection. It is also possible to predict the maximum temperature in the container for different container dimensions. Therefore, when the maximum acceptable temperature of the product is given, the maximum container dimensions may be calculated from the results of this study.

6.2 Suggestions for future research

The different model calculations can only give reliable results when values of the different physical properties of the stored product are correct. However the physical

properties at different temperatures and water vapour concentration are not always precisely known. Therefore more attention should be paid to the collection of precise and reliable experimental data. Moreover the work of this study emphasizes the need for better physical models of moisture loss.

The experiments on model material without moisture loss showed that a very simple model, predicting a linear temperature rise with height, was able to give a good prediction of the steady-state velocity of natural convection in systems with open bottom and open top. However this theory cannot be extended to products with moisture loss, because moisture loss influences temperature and therefore also the velocity of natural convection. Thus more experimental work is necessary to derive relations between rate of heat generation and velocity of natural convection, with moisture loss as an extra parameter, for real products.

The different models of natural convection for storage of agricultural and horticultural produce have shown that the representation of the ensemble of product and air by a porous medium gives good results, when a velocity-dependent permeability is used. In the calculation of the permeability a correction factor in the Ergun equation is used. However the correction factor of different products and under various storage conditions is not well known. It is therefore necessary to collect more relevant data about pressure drop for air flow through bulk-stored products.

Cooling by natural convection, without additional cooling by forced convection can be used in bulk storage when the size of the pieces of product is not too small. Under optimal storage conditions and at a bed height less than 3 m, the particle diameter should be larger than about 0.03 m at a relatively low rate of heat generation of the product (6 Wm^{-3}) and larger than about 0.06 m at a relatively high rate of heat generation of the product (60 Wm^{-3}). An economic analysis has to be made in order to decide whether costs of higher moisture loss, caused by the continuous air flow, are compensated by the advantage of lower energy costs. Energy costs decrease because fans to blow air through the stored produce are not necessary.

As shown by the experiments on potatoes and Brussels sprouts, for storage of real products in a closed container, the products lose moisture and condensation forms at different places in the container. These effects are not yet incorporated in the model equations of three-dimensional natural convection in a closed container. For better adaptation to practice the model has to be extended by incorporating these effects also. However the solution of the resulting set of equations will require much more computer-time than the solution of the actual model; for modelling moisture loss much smaller time steps should be used in the numerical calculations to avoid numerical instabilities.

During cooling of closed containers it is useful to know the time necessary to reduce the difference between average initial product temperature and average steady-state temperature by 90% (90% cooling time). These values may be calculated from the model of three-dimensional natural convection in a closed container. The results should be presented in a general correlation between 90% cooling time and various model parameters. The following model parameters could be introduced: container dimensions, rate of heat generation, particle diameter and difference between initial temperature and temperature of the colder surroundings. When the influence of moisture loss is included in the equations, this parameter can be introduced too. Here also reliable physical properties of the stored product are absolutely necessary.

Summary

In this study the influence of natural convection on heat and mass transfer during cooling and storage of agricultural or horticultural products is discussed. Natural convection is the flow of a fluid resulting from density differences. With storage of heat-generating products in a noninsulated container, a temperature gradient from the centre to the walls is created. At the walls heat is transferred to the environment. Natural convection occurs inside the container because of the nonuniform temperature distribution.

A review of literature shows that there are different models of bulk storage of agricultural or horticultural products and of conductive cooling of containers with these products. However in spite of its paramount importance, the influence of natural convection has not yet been incorporated in these models. Literature review also shows that several theories of natural convection in fluids and porous media with and without heat generation exist. I have extended these theories to conditions characteristic for storage of agricultural and horticultural products.

Three simple one-dimensional models of the steady-state temperature distribution in porous media with convective air flow and internal heat generation are developed. One of these models, which assumes heat transport by convection only, gives a proportionality between the velocity of natural convection and the square root of the rate of heat generation. Experimental results show that this relation offers a good prediction of the velocity of natural convection. The other models are a two-phase model and a one-phase model with velocity-dependent thermal conductivity. Both models describe heat transport by convection and conduction. They predict the measured steady-state temperatures in a cylindrical container, with insulated walls and open top and bottom, filled with heat-generating model material. Higher heat loss at the top than can be explained by radiation only, is modelled with an effective heat transfer coefficient, which rises linearly with the velocity of natural convection. Theoretical evidence for this rise is discussed. Experiments with the cylindrical container also show that natural convection gives rise to much lower temperatures when the air flow is not hindered by closing bottom, or top and bottom of the cylinder.

To model the influence of moisture loss and of the horizontally non-infinite extension of storage rooms too, a two-dimensional two-phase model of storage with natural convection (SNC-model) has been developed. In modelling natural convection, the air flow is assumed to be vertical and the ensemble of product and air is considered to be a continuous porous medium. The temperature and moisture distribution are calculated numerically from the energy and mass balance equations in a cylindrical system with heat generation, evaporation, condensation, moisture diffusion, heat conduction and convective transport. The SNC-model correctly predicts self-heating of a cylinder with model material or potatoes. A sensitivity analysis with the SNC-model demonstrates the influence of various model parameters such as mass transfer, porosity, rate of heat genera-

tion, bed height, heat and moisture loss at the side walls, velocity of forced convection and moisture content of the cooling air. It is shown that especially the rate of moisture loss has a great influence on the temperature and moisture distribution.

Many products are stored in closed containers. Air flow in closed containers caused by natural convection cannot be one-dimensional. Therefore I have developed a one-phase model of three-dimensional natural convection in closed containers, filled with heat-generating products. This model is used to calculate the wall heat transfer coefficients at bottom, top and side walls for experimental cooling of a closed container with isothermal walls. A good prediction of the measured change in temperature with time during cooling of the container is obtained with this model. The calculations also indicate that cooling of the container is accelerated by natural convection. As shown by experimental work the position of the maximum temperature in the container rises with increasing rate of heat generation. During experiments on self-heating of Brussels sprouts and potatoes in the closed container condensation occurred on top and side walls and on the products in the upper part of the container. This condensation and the experimental temperature distribution indicate that natural convection occurs when real products are stored.

The practical implications and suggestions for future research are discussed in the final chapter of this book.

Samenvatting

In dit proefschrift wordt de invloed van vrije convectie op warmte- en stofoverdracht bij het afkoelen en bewaren van land- en tuinbouwprodukten beschreven. Vrije convectie is de stroming van een fluïdum ten gevolge van dichtheidsverschillen in het fluidum. Het treedt bijvoorbeeld op bij bewaring van warmteproducerende produkten in een niet geïsoleerde kist. Hierin ontstaat een temperatuursafname vanuit het centrum naar de wanden, waar warmteverlies naar de omgeving plaatsvindt. Door de temperatuurverschillen in de kist zal er vrije convectie optreden.

Een literatuuroverzicht toont aan dat er verschillende modellen ontwikkeld zijn voor het berekenen van de temperatuur- en vochtverdeling die optreedt tijdens het koelen en bewaren van land- of tuinbouwprodukten in grote stapelingen. Ook bestaan er modellen voor de bewaring in kisten. In deze modellen wordt tot nu toe echter geen rekening gehouden met het optreden van vrije convectie. Er bestaan verschillende theorieën voor het beschrijven van vrije convectie in een fluïdum of in een poreus medium, waarbij al dan niet warmteontwikkeling in het systeem optreedt. Deze theorieën zijn uitgebreid om ze te kunnen gebruiken onder de omstandigheden die optreden bij de koeling en bewaring van land- of tuinbouwprodukten.

Er is een model opgesteld van een warmteproducerend poreus medium, in één richting doorstroomd met lucht, waarbij alleen warmtetransport door convectie aangenomen wordt. Uit dit model volgt dat de luchtsnelheid door vrije convectie evenredig is met de wortel uit de warmteproductie. De vrije-convectiesnelheid in een stapeling model-materiaal met warmteproductie waarin vrije doorstroming in vertikale richting mogelijk is, is berekend uit het gemeten stationaire temperatuurprofiel. Uit metingen bij verschillende warmteproducties blijkt dat de theoretische relatie tussen vrije-convectiesnelheid en warmteproductie goed voldoet (zie fig. 50).

Twee andere een-dimensionale modellen (een twee-fase model en een een-fase model met snelheidsafhankelijke warmtegeleidingscoëfficiënt) beschrijven warmtetransport door convectie en geleiding. De met deze modellen berekende stationaire temperatuurverdeling komt goed overeen met de gemeten stationaire temperatuurverdeling in een cylinder met open onder- en bovenkant en geïsoleerde zijwand. In de genoemde modellen is aan de bovenkant warmteverlies door straling aangenomen. Tijdens de experimenten treedt er een groter warmteverlies aan de bovenkant op dan ten gevolge van straling alleen. Dit extra warmteverlies is in het model beschreven met een effectieve warmteoverdrachtscoëfficiënt die lineair stijgt met de vrije convectiesnelheid. Een theoretische verklaring voor deze afhankelijkheid is besproken. Proeven met de cylinder tonen duidelijk aan dat door de vrije convectie de temperatuur in de cylinder veel lager is als er luchtstroming door de cylinder mogelijk is. Na het afsluiten van de onderkant of de onderkant en de bovenkant van de cylinder is de temperatuur in de stationaire toestand beduidend hoger.

Omdat er tijdens koeling en opslag van land- of tuinbouwprodukten ook vochtverlies

optreedt en omdat bewaarplaatsen nooit oneindig uitgestrekt zijn, is een twee-dimensionaal twee-fasemodel (SNC-model) opgesteld. Dit model beschrijft de temperatuur- en vochtverdeling in een cylinder met warmteproductie, verdamping, condensatie, vochtdifusie, warmtegeleiding en convectief transport. Uit de energie- en massabalansen voor dit systeem worden de temperatuur- en vochtverdeling numeriek berekend. Voor de beschrijving van vrije convectie is aangenomen dat de lucht in verticale richting stroomt en dat het totaal van produkt en lucht als een poreus medium mag worden beschouwd. Het SNC-model geeft een correcte beschrijving van het gemeten temperatuurverloop tijdens de zelf-opwarming van een cylinder gevuld met modelmateriaal of aardappels. Een gevoelighedenanalyse met het SNC-model toont de invloed van verschillende parameters in het model, zoals: stofoverdrachtscoëfficiënt, porositeit, warmteproductie, hoogte van de stapeling, warmte- en vochtverlies aan de zijwanden, gedwongen convectiesnelheid en vochtgehalte van de omgevingslucht. Uit de berekeningen blijkt dat de snelheid waarmee het produkt vocht verliest de grootste invloed heeft op de temperatuur- en vochtverdeling.

Er is een drie-dimensionaal een-fasemodel afgeleid voor de beschrijving van vrije convectie in een gesloten kist, gevuld met warmteproducerende produkten. Dit model is ontwikkeld omdat veel produkten in kisten bewaard worden, terwijl de luchtstroming in een afgesloten kist natuurlijk nooit een-dimensionaal kan zijn. Het model is gebruikt om de waarde van de interne warmte-overdrachtscoëfficiënt aan onderkant, zijkanten en bovenkant tijdens de experimentele afkoeling van een kist te berekenen. De kist is gevuld met warmteproducerend modelmateriaal, terwijl de wanden isotherm zijn. Het model geeft een goede voorspelling van het gemeten temperatuurverloop op verschillende plaatsen in de kist tijdens afkoeling. De modelberekeningen laten ook zien dat de koeling versneld wordt door het optreden van vrije convectie. Uit de experimenten met modelmateriaal blijkt dat de plaats van de maximale temperatuur in de kist stijgt met toeneemende warmteproductie. Er zijn proeven uitgevoerd met de gekoelde kist, gevuld met aardappels of spruitkool. Hierbij is de temperatuurstijging in de kist ten gevolge van de warmteproductie van het produkt gemeten. Er ontstond condensatie op de bovenkant en zijkant en op de produkten in het bovenste deel van de kist. De plaats van deze condensatie en de gemeten temperatuurverdeling tonen aan dat vrije convectie optreedt tijdens de opslag van land- of tuinbouwprodukten in kisten.

In het laatste hoofdstuk van dit proefschrift worden zowel praktische toepassingen van dit werk als suggesties voor nader onderzoek besproken.

Appendix A. Solution of the equations of the SNC-model

In order to solve the parabolic differential equations (3.62) and (3.63) I have used an Alternating Direction Implicit Procedure (ADIP) (Peaceman & Rachford, 1955), as recommended by Marsall (1976). With this procedure the temperature and moisture distribution are calculated in the following way.

1. The average air temperature and concentration are calculated with the trapezoidal rule and used to calculate the value of v_{NC} and the variables dependent on v_{NC} .
2. The difference equation of (3.63) is written with the analog to the derivatives in the R direction on the new time-level and in the Z direction on the old time-level (implicit in R direction). The difference equations on every Z -level form a tridiagonal coefficient matrix which is solved by using the Thomas algorithm to give the θ_p values after the time $\Delta\tau$.
3. The difference equation of (3.62) is written with the analog to the derivatives in the R direction on the new time-level and in the Z direction on the old time-level. The resulting equations are again solved by using the Thomas algorithm and give the C values after the time $\Delta\tau$.
4. θ_a after a time step $\Delta\tau$ is calculated from the calculated values of θ_p in the grid points.
5. The values of C are checked to detect whether condensation occurs somewhere. If necessary C is set at the C_{sat} value and the amount of condensed water is calculated.
6. The difference equation of (3.63) is written with the analog to the derivatives in the Z direction on the new time-level and in the R direction on the old time-level (implicit in Z direction). The difference equations on every R -level form a tridiagonal coefficient matrix which is solved by using the Thomas algorithm to give θ_p -values after the time $2\Delta\tau$.
7. The difference equation of (3.62) is written with the analog to the derivatives in the Z direction on the new time-level and in the R direction on the old time-level. The resulting equations give the value of C on the grid points after the time $2\Delta\tau$ directly.
8. θ_a after the time $2\Delta\tau$ is calculated from the values of θ_p in the grid points.
9. As 5.
10. A new value of the time step, $\Delta\tau$, is calculated by introducing a $\Delta\tau$ value which causes a maximum estimated change in C at the different grid-points of 2% of the initial value of C . The choice of the new time-step is restricted by the demand that the new time-step is never more than three times the old time-step and never exceeds an upper limit ($\Delta\tau \leq 2 \times 10^{-6}$). Time steps above the upper limit cause instabilities in the numerical scheme.

With the values of θ_p , C and θ_a after the first two time-steps the procedure 1-10 is repeated and so on. The values of the different constants in Eqns (3.62) and (3.63) show

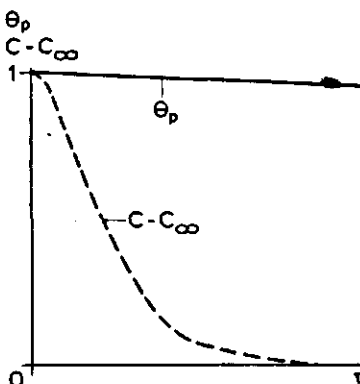


Fig. A₁. A stiff system.
 — Temperature
 --- Concentration.

that these two equations form a stiff system. Thus the change in C at the beginning of the cooling is much faster than the change in θ_p (see Fig. A1). Consequently the use of time steps is controlled by the calculation of the concentration. After some time the change in concentration becomes rather small and the calculation procedure is changed. A larger time-step is chosen which gives an estimated change in θ_p of 2%. The large time-step should not exceed a limiting value, above which the numerical scheme becomes unstable ($\Delta\tau \leq 3 \times 10^{-5}$). C is assumed to be constant during this time-step. The steps 1, 2, 4, 6 and 8 from the calculation procedure are performed with the large time step. Hereafter a new small time-step is calculated and the steps 1 to 9 from the calculation procedure are performed again.

By using alternately a small and a large time-step the computation time was reduced 10 times. A calculation with only small time-steps gave the same result as a calculation with alternately small time-steps and large time-steps with a constant value of C .

Appendix B. Physical properties of the potatoes used in the experiments

The potatoes in my experiments were grown on river clay and harvested in September. Variety: Bintje, size 35/45 mm. The potatoes were cured at the farm for 3 weeks at 15-20 °C. Some experiments started in February when the dormant period was already finished.

The rate of heat generation of the potatoes was measured by the Sprenger Institute with an adiabatic calorimeter as described by Rudolphy et al. (1977). The results are given in Table B1. The rate of heat generation in November was rather low compared

Table B₁. Rate of heat generation on two occasions at different temperatures.

Date	T (°C)	Q (W/kg)
Nov. '78	20.0	0.016
March '79	15.0	0.030
March '79	20.0	0.039
March '79	25.0	0.050

Table B₂. Physical properties of the potatoes used in the experiments.

λ_0 (W/m K)	0.25
ρ_p (kg/m ³)	1090
ρ_b (kg/m ³)	710
c_p (J/kg K)	3590
d_p (m)	0.046
A (m ² /m ³)	132
Q_0 (W/kg)	1.261×10^5
Q_1 (K)	4396

with data of Grähs et al. (1978) who found a rate of heat generation of 0.019 W kg⁻¹ of Bintjes at 14 °C. These data were however measured at the start of the storage period when the rate of heat generation is higher as reported by Schippers (1977b). The measured rate of heat generation in March was much higher than the values of Grähs et al. (1978) because the dormant period was already finished when these measurements were made. It is well known (Schippers, 1977a, 1977b) that the rate of heat generation rises after the dormant period.

The temperature dependence of the rate of heat generation is described with the Arrhenius type equation:

$$Q = Q_0 e^{-\frac{Q_1}{T}} \quad (B.1)$$

where T represents the absolute temperature (K). The values of Q_0 and Q_1 are given in Table B2. This table also gives the other physical properties of the potatoes. The bulk thermal conductivity (λ_0) was measured by the Sprenger Institute with a Poensgen apparatus as described by Van Beek (1974) and Bouwman (1977). The product density (ρ_p) is determined by weighing the product in water and in air. The bulk density (ρ_b) is calculated from the weight and the volume of the potatoes in the cylindrical set-up. The specific heat (c_p) is calculated by the Sprenger Institute from the experimentally determined composition as described by Van Beek & Verbeek (1978). The particle diameter (d_p) is the diameter of a spherical potato with the same weight as the average weight of a single potato in these experiments. The specific surface area (A) follows from the assumption of spherical products: $A = 6/d_p$ m² m⁻³ product.

References

Arsdel, W.B. van, 1955. Simultaneous heat and mass transfer in a non isothermal system: Through flow drying in the low-moisture range. Am. Inst. Chem. Eng. Symposium Series No. 16 p. 47-58.

Anzelius, A., 1926. Über Erwärmung vermittels durchströmender Medium, Z. angew. Math. Mech. 6: 291-294.

Aziz, K. & J.D. Hellums, 1967. Numerical solution of the three-dimensional equations of motion for laminar natural convection. Physics Fluids 10: 314-324.

Baird, C.D. & J.J. Gafney, 1976. A numerical procedure for calculating heat transfer in bulk loads of fruits and vegetables. ASHRAE Trans. 82: 525-540.

Bakker Arkema, F.W., R.C. Brook & L.E. Lerew, 1977. Cereal grain drying. Advances in cereal science and technology, Vol. II. In: Y. Pomeranz (Ed.) Am. Ass. Cereal Chem. Inc., St. Paul, Minnesota.

Bakker Arkema, F.W., R.J. Patterson & W.G. Bickert, 1969. Static pressure-airflow relationships in packed beds of granular biological materials such as cherry pits. Trans. Am. Soc. agric. Engrs 12: 134-136, 140.

Balakrishnan, A.R. & D.C.T. Pei, 1979. Heat transfer in gas-solid packed bed systems. 1. A critical review. Ind. Engng Chem. Proc. Des. Dev. 18: 30-40.

Barker, J.J., 1965. Heat transfer in packed beds. Ind. Engng Chem. 57: 43-51.

Bauer, R. & E.U. Schlünder, 1977. Die effektive radiale Wärmeleitfähigkeit gasdurchströmter Schüttungen. Verfahrenstechnik 11: 605-614.

Beck, J.L., 1972. Convection in a box of porous material saturated with fluid. Physics Fluids 15: 1377-1383.

Beek, G. van, 1974. Heat transfer through layers of agricultural products of near spherical shape. Ann. Bull. IIR 1974-3: 183-188.

Beek, G. van & L. Ficek, 1979. Prediction of relative humidity in a transport container. Proc. 15th int. Congr. Refr., Venice.

Beek, G. van & W. Verbeek, 1978. Calculation of thermophysical properties of horticultural produce from their composition between -40 °C and +20 °C. Report Nr 1959, Sprenger Institute, Wageningen.

Berg, L. van den & C.P. Lentz, 1973. High humidity storage of carrots, parsnips, rutabagas and cabbage. J. am. Soc. hort. Sci. 98: 129-132.

Berg, L. van den & C.P. Lentz, 1975. Effect of composition on thermal conductivity of fresh and frozen foods. Can. Inst. Food Sci. Technol. J. 8: 79-83.

Beukema, K.J. & J.G. de Swart, 1979. An accurate thermistor based temperature measuring system. Technical and preliminary research report No 87, ITAL, Wageningen.

Bird, R.B., W.E. Stewart & E.N. Lightfoot, 1960. Transport phenomena. John Wiley & Sons, Inc., New York.

Bloome, P.D. & G.C. Shove, 1971. Near equilibrium simulation of shelled corn drying. Trans. Am. Soc. agric. Engrs 14: 709-712.

Boon-Long, P., T.W. Lester & R.E. Faw, 1979. Convective heat transfer in an internally heated horizontal fluid layer with unequal boundary temperatures. Int. J. Heat Mass Transfer 22: 437-445.

Bories, S.A. & M.A. Combarnous, 1973. Natural convection in a sloping porous layer. J. Fluid Mech. 57: 63-79.

Bouwman, P., 1977. Bepaling van de warmtegeleidingscoëfficiënt van rozen met het Poensgen-apparaat. Report No 1990, Sprenger Institute, Wageningen.

Brinkman, H.C., 1947. A calculation of the viscous force exerted by a flowing fluid on a dense swarm of particles. *Appl. sci. Res.* A1: 27-34.

Brooker, D.B., 1967. Mathematical model of the psychrometric chart. *Trans. Am. Soc. agric. Engrs* 10: 558-560, 563.

Brunovska, A., V. Hlavacek, J. Ilavsky & J. Valtyni, 1978. An analysis of non isothermal one-component sorption in a single adsorbent particle. *Chem. Engng Sci.* 33: 1385-1390.

Buretta, R.J., 1972. Thermal convection in a fluid filled porous layer with uniform internal heat sources. *Ph. D. Thesis, Univ. of Minnesota.*

Buretta, R.J. & A.S. Berman, 1976. Convective heat transfer in a liquid saturated porous layer. *J. appl. Mech.* 43: 249-253.

Burton, W.G., 1963. The basic principles of potato storage as practised in Great Britain. *Eur. Potato J.* 6: 77-92.

Burton, W.G., 1977. Storage requirements as determined by potential deterioration. *Ann. appl. Biol.* 85: 157-158.

Burton, W.G., G. Mann & H.G. Wager, 1955. The storage of ware potatoes in permanent buildings. II The temperature of unventilated stacks of potatoes. *J. agric. Sci.* 46: 150-163.

Businger, J.A., 1954. Luchtbehandeling van producten in gestorte toestand. *Verwarming en Ventilatie* 11: 31-35.

Cannon, J.N., W.B. Krantz, F. Kreith & D. Naot, 1979. A study of transpiration from porous flat plates simulating plant leaves. *Int. J. Heat Mass Transfer* 22: 469-483.

Carlaw, G.S. & J.C. Jaeger, 1959. Conduction of heat in solids. Oxford University Press, Oxford.

Carter, D.G. & M.D. Farrat, 1943. Redistribution of moisture in soybean bins. *Agric. Engng* 24: 296.

Catton, I. & A.J. Suo-Antilla, 1974. Heat transfer from a volumetric heated horizontal fluid layer. *Proc. 5th Int. Heat Transf. Conf., Tokio (3) p. 69-73.*

Cheftel, J.C. & H. Cheftel, 1976. Introduction à la biochémie et à la technologie des aliments. P.I.C., Genève.

Cheung, F.B., 1977. Natural convection in a volumetric heated fluid layer at high Rayleigh numbers. *Int. J. Heat Mass Transfer* 20: 499-506.

Cheung, F.B., 1978. Correlation equations for turbulent thermal convection in a horizontal fluid layer heated internally and from below. *J. Heat Transfer* 100: 416-422.

Colquhoun-Lee, B.I. & J. Stepanek, 1974. Mass transfer in single phase flow in packed beds. *The Chemical Engineer* 282 February, p. 108-111.

Dixon, A.G., W.G. Paterson & D.L. Cresswell, 1978. Heat transfer in packed beds of low tube/particle diameter ratio. *Chemical Reaction Engineering-Houston.* V.W. Weekman & D. Luss (Eds.), ACS Symp. Series 65, Am. Chem. Soc., Washington.

Douglas Jr., J. & H.H. Rachford Jr., 1956. On the numerical solution of heat conduction problems in two and three space variables. *Trans. am. math. Soc.* 82: 421-439.

Dullien, F.A.L., 1975. Single phase flow through porous media and pore structures (invited review). *Chem. Engng J.* 10: 1-34.

Dwivedi, P.N. & S.N. Upadhyay, 1977. Particle-fluid mass transfer in fixed and fluidized beds. *Ind. Engng Chem. Proc. Des. Dev.* 16: 157-165.

Eelkman Rooda, J. & F.P.H. van Beckum, 1978. Heat-transfer during the cooling process of exponential heat generating produce. *Lebensm. Wiss. Technol.* 11: 209-214.

Elder, J.W., 1967. Steady free convection in a porous medium heated from below. *J. Fluid Mech.* 27: 29-48.

Epherre, J.F., M. Combarnous & S. Klarsfeld, 1976. Critère d'apparition de la convection naturelle dans des couches poreuses anisotropes saturées d'air et soumises à de grandes différences de température. *Ann. Bull. IIR* 1976-2: 55-62.

Ergun, S., 1952. Fluid flow through packed columns. *Chem. Engng Prog.* 48: 89-94.

Eucken, A., 1940. Allgemeine Gesetzmässigkeiten für das Wärmeleitvermögen verschiedener Stoffarten und Aggregatzustände. *Forsch. Geb. Ingenieurwes.* 11: 6-20.

Ferrel, J.K., R.W. Rousseau & M.R. Branscome, 1976. The development and testing of a mathematical model for complex adsorption beds. *Ind. Engng Chem. Proc. Des. Dev.* 15: 114-122.

Fischer, R., 1967. Pulsierende Strömung durch Schüttungen. *VDI-Forschungsheft* 524.

Fockens, F.H., 1967. Fysische transportverschijnselen tijdens het afkoelen van tuinbouwprodukten. Ph. D. Thesis, Techn. Univ. Delft.

Fockens, F.H. & H.F.Th. Meffert, 1972. Biophysical properties of horticultural products as related to loss of moisture during cooling down. *J. Sci. Food Agric.* 23: 285-298.

Froment, G.F., 1974. Fixed bed catalytic reactors. Technological and fundamental design aspects. *Chem. Ing. Tech.* 46: 374-386.

Furnas, C.C., 1930. Heat transfer from a gas stream to a bed of broken solids. *Trans. Am. Inst. chem. Engrs* 24: 142-193.

Gafney, J.J., 1977. Engineering principles related to the design of systems for air cooling of fruits and vegetables in shipping containers. *Proc. 29th Int. Conf. on Handling Perishable Agricultural Commodities*, Michigan State Univ..

Gasser, R.D. & M.S. Kazimi, 1976. Onset of convection in a porous medium with internal heat generation. *J. Heat Transfer* 98: 49-54.

Geel, J.L.C. van, 1966. Safe radius of heat generating substances. *Ind. Engng Chem.* 58: 24-32.

Gilles, E.D., 1976. Reactor models. *Proc. Chem. React. Engng. 4th Int./6th Eur. Symp.* Heidelberg, DecHEMA, Frankfurt am M..

Gögüs, A.Y., M. Akyurt & S. Yavuzkurt, 1972. Unsteady cooling of unit loads with exponential heat generation. *Ann. Bull. IIR* 1972-1: 227-239.

Gonlag, H.M., 1974. Temperatuurontwikkeling in stapels tuinbouwprodukten met temperatuurafhankelijke warmteproductie tijdens koelen. M. Sc. thesis, Wageningen. Also: Report nr 1916, Sprenger Institute, Wageningen.

Grähs, L., B. Hylmö, A. Johansson & C. Wikberg, 1978. The two-point temperature measurement. A method to determine the rate of respiration in a potato pile. *Acta Agric. scand.* 28: 231-236.

Hardee, H.C. & R.H. Nilson, 1977. Natural convection in porous media with heat generation. *Nucl. Sci. Engng* 63: 119-132.

Hirasaki, G.J. & J.D. Hellums, 1968. A general formulation of the boundary conditions on the vector potential in three-dimensional hydronamics. *Q. appl. Math.* 26: 331-342.

Hlavacek, V., 1970. Aspects in design of packed catalytic reactors. *Ind. Engng Chem.* 62: 8-26.

Hofmann, H., 1974. Probleme bei der mathematischen Modellierung von Schütschicht Reaktoren. *Chem. Ing. Tech.* 46: 236-242.

Holst, P.H. & K. Aziz, 1972a. A theoretical and experimental study of natural convection in a confined porous medium. *Can. J. chem. Engng* 50: 232-241.

Holst, P.H. & K. Aziz, 1972b. Transient three-dimensional natural convection in confined porous media. *Int. J. Heat Mass Transfer* 15: 73-90.

Horne, R.N. & M.J. O'Sullivan, 1978. Convection in a porous medium heated from below: the effect of temperature dependent viscosity and thermal expansion coefficient. *J. Heat Transfer* 100: 448-452.

Hunter, J.H., 1976. Mathematical simulation of the physiological interactions of the white potato in bulk storage. First Int. Cong. Engng and Food, Boston p. 36.

Hwang, I., 1971. Finite amplitude thermal convection in porous media with heat source and variable viscosity. Ph. D. Thesis, Univ. of Minnesota.

Hylmö, B., T. Persson, C. Wikberg & W.C. Sparks, 1975a. The heat balance in a potato pile. I The influence of the latent heat of the removed water. *Acta Agric. scand.* 25: 81-87.

Hylmö, B., T. Persson, C. Wikberg & W.C. Sparks, 1975b. The heat balance in a potato pile. II The temperature distribution at intermittent ventilation. *Acta Agric. scand.* 25: 88-91.

Jaffrennou, J.Y., S.A. Bories & M.A. Combarnous, 1974. Natural convective flows and mean heat transfer in a sloping porous layer. *Proc. 5th Int. Heat Transf. Conf.*, Tokio (3) p. 83-87.

Jahn, M. & H.H. Reineke, 1974. Free convection heat transfer with internal heat sources, calculations and measurements. *Proc. 5th Int. Heat Transf. Conf.*, Tokio (3) p. 74-78.

Jones, D.R., 1974. Convective effects in enclosed, exothermally reacting gases. *Int. J. Heat Mass Transfer* 17: 11-21.

Kaneko, T., M.F. Mohtadi & K. Aziz, 1974. An experimental study of natural convection in inclined porous media. *Int. J. Heat Mass Transfer* 17: 485-496.

Käppel, R. & J. Weichmann, 1977. Gemüse Lagerung bei der Verwertungsindustrie. *Ind. Obst und Gemüseverwert.* 62: 131-133.

Kassoy, D.R. & A. Zebib, 1975. Variable viscosity effects on the onset of convection in porous media. *Physics Fluids* 18: 1649-1651.

Katto, Y. & T. Masuoka, 1967. Criterion for the onset of convective flow in a fluid in a porous medium. *Int. J. Heat Mass Transfer* 10: 297-309.

Kee, R.J., C.S. Landram & J.C. Miles, 1976. Natural convection of a heat generating fluid within closed vertical cylinders and spheres. *J. Heat Transfer* 98: 55-61.

Kostaropoulos, A.E., W. Wolf & W.E.L. Spiess, 1975. Modelle für die theoretische Bestimmung der Wärmeleitzahl inhomogener poröser Stoffe. *Lebensm. Wiss. Technol.* 8: 177-180.

Kulacki, F.A. & A.A. Emara, 1977. Steady and transient thermal convection in a fluid layer with uniform volumetric energy sources. *J. Fluid Mech.* 83: 375-395.

Kulacki, F.A. & R.J. Goldstein, 1972. Thermal convection in a horizontal fluid layer with uniform volumetric energy sources. *J. Fluid Mech.* 55: 271-287.

Kulacki, F.A. & R.J. Goldstein, 1974. Eddy heat transport in thermal convection with volumetric energy sources. *Proc. 5th int. Heat Transf. Conf.*, Tokio (3) p. 64-68.

Kulacki, F.A. & R. Ramchandani, 1975. Hydrodynamic instability in a porous layer saturated with a heat generating fluid. *Wärme und Stoffübertragung* 8: 179-185.

Labuza, T.P., 1970. Properties of water as related to keeping quality of foods. *Proc. 3th int. Cong. Food, Science and Technol.*, Washington, p. 618-635.

Lawson, M.L. & W.J. Yang, 1975. Thermal stability of binary gas mixtures in a porous medium. *J. Heat Transfer* 97: 378-381.

Lawson, M.L., W.J. Yang & S. Bunditkul, 1976. Theory on thermal instability of binary gas mixtures in porous media. *J. Heat Transfer* 98: 35-41.

Lapwood, E.R., 1948. Convection of a fluid in a porous medium. *Proc. Cambridge philos. Soc.* 44: 508-521.

Lentz, C.P., L. van den Berg & R.S. Mac Cullough, 1971. Study of affecting temperature, relative humidity and moisture loss in fresh fruit and vegetable storages. *J. Can. Inst. Food Technol.* 4: 146-153.

Lerew, L.E., 1978. Development of a temperature-weight loss model for bulk stored potatoes. Ph. D. Thesis, Univ. Michigan State University.

Lerou, J.J. & G.F. Froment, 1977. Velocity, temperature and conversion profiles in fixed bed catalytic reactors. *Chem. Engng Sci.* 32: 853-861.

Li, C.H. & B.A. Finlayson, 1977. Heat transfer in packed beds – a reevaluation. *Chem. Engng Sci.* 32: 1055-1066.

Ligny, C.L. de, 1970. Coupling between diffusion and convection in radial dispersion of matter by fluid flow through packed beds. *Chem. Engng Sci.* 25: 1177-1181.

Loughlin, J.B. O', 1976. Cold storage of fresh fruit and vegetables. *Tasmanian J. Hort.* 47: 119-126.

Lukov, A.V., 1968. Analytical heat diffusion theory. Academic Press, New York.

Macdonald, I.F., M.S. El-Sayed, K. Mow & F.A.L. Dullien, 1979. Flow through porous media – the Ergun equation revisited. *Ind. Engng Chem. Fund.* 18: 199-208.

Marsal, D., 1976. Die numerische Lösung partieller Differentialgleichungen. Bibliographisches Institut AG, Zürich.

Matthies, H.J., 1956. Der Strömungswiderstand beim belüfteten landwirtschaftlichen Erntegut. *VDI-Forschungsheft* 454.

Matthies, H.J. & H. Petersen, 1974. New data for calculating the resistance to air flow of stored granular materials. *Trans. Am. Soc. agric. Engrs* 17: 1144-1149.

Meffert, H.F.Th. & G. van Beek, 1976. Safe radius is an important physical propertie. *Ann. Bull. IIR* 1976-1: 341-348.

Meffert, H.F.Th. & M.L. Potters, 1970. Development of the temperature field in a cube with heat generation. *Ann. Bull. IIR* 1970-1: 97-106.

Meffert, H.F.Th. & J.W. Rudolphy, 1972. The cooling process of heat generating bodies. *Int. Symp. Heat and Mass Transfer problems in Food Engng*, Paper B6, Wageningen.

Meijer, O.A. & T.W. Weber, 1967. Nonisothermal adsorption in fixed beds. *A.I.Ch.E.J.* 13: 457-465.

Mellor, J.D., 1979. Thermophysical properties of foodstuffs 3. Measurements. *Bull IIR* 59: 551-564.

Mellor, J.D., E.G. Hall & D. Martin, 1962. Cooling of fruit in bulk bins. *Proc. 1st int. Congr. Food Sci. Technol.*: 625-631.

Misener, G.C. & M.L. Mac Donald, 1975. Simulated moisture loss and cooling time for bulk potatoes. Canadian agric. Engng 17: 72-74.

Misener, G.C. & G.C. Shove, 1976a. Simulated cooling of potatoes. Trans. Am. Soc. agric. Engrs 19: 954-957, 961.

Misener, G.C. & G.C. Shove, 1976b. Moisture loss from Kennebec potato tubers during initial storage period. Trans. Am. Soc. agric. Engrs 19: 967-969.

Molerus, O., 1977. Druckverlustgleichung für die Durchströmung von Kugelschüttungen im laminaren und im Übergangsbereich. Chem. Ing. Techn. 49: 675.

Muir, W.E., 1973. In: R.H. Sinha & W.E. Muir, (Eds) *Grain Storage: Part of a system*. The Avi Publishing Comp., Inc. Westport, Connecticut. p. 63.

Neale, M.A. & H.J.M. Messer, 1976. Resistance of root and bulb vegetables to airflow. J. agric. Engng Res. 21: 221-231.

Palm, E., J.E. Weber & O. Kvernold, 1972. On steady convection in a porous medium. J. Fluid Mech. 54: 153-161.

Patterson, R.J., F.W. Bakker Arkema & W.G. Bickert, 1971. Static pressure - airflow relationships in packed beds of granular biological materials such as grain II. Trans. Am. Soc. agric. Engrs 14: 172-174, 178.

Peaceman, P.W. & H.H. Rachford Jr., 1955. The numerical solution of parabolic and elliptic differential equations. J. Soc. indstr. appl. Math. 3: 28-41.

Ray, W.H., 1972. Fixed bed reactors: dynamics and control. Proc. 5th Eur. 2nd int. Symp. chem. Reactor Engng., Amsterdam, Paper A8. Elsevier Publ. Co., Amsterdam. p. 1-19.

Reidy, G.A. & A.L. Rippen, 1971. Methods for determining thermal conductivity in foods. Trans. Am. Soc. agric. Engrs 14: 248-254.

Ribando, R.J. & K.E. Torrance, 1976. Natural convection in a porous medium: effects of confinement, variable permeability and thermal boundary conditions. J. Heat Transfer 98: 42-48.

Rice, B., 1974. Computer simulation of temperature control systems in potato stores. Acta Hort. 38: 91-94.

Rudolphy, J.W., W. Verbeek & F.H. Fockens, 1977. Measuring heat production of respiring produces under normal and CA-storage conditions with an adiabatic calorimeter. Lebensm. Wiss. Technol. 10: 153-158.

Rudraiah, N. & P.R. Prabhramani, 1974. Thermal diffusion and convective stability of two component fluid in a porous medium. Proc. 5th Int. Heat Transf. Conf., Tokio (5) 79-82.

Rumpf, H. & A.R. Gupte, 1971. Einflüsse der Porosität und Korngrößenverteilung im Widerstandsgesetz der Porenströmung. Chem. Ing. Techn. 43: 367-375.

Sastry, S.K., C.D. Baird & D.E. Buffington, 1978. Transpiration rates of certain fruits and vegetables. ASHRAE Trans. 84: 237-255.

Schippers, P.A., 1977a. The rate of respiration of potato tubers during storage. 1. Review of literature. Potato Res. 20: 173-188.

Schippers, P.A., 1977b. The rate of respiration of potato tubers during storage. 2. Results of experiments in 1972 and 1973. Potato Res. 20: 189-206.

Schumann, T.E.W., 1929. Heat transfer: a liquid flowing through a porous prism. J. Franklin Inst. 208: 405-416.

Seiki, N., S. Fukusako & H. Inaba, 1978. Heat transfer in a confined rectangular cavity packed with porous media. Int. J. Heat Mass Transfer 21: 985-989.

Serpemen, Y. & W.D. Deckwer, 1977. Vergleich ein- und zweidimensionaler Modelle für Festbettreaktoren mit Wandkühlung. Chem. Ing. Tech. 49: 365.

Simon, B. & D. Vortmeyer, 1978. Measured and calculated migration speeds of reaction zones in a fixed bed reactor, a quantitative comparison. Chem. Engng Sci. 33: 109-114.

Spaninks, J.A.M., 1979. Design procedures for solid-liquid extractors. Agric. Res. Rep. 885, Pudoc Wageningen. Also doctoral thesis, Agric. Univ. Wageningen. 100 p.

Sprenger Institute, 1972. *Productgegevens groente en fruit*. Sprenger Instituut, Wageningen.

Strauss, J.M., 1974. Large amplitude convection in porous media. J. Fluid Mech. 64: 51-63.

Strauss, J.M. & G. Schubert, 1978. On the existance of three-dimensional convection in a rectangular box containing fluid-saturated porous material. J. Fluid Mech. 87: 385-394.

Sun, W.J., 1973. Convective instability in superposed porous and free layers. Ph. D. Thesis, Univ. of Minnesota.

Tchumak, I.G., V.S. Murashov & V.P. Petrovsky, 1970. Heat and moisture exchange in fruit storage rooms. *Ann. Bull. IIR* 1970-3: 321-324.

Thompson, T.L., R.M. Peart & G.H. Foster, 1968. Mathematical simulation of corn drying – a new model. *Trans. Am. Soc. agric. Engrs* 11: 582-586.

Tveitereid, M., 1977. Thermal convection in a horizontal porous layer with internal heat sources. *Int. J. Heat Mass Transfer* 20: 1045-1050.

Tveitereid, M., 1978. Thermal convection in a horizontal fluid layer with internal heat sources. *Int. J. Heat Mass Transfer* 21: 335-339.

Villa, L.G., 1973. Single particle convective moisture losses from horticultural products in storage. Ph. D. Thesis, Michigan State University.

Vortmeyer, D., K. Dietrich & K.O. Ring, 1974. Comparison of one- and two-phase model predictions for adiabatic packed bed chemical reactors. *Adv. Chem. Ser.* 133. Chemical Reaction Engng II: 588-599.

Vortmeyer, D. & R.J. Schaefer, 1974. Equivalence of one- and two-phase models for heat transfer processes in packed beds: one dimensional theory. *Chem. Engng Sci.* 29: 485-491.

Wakao, N. & T. Funazkri, 1978. Effect of fluid dispersion coefficients in particle-to-fluid mass transfer coefficients in packed beds. Correlation of Sherwood numbers. *Chem. Engng Sci.* 33: 1375-1384.

Wakao, N., S. Kaguci & T. Funazkri, 1979. Effect of fluid dispersion coefficients on particle-to-fluid heat transfer coefficients in packed beds. Correlation of Nusselt numbers. *Chem. Engng Sci.* 34: 325-336.

Wakao, N. & K. Kato, 1969. Effective thermal conductivity of packed beds. *J. chem. Engng Japan* 2: 24-33.

Walker, K. & G.M. Homsy, 1977. A note on convective instabilities in Boussinesq fluids and porous media. *J. Heat Transfer* 99: 338-339.

Weast, R.C. (Ed.), 1975. *Handbook of Chemistry an Physics*, 56th ed. CRC Press, Ohio.

Weber, J.E., 1975a. Thermal convection in a tilted porous layer. *Int. J. Heat Mass Transfer* 18: 474-475.

Weber, J.E., 1975b. The boundery layer regime for convection in a vertical porous layer. *Int. J. Heat Mass Transfer* 18: 569-573.

Whithaker, S., 1966. The equation of motion in porous media. *Chem. Engng Sci.* 21: 291-300.

Whitaker, S., 1969. Advances in theory of fluid motion in porous media. *Ind. Engng Chem.* 61: 15-28.

Willet, J.W., 1976. The world food situation. Vol. I. Oceana Publications Inc. Dobbs Ferry: 219, 326-327.

Yagi, S. & D. Kunii, 1957. Studies on effective thermal conductivities in packed beds. *A.I.Ch.E.J.* 3: 373-381.

Yavuzkurt, S., A.Y. Gögüs & T. Ceylan, 1976. Heat and mass transfer during precooling. *Ann. Bull. IIR* 1976-2: 87-96.

Zebib, A. & D.R. Kassoy, 1977. Onset of natural convection in a box of water saturated porous media with large temperature variation. *Physics Fluids* 20: 4-9.

Zehner, P. & E.U. Schlünder, 1970. Wärmeleitfähigkeit von Schüttungen bei mässigen Temperaturen. *Chem. Ing. Tech.* 42: 933-941.

Zehner, P. & E.U. Schlünder, 1973. Die effektive Wärmeleitfähigkeit durchströmten Kugelschüttungen bei mässigen und hohen Temperaturen. *Chem. Ing. Tech.* 45: 272-276.